MONONUCLEAR AND HETEROTRINUCLEAR RUTHENIUM COMPLEXES: SYNTHESIS AND WATER OXIDATION ACTIVITY.

Lorenzo Mognon

Dipòsit Legal: T 1359-2015

UNIVERSITAT ROVIRA I VIRGILI
MONONUCLEAR AND HETEROTRINUCLEAR RUTHENIUM COMPLEXES: SYNTHESIS AND WATER OXIDATION ACTIVITY.
Lorenzo Mognon
Dipòsit Legal: T 1359-2015

UNIVERSITAT ROVIRA I VIRGILI
MONONUCLEAR AND HETEROTRINUCLEAR RUTHENIUM COMPLEXES: SYNTHESIS AND WATER OXIDATION ACTIVITY.
Lorenzo Mognon
Dipòsit Legal: T 1359-2015

Lorenzo Mognon

Mononuclear and Heterotrinuclear Ruthenium Complexes: Synthesis and Water Oxidation Activity

Doctoral Thesis

Supervised by Prof. Antoni Llobet Dalmases

Institute of Chemical Research of Catalonia (ICIQ)

UNIVERSITAT ROVIRA I VIRGILI

Tarragona

2015

UNIVERSITAT ROVIRA I VIRGILI
MONONUCLEAR AND HETEROTRINUCLEAR RUTHENIUM COMPLEXES: SYNTHESIS AND WATER OXIDATION ACTIVITY.
Lorenzo Mognon
Dipòsit Legal: T 1359-2015

UNIVERSITAT ROVIRA I VIRGILI

I STATE that the present study, entitled "Mononuclear and Heterotrinuclear Ruthenium Complexes: Synthesis and Water Oxidation Activity", presented by Lorenzo Mognon for the award of the degree of Doctor, has been carried out under my supervision at the Institute of Chemical Research of Catalonia.

Tarragona, June 2015

Doctoral Thesis Supervisor

Prof. Antoni Llobet Dalmases

UNIVERSITAT ROVIRA I VIRGILI
MONONUCLEAR AND HETEROTRINUCLEAR RUTHENIUM COMPLEXES: SYNTHESIS AND WATER OXIDATION ACTIVITY.
Lorenzo Mognon
Dipòsit Legal: T 1359-2015

UNIVERSITAT ROVIRA I VIRGILI
MONONUCLEAR AND HETEROTRINUCLEAR RUTHENIUM COMPLEXES: SYNTHESIS AND WATER OXIDATION ACTIVITY.
Lorenzo Mognon
Dipòsit Legal: T 1359-2015

Alla mia famiglia

A la meva rosa dels vents

UNIVERSITAT ROVIRA I VIRGILI
MONONUCLEAR AND HETEROTRINUCLEAR RUTHENIUM COMPLEXES: SYNTHESIS AND WATER OXIDATION ACTIVITY.
Lorenzo Mognon
Dipòsit Legal: T 1359-2015

Acknowledgments

In these few lines I would like to express my gratitude to the people who somehow helped me accomplish this objective. I will use the four languages that accompanied me in this experience: Catalan, English, Spanish, and, obviously, Italian.

Primer de tot, vull donar les gràcies al meu director de tesis, el Toni, per haver-me permès treballar amb ell i aprendre d'ell com "fer" química i com investigar.

Voglio anche ringraziare Marcella, Mauro e Giulia, del laboratorio di Padova, per avermi aiutato a fare i primi passi nel mondo della ricerca, e avermi incoraggiato a seguire questa strada.

I want to thank all the people that collaborated in one way or another with the chemistry I'm presenting in this work. In particular I'd like to thank the people from the Research Support Area that helped me every time I needed them, for their professionalism and competence.

I also want to thank the people of the group of the Universitat Autònoma de Barcelona, because even if in the end we didn't meet so much, every time was very enjoyable.

I want to thank all the people that worked in the group, for longer or shorter time, who helped me growing both on professional and personal side, inside and out of the lab; rigorously not in rigorous time order: Stephan, Carlo, Lydia, Isidoro, Somnath, Pau, Tomasz, Sukanta, Takashi, Craig, Laia, Arianna, Joan, Roc, Carolina, Sven, Haijie, Anett, Samuel, Pablo, Stephanie, Serena, Ana, Ana and Ana, Edyta, Kentaro, Jordi, Costance, Jann, Tanja, Yuanyuan and Sergi.

Una menció especial la vull reservar per la Maria José, per ser una secretaria de grup exemplar, i ajudar-nos, crec que algun cop més enllà del que toca.

Gràcies també a la gent que he conegut a Tarragona fora del laboratori: la Mariona i el Txepo (i l'Isard), el Robert, el Carles i la Laura, la Maribel, la Neus, el Xevi, la Eloise, la Marta i el Francesco (anche se in reltá ci conoscevamo anche prima), perquè no es pot viure només treballant.

Quiero agradecer también a tod@s l@s chic@s del curso de castellano, y especialmente a Sandra, para ser mucho más que una simple profe de idiomas.

Deixant Tarragona, vull donar les gràcies a la gent de la UAB people, a les químiques i els seus marits, i a la colla d'Artés, per haver-me acceptat com un més del grup, encara que els primers mesos no entenia res del que deien.

Ja que estem per al Bages, vull donar les gràcies a la tribu Forcada i als de Avinyó, per tractar-me com un d'ells des del principi, quan l'únic que feia era esperar que la Laia em traduïes el que deien. I gràcies especialment a l'Albert per ajudar-me amb la portada d'aquesta tesis.

Devo invece chiedere scusa a quei due, Alessio e Marco, perché avevo detto che avrei avuto più tempo per loro sanno cosa, e invece sono andato a Tarragona. E grazie, perché anche quando ve lo dico una settimana prima, riuscite a liberarvi per andare a fare una birra e rimetterci in pari con la vita.

Siamo quasi alla fine, e qui vengono i ringraziamenti più sentiti. Grazie ai miei genitori, per avermi appoggiato durante tutto il percorso, per avermi incoraggiato a seguire la mia strada e per aver fatto di tutto per farmi arrivare fin qui con le mie gambe. Grazie ad Andrea e a Martina, per essere un esempio da seguire, per avermi spronato ad arrivare fino alla fine, e per cercare sempre di trovare il tempo di parlare, anche avendo due bimbe (bellissime, bisogna dirlo) da seguire.

Finalment, gràcies a la Laia, el millor que m'ha passat durant aquest quatre anys, i espero que continuarà passant. Gràcies per tot.

The work performed in the present doctoral thesis has been possible thanks to the funding of:

- Institut Català de Investigació Quimica (ICIQ).
- Agencia de Gestió d'Ajuts Universitaris i de Recerca (AGAUR) through projects: 2009 SGR 69 and 2014 SGR 915.
- Ministerio de Ciencia e Innovación through project: CTQ2010-21497.
- Ministerio de Economía y Competitividad through projects: PRI-PIBIN-2011-1278, CTQ2013-49075-R and Severo Ochoa Excellence Accreditation 2014-2018 (SEV-2013-0319).

UNIVERSITAT ROVIRA I VIRGILI
MONONUCLEAR AND HETEROTRINUCLEAR RUTHENIUM COMPLEXES: SYNTHESIS AND WATER OXIDATION ACTIVITY.
Lorenzo Mognon
Dipòsit Legal: T 1359-2015

UNIVERSITAT ROVIRA I VIRGILI
MONONUCLEAR AND HETEROTRINUCLEAR RUTHENIUM COMPLEXES: SYNTHESIS AND WATER OXIDATION ACTIVITY.
Lorenzo Mognon
Dipòsit Legal: T 1359-2015

UNIVERSITAT ROVIRA I VIRGILI
MONONUCLEAR AND HETEROTRINUCLEAR RUTHENIUM COMPLEXES: SYNTHESIS AND WATER OXIDATION ACTIVITY.
Lorenzo Mognon
Dipòsit Legal: T 1359-2015

Graphical Abstracts

Chapter 1. Introduction

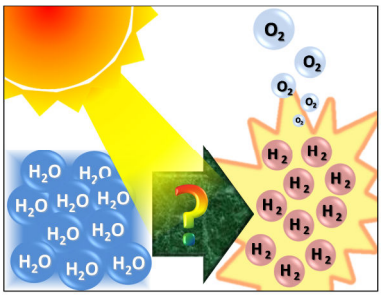

A general introduction about the energy problem, the study of the mechanism of natural photosynthesis, and the challenges of artificial photosynthesis is presented. The paramount importance of water oxidation and how the properties of ruthenium complexes are optimal to deal with its optimization is discussed. A brief history of the cornerstones of water oxidation catalysis and an analysis of the state of the art are exposed.

Chapter 2. Objectives

Chapter 3. Ru–Zn Heteropolynuclear Complexes Containing a Dinucleating Bridging Ligand: Synthesis, Structure, and Isomerism

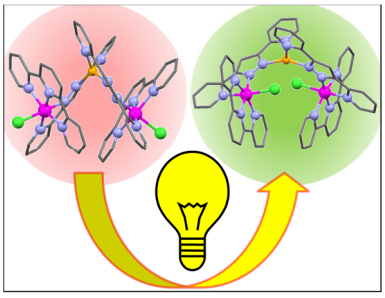

New heteropolynuclear complexes of ruthenium and zinc based on 2,2'-(1*H*-pyrazole-3,5-diyl)dipyridine are synthesized and characterized by spectroscopic and electrochemical methods. The electronic communication through the bridging ligand is

discussed. Reactivity towards isomerization is observed by means of NMR and rationalized by density functional theory based calculations.

Chapter 4. Synthesis, Structure, Spectroscopy and Reactivity of New Heterotrinuclear Water Oxidation Catalysts

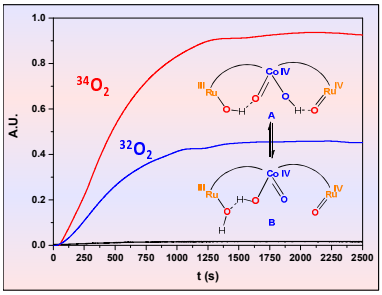

New heterotrinuclear complexes containing ruthenium and manganese or cobalt, based on 2,2'-(1*H*-pyrazole-3,5-diyl)dipyridine are synthesized. Electrochemical, UV-vis and EPR experiments are carried out on different complexes. Photochemical water oxidation activity is tested with $[Ru(bpy)_3]^{2+}$ as photosensitizer and $Na_2S_2O_8$ as sacrificial electron acceptor. Oxone is used as sacrificial oxidant to study the reaction at pH = 7 and labelled water experiments shine light on the oxygen evolving mechanism.

Chapter 5. Single Site Isomeric Ru WOCs with Electron Withdrawing Groups: Synthesis, Electrochemical Characterization and Reactivity

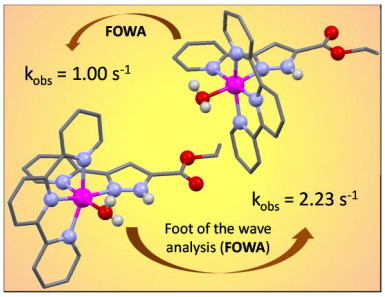

New mononuclear ruthenium complexes based on 1*H*-Pyrazole-3-Carboxylic Acid, 5-(2-pyridinil)-, ethyl ester are synthesized and extensively characterized. A linkage isomerism is identified and analyzed by

electrochemical methods. Foot-of-the-wave analysis is applied to the electrocatalytic water oxidation and kinetic constants are obtained. Ce(IV) is used as sacrificial oxidant to study chemically driven water oxidation.

Chapter 6. Supported Single Site Isomeric Ru WOCs: Synthesis, Electrochemical Characterization, Reactivity and Anchoring

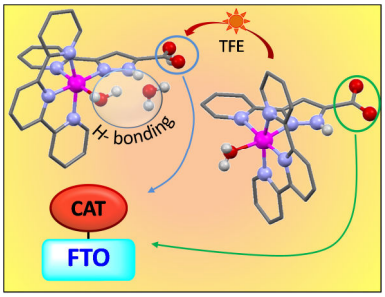

Modified mononuclear ruthenium complexes are synthesized and extensively characterized by spectroscopic and electrochemical methods. Homogeneous water oxidation is tested using Ce(IV) as sacrificial oxidant. The complexes are attached on solid support and characterized by electrochemical methods. Preliminary studies on heterogeneous water oxidation are carried out.

Chapter 7. Summary and Conclusions

UNIVERSITAT ROVIRA I VIRGILI
MONONUCLEAR AND HETEROTRINUCLEAR RUTHENIUM COMPLEXES: SYNTHESIS AND WATER OXIDATION ACTIVITY.
Lorenzo Mognon
Dipòsit Legal: T 1359-2015

Table Of Contents

UNIVERSITAT ROVIRA I VIRGILI
MONONUCLEAR AND HETEROTRINUCLEAR RUTHENIUM COMPLEXES: SYNTHESIS AND WATER OXIDATION ACTIVITY.
Lorenzo Mognon
Dipòsit Legal: T 1359-2015

Glossary of terms and abbreviations

bpy	2,2'-bypiridine
CFSE	Crystal Field Stabilization Energy
COSY	Correlation Spectroscopy
CPE	Controlled Potential Electrolysis
CV	Cyclic Voltammetry
DCM	Dichloromethane
DFT	Density Functional Theory
DMF	*N, N*-Dimethylformamide
DMSO	Dimethyl sulfoxide
DPV	Differential Pulse Voltammetry
ΔE	Difference between two redox potentials
ΔE_p	Difference between the potentials of the two peak of the same redox process: $\Delta E_p = E_{p,A} - E_{p,C}$
E	Potential
$E_{1/2}$	Half wave potential
$E_{p,A}$	Anodic peak potential
$E_{p,C}$	Cathodic peak potential
ET	Electron Transfer
FOWA	Foot-of-the-wave Analysis
FTO	Fluorine-doped Tin Oxide
H_2pcp	1*H*-Pyrazole-3-Carboxylic Acid, 5-(2-pyridinil)-
Hbpp	2,2'-(1*H*-pyrazole-2,5-diyl)dipyridine
HL	1*H*-Pyrazole-3-Carboxylic Acid, 5-(2-pyridinil)-, ethyl ester

HSAB	Hard Soft Acid Base theory
I2M	Interaction between two M-O entities
i_a	Current intensity of the anodic peak
i_c	Current intensity of the cathodic peak
MeCN	Acetonitrile, CH_3CN
MLCT	Metal to Ligand Charge Transfer
NHE	Normal Hydrogen Electrode
NOESY	Nuclear Overhauser Effect Spectroscopy
OEC	Oxygen Evolving Complex
OCP	Open Circuit Potential
ORTEP	Oak Ridge Thermal Ellipsoid Plot
PCET	Proton Coupled Electron Transfer
RDE	Rotating Disk Electrode
rds	Rate determining step
SCE	Saturated Calomel Electrode
SSCE	Sodium Saturated Calomel Electrode
trpy	2,2':6',2''-terpyridine
TBAH	Tetrabutylammonium hexafluorophosphate, $[(n\text{Bu}_4\text{N})PF_6]$
TFE	Trifluoroethanol, CF_3CH_2OH
TOF_i	Initial Turn Over Frequency
TON	Turn Over Number
WNA	Water Nucleophilic Attack
WOC	Water Oxidation Catalyst
ZFS	Zero Field Splitting

UNIVERSITAT ROVIRA I VIRGILI
MONONUCLEAR AND HETEROTRINUCLEAR RUTHENIUM COMPLEXES: SYNTHESIS AND WATER OXIDATION ACTIVITY.
Lorenzo Mognon
Dipòsit Legal: T 1359-2015

UNIVERSITAT ROVIRA I VIRGILI
MONONUCLEAR AND HETEROTRINUCLEAR RUTHENIUM COMPLEXES: SYNTHESIS AND WATER OXIDATION ACTIVITY.
Lorenzo Mognon
Dipòsit Legal: T 1359-2015

Chapter 1. Introduction

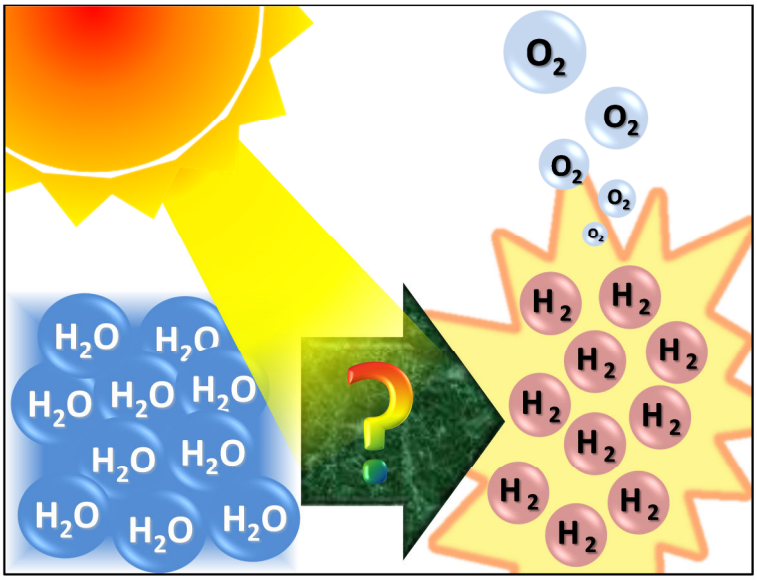

A general introduction about the energy problem, the study of the mechanism of natural photosynthesis, and the challenges of artificial photosynthesis is presented. The paramount importance of water oxidation and how the properties of ruthenium complexes are optimal to deal with its optimization is discussed. A brief history of the cornerstones of water oxidation catalysis and an analysis of the state of the art are exposed.

UNIVERSITAT ROVIRA I VIRGILI
MONONUCLEAR AND HETEROTRINUCLEAR RUTHENIUM COMPLEXES: SYNTHESIS AND WATER OXIDATION ACTIVITY.
Lorenzo Mognon
Dipòsit Legal: T 1359-2015

Chapter 1. Introduction

UNIVERSITAT ROVIRA I VIRGILI
MONONUCLEAR AND HETEROTRINUCLEAR RUTHENIUM COMPLEXES: SYNTHESIS AND WATER OXIDATION ACTIVITY.
Lorenzo Mognon
Dipòsit Legal: T 1359-2015

Chapter 1. Introduction

1.1 The energy problem

Ever since the industrial revolution, human society has relied mostly on fossil fuels for the satisfaction of its energetic demands. Through the decades, the uncontrolled consumption of coal in the beginning and oil and gas in later years (Figure 1), has brought two main problems: (1) The fossil fuels reserves are running out, and the new ones are less and less feasible in terms of price and/or extraction;[1] moreover, the usage of these already scarce resources for mere burning and energy extraction subtracts useful raw material for fine chemicals production. (2) The CO_2 generated from their burning is one of the main reasons for the climate change, with all its catastrophic consequences.[1]

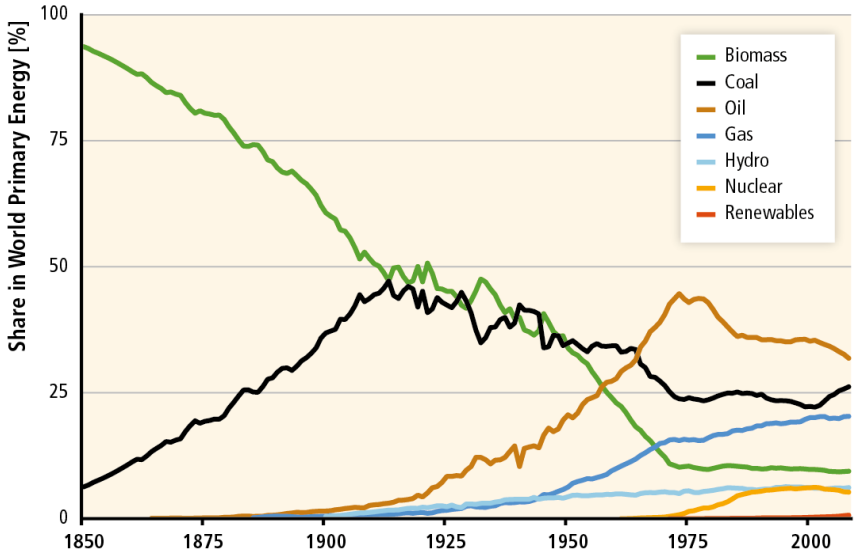

Figure 1. Structural change in world primary energy (in percent) over 1850 – 2008 illustrating the substitution of traditional biomass (mostly non-commercial) by coal and later by oil and gas. The emergence of hydro, nuclear and new renewables is also shown.[1]

I

Alternatives to fossil fuels energy sources include nuclear fission and renewable resources. While nuclear energy has a low impact on CO_2 production, problems related to its safety (illustrated by the accidents in Three Mile Island, Chernobyl, and Fukushima) and treatment of waste led to a global decrease in its usage over the years, from 17% in 1993 to 11% in 2012. [1]

On the other hand, renewable resources include biomass, hydro power, geothermal energy, wind power and solar energy. In particular, the latter is very promising because the energy coming from the Sun every hour is almost as much as the yearly world consumption (ca. 16TW, 2009). For this reason, a huge burst of researches in this field has been registered in the last years. [2] Up to now most of the research has been focused on the direct conversion of solar energy into electricity using solar cells.[3] However, this technology depends dramatically on constant sunshine, mostly because of the difficulties in efficient storage and transport. To overcome the storage, transport and solar light intermittence problems, a different approach has to be considered. This is the so-called artificial photosynthesis (inspired by the natural photosynthesis), which consists in generating a fuel (solar fuel) from sunlight energy, thus avoiding the sunshine dependence, the storage and the transport problems (See Section 1.1.2)

1.1.1 Natural photosynthesis

In nature, the energy from the Sun is harvested and stored in form of chemical bonds through photosynthesis. The process consists in using the energy from sunlight radiation to oxidize water to generate protons, which are later recombined with CO_2 to give carbohydrates, and oxygen, which is released as molecular oxygen side product (Equation 1). The water oxidation

reaction presents intrinsic challenges: (1) thermodynamic, due to the quantity of electrons involved in the process, and (2) mechanistic, due to the number of bonds that have to be broken and formed.[4]

$$nCO_2 + nH_2O + h\nu \rightarrow (CH_2O)_n + nO_2 \qquad \textbf{Eq.1}$$

This process is performed by a series of proteins, namely photosystem II (PSII), cytochrome b_6f, photosystem I (PSI) and ATPsynthase, which are distributed in the thylakoid membrane in chloroplasts of green plants, algae and oxyphotobacteria.

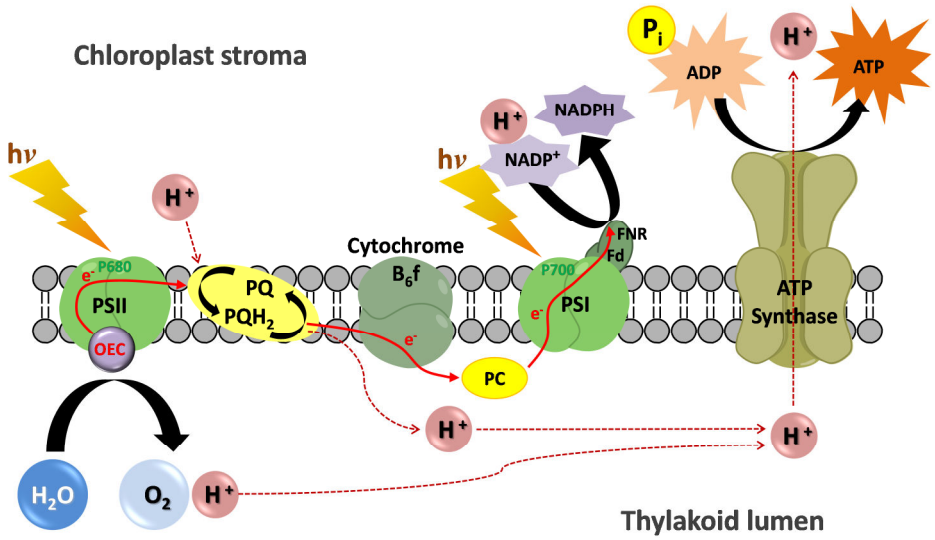

Figure 2. Schematic view of the thylakoid membrane and of the processes taking place in it.

The process is initiated by the absorption of a photon by chlorophyll P680 and other pigments. Here the charge separation takes place: the excited P680* transfers an electron through a series of acceptors until it reaches PSI, where a

second photon is absorbed. At this point the energy accumulated is enough to drive the fixation of carbon dioxide, generating first the reduced NADPH (Nicotinamide Adenine Dinucleotide Phosphate) as a hydrogen carrier and then the energy rich molecule ATP (Adenosine Triphosphate). On the other hand, a tyrosine residue in the PSII transfers an electron to the oxidized chlorophyll, which is then ready for the next photon absorption. The tyrosine then proceeds to oxidize the oxygen evolving complex (OEC).[5] For the OEC to oxidize a water molecule, the same pattern has to be repeated four times.

For the scope of this work, the OEC and the reaction taking place in it are the most relevant topic and for this reason they will be further developed. OEC structure has been the focus of multiple X-ray crystallographic studies,[6] each with increasing resolution, up to the 1.9 Å obtained by Umena et al. (Figure 3).[7] The OEC is a manganese cluster of formula Mn_4O_5Ca. It consists of a cubane-like structure where three Mn and one Ca atoms are linked by oxo bridges. The fourth Mn atom is located outside the cubane and is linked to two other manganese atoms through a di-μ-oxo bridge. The cluster is surrounded by amino acid residues that provide a coordination framework for the metal atoms, or a hydrogen bonding network, and by a number of water molecules.

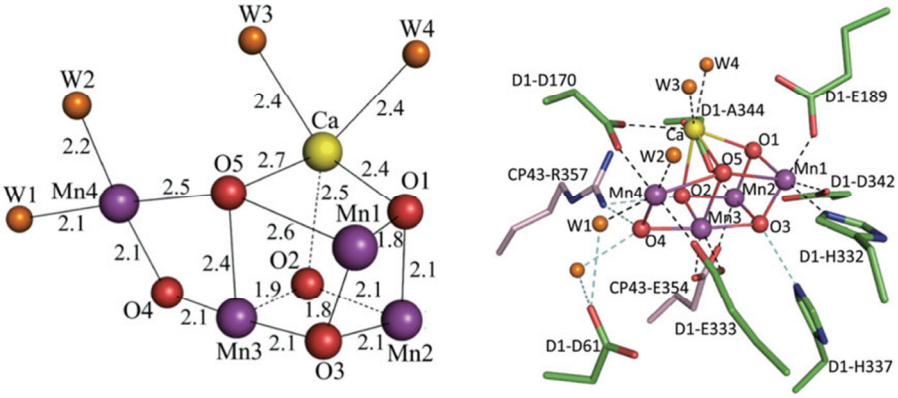

Figure 3. (Left) Distances (in angstroms) between metal atoms and oxo bridges or water molecules in OEC. (Right) Ligand environment of the OEC. Manganese, purple; calcium, yellow; oxygen, red; water, orange.

As previously mentioned, the OEC has to accumulate 4 oxidative equivalents to generate oxygen, passing through five intermediate states S_i(i=0-4). The stepwise change from the most reduced state S_0 to the most oxidized S_4 is mediated by electron abstraction from a nearby tyrosine residue (Y_Z), which in turn is reduced by P680*.

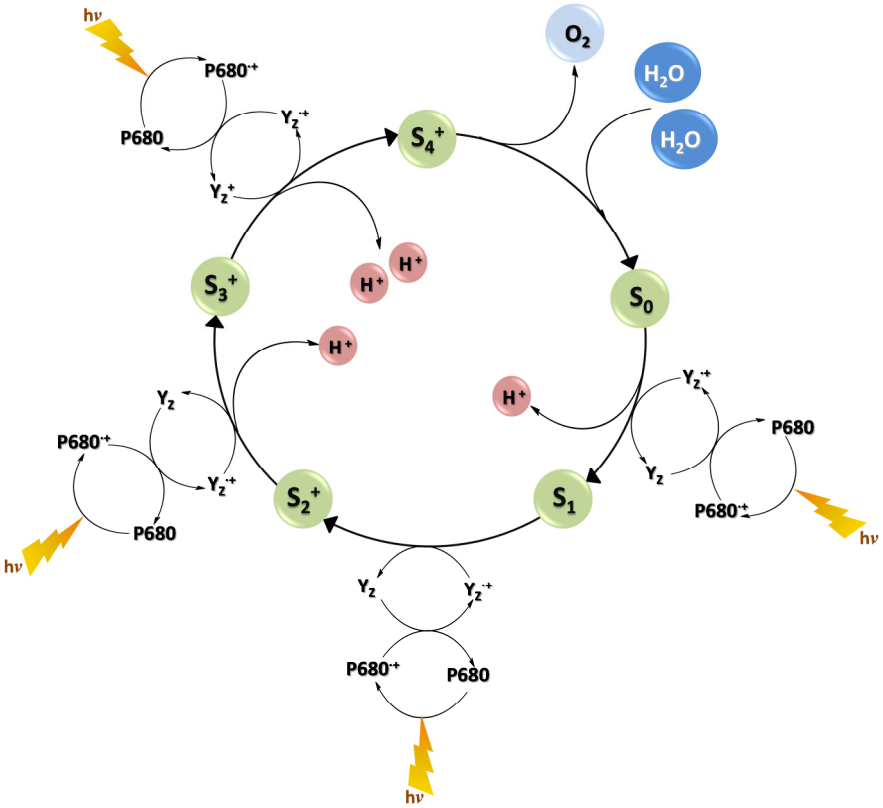

Figure 4. The S-state cycle for the photooxidation of two water molecules.

While the proposed structure is generally accepted, there is no accordance on the oxygen atoms involved in the oxygen-oxygen bound formation, and therefore on its mechanism. Two general pathways constitute the main proposal (Figure 5):

1) A nucleophilic attack, either from an hydroxide (a)[8] or a water molecule (b)[6a, 9] bound and activated by Ca or Mn,[10] or directly from an outer sphere H_2O (c),[10b, 11] on a terminal oxygen (Mn^{V}=O);

2) a radical coupling between oxyl or oxido bridging μ-O^{2-} ligands (d),[12] or μ_2- and μ_3-O^{2-} (e),[12a] or between a terminal oxyl bound to a Mn and a μ_3-O^{2-} bridging two Mn and a Ca (f).

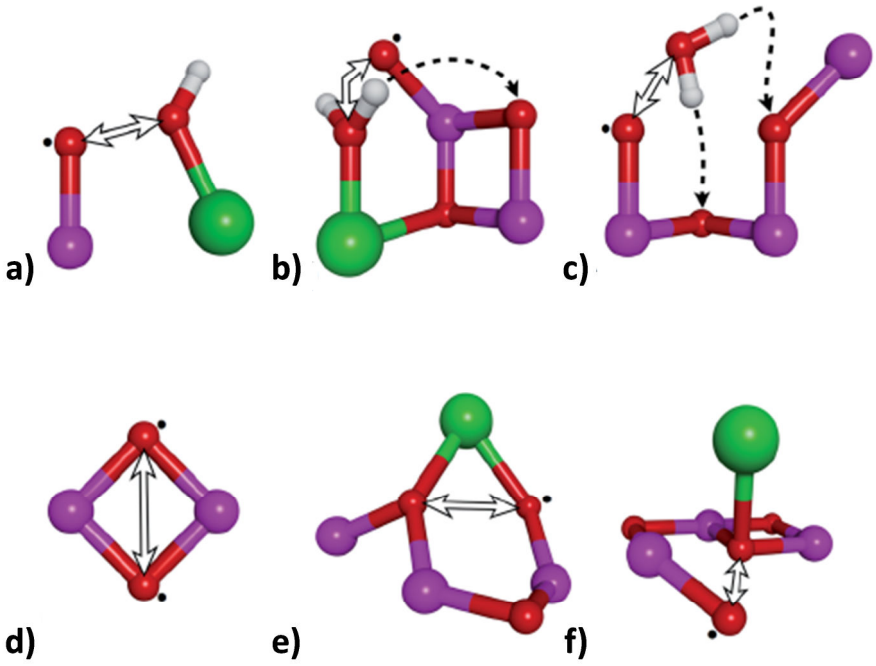

Figure 5. Proposed mechanisms for O-O bond formation in water oxidation catalyzed by OEC. Color code: Ca in green, Mn in purple, O in red, and H in light gray.[13]

It is important to note that the Ca atom has been proposed to act as a water binding and activation site, but its complete role is still not fully understood. Removal of Ca from OEC inhibits its activity, which can be restored by addition of Ca^{2+} to the deactivated OEC.[14] A number of other Lewis acids have been tested in this sense,[14d-f] but only Sr^{2+} has shown any activity, even if much lower.[14a, 14d, 14f, 15]

1.1.2 Artificial photosynthesis

The idea behind artificial photosynthesis is to mimic the natural occurring process of photo collection to oxidize water and use the generated protons and electrons to produce a high energy molecule (sugars in natural photosynthesis) such as hydrogen. When the final products are O_2 and H_2, the reaction can be described as water splitting, as a H_2O is broken down to its fundamental constituents. To rationalize this process, the water splitting reaction (3) is commonly separated in two half reactions, water oxidation (1) and proton reduction (2) (Scheme 1). This separation allows for independent study and optimization of the processes.

$$2H_2O \rightarrow O_2 + 4H^+ + 4e^- (\mathbf{1})$$
$$\underline{4H^+ + 4e^- \rightarrow 2H_2 (\mathbf{2})}$$
$$2H_2O \rightarrow O_2 + 2H_2 (\mathbf{3})$$

Scheme 1. Water splitting half reactions

This separation also allows the rational design of a device capable to perform the artificial photosynthesis process, such as the Photoelectrochemical Cell (PEC) presented in Figure 6.[16] This should be formed of an antenna or photosensitive material for light absorption and charge separation (D), a water oxidation semi cell, a proton-exchange membrane (PEM), and a proton reduction semi cell.

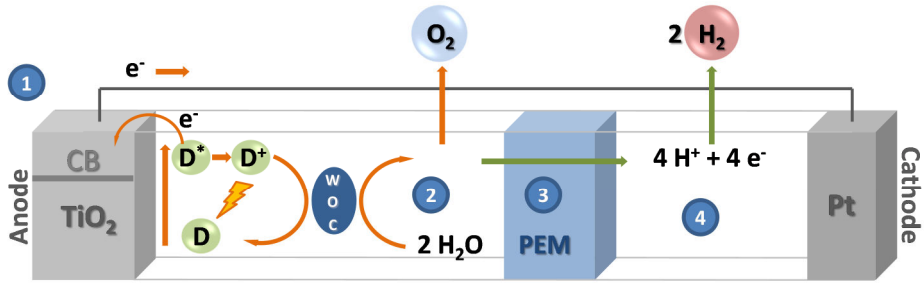

Figure 6. Schematic drawing of an example of a water splitting photoelectrochemical cell.

As in natural photosynthesis, the water splitting process starts with the absorption of a photon by the photosensitizer which is excited and injects an electron in the conduction band of the anode semiconductor, usually TiO_2, generating the oxidized photosensitizer (1). The injected electrons proceed through the wires to the cathode, where the proton reduction catalyst, in the example a platinum electrode, produces hydrogen (4). The now oxidized photosensitizer is reduced by the water oxidation catalyst (WOC) to regenerate its initial form. Once the WOC has accumulated four oxidizing equivalents, an oxygen molecule is released (2), and the protons generated in the process migrate through the PEM (3) to the cathode semi cell where their reduction is carried out.

For the PEC to work efficiently, many simultaneous reactions and processes have to take place harmoniously. However, the main bottleneck of the whole process is the water oxidation reaction due to the previously discussed problems.[16d, 17]

1.2 Water oxidation catalysis

As appointed in the previous part, the bottleneck of the whole water splitting process is the water oxidation reaction, due to its high potential (1.23 V vs NHE at pH = 0) and the intrinsic molecular complexity generated by the synchronized reorganization of multiple bonds. For this reason the use of a suitable catalyst is pivotal to perform this reaction efficiently.

Several compounds have been reported to catalyze this reaction. One attractive approach is the use of molecular catalysts, which usually are complexes of transition metals as ruthenium, cobalt, iridium, manganese, iron and more recently copper. Polyoxometalates of ruthenium, cobalt and other metals have also been reported to catalyze water oxidation.

Another approach is the use of heterogeneous catalysts such as metal oxides or anchored molecular catalysts. While heterogeneous catalysis allows for easy catalysts and/or products separation and recovery from the reaction medium, they often lack a good characterization on the molecular level, complicating mechanistic studies. On the other hand molecular catalysts are excellent candidates to carry out this kind of studies. For the scope of this work, the catalysis with metal oxides will not be discussed; however, some examples of supported molecular catalysts will be considered in Section 2.1.3.

From the mechanistic point of view, as in the case of the proposed mechanisms for the OEC, the formation of an oxygen-oxygen bond promoted by a transition metal center is usually classified under the two following possible scenarios (Figure 7): (a) Water Nucleophilic Attack to an M-O bond (WNA), or (b) Interaction between two M-O entities (I2M). The nuclearity of the complex is not fundamental in determine the mechanism.

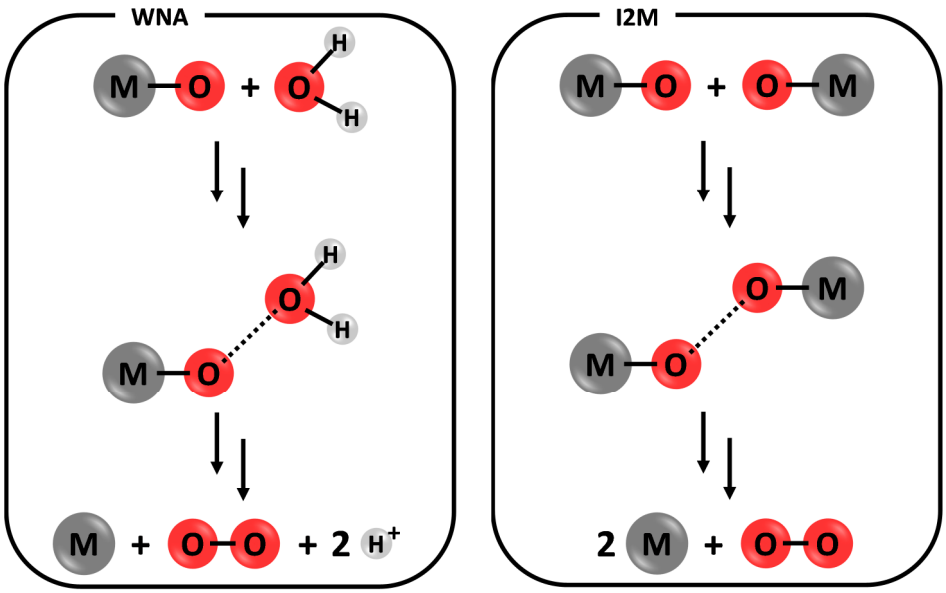

Figure 7. Possible mechanisms for oxygen-oxygen bond formation.

As in the natural photosynthesis, the artificial WOCs have to be able to accumulate four oxidative equivalents to drive the O_2 generation. Ideally, this oxidation process would take place using photons. However, to allow a quick screening of newly synthetized compounds, homogenous catalysts are tested using sacrificial oxidants: molecules that supply the oxidative equivalents required for the reaction, without the need for a full PEC device. The most common sacrificial oxidants are cerium ammonium nitrate (CAN), $[Ru(bpy)_3]^{3+}$, sodium peroxodisulfate and potassium peroxymonosulfate (or OXONE).[18]

I

1.2.1 Ruthenium polypyridilic catalysts

Ruthenium complexes are widely used in a number of fields, ranging from nonlinear optics,[19] liquid crystals[20] and magnetism[21] to molecular sensing[22] and chemotherapy.[23]

Ruthenium is a metal from the second row of the d group of the periodic table. Its electronic configuration [Kr] $4d^7\ 5s^1$ gives it access to the widest variety (together with osmium) of oxidation states, from +8 in RuO_4, to -2 in $[Ru(CO)_4]^{2-}$, corresponding to d^0 and d^{10} electronic configurations. Ruthenium complexes are generally stable and their properties can be tuned through ligand design and carefully controlled synthetic methods. These peculiar characteristics make ruthenium complexes appealing for catalysis: they are employed in a variety of reactions, as for example oxidation of organic substrates,[24] hydrogenations[25] or hydrogen abstractions,[26] C-H insertions[27] and metathesis.[28]

In particular, Ru aqua complexes exhibit a special redox behavior due to the possibility to exchange protons and electrons. As shown in Scheme 2, the successive oxidations from Ru(II) to Ru(IV) can be accompanied by proton loss, favored by the increased acidity induced in the aqua ligand.[29]

$$Ru^{II}\text{-}OH_2 \underset{+H^+ +e^-}{\overset{-H^+ -e^-}{\rightleftharpoons}} Ru^{III}\text{-}OH \underset{+H^+ +e^-}{\overset{-H^+ -e^-}{\rightleftharpoons}} Ru^{IV}{=}O$$

Scheme 2. Proton coupled electron transfer processes for ruthenium aqua species.

These proton coupled electron transfer (PCET) reactions avoid the formation of high energy intermediates due to charge accumulation.[30] The

relationship between pH and redox potential is rationalized by the Nernst equation:

$$E_{1/2} = E^0_{1/2} - 0.059(\mathrm{m/n})\mathrm{pH} \qquad \textbf{Eq.2}$$

where *m* and *n* are the number of protons and of electrons, respectively, exchanged in the redox process.

The dependence of the redox potential on the pH is graphically represented in the Pourbaix diagrams, which plot the half wave potentials of the species involved against a range of pH, thus giving information about the various equilibriums in the system.

In the late 70s, Meyer et al.[31] showed how polypyridilic aqua ruthenium (II) complexes can reach high oxidation state (IV) in a narrow potential window through simultaneous loss of electrons and protons. This is illustrated by the Latimer diagrams of $[Ru(bpy)_2Cl_2]$ and $[Ru(bpy)(py)(H_2O)]^{2+}$ shown in Scheme 3.[29]

$$\underset{(d\pi^4)}{cis\text{-}[Ru^{IV}(bpy)_2(Cl)_2]^{2+}} \xrightarrow{1.7\ V} \underset{(d\pi^5)}{cis\text{-}[Ru^{III}(bpy)_2(Cl)_2]^{+}} \xrightarrow{0\ V} \underset{(d\pi^6)}{cis\text{-}[Ru^{II}(bpy)_2(Cl)_2]} \qquad \text{(a)}$$

$$\underset{(d\pi^4)}{cis\text{-}[Ru^{IV}(bpy)_2(py)(O)]^{2+}} \xrightarrow{0.78\ V} \underset{(d\pi^5)}{cis\text{-}[Ru^{III}(bpy)_2(py)(OH)]^{2+}} \xrightarrow{0.67\ V} \underset{(d\pi^6)}{cis\text{-}[Ru^{II}(bpy)_2(py)(H_2O)]^{2+}} \qquad \text{(b)}$$

Scheme 3. Latimer diagrams for $[Ru(bpy)_2Cl_2]$ (a) and $[Ru(bpy)(py)(H_2O)]^{2+}$ (b). Potentials vs NHE.

For the chlorido complex (a) the first oxidation to Ru(III) takes places at a low potential (0 V), while the second oxidation rise to high potential (1.7 V), due to the increase in oxidation state and loss of negative charge. If the chlorido ligands are substituted by neutral pyridine and H_2O ligands (b), the first potential rises (0.67 V), whereas the second drops drastically (0.78 V). This is possible thanks to the increase in acidity of the M-H_2O system, which favors proton release and thus the preservation of the total charge, and to the stability of the Ru(IV)-oxo moiety, due to the $d\pi_{Ru}$-$2p\pi_O$ multiple bond interaction, as shown in Figure 8.

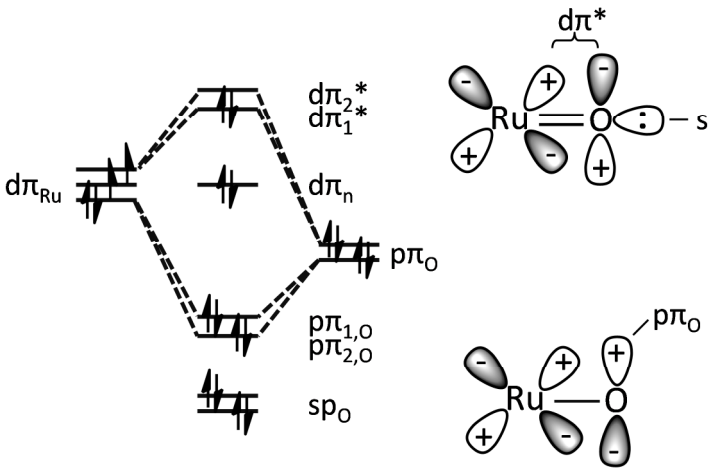

Figure 8. Ru^{IV}=O schematic energy orbital diagram.

The Ru(IV)-oxo system plays a key role in catalytic oxidations: in addition to stabilize high oxidation states, its LUMO orbital is a suitable site for initial interaction with electron donors.

As previously mentioned, the properties of ruthenium complexes are influenced by their ligands. To illustrate these effects, Table 1 shows the

electrochemical potentials of a number of ruthenium complexes with different N-containing and non N-containing ligands.[32]

Entry	Complex[a]	$E_{1/2}$(V vs NHE)[b]			
		$Ru^{III/II}$	$Ru^{IV/III}$	$Ru^{IV/II}$	$\Delta E_{1/2}$[c]
1	$[Ru(NH_3)_5(OH_2)]^{2+}$	-0.09	0.59	0.25	0.68
2	*cis*-$[Ru(bpy)_2(py)(H_2O)]^{2+}$	0.67	0.78	0.72	0.11
3	*cis*-$[Ru(bpy)_2(PPh_3)(H_2O)]^{2+}$	0.74	1.00	0.87	0.26
4	$[Ru(trpy)(4,4'\text{-}Me_2\text{-}bpy)(H_2O)]^{2+}$	0.71	0.85	0.78	0.14
5	$[Ru(trpy)(4,4'\text{-}(CO_2Et)bpy)(H_2O)]^{2+}$	0.90	1.04	0.97	0.14
6	$[Ru(trpy)(bpy)(H_2O)]^{2+}$	0.73	0.86	0.80	0.13
7	$[Ru(trpy)(acac)(H_2O)]^{+}$	0.43	0.80	0.62	0.37
8	$[Ru(trpy)(C_2O_4)(H_2O)]$	0.40	0.69	0.55	0.29

Table 1. Electrochemical properties for ruthenium aqua complexes.[a] Ligand abbreviations: bpy = 2,2'-bipyridine; py = pyridine; PPh_3 = triphenylphosphine; trpy = 2,2';6',2''-terpyridine; acac = acetyl acetonate anion.[b] $E_{1/2}$ values for Ru^{III}-OH/Ru^{II}-OH_2, Ru^{IV}=O/Ru^{III}-OH, and Ru^{IV}=O/Ru^{II}-OH_2 couples.[c] $\Delta E_{1/2} = E_{1/2}(Ru(IV/III)) - E_{1/2}(Ru(III/II))$

It can be observed that the Ru(III)/Ru(II) couple is strongly influenced by the ligands: Ru(II) is stabilized by dπ-π*(L) backbonding in presence of ligands as PPh_3 (entries 2 and 3) or electronrich π systems (entries 4 and 5), while Ru(III) is stabilized by the electrondonating characteristics of oxygen containing ligands (entries 6, 7 and 8).

In summary, ruthenium aqua complexes are excellent candidates to carry out the water oxidation reaction because: (1) they are able to accumulate high oxidation states in a narrow range of potentials thanks to PCET and (2) their

redox properties, and so the performance in the catalytic reaction, can be modulated by changing the ligands, allowing the rational design of the system.

1.2.1.1 Dinuclear complexes

The first well characterized molecular complex able to perform water oxidation was reported in 1982 by Meyer's group.[33] The so-called blue dimer was a dinuclear μ-oxo-bridged ruthenium complex *cis, cis*-$[(bpy)_2(H_2O)Ru(\mu\text{-}O)Ru(H_2O)(bpy)_2]^{4+}$, **1**, able to carry out the reaction with a TON of 13.2 and a TOF_i of 4.2 x 10^{-3} s^{-1} using CAN as sacrificial oxidant. The main deactivation pathway for this catalyst is thought to be the cleavage of the μ-oxo bridge,[34] but ligand oxidation[35] and anation[36] have also been proposed.

In 2004, Llobet et al.[37] reported a new dinuclear WOC, $[Ru_2(H_2O)_2(bpp)(trpy)_2]^{3+}$, **2**, bearing the much rugged bpp^- (Hbpp is 2,2'-(1-H-pyrazole-3,5-diyl)dipyridine) as bridging ligand. The complex catalytic performance is three times faster than that of the blue dimer, with a higher TON (17.5). Extensive mechanistic studies[38] demonstrated an I2M pathway for the formation of the O-O bond, in contrast to its predecessor.

During following years, an increasing number of dinuclear compounds have been synthesized and tested for water oxidation.[39] An interesting development was presented by Meyer and Llobet [40] with complex **3**, bearing a ligand similar to Hbpp, with an extra pyridine forcing a higher distance between the metal centers: water labelled mechanistic studies showed how subtle change in the geometry of the active site could reduce the space interaction between the two ruthenium metals, thus shifting the mechanism from the I2M seen for **2** to a WNA.

Presently the best results are reported by Llobet and Meyer[41] with complex **4**, based on a ligand structurally analogous to Hbpp. With two carboxylic moieties on the pyridine rings, this strongly anionic ligand allows for an impressive TOF_i of 1.4 s^{-1} using CAN, bringing this catalyst at the frontline of dinuclear complexes, and demonstrates the importance of rational design of the ligands.

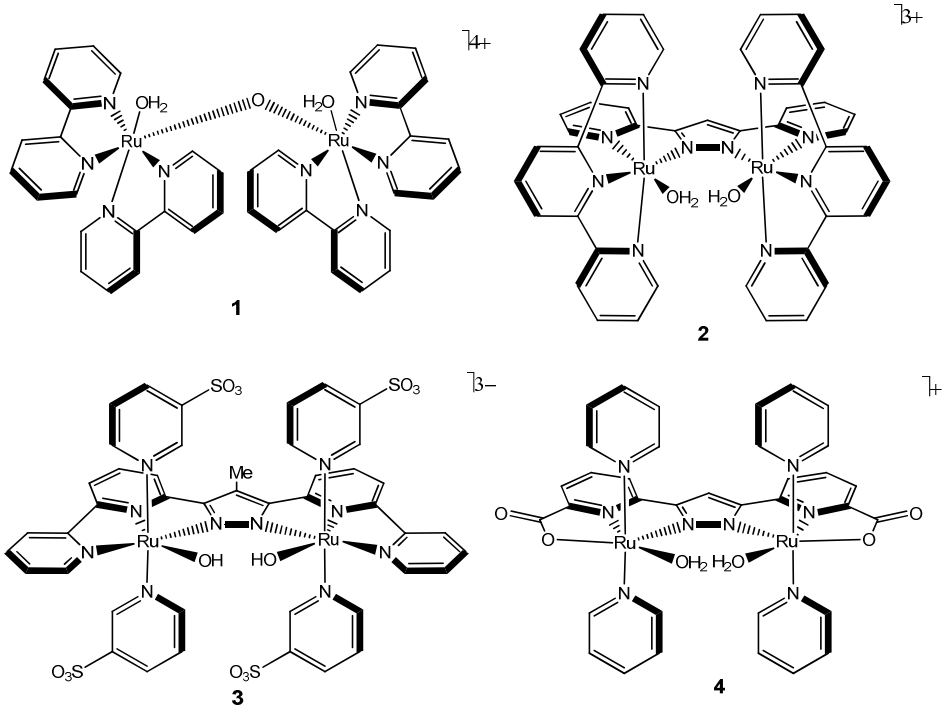

Figure 9. Dinuclear ruthenium complexes

1.2.1.2 Mononuclear complexes

Mononuclear ruthenium complexes represent a simpler approach, thanks to their generally easier synthesis and fine tuning of properties. However, due to the multimetallic nature of the OEC, it was long envisioned that an artificial WOC would need to accommodate multiple metal centers to account for the four oxidative equivalents needed for water oxidation.

In 2005 Thummel et al.[39a, 42] invalidated this notion with the first single site metal complex capable of oxidizing water. They later went on and synthetized and evaluated the catalytic performances of various mononuclear complexes (**5-7**).[42]

A thoroughly mechanistic characterization to verify the mononuclear nature of the catalysis was presented in 2008 by Meyer and co-workers.[43] The proposed pathway has been later adapted to other catalytic systems based on Ru[44] or other metals.[45]

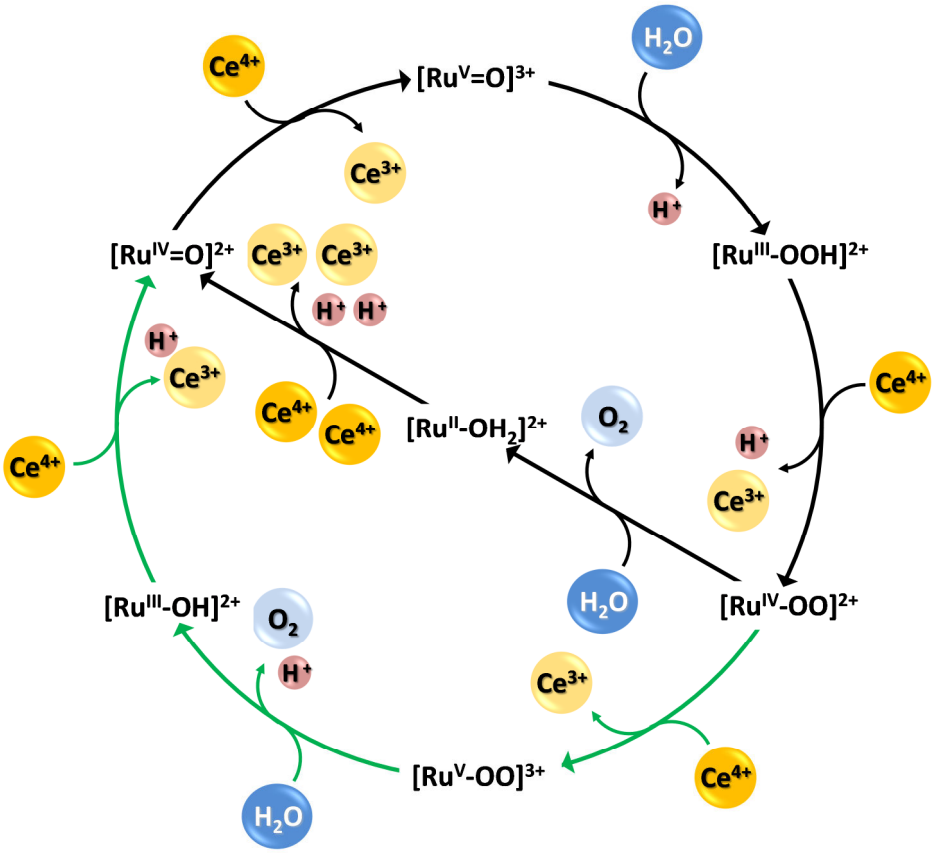

Scheme 4. Proposed WNA mechanism for catalytic water oxidation by mononuclear ruthenium complexes. The green arrows represent the pathway in 1 M HNO_3.

The process starts with three stepwise oxidations of Ru^{II}-OH_2 to Ru^{V}=O, the first two proceeding through PCET. The highly electrophilic oxo group then undergoes a water nucleophilic attack, with the formation of the O-O bond, to generate the hydroperoxide intermediate Ru^{III}-OOH. A new PCET oxidation takes places, forming Ru^{IV}-OO, the dominant species in the catalytic steady state. In 0.1 M HNO_3 the peroxo species release O_2 and the original Ru^{II}-OH_2

species is regenerated. In 1 M HNO_3 Ru^{IV}-OO is further oxidized to Ru^{V}-OO, which evolves oxygen and re-enters the catalytic cycle as Ru^{III}-OH.

Mononuclear complexes structurally related to **2** have also been synthetized, characterized and tested for catalytic activity.[46] Due to the asymmetric nature of the ligands, isomeric complexes were obtained, referred to as *in* or *out*, depending on the relative positions of the ligands (Figure 10). The authors stress the importance of PCET in the water oxidation catalysis comparing the electrochemical behavior of the precursor chlorido complexes and the aqua complexes **8-9**: the former displayed only one redox process, associated to a Ru(III)/Ru(II) couple, while the latter showed three redox processes, assigned to the Ru(III)/Ru(II), Ru(IV)/Ru(III) and Ru(V)/Ru(IV) couples.

During the last few years, very fast catalysts (**10-11**) have been reported by Sun, Llobet at al. [47] based on the bda^{2-} ligand (H_2bda is 2,2'-bipyridine-6,6'-dicarboxylic acid). Kinetic studies demonstrated the I2M mechanism, favored by the π- π stacking of the ancillary ligands, and showed once more how modification of the ligands can affect the catalytic properties of the complex.

On the mechanistic side, a particular case was recently reported by Llobet et al.[48] for the mononuclear active complex $[Ru(trpy)(bpy)(H_2O)]^{2+}$, **12**, which under catalytic conditions underwent ligand removal, with formation of a dinuclear species, **13**. Thorough characterization of the system, supported by theoretical studies, showed a slow interconversion to the more stable dinuclear system, where one center acts as electron relay and the other is responsible for the primary interaction with the water molecules through

PCET. Furthermore, the terminal Ru=O group can act as anchor for hydrogen bonding, to reduce the activation energy of transition states.

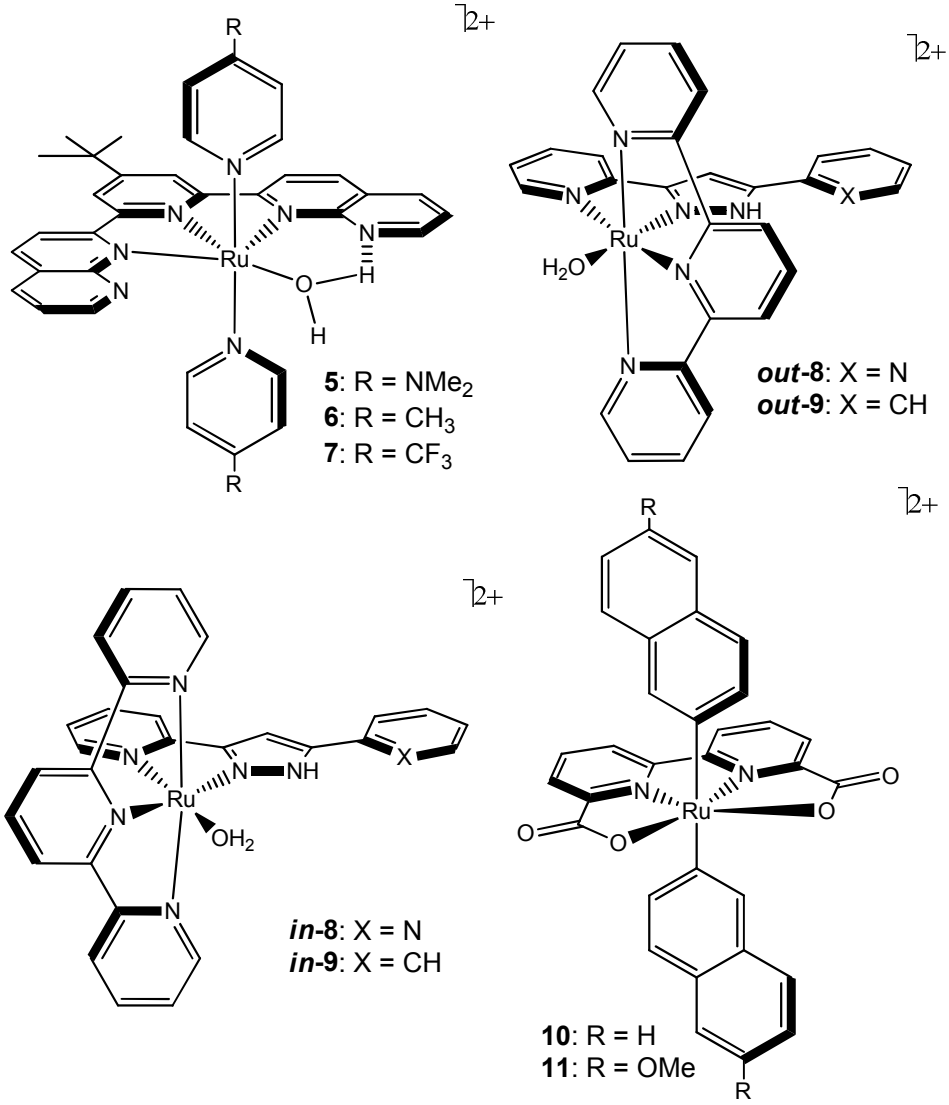

Figure 10. Mononuclear ruthenium complexes.

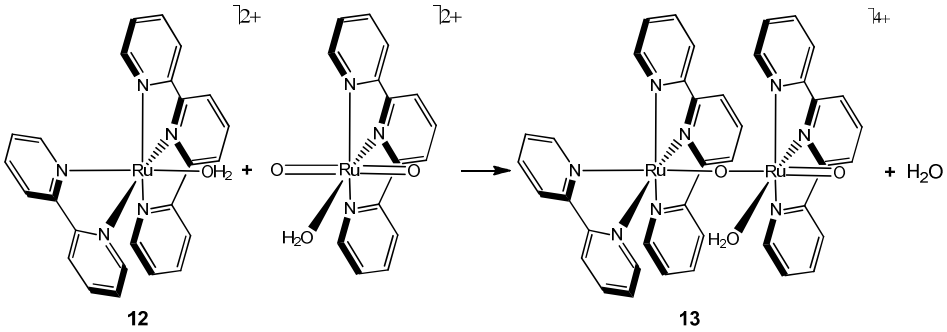

Figure 11. Formation of complex **13**.

1.2.1.3 Supported complexes

As is well known, homogenous and heterogeneous catalysis present different advantages. On the one hand homogenous catalysis shows high selectivity and reaction rates, and allows for fine tuning of the catalyst properties. On the other hand heterogeneous catalysis grants for easier separation of the products and recycle of the catalyst. In order to get the advantages of both sides, a good strategy is that of attaching a molecular catalyst on conducting solid surfaces. Moreover, this strategy is a step further towards the development of a PEC, and it allows to get rid of the chemical oxidant to use an applied potential to achieve the oxidation state where the catalytic cycle starts.

Several approaches have been developed with this objective, hereby some examples are reported:

- Covalent bond. The complex presents a functional group that can react with the surface to form a covalent bond. Typical examples are phosphonate,[49] carboxylate[50] and sulfonate[40] moieties on the catalyst,

which can condense with the hydroxyl groups of a metal oxide support. Complex **14**, a functionalized analogue of **2** (Figure 12) have been anchored on different supports,[50] retaining its water oxidation activity. Similar complexes can show different activities depending on the position and orientation of the anchoring group.

A slightly different approach involves electrografting of diazonium salts on a glassy carbon electrode, yielding a new C-C bond between the catalyst and the (carbon based) surface.[51]

- Electropolymerization. A ligand of the complex is functionalized with a species that can generate a polymer (for example pyrrole or thiophene). The complex is then electropolymerized, forming a film on the surface. Complex **15,** a different analogue of **2** has been electropolymerized on vitreous carbon sponges and FTO electrodes, thanks to the pyrrolic rings on the modified trpy.[52]
- Electrostatic interaction. The anchoring is obtained through the interaction of the opposite charges between the complex and the support. Complex **16**, similar to the one previously referred, has been successfully anchored on a number of different support, in virtue of its pyridinium moieties.[53]
- Intermolecular forces. The complex is anchored by means of intermolecular interactions as H-bond or π-π stacking. Complex **17**, a modified version of **10,** has been attached on multiwalled nanotubes previously coated on an ITO glass electrode, thanks to the pyrene moieties of the ligand.[54]

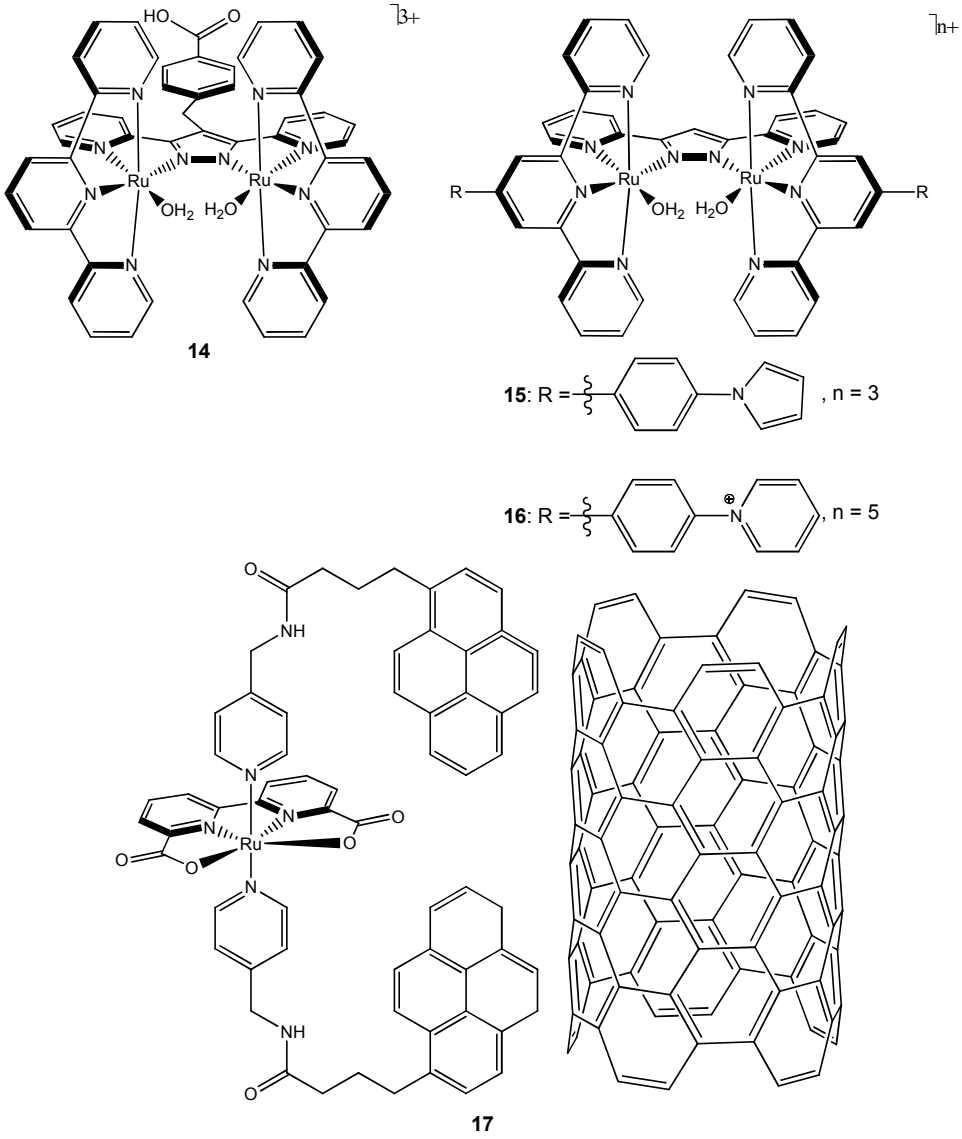

Figure 12. Supported molecular catalysts.

1.2.2 Other redox active metals catalysts

Although in water oxidation the chemistry of ruthenium complexes is the most extensive studied, other metals have recently gained importance in this field, due to their higher abundance and/or their high reactivity.

1.2.2.1 Cobalt

In 2011 Berlinguette et al.[45b] reported the first example of a molecular single-site cobalt WOC, using the pentadentate 2,6-(bis(bis-2-pyridyl)methoxy-methane)-pyridine ligand, **18**. The complex showed electrochemical water oxidation via a PCET mechanism, but homogeneity concerns were raised. Subsequent studies highlighted how small quantities, as low as 1-2%, of free Co(II) oxides can catalyze water oxidation. [55]

In order to avoid the formation of oxides, corrole[56] and porphyrine[57] based complexes were synthetized and successfully tested for electrochemical and photochemical[58] water oxidation.

Llobet et al.[59] reported a dinuclear μ-peroxo bridge complex based on the bpp^- ligand, **19**. The electrochemical characterization showed activity at low pH, without formation of nanoparticles.

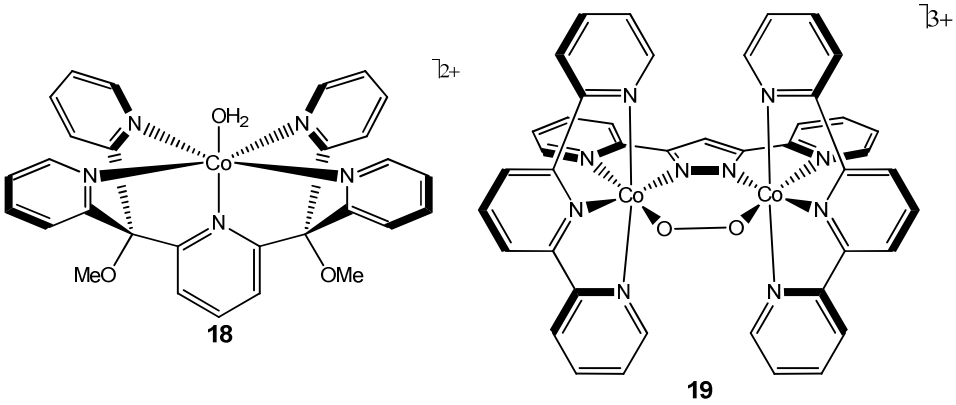

Figure 13. Cobalt molecular catalysts.

1.2.2.2 Iridium

Although not considered as an earth abundant element, iridium has also gained popularity in the field over the last years. The first iridium molecular catalysts for water oxidation were published in 2008 by Bernhard et al.[60] These cyclometalated complexes take advantage of the strong carbon-iridium bond to afford the robustness necessary to catalyze the reaction with CAN.

Different approaches see the use of cyclopentadiene-type,[45a, 61] carbene[62] and mesoionic carbene[63] ligands. However the oxidation of the ligands in the early stage of the catalysis has been demonstrated,[64] indicating that the initial complex is a precursor for the real catalyst,[45a] which nature most of the times remains unknown.

In addition these iridium based catalysts have the tendency to decompose to iridium oxides, in form of nanoparticles[65] or deposited films,[66] which are known to be good water oxidation catalysts.[67] The molecular nature of the

active species in iridium catalyzed systems is therefore not always straightforward.

1.2.2.3 Manganese

Its use by nature in PSII, rich redox chemistry, earth abundance and low cost made manganese popular in the pursuit of efficient WOCs.

A dimeric complex was first developed by Crabtree at al.,[68] which showed to promote chemically driven water oxidation. Labelled water experiments with different oxo-transfer oxidants[68b, 69] indicated a mixed origin of the oxygen atom incorporated in the evolved gas. Various other complexes with higher[70] or lower[71] nuclearity were also developed, but they showed to share the same oxo-transfer problem.

Biomimetically inspired ligands containing imidazole and carboxylate ligands allowed Akermark et al.[72] to develop complexes capable of achieve high oxidation states at lower potential. These complexes are thus more oxidatively rugged and compatible with non oxo-transfer oxidants, like $[Ru(bpy)_3]^{3+}$. However, the nature of the active species during the catalytic cycle still remains under debate.

1.2.2.4 Iron

In the last years, iron based WOCs were reported.[73] Lau et al.[74] tested a number of these, showing how the isolated compound was not the active catalyst, which turned out to be iron nanoparticles, influenced in the formation by the ligands of the starting complexes. Similar behavior have been observed also by Llobet and Nam.[75]

Iron is anyway an appealing alternative to more expensive and scarce metals, and is thus still the object of research, focused on more oxidatively rugged ligands.[76]

1.2.2.5 Copper

Copper is a relatively new actor in this research area. In 2012 Mayer et al.[77] reported the first electrochemical homogeneous copper WOC, a bipyridine dimer. Subsequently Meyer et al.[78] showed how simple salts were also electrocatalytically active, and reported the formation, over long term electrolysis, of a film on the electrode surface, active towards water oxidation.

Meyer[45c] also reported a triglycylglycine complex able of electrocatalytically oxidize water, maintaining its molecular structure. Llobet et al.[79] recently described a family of very stable copper complexes, containing a redox non-innocent ligand, and illustrated how the fine tuning of the latter could lower the potential for water oxidation by more than 500 mV, at basic pH.

1.2.3 Polyoxometalates

As illustrated in the previous sections, one of the main drawbacks of most of the reported WOCs is the degradation of the ligand in the oxidative conditions necessary for water oxidation catalysis. Under this premise, use of polyoxometalates (POMs), containing all-inorganic ligands, constitute a valid alternative to organic-ligand based WOC.

POMs are polyanionic molecular oxo-clusters of early transition metals (V, Nb, Ta, Mo, and W). The metals are usually in their higher oxidation state, making POMs oxidatively inert. While their synthesis is relatively

straightforward, it's possible to modulate and tune the properties of the obtained POMs by control of the reaction conditions (concentration, pH, temperature, nature of anions, heteroatoms or solvent, etc.).

In recent years, POMs based on manganese,[80] molybdenum,[81] iridium[82] and nickel[83] have been reported as active WOCs, but the most extensive studies have been performed on ruthenium and cobalt based WOCs. In the following paragraphs, some of the most notable examples are reported.

In 2004 Shannon et al.[84] reported a dinuclear ruthenium based POM, the first able to mediate water oxidation. Interestingly, the mononuclear analogue was not active. Later, Bonchio et al.[85] reported the tetranuclear ruthenium POM **17** able to perform water oxidation using CAN as sacrificial oxidant in acidic pH. Hill et al.[86] independently reported the same POM as active in neutral conditions with $[Ru(bpy)_3]^{3+}$. The WOC underwent extensively photocatalytic,[87] computational [88] and mechanistic studies,[89] and was successfully anchored on TiO_2[90] and multiwalled carbon nanotubes, [91] via electrostatic interaction.

In 2010 Hill at al.[92] reported the cobalt based POM **18**, able to perform water oxidation. However, as for some organic-based cobalt WOCs, the homogeneous nature of the catalyst has been questioned,[55a, 93] and the exact nature of the active species has been found to strongly depend on the applied conditions.[94]

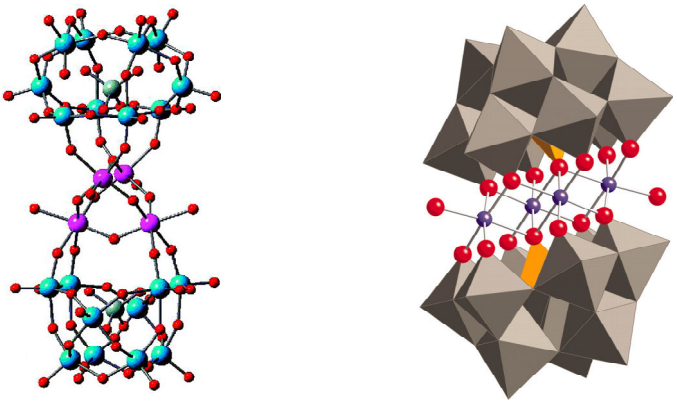

17 18

Figure 13. Polyoxometalate WOCs. Images taken from the original references

1.2.4 Use of redox inactive metals

As the OEC in PSII contains a calcium atom, which is a non redox active Lewis acid, increasing interest has been growing around the effect of Lewis acids on the properties of water oxidation catalysts.

For this purpose mixed metal complexes of Fe and Ca[95] or Sc[96], Mn and Zn[97] or Sc,[98] Co and Sc[99], all bounded through high valence M=O moieties, have been characterized. Electrochemical analyses generally agree that the coordination of Lewis acids lowers the redox potential of the metals, enhancing the ET rates to the point that, for example, oxidations of thyoanisoles pass from direct oxygen atom transfer to an electron-transfer-oxygen-transfer mechanism.[98b, 100]

Further insight were obtained by Nam et al.[101] by comparing the effects of several Lewis acids on the oxygen release of an in situ generated $[(TMC)Fe^{III}(\mu,\eta^2{:}\eta^2\text{-}O_2)]^{+}$–$M^{n+}$ (TMC, 1,4,8,11-tetramethyl-1,4,8,11-

tetraazacyclotetradecane, M^{n+} = Ca^{2+}, Sr^{2+}, Zn^{2+}, Lu^{3+},Sc^{3+} or Y^{3+}), **19**, when CAN was added. The results illustrate how strong Lewis acids, like zinc or scandium, interfere with the oxygen release, while mild Lewis acids like calcium or strontium do not interfere.

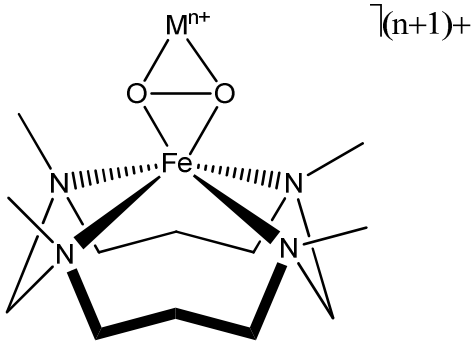

19

Figure 14. Redox inactive metal containing complex

1.3 References

(1) Edenhofer, O., R. Pichs-Madruga, Y. Sokona, E. Farahani, S. Kadner, K. Seyboth, A. Adler, I. Baum, S. Brunner, P. Eickemeier, B. Kriemann, J. Savolainen, S. Schlömer, C. von Stechow, T. Zwickel and J.C. Minx (eds.) *IPCC: Climate Change 2014: Mitigation of Climate Change. Contribution of Working Group III to the Fifth Assessment Report of the Intergovernmental Panel on Climate Change.*; Cambridge University Press: Cabridge, UK, 2014.

(2) Styring, S. *Faraday Discuss.* **2012,** *155*, 357-376.

(3) Branker, K.; Pathak, M. J. M.; Pearce, J. M. *Renew. Sust. Energ. Rev.* **2011,** *15*, 4470-4482.

(4) Romain, S.; Vigara, L.; Llobet, A. *Acc. Chem. Res.* **2009,** *42*, 1944-1953.

(5) Karlsson, S.; Boixel, J.; Pellegrin, Y.; Blart, E.; Becker, H.-C.; Odobel, F.; Hammarstrom, L. *Faraday Discuss.* **2012,** *155*, 233-252.

(6) a) Ferreira, K. N.; Iverson, T. M.; Maghlaoui, K.; Barber, J.; Iwata, S. *Science* **2004,** *303*, 1831-1838; b) Guskov, A.; Kern, J.; Gabdulkhakov, A.; Broser, M.; Zouni, A.; Saenger, W. *Nat. Struct. Mol. Biol.* **2009,** *16*, 334-342; c) Loll, B.; Kern, J.; Saenger, W.; Zouni, A.; Biesiadka, J. *Nature* **2005,** *438*, 1040-1044.

(7) Umena, Y.; Kawakami, K.; Shen, J.-R.; Kamiya, N. *Nature* **2011,** *473*, 55-60.

(8) V. L. Pecoraro, M. J. B., M. T. Caudle, W.-Y. Hsieh, N. A. Law *Pure Appl. Chem.* **1998,** *70*, 925-929.

(9) a) Dau, H.; Limberg, C.; Reier, T.; Risch, M.; Roggan, S.; Strasser, P. *ChemCatChem* **2010,** *2*, 724-761; b) McEvoy, J. P.; Brudvig, G. W. *Chem. Rev.* **2006,** *106*, 4455-4483; c) McEvoy, J. P.; Gascon, J. A.; Batista, V. S.; Brudvig, G. W. *Photochem. Photobiol. Sci.* **2005,** *4*, 940-949; d) Vrettos, J. S.; Limburg, J.; Brudvig, G. W. *Biochim. Biophys. Acta* **2001,** *1503*, 229-245.

(10) a) Barber, J.; Ferreira, K.; Maghlaoui, K.; Iwata, S. *Phys. Chem. Chem. Phys.* **2004,** *6*, 4737-4742; b) Messinger, J.; Badger, M.; Wydrzynski, T. *Proc. Natl. Acad. Sci. U.S.A.* **1995,** *92*, 3209-3213; c) Sproviero, E. M.; Gascón, J. A.; McEvoy, J. P.; Brudvig, G. W.; Batista, V. S. *J. Am. Chem. Soc.* **2008,** *130*, 3428-3442; d) Kusunoki, M. *Biochim. Biophys. Acta* **2007,** *1767*, 484-492; e) Kusunoki, M. *Biochim. Biophys. Acta* **2008,** *1777*, 477; f) Dau, H.; Haumann, M. *Biochim. Biophys. Acta* **2007,** *1767*, 472-483.

(11) a) Dau, H.; Iuzzolino, L.; Dittmer, J. *Biochim. Biophys. Acta* **2001,** *1503*, 24-39; b) Hillier, W.; Wydrzynski, T. *Biochim. Biophys. Acta* **2001,** *1503*, 197-209.

(12) a) Siegbahn, P. E. M. *Acc. Chem. Res.* **2009,** *42*, 1871-1880; b) Ruettinger, W.; Yagi, M.; Wolf, K.; Bernasek, S.; Dismukes, G. C. *J. Am. Chem. Soc.* **2000,** *122*, 10353-10357; c) Yachandra, V. K.; Sauer, K.; Klein, M. P. *Chem. Rev.* **1996,** *96*, 2927-2950.

(13) Wiechen, M.; Najafpour, M. M.; Allakhverdiev, S. I.; Spiccia, L. *Energy Environ. Sci.* **2014,** *7*, 2203-2212.

(14) a) Boussac, A.; Rutherford, A. W. *Biochemistry* **1988,** *27*, 3476-3483; b) Boussac, A.; Zimmermann, J.-L.; Rutherford, A. W. *FEBS Lett. 277*, 69-74; c) Boussac, A.; Zimmermann, J. L.; Rutherford, A. W. *Biochemistry* **1989,** *28*, 8984-8989; d) Ghanotakis, D. F.; Babcock, G. T.; Yocum, C. F. *FEBS Lett. 167*, 127-130; e) Miyao, M.; Murata, N. *FEBS Lett. 168*, 118-120; f) Ono, T.-a.; Inoue, Y. *FEBS Lett. 227*, 147-152.

(15) Boussac, A.; Rappaport, F.; Carrier, P.; Verbavatz, J.-M.; Gobin, R.; Kirilovsky, D.; Rutherford, A. W.; Sugiura, M. *J. Biol. Chem.* **2004,** *279*, 22809-22819.

(16) a) Sala, X.; Romero, I.; Rodríguez, M.; Escriche, L.; Llobet, A. *Angew. Chem. Int. Ed.* **2009,** *48*, 2842-2852; b) Herrero, C.; Lassalle-Kaiser, B.; Leibl, W.;

Rutherford, A. W.; Aukauloo, A. *Coord. Chem. Rev.* **2008,** *252*, 456-468; c) McConnell, I.; Li, G.; Brudvig, G. W. *Chem. Biol.* **2010,** *17*, 434-447; d) Sanderson, K. *Nature* **2008,** *452*, 400.

(17) Nocera, D. G. *Acc. Chem. Res.* **2012,** *45*, 767-776.

(18) Parent, A. R.; Crabtree, R. H.; Brudvig, G. W. *Chem. Soc. Rev.* **2013,** *42*, 2247-2252.

(19) a) Whittall, I. R.; McDonagh, A. M.; Humphrey, M. G.; Samoc, M., Organometallic Complexes in Nonlinear Optics I: Second-Order Nonlinearities. in *Advances in Organometallic Chemistry*, Stone, F. G. A.; Robert, W., Eds. Academic Press: 1998; b) Ian R, W.; Andrew M, M.; Mark G, H.; Samoc, M., Organometallic Complexes in Nonlinear Optics II: Third-Order Nonlinearities and Optical Limiting Studies. in *Advances in Organometallic Chemistry*, Robert, W.; Anthony, F. H., Eds. Academic Press: 1999; c) Coe, B. J. *Acc. Chem. Res.* **2006,** *39*, 383-393; d) Green, K. A.; Cifuentes, M. P.; Corkery, T. C.; Samoc, M.; Humphrey, M. G. *Angew. Chem. Int. Ed.* **2009,** *48*, 7867-7870; e) Zhao, G.-J.; Han, K.-L. *Acc. Chem. Res.* **2011,** *45*, 404-413.

(20) a) Hudson, S. A.; Maitlis, P. M. *Chem. Rev.* **1993,** *93*, 861-885; b) Aquino, M. A. S. *Coord. Chem. Rev.* **1998,** *170*, 141-202.

(21) a) Larionova, J.; Mombelli, B.; Sanchiz, J.; Kahn, O. *Inorg. Chem.* **1998,** *37*, 679-684; b) Desplanches, C.; Ruiz, E.; Alvarez, S. *Eur. J. Inorg. Chem.* **2003,** *2003*, 1756-1760; c) Mikuriya, M.; Yoshioka, D.; Handa, M. *Coord. Chem. Rev.* **2006,** *250*, 2194-2211.

(22) Fillaut, J.-L.; Andriès, J.; Marwaha, R. D.; Lanoë, P.-H.; Lohio, O.; Toupet, L.; Gareth Williams, J. A. *J. Organomet. Chem.* **2008,** *693*, 228-234.

(23) a) Bergamo, A.; Sava, G. *Dalton Trans.* **2007**, 1267-1272; b) Groessl, M.; Reisner, E.; Hartinger, C. G.; Eichinger, R.; Semenova, O.; Timerbaev, A. R.; Jakupec, M. A.; Arion, V. B.; Keppler, B. K. *J. Med. Chem.* **2007,** *50*, 2185-2193.

(24) a) Ishizuka, T.; Ohzu, S.; Kojima, T. *Synlett* **2014,** *25*, 1667-1679; b) Farràs, P.; Benniston, A. C. *Tetrahedron Lett.* **2014,** *55*, 7011-7014; c) Li, F.; Yu, M.; Jiang, Y.; Huang, F.; Li, Y.; Zhang, B.; Sun, L. *Chem. Commun.* **2011,** *47*, 8949-8951.

(25) a) Bagh, B.; McKinty, A. M.; Lough, A. J.; Stephan, D. W. *Dalton Trans.* **2015,** *44*, 2712-2723; b) Wang, W.-W.; Li, Z.-M.; Su, L.; Wang, Q.-R.; Wu, Y.-L. *J. Mol. Catal. A: Chem.* **2014,** *387*, 92-102; c) Zirakzadeh, A.; Schuecker, R.; Gorgas, N.; Mereiter, K.; Spindler, F.; Weissensteiner, W. *Organometallics* **2012,** *31*, 4241-4250.

(26) a) Dhuri, S. N.; Lee, Y.-M.; Seo, M. S.; Cho, J.; Narulkar, D. D.; Fukuzumi, S.; Nam, W. *Dalton Trans.* **2015,** *44*, 7634-7642; b) Ishizuka, T.; Ohzu, S.; Kotani, H.; Shiota, Y.; Yoshizawa, K.; Kojima, T. *Chem. Sci.* **2014,** *5*, 1429-1436; c) Guo, Z.; Guan, X.; Huang, J.-S.; Tsui, W.-M.; Lin, Z.; Che, C.-M. *Chem. Eur. J.* **2013,** *19*, 11320-11331.

(27) a) Zuo, Z.; Yang, X.; Liu, J.; Nan, J.; Bai, L.; Wang, Y.; Luan, X. *J Org. Chem.* **2015,** *80*, 3349-3356; b) Ruiz, S.; Villuendas, P.; Ortuño, M. A.; Lledós, A.; Urriolabeitia, E. P. *Chem. Eur. J.* **2015,** *21*, 8626-8636; c) Ackermann, L. *Acc. Chem. Res.* **2014,** *47*, 281-295.

(28) a) Manzini, S.; Urbina Blanco, C. A.; Nelson, D. J.; Poater, A.; Lebl, T.; Meiries, S.; Slawin, A. M. Z.; Falivene, L.; Cavallo, L.; Nolan, S. P. *J. Organomet. Chem.* **2015,** *780*, 43-48; b) Baraut, J.; Massard, A.; Chotard, F.; Bodio, E.; Picquet, M.; Richard, P.; Borguet, Y.; Nicks, F.; Demonceau, A.; Le Gendre, P. *Eur. J. Inorg. Chem.* **2015,** *2015*, 2671-2682; c) de O. Romera, C.; Cardoso, P. B.; Meier, M. A. R.; Sayer, C.; Araújo, P. H. H. *Eur. J. Lipid Sci. Technol.* **2015,** *117*, 235-241.

(29) Meyer, T. J.; Huynh, M. H. V. *Inorg. Chem.* **2003,** *42*, 8140-8160.

(30) a) Meyer, T. J. *J. Electrochem. Soc.* **1984,** *131*, 221C-228C; b) Masllorens, E.; Rodríguez, M.; Romero, I.; Roglans, A.; Parella, T.; Benet-Buchholz, J.; Poyatos, M.; Llobet, A. *J. Am. Chem. Soc.* **2006,** *128*, 5306-5307.

(31) a) Moyer, B. A.; Meyer, T. J. *J. Am. Chem. Soc.* **1978,** *100*, 3601-3603; b) Moyer, B. A.; Meyer, T. J. *Inorg. Chem.* **1981,** *20*, 436-444.

(32) Dovletoglou, A.; Adeyemi, S. A.; Meyer, T. J. *Inorg. Chem.* **1996,** *35*, 4120-4127.

(33) a) Gilbert, J. A.; Eggleston, D. S.; Murphy, W. R.; Geselowitz, D. A.; Gersten, S. W.; Hodgson, D. J.; Meyer, T. J. *J. Am. Chem. Soc.* **1985,** *107*, 3855-3864; b) Gersten, S. W.; Samuels, G. J.; Meyer, T. J. *J. Am. Chem. Soc.* **1982,** *104*, 4029-4030.

(34) Lebeau, E. L.; Adeyemi, S. A.; Meyer, T. J. *Inorg. Chem.* **1998,** *37*, 6476-6484.

(35) Hurst, J. K. *Coord. Chem. Rev.* **2005,** *249*, 313-328.

(36) a) Liu, F.; Concepcion, J. J.; Jurss, J. W.; Cardolaccia, T.; Templeton, J. L.; Meyer, T. J. *Inorg. Chem.* **2008,** *47*, 1727-1752; b) Binstead, R. A.; Chronister, C. W.; Ni, J.; Hartshorn, C. M.; Meyer, T. J. *J. Am. Chem. Soc.* **2000,** *122*, 8464-8473.

(37) Sens, C.; Romero, I.; Rodríguez, M.; Llobet, A.; Parella, T.; Benet-Buchholz, J. *J. Am. Chem. Soc.* **2004,** *126*, 7798-7799.

(38) a) Bozoglian, F.; Romain, S.; Ertem, M. Z.; Todorova, T. K.; Sens, C.; Mola, J.; Rodríguez, M.; Romero, I.; Benet-Buchholz, J.; Fontrodona, X.; Cramer, C. J.; Gagliardi, L.; Llobet, A. *J. Am. Chem. Soc.* **2009,** *131*, 15176-15187; b) Romain, S.; Bozoglian, F.; Sala, X.; Llobet, A. *J. Am. Chem. Soc.* **2009,** *131*, 2768-2769.

(39) a) Zong, R.; Thummel, R. P. *J. Am. Chem. Soc.* **2005,** *127*, 12802-12803; b) Wada, T.; Tsuge, K.; Tanaka, K. *Inorg. Chem.* **2001,** *40*, 329-337; c)

Wasylenko, D. J.; Ganesamoorthy, C.; Koivisto, B. D.; Berlinguette, C. P. *Eur. J. Inorg. Chem.* **2010,** *2010*, 3135-3142.

(40) Neudeck, S.; Maji, S.; López, I.; Meyer, S.; Meyer, F.; Llobet, A. *J. Am. Chem. Soc.* **2013,** *136*, 24-27.

(41) Sander, A. C.; Maji, S.; Francàs, L.; Böhnisch, T.; Dechert, S.; Llobet, A.; Meyer, F. *ChemSusChem* **2015,** *8*, 1697-1702.

(42) Tseng, H.-W.; Zong, R.; Muckerman, J. T.; Thummel, R. *Inorg. Chem.* **2008,** *47*, 11763-11773.

(43) a) Concepcion, J. J.; Jurss, J. W.; Templeton, J. L.; Meyer, T. J. *J. Am. Chem. Soc.* **2008,** *130*, 16462-16463; b) Concepcion, J. J.; Tsai, M.-K.; Muckerman, J. T.; Meyer, T. J. *J. Am. Chem. Soc.* **2010,** *132*, 1545-1557; c) Chen, Z.; Concepcion, J. J.; Luo, H.; Hull, J. F.; Paul, A.; Meyer, T. J. *J. Am. Chem. Soc.* **2010,** *132*, 17670-17673.

(44) Murakami, M.; Hong, D.; Suenobu, T.; Yamaguchi, S.; Ogura, T.; Fukuzumi, S. *J. Am. Chem. Soc.* **2011,** *133*, 11605-11613.

(45) a) Blakemore, J. D.; Schley, N. D.; Balcells, D.; Hull, J. F.; Olack, G. W.; Incarvito, C. D.; Eisenstein, O.; Brudvig, G. W.; Crabtree, R. H. *J. Am. Chem. Soc.* **2010,** *132*, 16017-16029; b) Wasylenko, D. J.; Ganesamoorthy, C.; Borau-Garcia, J.; Berlinguette, C. P. *Chem. Commun.* **2011,** *47*, 4249-4251; c) Zhang, M.-T.; Chen, Z.; Kang, P.; Meyer, T. J. *J. Am. Chem. Soc.* **2013,** *135*, 2048-2051.

(46) Roeser, S.; Farràs, P.; Bozoglian, F.; Martínez-Belmonte, M.; Benet-Buchholz, J.; Llobet, A. *ChemSusChem* **2011,** *4*, 197-207.

(47) a) Duan, L.; Bozoglian, F.; Mandal, S.; Stewart, B.; Privalov, T.; Llobet, A.; Sun, L. *Nat. Chem.* **2012,** *4*, 418-423; b) Richmond, C. J.; Matheu, R.; Poater, A.; Falivene, L.; Benet-Buchholz, J.; Sala, X.; Cavallo, L.; Llobet, A. *Chem. Eur. J.* **2014,** *20*, 17282-17286.

(48) López, I.; Ertem, M. Z.; Maji, S.; Benet-Buchholz, J.; Keidel, A.; Kuhlmann, U.; Hildebrandt, P.; Cramer, C. J.; Batista, V. S.; Llobet, A. *Angew. Chem. Int. Ed.* **2014,** *53*, 205-209.

(49) Liu, F.; Cardolaccia, T.; Hornstein, B. J.; Schoonover, J. R.; Meyer, T. J. *J. Am. Chem. Soc.* **2007,** *129*, 2446-2447.

(50) Francàs, L.; Sala, X.; Benet-Buchholz, J.; Escriche, L.; Llobet, A. *ChemSusChem* **2009,** *2*, 321-329.

(51) Matheu, R.; Francàs, L.; Chernev, P.; Ertem, M. Z.; Batista, V.; Haumann, M.; Sala, X.; Llobet, A. *ACS Catal.* **2015,** *5*, 3422-3429.

(52) Mola, J.; Mas-Marza, E.; Sala, X.; Romero, I.; Rodríguez, M.; Viñas, C.; Parella, T.; Llobet, A. *Angew. Chem. Int. Ed.* **2008,** *47*, 5830-5832.

(53) Aguilo, J.; Francas, L.; Liu, H. J.; Bofill, R.; Garcia-Anton, J.; Benet-Buchholz, J.; Llobet, A.; Escriche, L.; Sala, X. *Catal. Sci. Technol.* **2014,** *4*, 190-199.

(54) Li, F.; Zhang, B.; Li, X.; Jiang, Y.; Chen, L.; Li, Y.; Sun, L. *Angew. Chem. Int. Ed.* **2011,** *50*, 12276-12279.

(55) a) Stracke, J. J.; Finke, R. G. *J. Am. Chem. Soc.* **2011,** *133*, 14872-14875; b) Wasylenko, D. J.; Palmer, R. D.; Schott, E.; Berlinguette, C. P. *Chem. Commun.* **2012,** *48*, 2107-2109.

(56) a) McGuire Jr, R.; Dogutan, D. K.; Teets, T. S.; Suntivich, J.; Shao-Horn, Y.; Nocera, D. G. *Chem. Sci.* **2010,** *1*, 411-414; b) Lei, H.; Han, A.; Li, F.; Zhang, M.; Han, Y.; Du, P.; Lai, W.; Cao, R. *Phys. Chem. Chem. Phys.* **2014,** *16*, 1883-1893.

(57) Wang, D.; Groves, J. T. *Proc. Natl. Acad. Sci. U.S.A.* **2013,** *110*, 15579-15584.

(58) Nakazono, T.; Parent, A. R.; Sakai, K. *Chem. Commun.* **2013,** *49*, 6325-6327.

(59) Rigsby, M. L.; Mandal, S.; Nam, W.; Spencer, L. C.; Llobet, A.; Stahl, S. S. *Chem. Sci.* **2012,** *3*, 3058-3062.

(60) McDaniel, N. D.; Coughlin, F. J.; Tinker, L. L.; Bernhard, S. *J. Am. Chem. Soc.* **2008,** *130*, 210-217.

(61) Hull, J. F.; Balcells, D.; Blakemore, J. D.; Incarvito, C. D.; Eisenstein, O.; Brudvig, G. W.; Crabtree, R. H. *J. Am. Chem. Soc.* **2009,** *131*, 8730-8731.

(62) a) Brewster, T. P.; Blakemore, J. D.; Schley, N. D.; Incarvito, C. D.; Hazari, N.; Brudvig, G. W.; Crabtree, R. H. *Organometallics* **2011,** *30*, 965-973; b) Hetterscheid, D. G. H.; Reek, J. N. H. *Chem. Commun.* **2011,** *47*, 2712-2714; c) Volpe, A.; Sartorel, A.; Tubaro, C.; Meneghini, L.; Di Valentin, M.; Graiff, C.; Bonchio, M. *Eur. J. Inorg. Chem.* **2014,** *2014*, 665-675.

(63) a) Lalrempuia, R.; McDaniel, N. D.; Müller-Bunz, H.; Bernhard, S.; Albrecht, M. *Angew. Chem. Int. Ed.* **2010,** *49*, 9765-9768; b) Hetterscheid, D. G. H.; van der Vlugt, J. I.; de Bruin, B.; Reek, J. N. H. *Angew. Chem. Int. Ed.* **2009,** *48*, 8178-8181.

(64) Savini, A.; Belanzoni, P.; Bellachioma, G.; Zuccaccia, C.; Zuccaccia, D.; Macchioni, A. *Green Chem.* **2011,** *13*, 3360-3374.

(65) a) Grotjahn, D. B.; Brown, D. B.; Martin, J. K.; Marelius, D. C.; Abadjian, M.-C.; Tran, H. N.; Kalyuzhny, G.; Vecchio, K. S.; Specht, Z. G.; Cortes-Llamas, S. A.; Miranda-Soto, V.; van Niekerk, C.; Moore, C. E.; Rheingold, A. L. *J. Am. Chem. Soc.* **2011,** *133*, 19024-19027; b) Wöhler, L.; Witzmann, W. *Z. Anorg. Allg. Chem.* **1908,** *57*, 323-352.

(66) Blakemore, J. D.; Schley, N. D.; Olack, G. W.; Incarvito, C. D.; Brudvig, G. W.; Crabtree, R. H. *Chem. Sci.* **2011,** *2*, 94-98.

(67) a) Harriman, A.; Pickering, I. J.; Thomas, J. M.; Christensen, P. A. *J. Chem. Soc. Faraday Trans. 1* **1988,** *84*, 2795-2806; b) Nahor, G. S.; Hapiot, P.; Neta, P.; Harriman, A. *J. Phys. Chem.* **1991,** *95*, 616-621; c) Hara, M.; Waraksa,

C. C.; Lean, J. T.; Lewis, B. A.; Mallouk, T. E. *J. Phys. Chem. A* **2000,** *104*, 5275-5280.

(68) a) Limburg, J.; Vrettos, J. S.; Liable-Sands, L. M.; Rheingold, A. L.; Crabtree, R. H.; Brudvig, G. W. *Science* **1999,** *283*, 1524-1527; b) Limburg, J.; Vrettos, J. S.; Chen, H.; de Paula, J. C.; Crabtree, R. H.; Brudvig, G. W. *J. Am. Chem. Soc.* **2001,** *123*, 423-430; c) Cady, C. W.; Shinopoulos, K. E.; Crabtree, R. H.; Brudvig, G. W. *Dalton Trans.* **2010,** *39*, 3985-3989; d) Chen, H.; Tagore, R.; Das, S.; Incarvito, C.; Faller, J. W.; Crabtree, R. H.; Brudvig, G. W. *Inorg. Chem.* **2005,** *44*, 7661-7670.

(69) Chen; Tagore, R.; Olack, G.; Vrettos, J. S.; Weng, T.-C.; Penner-Hahn, J.; Crabtree, R. H.; Brudvig, G. W. *Inorg. Chem.* **2007,** *46*, 34-43.

(70) a) Kurz, P.; Berggren, G.; Anderlund, M. F.; Styring, S. *Dalton Trans.* **2007**, 4258-4261; b) Berggren, G.; Thapper, A.; Huang, P.; Kurz, P.; Eriksson, L.; Styring, S.; Anderlund, M. F. *Dalton Trans.* **2009**, 10044-10054; c) Berggren, G.; Thapper, A.; Huang, P.; Eriksson, L.; Styring, S.; Anderlund, M. F. *Inorg. Chem.* **2011,** *50*, 3425-3430.

(71) Young, K. J.; Takase, M. K.; Brudvig, G. W. *Inorg. Chem.* **2013,** *52*, 7615-7622.

(72) Karlsson, E. A.; Lee, B.-L.; Åkermark, T.; Johnston, E. V.; Kärkäs, M. D.; Sun, J.; Hansson, Ö.; Bäckvall, J.-E.; Åkermark, B. *Angew. Chem. Int. Ed.* **2011,** *50*, 11715-11718.

(73) a) Ellis, W. C.; McDaniel, N. D.; Bernhard, S.; Collins, T. J. *J. Am. Chem. Soc.* **2010,** *132*, 10990-10991; b) Ertem, M. Z.; Gagliardi, L.; Cramer, C. J. *Chem. Sci.* **2012,** *3*, 1293-1299; c) Liao, R.-Z.; Li, X.-C.; Siegbahn, P. E. M. *Eur. J. Inorg. Chem.* **2014,** *2014*, 728-741; d) Fillol, J. L.; Codolà, Z.; Garcia-Bosch, I.; Gómez, L.; Pla, J. J.; Costas, M. *Nat. Chem.* **2011,** *3*, 807-813.

(74) Chen, G.; Chen, L.; Ng, S.-M.; Man, W.-L.; Lau, T.-C. *Angew. Chem. Int. Ed.* **2013,** *52*, 1789-1791.

(75) Hong, D.; Mandal, S.; Yamada, Y.; Lee, Y.-M.; Nam, W.; Llobet, A.; Fukuzumi, S. *Inorg. Chem.* **2013,** *52*, 9522-9531.

(76) a) Coggins, M. K.; Zhang, M.-T.; Vannucci, A. K.; Dares, C. J.; Meyer, T. J. *J. Am. Chem. Soc.* **2014,** *136*, 5531-5534; b) Hoffert, W. A.; Mock, M. T.; Appel, A. M.; Yang, J. Y. *Eur. J. Inorg. Chem.* **2013,** *2013*, 3846-3857.

(77) Barnett, S. M.; Goldberg, K. I.; Mayer, J. M. *Nat. Chem.* **2012,** *4*, 498-502.

(78) Chen, Z.; Meyer, T. J. *Angew. Chem. Int. Ed.* **2013,** *52*, 700-703.

(79) Garrido-Barros, P.; Funes-Ardoiz, I.; Drouet, S.; Benet-Buchholz, J.; Maseras, F.; Llobet, A. *J. Am. Chem. Soc.* **2015,** *137*, 6758-6761.

(80) a) Bassil, B. S.; Ibrahim, M.; Al-Oweini, R.; Asano, M.; Wang, Z.; van Tol, J.; Dalal, N. S.; Choi, K.-Y.; Ngo Biboum, R.; Keita, B.; Nadjo, L.; Kortz, U. *Angew. Chem. Int. Ed.* **2011,** *50*, 5961-5964; b) Al-Oweini, R.; Bassil, B. S.; Palden, T.; Keita, B.; Lan, Y.; Powell, A. K.; Kortz, U. *Polyhedron* **2013,** *52*, 461-466.

(81) Gao, J.; Cao, S.; Tay, Q.; Liu, Y.; Yu, L.; Ye, K.; Mun, P. C. S.; Li, Y.; Rakesh, G.; Loo, S. C. J.; Chen, Z.; Zhao, Y.; Xue, C.; Zhang, Q. *Sci. Rep.* **2013,** *3*.

(82) Cao, R.; Ma, H.; Geletii, Y. V.; Hardcastle, K. I.; Hill, C. L. *Inorg. Chem.* **2009,** *48*, 5596-5598.

(83) Zhu, G.; Glass, E. N.; Zhao, C.; Lv, H.; Vickers, J. W.; Geletii, Y. V.; Musaev, D. G.; Song, J.; Hill, C. L. *Dalton Trans.* **2012,** *41*, 13043-13049.

(84) Howells, A. R.; Sankarraj, A.; Shannon, C. *J. Am. Chem. Soc.* **2004,** *126*, 12258-12259.

(85) Sartorel, A.; Carraro, M.; Scorrano, G.; Zorzi, R. D.; Geremia, S.; McDaniel, N. D.; Bernhard, S.; Bonchio, M. *J. Am. Chem. Soc.* **2008,** *130*, 5006-5007.

(86) Geletii, Y. V.; Botar, B.; Kögerler, P.; Hillesheim, D. A.; Musaev, D. G.; Hill, C. L. *Angew. Chem. Int. Ed.* **2008,** *47*, 3896-3899.

(87) a) Geletii, Y. V.; Huang, Z.; Hou, Y.; Musaev, D. G.; Lian, T.; Hill, C. L. *J. Am. Chem. Soc.* **2009,** *131*, 7522-7523; b) Puntoriero, F.; La Ganga, G.; Sartorel, A.; Carraro, M.; Scorrano, G.; Bonchio, M.; Campagna, S. *Chem. Commun.* **2010,** *46*, 4725-4727.

(88) Piccinin, S.; Sartorel, A.; Aquilanti, G.; Goldoni, A.; Bonchio, M.; Fabris, S. *Proc. Natl. Acad. Sci. U.S.A.* **2013,** *110*, 4917-4922.

(89) a) Sartorel, A.; Miró, P.; Salvadori, E.; Romain, S.; Carraro, M.; Scorrano, G.; Valentin, M. D.; Llobet, A.; Bo, C.; Bonchio, M. *J. Am. Chem. Soc.* **2009,** *131*, 16051-16053; b) Geletii, Y. V.; Besson, C.; Hou, Y.; Yin, Q.; Musaev, D. G.; Quiñonero, D.; Cao, R.; Hardcastle, K. I.; Proust, A.; Kögerler, P.; Hill, C. L. *J. Am. Chem. Soc.* **2009,** *131*, 17360-17370; c) Liu, Y.; Guo, S.-X.; Bond, A. M.; Zhang, J.; Geletii, Y. V.; Hill, C. L. *Inorg. Chem.* **2013,** *52*, 11986-11996.

(90) Orlandi, M.; Argazzi, R.; Sartorel, A.; Carraro, M.; Scorrano, G.; Bonchio, M.; Scandola, F. *Chem. Commun.* **2010,** *46*, 3152-3154.

(91) Toma, F. M.; Sartorel, A.; Iurlo, M.; Carraro, M.; Parisse, P.; Maccato, C.; Rapino, S.; Gonzalez, B. R.; Amenitsch, H.; Da Ros, T.; Casalis, L.; Goldoni, A.; Marcaccio, M.; Scorrano, G.; Scoles, G.; Paolucci, F.; Prato, M.; Bonchio, M. *Nat. Chem.* **2010,** *2*, 826-831.

(92) Yin, Q.; Tan, J. M.; Besson, C.; Geletii, Y. V.; Musaev, D. G.; Kuznetsov, A. E.; Luo, Z.; Hardcastle, K. I.; Hill, C. L. *Science* **2010,** *328*, 342-345.

(93) Natali, M.; Berardi, S.; Sartorel, A.; Bonchio, M.; Campagna, S.; Scandola, F. *Chem. Commun.* **2012,** *48*, 8808-8810.

(94) Stracke, J. J.; Finke, R. G. *ACS Catal.* **2013,** *3*, 1209-1219.

(95) Fukuzumi, S.; Morimoto, Y.; Kotani, H.; Naumov, P.; Lee, Y.-M.; Nam, W. *Nat. Chem.* **2010,** *2*, 756-759.

(96) Morimoto, Y.; Kotani, H.; Park, J.; Lee, Y.-M.; Nam, W.; Fukuzumi, S. *J. Am. Chem. Soc.* **2011,** *133*, 403-405.

(97) Chen, J.; Lee, Y.-M.; Davis, K. M.; Wu, X.; Seo, M. S.; Cho, K.-B.; Yoon, H.; Park, Y. J.; Fukuzumi, S.; Pushkar, Y. N.; Nam, W. *J. Am. Chem. Soc.* **2013,** *135*, 6388-6391.

(98) a) Leeladee, P.; Baglia, R. A.; Prokop, K. A.; Latifi, R.; de Visser, S. P.; Goldberg, D. P. *J. Am. Chem. Soc.* **2012,** *134*, 10397-10400; b) Yoon, H.; Lee, Y.-M.; Wu, X.; Cho, K.-B.; Sarangi, R.; Nam, W.; Fukuzumi, S. *J. Am. Chem. Soc.* **2013,** *135*, 9186-9194.

(99) Pfaff, F. F.; Kundu, S.; Risch, M.; Pandian, S.; Heims, F.; Pryjomska-Ray, I.; Haack, P.; Metzinger, R.; Bill, E.; Dau, H.; Comba, P.; Ray, K. *Angew. Chem. Int. Ed.* **2011,** *50*, 1711-1715.

(100) Park, J.; Morimoto, Y.; Lee, Y.-M.; Nam, W.; Fukuzumi, S. *J. Am. Chem. Soc.* **2011,** *133*, 5236-5239.

(101) Bang, S.; Lee, Y.-M.; Hong, S.; Cho, K.-B.; Nishida, Y.; Seo, M. S.; Sarangi, R.; Fukuzumi, S.; Nam, W. *Nat. Chem.* **2014,** *6*, 934-940.

UNIVERSITAT ROVIRA I VIRGILI
MONONUCLEAR AND HETEROTRINUCLEAR RUTHENIUM COMPLEXES: SYNTHESIS AND WATER OXIDATION ACTIVITY.
Lorenzo Mognon
Dipòsit Legal: T 1359-2015

Chapter 2. Objectives

UNIVERSITAT ROVIRA I VIRGILI
MONONUCLEAR AND HETEROTRINUCLEAR RUTHENIUM COMPLEXES: SYNTHESIS AND WATER OXIDATION ACTIVITY.
Lorenzo Mognon
Dipòsit Legal: T 1359-2015

Chapter 2. Objectives

The general aim of this thesis is the synthesis and characterization of new ruthenium complexes suitable for water oxidation. The spectroscopic and electronic properties and the oxidative activity of the new compounds will be related to the structure and synthetic pathways, so to shine more light on the possibilities afforded by the fine tuning of this kind of complexes.

This general objective will be pursued through different approaches:

- Starting from previously described mononuclear ruthenium complexes, new heteromultinuclear complexes bearing a redox inactive zinc center will be synthetized, characterized and tested for stability and reactivity.
- Using the same previously described mononuclear complexes, new heteromultinuclear complexes containing a water oxidation active manganese or cobalt metal center will be synthesized and characterized. The effect of the presence of a further potential catalytic center on the mechanism will be investigated;
- A new ligand bearing versatile moieties will be employed for the synthesis of new ruthenium mononuclear complexes. The effects of electron withdrawing groups, acid base equilibriums and

II

hydrogen bonds on the electrochemical properties and oxidation reactivity will be discussed;

- Taking advantage of the previously mentioned ligand versatility, newly synthesized mononuclear ruthenium complexes will be anchored on metal oxide surfaces and tested for heterogeneous water oxidation.

UNIVERSITAT ROVIRA I VIRGILI
MONONUCLEAR AND HETEROTRINUCLEAR RUTHENIUM COMPLEXES: SYNTHESIS AND WATER OXIDATION ACTIVITY.
Lorenzo Mognon
Dipòsit Legal: T 1359-2015

UNIVERSITAT ROVIRA I VIRGILI
MONONUCLEAR AND HETEROTRINUCLEAR RUTHENIUM COMPLEXES: SYNTHESIS AND WATER OXIDATION ACTIVITY.
Lorenzo Mognon
Dipòsit Legal: T 1359-2015

Chapter 3. Ru-Zn Heteropolynuclear Complexes Containing a Dinucleating Bridging Ligand: Synthesis, Structure and Isomerism

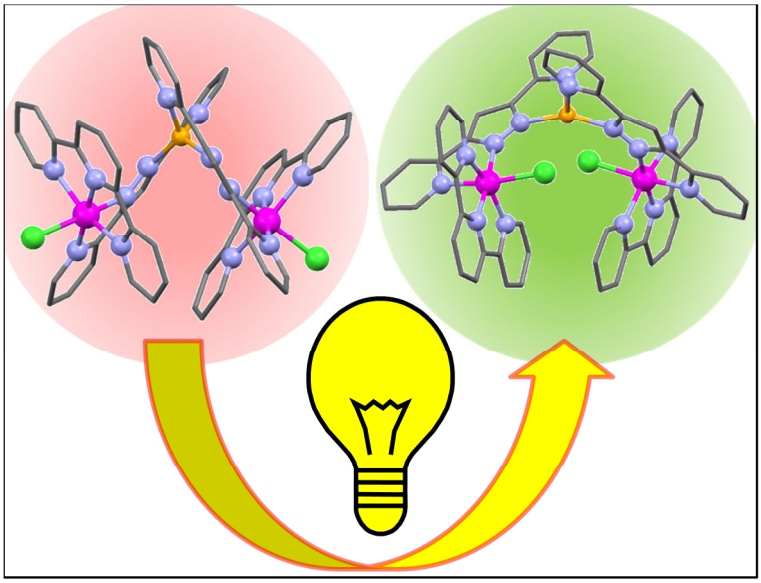

New heteropolynuclear complexes of ruthenium and zinc based on 2,2'-(1*H*-pyrazole-3,5-diyl)dipyridine are synthesized and characterized by spectroscopic and electrochemical methods. The electronic communication through the bridging ligand is discussed. Reactivity towards isomerization is observed by means of NMR and rationalized by density functional theory based calculations.

UNIVERSITAT ROVIRA I VIRGILI
MONONUCLEAR AND HETEROTRINUCLEAR RUTHENIUM COMPLEXES: SYNTHESIS AND WATER OXIDATION ACTIVITY.
Lorenzo Mognon
Dipòsit Legal: T 1359-2015

Chapter 3. Ru-Zn Heteropolynuclear Complexes Containing a Dinucleating Bridging Ligand: Synthesis, Structure and Isomerism

UNIVERSITAT ROVIRA I VIRGILI
MONONUCLEAR AND HETEROTRINUCLEAR RUTHENIUM COMPLEXES: SYNTHESIS AND WATER OXIDATION ACTIVITY.
Lorenzo Mognon
Dipòsit Legal: T 1359-2015

Chapter 3. Ru-Zn Heteropolynuclear Complexes Containing a Dinucleating Bridging Ligand: Synthesis, Structure and Isomerism

Inorg. Chem. **2014**, *53*, 12407-12415

Lorenzo Mognon,[a] Jordi Benet-Buchholz,[a] Wahidur Rahaman,[a] Carles Bo,[a,b] and Antoni Llobet[a,c]

[a] Institute of Chemical Research of Catalonia (ICIQ), Avinguda Països Catalans 16, 43007 Tarragona, Spain

[b] Departament de Química Física i Inorgànica, Universitat Rovira i Virgili, 43007 Tarragona, Spain

[c] Departament de Química, Universitat Autònoma de Barcelona, Cerdanyola del Vallès, 08193 Barcelona, Spain

3.1 Abstract

Mononuclear complexes *out*- and *in*-[Ru(Cl)(Hbpp)(trpy)]$^{+}$ (***out*-0** and ***in*-0**; Hbpp is 2,2'-(1H-pyrazole-3,5-diyl)dipyridine and trpy is 2,2':6',2"-terpyridine) are used as starting materials for preparation of Ru-Zn heterodinuclear *out*-{[Ru(Cl)(trpy)][$ZnCl_2$](μ-bpp)} (***out*-2**) and heterotrinuclear *out,out*- and *in,in*-{[Ru(Cl)(trpy)]$_2$(μ-[Zn(bpp)$_2$])}$^{2+}$ (***out*-3**, ***in*-3**) constitutional isomers. Further substitution of the Cl ligand from the former complexes leads to Ru-aqua *out,out*-{[Ru(trpy)(H_2O)]$_2$(μ-[Zn(bpp)$_2$])}$^{4+}$ (***out*-4**) and the oxo-bridged Ru-O-Ru complex *in,in*-{[Ru^{III}(trpy)]$_2$(μ-[Zn(bpp)$_2$(H_2O)]μ-(O)}$^{4+}$ (***in*-5**). All complexes are thoroughly characterized by the usual analytical techniques as well as by

spectroscopy by means of UV-vis, MS and when diamagnetic NMR. CV and DPV are used to extract electrochemical information and monocrystal X-ray diffraction to characterize complexes ***out*-2**, ***out*-3**, ***in*-3** and ***in*-5** in the solid state. Complex ***out*-3** photochemically isomerizes towards ***in*-3**, as can be observed by NMR spectroscopy and rationalized by density functional theory based calculations.

3.2 Introduction

Polynuclear transition metal complexes are a very interesting class of complexes whose properties can be tuned by the type of bridging ligands bonded to the transition metals. The bridging ligand thus dictates the degree of electronic communication between two or more transition metals. In addition, the structure of the ligand can generate a particular spatial disposition of the metal centers that can favor a cooperative effect for a given reaction.[1] Taking into account the relatively large number of transition metals and the huge variety of bridging ligands, an immense number of complexes can be potentially obtained with a large diversity of properties.

Polynuclear transition metal complexes have found interesting application in fields where cooperation between metal centers is important such as: magnetochemistry,[2] optical properties,[3] reactivity,[1d] catalysis[4,5] etc. Nature also benefits from metal cooperation in a number of metalloproteins whose functions range from small molecule activation (N_2, O_2, and H_2)[6] to hydrolysis.[6d, 7] Low molecular weight models have been proven crucial in some cases for understanding the spectroscopic and structural properties of the active site of these proteins.[7g, 8]

A fundamental characteristic of coordination complexes is the multiple different types of isomers that they can display. Regarding Ru complexes containing the Hbpp ligand (Hbpp is 2,2'-(1H-pyrazole-3,5-diyl)dipyridine), we previously described examples where Ru-dmso linkage isomerism takes place induced by a change in oxidation state.[9] We also described the presence of axial chirality due to the through-space supramolecular interaction and different ligand space arrangement in Ru-bpp$^-$ complexes containing the MeCN ligand.[10] In addition we also described constitutional isomerism in mononuclear Ru-Hbpp complexes containing the tridentate meridional 2,2':6',2"-terpyridine (trpy) ligand and Cl or H_2O ligands in the case of *out*- and *in*-[Ru(Cl)(Hbpp)(trpy)]$^+$ (***out*-0**, ***in*-0**) and *out*- and *in*-[Ru(Hbpp)(trpy)(H_2O)]$^{2+}$ (***out*-1**, ***in*-1**).[11]

The non-symmetric nature of the Hbpp ligand allows to easily prepare mononuclear complexes and use the latter as starting materials for preparation of the corresponding multinuclear complexes. On the other hand symmetric ligands generally lead to homodinuclear complexes and sometimes to even coordination oligomers or polymers[12] especially with first row transition metal complexes.

Here on we present the synthesis and reactivity of new hetero-, di-, and trinuclear complexes containing the bpp$^-$ ligand, using the corresponding mononuclear Ru-Hbpp complexes, ***out*-0** and ***in*-0**, as synthetic intermediates.

3.3 Experimental section

Preparations. The starting complexes *out*-[Ru(Cl)(Hbpp)(trpy)](PF_6), ***out*-0**, and *in*-[Ru(Cl)(Hbpp)(trpy)](PF_6), ***in*-0**, and their respective aqua complexes *out*-

[Ru(Hbpp)(trpy)(H_2O)](ClO_4)$_2$, ***out*-1**, and *in*-[Ru(Hbpp)(trpy)(H_2O)](ClO_4)$_2$, ***in*-1**, were prepared as described in the literature.[11a]

***out*-{[Ru(Cl)(trpy)][$ZnCl_2$](μ-bpp)}·H_2O, *out*-2·H_2O.** A 100 mg (0.132 mmol) sample of *out*-[Ru(Cl)(Hbpp)(trpy)](PF_6) was dissolved in 40 mL of methanol, and then 19.0 mL of triethylamine (0.136 mmol) was slowly added to the solution under magnetic stirring and heating at 50 °C. Afterwards, 90 mg of $ZnCl_2$ (0.660 mmol) previously dissolved in 10 mL of methanol was added, and the solution was kept stirring for 1 h at 50°C. A black solid is then filtered from the solution and washed with methanol (3 x 10 mL) and diethylether (3 x 10 mL). Yield: 89 mg (92.8%). Anal. Calcd for $C_{28}H_{20}Cl_3N_7RuZn·H_2O$: C, 45.12; H, 2.98; N, 13.15. Found: C, 44.90; H, 2.66; N, 12.96. ^{1}H NMR (400MHz, d_6-DMSO): δ = 9.92 (d, $^3J_{16\text{-}17}$ = 5.5 Hz, H16), 8.57 (d, $^3J_{7\text{-}8}$ = $^3J_{9\text{-}8}$ = 8.3 Hz, H7, H9), 8.48 (d, $^3J_{4\text{-}3}$ = $^3J_{12\text{-}13}$ = 7.9 Hz, H4,H12), 8.30 (d, $^3J_{19\text{-}18}$ = 7.6 Hz, H19), 8.19 (dd, $^3J_{18\text{-}19}$ = 7.6 Hz, $^3J_{18\text{-}17}$ = 7.4 Hz, H18), 8.11 (d, $^3J_{28\text{-}27}$ = 4.5 Hz, H28), 8.03 (dd, $^3J_{26\text{-}25}$ = 8.0 Hz, $^3J_{26\text{-}27}$ = 7.9 Hz, H26), 7.97 (t, $^3J_{8\text{-}7}$ = $^3J_{8\text{-}9}$ = 8.3 Hz, H8), 7.85 (dd, $^3J_{3\text{-}4}$ = $^3J_{13\text{-}12}$ = 7.9 Hz, $^3J_{3\text{-}2}$ = $^3J_{13\text{-}14}$ = 7.8 Hz, H3, H13), 7.79 (d, $^3J_{25\text{-}26}$ = 8.0 Hz, H25), 7.74 (s, H22), 7.72 (dd, $^3J_{17\text{-}18}$ = 7.4 Hz, $^3J_{17\text{-}16}$ = 5.5 Hz, H17), 7.56 (d, $^3J_{1\text{-}2}$ = $^3J_{15\text{-}14}$ = 5.2 Hz, H1, H15), 7.37 (dd, $^3J_{27\text{-}26}$ = 7.92, $^3J_{27\text{-}28}$ = 4.5 Hz, H27), 7.29 (dd, $^3J_{2\text{-}3}$ = $^3J_{14\text{-}13}$ = 7.8 Hz, $^3J_{2\text{-}1}$ = $^3J_{14\text{-}15}$ = 5.2 Hz, H2, H14). NMR is assigned following the labels in Figure 1. MALDI-MS (CH_2Cl_2): *m/z* = 727.0 ([M]$^+$). Cyclic Voltammetry (CH_2Cl_2, TBAH): $E_{1/2}$ = 0.543 V *vs.* SSCE (ΔE_p = 76 mV).

***out,out*-{[Ru(Cl)(trpy)]$_2$(μ-[Zn(bpp)$_2$])}(PF_6)$_2$·H_2O, *out*-3·H_2O.** A 80 mg (0.110 mmol) sample of *out*-{[Ru(Cl)(trpy)][$ZnCl_2$](μ-bpp)} was dissolved in a minimum amount of DMF, then a few drops of a saturated aqueous KPF_6 solution were added. Afterward water was added until a precipitate appeared. The mixture was cooled in the fridge for 2 hours, and then the solid filtered on a frit and

washed with water (3 x 10 mL) and diethyl ether (3 x 10 mL). Yield: 75 mg (88.7%). Anal. Calcd for $C_{56}H_{40}Cl_2F_{12}N_{14}P_2Ru_2Zn{\cdot}H_2O$: C, 43.24; H, 2.72; N, 12.61. Found: C, 43.33; H, 2.69; N, 12.47. ^{1}H NMR (400MHz, d_6-acetone): δ = 9.82 (d, $^3J_{16\text{-}17} = {}^3J_{41\text{-}40}$ = 5.1 Hz, H16, H41), 8.65 (d, $^3J_{19\text{-}18} = {}^3J_{38\text{-}39}$ = 7.7 Hz, H19, H38), 8.40 (dd, $^3J_{18\text{-}17} = {}^3J_{39\text{-}40}$ = 7.7 Hz, $^3J_{18\text{-}19} = {}^3J_{39\text{-}38}$ = 7.7 Hz, H18, H39), 8.36 (dd, $^3J_{26\text{-}25} = {}^3J_{31\text{-}32}$ = 7.9 Hz, $^3J_{26\text{-}27} = {}^3J_{31\text{-}30}$ = 7.9 Hz, H26, H31), 8.23 (d, $^3J_{28\text{-}27} = {}^3J_{29\text{-}30}$ = 4.9 Hz, H28, H29), 8.16 (d, $^3J_{7\text{-}8} = {}^3J_{50\text{-}49}$ = 8.0 Hz, H7, H50), 8.15 (d, $^3J_{4\text{-}3} = {}^3J_{53\text{-}54}$ = 7.8 Hz, H4, H53), 8.11 (d, $^3J_{12\text{-}13} = {}^3J_{45\text{-}44}$ = 7.9 Hz, H12, H45), 8.10 (d, $^3J_{25\text{-}26} = {}^3J_{32\text{-}31}$ = 7.9 Hz, H25, H32), 8.07 (s, H22, H35), 7.79 (dd, $^3J_{17\text{-}18} = {}^3J_{40\text{-}39}$ = 7.7 Hz, $^3J_{17\text{-}16} = {}^3J_{40\text{-}41}$ = 5.1 Hz, H17, H40), 7.77 (d, $^3J_{9\text{-}8} = {}^3J_{48\text{-}49}$ = 7.6 Hz, H9, H48), 7.74 (dd, $^3J_{13\text{-}12} = {}^3J_{44\text{-}45}$ = 7.9 Hz, $^3J_{13\text{-}14} = {}^3J_{44\text{-}43}$ = 7.8 Hz, H13, H44), 7.64 (dd, $^3J_{27\text{-}26} = {}^3J_{30\text{-}31}$ = 7.9 Hz, $^3J_{27\text{-}28} = {}^3J_{30\text{-}29}$ = 4.9 Hz, H27, H30), 7.57 (d, $^3J_{1\text{-}2} = {}^3J_{56\text{-}55}$ = 5.3 Hz, H1, H56), 7.43 (dd, $^3J_{2\text{-}3} = {}^3J_{55\text{-}54}$ = 7.8 Hz, $^3J_{2\text{-}1} = {}^3J_{55\text{-}56}$ = 5.3 Hz, H2, H55), 7.38 (dd, $^3J_{3\text{-}4} = {}^3J_{54\text{-}53}$ = 7.8 Hz, $^3J_{3\text{-}2} = {}^3J_{54\text{-}55}$ = 7.8 Hz, H3, H54), 7.29 (d, $^3J_{15\text{-}14} = {}^3J_{42\text{-}43}$ = 4.7 Hz, H15, H42), 7.21 (dd, $^3J_{8\text{-}7} = {}^3J_{49\text{-}50}$ = 8.0 Hz, $^3J_{8\text{-}9} = {}^3J_{49\text{-}48}$ = 7.6 Hz, H8, H49), 7.20 (dd, $^3J_{14\text{-}13} = {}^3J_{43\text{-}44}$ = 7.8 Hz, $^3J_{14\text{-}15} = {}^3J_{43\text{-}42}$ = 4.7 Hz, H14, H43). NMR is assigned following the labels in Figure 5. MALDI-MS (CH_2Cl_2): *m/z* = 592.2 ([Ru(Cl)(Hbpp)(trpy)]$^+$). Cyclic Voltammetry (CH_2Cl_2, TBAH): $E_{1/2}$ = 0.669 V *vs*. SSCE (ΔE_p = 185 mV).

***out,out*-{[Ru(trpy)(H$_2$O)]$_2$(μ-[Zn(bpp)$_2$])}(ClO$_4$)$_4$,·(CH$_3$)$_2$CO, *out*-4·(CH$_3$)$_2$CO.** A 50 mg (0.033 mmol) sample of *out,out*-{[Ru(Cl)(trpy)]$_2$(μ-[Zn(bpp)$_2$])}(PF$_6$)$_2$ was placed in a 5 mL round-bottom flask together with 13.3 mg (0.064 mmol) of $AgClO_4$. The solids were dissolved with 10 mL of a 1:3 water/acetone solution (v/v) and refluxed for 1.5 h in the dark. The solution was then cooled in an ice bath and filtered over Celite to remove precipitated AgCl. A few drops of a saturated aqueous $NaClO_4$ solution was added to the filtrate, and the volume

reduced under vacuum, keeping the temperature below 30 °C, until a precipitate appeared. Precipitation was completed by immersion in an ice bath for 30 minutes and the solid obtained filtered through a frit, washed with cold water (3 x 10 mL) and diethyl ether (3 x 10 mL), and dried in a vacuum. Yield: 49 mg (92.9%). Anal. Calcd for $C_{56}H_{44}Cl_4N_{14}O_{18}Ru_2Zn\cdot(CH_3)_2CO$: C, 42.47; H, 3.02; N, 11.75. Found: C, 42.16; H, 3.16; N, 11.65. MALDI-MS (H_2O): *m/z* = 556.2 ($[Ru(bpp)(trpy)]^+$), 598.6 ($[Ru(bpp)(trpy)(OH)(Na)]^+$).

***in,in*-{[Ru(Cl)(trpy)]$_2$(μ-[Zn(bpp)$_2$])}(PF$_6$)$_2$, *in*-3. ROUTE A.** A 100 mg (0.132 mmol) sample of *in*-[Ru(Cl)(Hbpp)(trpy)](PF_6) was dissolved in 40 mL of methanol, and then 19.0 mL of triethylamine (0.136 mmol) was slowly added to the solution under magnetic stirring and heating at 50 °C. Afterwards, 90 mg of $ZnCl_2$ (0.660 mmol) previously dissolved in 10 mL of methanol was added, and the solution was kept stirring for 1 h at 50 °C. The solvent was evaporated and the red solid dissolved in acetone. Some drops of a saturated KPF_6 aqueous solution and water were added and the volume reduced until formation of a precipitate. The mixture was then left in a fridge overnight to complete precipitation and then filtered and washed with water (3 x 10 mL) and diethyl ether (3 x 10 mL). Yield: 87 mg (85.7%). Anal. Calcd for $C_{56}H_{40}Cl_2F_{12}N_{14}P_2Ru_2Zn\cdot2.8(KPF_6)$: C, 32.52; H, 1.95; N, 9.48. Found: C, 32.99; H, 2.01; N, 9.15. ^{1}H NMR (400 MHz, d_6-acetone): δ = 8.69 (d, $^3J_{7\text{-}8}$ = $^3J_{50\text{-}49}$ = 7.9 Hz, H7, H50), 8.67 (d, $^3J_{9\text{-}8}$ = $^3J_{48\text{-}49}$ = 8.0 Hz, H9, H48), 8.57 (d, $^3J_{12\text{-}13}$ = $^3J_{45\text{-}44}$ = 5.0 Hz, H12, H45), 8.53 (d, $^3J_{28\text{-}27}$ = $^3J_{29\text{-}30}$ = 7.9 Hz, H28, H29), 8.40 (d, $^3J_{4\text{-}3}$ = $^3J_{53\text{-}54}$ = 7.9 Hz, H4, H53), 8.18 (m, H15, H42), 8.17 (d, $^3J_{19\text{-}18}$ = $^3J_{38\text{-}39}$ = 8.4 Hz, H19, H38), 8.14 (dd, $^3J_{8\text{-}9}$ = $^3J_{49\text{-}48}$ = 8.0 Hz, $^3J_{8\text{-}7}$ = $^3J_{49\text{-}50}$ = 7.9 Hz, H8, H49), 8.09 (m, H14, H43), 8.00 (d, $^3J_{25\text{-}26}$ = $^3J_{32\text{-}31}$ = 6.9 Hz, H25, H32), 7.99 (s, H22, H35), 7.94 (dd, $^3J_{27\text{-}28}$ = $^3J_{30\text{-}29}$ = 7.9 Hz, $^3J_{27\text{-}26}$ = $^3J_{30\text{-}31}$ = 7.0 Hz, H27, H30), 7.77 (d, $^3J_{1\text{-}2}$ = $^3J_{56\text{-}55}$ =

5.7 Hz, H1, H56), 7.65 (dd, $^3J_{3\text{-}4} = {}^3J_{54\text{-}53} = 7.9$ Hz, $^3J_{3\text{-}2} = {}^3J_{54\text{-}55} = 7.7$ Hz, H3, H54), 7.60 (dd, $^3J_{18\text{-}19} = {}^3J_{39\text{-}38} = 8.4$, $^3J_{18\text{-}17} = {}^3J_{39\text{-}40} = 7.5$ Hz, H18, H39), 7.59 (dd, $^3J_{26\text{-}27} = {}^3J_{31\text{-}30} = 7.0$ Hz, $^3J_{26\text{-}25} = {}^3J_{31\text{-}32} = 6.9$ Hz, H26, H31), 7.42 (dd, $^3J_{13\text{-}14} = {}^3J_{44\text{-}43} = 6.9$ Hz, $^3J_{13\text{-}12} = {}^3J_{44\text{-}45} = 5.0$ Hz, H13, H44), 7.10 (d, $^3J_{16\text{-}17} = {}^3J_{41\text{-}40} = 6.4$ Hz, H16, H41), 6.76 (dd, $^3J_{17\text{-}18} = {}^3J_{40\text{-}39} = 7.5$ Hz, $^3J_{17\text{-}16} = {}^3J_{40\text{-}41} = 6.4$ Hz, H17, H40), 6.42 (dd, $^3J_{2\text{-}3} = {}^3J_{55\text{-}54} = 7.7$ Hz, $^3J_{2\text{-}1} = {}^3J_{55\text{-}56} = 5.7$ Hz, H2, H55). NMR is assigned following the labels in Figure 5. MALDI-MS (CH_2Cl_2): *m/z* = 1391.2 ($[M\text{-}PF_6]^+$). Cyclic Voltammetry (CH_2Cl_2, TBAH): $E_{1/2}$ = 0.665 V *vs*. SSCE (ΔE_p = 68 mV), $E_{1/2}$ = 0.765 V vs SSCE (ΔE_p = 66 mV).

ROUTE B. A 150 mg (0.098 mmol) sample of *out,out*-{[Ru(Cl)(trpy)]$_2$(μ-[Zn(bpp)$_2$])}$(PF_6)_2$ was dissolved in 130 mL of acetone and refluxed in the presence of a 100 W lamp for 72 h. Then a few drops of a saturated KPF_6 aqueous solution and water were added, and the volume was reduced until the formation of a precipitate. The mixture was left in a fridge overnight to complete precipitation and then filtered and washed with water (3 x 10 mL) and diethyl ether (3 x 10 mL).Yield: 128 mg (85.3 %).

***in,in*-{[Ru^{III}(trpy)]$_2$(μ-[Zn(bpp)$_2$(H$_2$O)]μ-(O)}$(ClO_4)]_4$, *in*-5.** A 50 mg (0.033 mmol) sample of *in,in*-{[Ru(Cl)(trpy)]$_2$(μ-[Zn(bpp)$_2$])}$(PF_6)_2$ was placed in a 5 mL round-bottom flask together with a 13.3 mg (0.064 mmol) of $AgClO_4$. The solids were dissolved with 10 mL of a 1:3 water/acetone solution (v/v) and refluxed for 1.5 h in the dark. The solution was then cooled in an ice bath and filtered over Celite to remove precipitated AgCl. A few drops of a saturated aqueous $NaClO_4$ solution was added to the filtrate, and the volume reduced under vacuum, keeping the temperature below 30 °C, until a precipitate appeared. Precipitation was completed by immersion in an ice bath for 30 min, and the solid obtained was filtered through a frit, washed with cold water (3 x 10 mL)

and diethyl ether (3 x 10 mL), and dried in a vacuum. Yield: 11 mg (19.5 %). Anal. Calcd for $C_{56}H_{42}Cl_4N_{14}O_{18}Ru_2Zn \cdot 2(LiClO_4) \cdot (CH_3)_2CO$: C, 37.71; H, 2.57; N, 10.43. Found: C, 37.98; H, 2.40; N, 10.64. MALDI-MS (CH_2Cl_2): *m/z* = 656.2 ([Ru(bpp)(trpy)]$(ClO_4)^+$). Cyclic Voltammetry (H_2O, pH = 1.0 CF_3SO_3H): $E_{1/2}$ = 0.310 V vs SSCE (ΔE = 93 mV), $E_{1/2}$ = 0.730 V vs SSCE (ΔE_p = 81 mV); (H_2O, pH = 7.0 phosphate buffer): $E_{1/2}$ = 0.152 V vs SSCE (ΔE_p = 204 mV), $E_{1/2}$ = 0.780 V vs SSCE (ΔE_p = 101 mV).

X-ray Crystal Structure Determination. Black crystals of *out*-{[Ru(Cl)(trpy)][$ZnCl_2$](μ-bpp)}, ***out*-2**, were obtained by slow diffusion of acetone into a dimethylformamide solution of the complex. Brown crystals of *out,out*-{[Ru(Cl)(trpy)]$_2$(μ-[Zn(bpp)$_2$])}$(PF_6)_2$, ***out*-3**, were obtained by slow diffusion of ether in a methanolic solution of the complex. Dark red crystals of *in,in*-{[Ru(Cl)(trpy)]$_2$(μ-[Zn(bpp)$_2$])}$(PF_6)_2$, ***in*-3**, could be obtained by slow diffusion of ether in a methanolic solution of the complex. Green crystals of *in,in*-{[Ru^{III}(trpy)]$_2$μ-[Zn(bpp)$_2$(H_2O)]μ-(O)}$(ClO_4)]_4$, ***in*-5**, were obtained by slow diffusion of ether in acetone solution of the complex. The measured crystals were prepared under inert conditions immersed in perfluoropolyether as protecting oil for manipulation.

Data collection: Crystal structure determination for ***out*-2** was carried out using a Apex DUO Kappa 4-axis goniometer equipped with an APPEX 2 4K CCD area detector, a Microfocus Source E025 IuS using MoK_α radiation, Quazar MX multilayer Optics as monochromator and a Oxford Cryosystems low temperature device Cryostream 700 plus (T = -173 °C). Full-sphere data collection was used with ω and φ scans. *Programs used:* Data collection APEX-2,[13] data reduction Bruker Saint[14] V/.60A and absorption correction SADABS.[15,16] Crystal structure determinations for ***out*-3, *in*-3** and ***in*-5** were

carried out using a Bruker-Nonius diffractometer equipped with an APPEX 2 4K CCD area detector, a FR591 rotating anode with MoK_α radiation, Montel mirrors as monochromator and an Oxford Cryosystems low temperature device Cryostream 700 plus (T = -173 °C).

Structure Solution and Refinement: Crystal structure solution was achieved using direct methods as implemented in SHELXTL[17] and visualized using the program XP. Missing atoms were subsequently located from difference Fourier synthesis and added to the atom list. Least-squares refinement on F^2 using all measured intensities was carried out using the program SHELXTL. All non hydrogen atoms were refined including anisotropic displacement parameters.

Comments to the structures: ***out*-2**: The asymmetric unit contains two independent molecules of the bimetallic complex, three DMF molecules and three water molecules. One of the DMF molecules and one of the water molecules are disordered in two positions (ratio respectively: 75:25 and 50:50). Due to the disorder of the water molecules the positions of the corresponding hydrogen atoms could not be clearly localized and these were added to approximate positions to satisfy the crystal stoichiometry. This disorder is thus responsible for the B alerts that appear in the checkcif file. ***out*-3**: The asymmetric unit contains two independent molecules of the metallic complex, four PF_6 anions and 4.6 water molecules which are highly disordered distributed in 7 positions (1:1:0.6:0.6:0.6:0.4:0.4). As in the previous case hydrogen atoms could not be clearly localized and were added at approximate. ***in*-3**: The asymmetric unit contains one molecules of the metallic complex, two PF_6 anions, one acetone molecule and one methanol molecule. One of the PF_6 anions is disordered in two orientations (ratio: 80:20). The methanol molecule is disordered in three positions (ratio: 62.5:25:12.5). ***in*-5**: The asymmetric unit contains one molecule of the metallic complex, four ClO_4 anions and one and

half nonmetal coordinated water molecules. Three of the ClO_4 anions are disordered in two orientations (ratios: 60:40; 36:74; 81:19). The one and half nonmetal coordinated water molecules are disordered in three positions (ratio: 65:35:50).

Computational details: All calculations were carried out by using the Amsterdam Density Functional (ADF v2013.01) package.[18] DFT-based methods employed the generalized-gradient-approximation (GGA) level, with the Becke exchange[19] and the Perdew correlation[20] functionals (BP86). A triple-ξ plus polarization Slater basis set was used on all atoms. Relativistic corrections were introduced by scalar-relativistic zero-order regular approximation (ZORA).[21] Full geometry optimizations were performed without constraints, and also including Grimme's DFT-D empirical dispersion energy corrections.[22]

3.4 Results and discussion

Synthesis and structure. The non-symmetric dinucleating nature of Hbpp ligand[23] allows for the easy preparation of heteronuclear complexes given the different reactivity of the two available sites. Initially mononuclear complexes can be prepared leaving the second site ready for a second transition metal to coordinate. In the present report we have used the mononuclear isomeric complexes *out*- and *in*-[RuCl(Hbpp)(trpy)]$^+$, ***out*-0** and ***in*-0**,[11a] as starting materials following the synthetic strategy described in Scheme 1.

Ru-Zn Heteropolynuclear Complexes Containing a Dinucleating Bridging Ligand: Synthesis, Structure and Isomerism

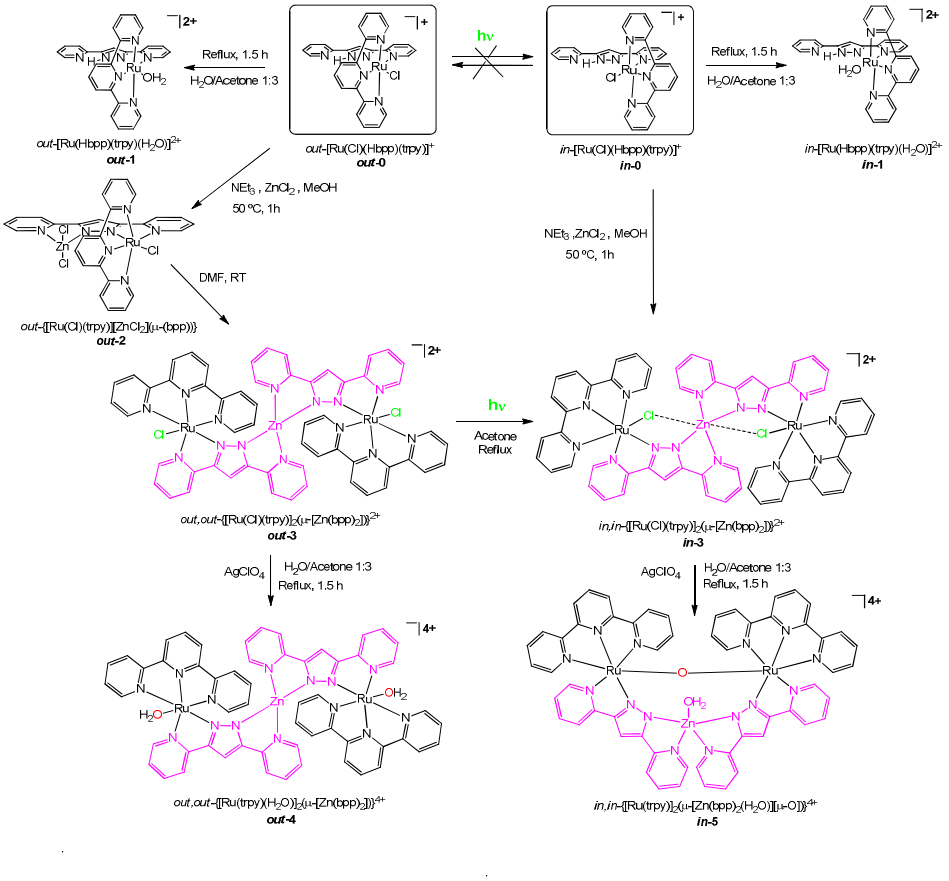

Scheme 1. Synthetic pathway.

Reaction of *out*-[RuCl(Hbpp)(trpy)]$^{+}$, ***out*-0**, with excess $ZnCl_2$ in the presence of triethylamine, which acts as a base, in methanol at 50 °C for 1 hour produces the complex *out*-{[Ru(Cl)(trpy)][$ZnCl_2$](μ-bpp)}, ***out*-2**, almost quantitatively.

out-[RuCl(Hbpp)(trpy)]$^{+}$ + NEt_3 + $ZnCl_2$

***out*-0**

-> ***out*-**{[RuCl(trpy)][$ZnCl_2$](μ-bpp)} + $HNEt_3^{+}$ **Eq.1**

***out*-2**

Complex ***out*-2** precipitates readily from the methanolic solution and it is insoluble in water and in most organic solvents except in DCM, DMSO and DMF. Dissolved in the latter the complex has a strong tendency to dimerize generating a heterotrinuclear complex, according to

2 *out*-{[RuCl(trpy)][$ZnCl_2$](μ-bpp)}

***out*-2**

-> *out,out*-{[RuCl(trpy)]$_2$(μ-[Zn(bpp)$_2$])}$^{2+}$ + $ZnCl_4^{2-}$ **Eq.2**

***out*-3**

where the Zn metal is now bonded to two bpp^{-} ligands in an tetrahedral fashion and acts as bridged for the two [RuCl(trpy)] moieties. Addition of Ag(I) to ***out*-3** generates the corresponding Ru diaqua complex

out,out-{[RuCl(trpy)]$_2$(μ-[Zn(bpp)$_2$])}$^{2+}$ + 2 Ag^{+}

***out*-3**

-> *out,out*-{[Ru(trpy)(H_2O)]$_2$(μ-[Zn(bpp)$_2$])}$^{4+}$ + 2 AgCl **Eq.3**

***out*-4**

It is interesting to realize here that the yield for this reaction is nearly quantitative (93 %) in sharp contrast to the yield obtained for formation of the aqua complex ***out*-1** from ***out*-0** of 53%, under comparable conditions. This is a consequence of the potential coordination of Ag to the available coordination position of the bpp^{-} ligand in ***out*-0** that can drive the system to additional

undesired pathways thus lowering the yield. In the present case the Zn metal avoids the interaction of silver with the bpp^- ligands and thus is responsible for this large enhancement of the yield.

The parallel chemistry with the *in* isomer *in*-$[RuCl(Hbpp)(trpy)]^+$, ***in*-0**, is radically different from the previously described reactions. In this case the addition of $ZnCl_2$ generates directly the heterotrinuclear complex,

$$2\ \textit{in}\text{-}[RuCl(Hbpp)(trpy)]^+ + 2\ NEt_3 + 2\ ZnCl_2 \xrightarrow[\textit{in}\text{-}\mathbf{0}]{} \textit{in,in}\text{-}\{[RuCl(trpy)]_2(\mu\text{-}[Zn(bpp)_2])\}^{2+} + ZnCl_4^{2-} + 2\ HNEt_3^+ \qquad \textbf{Eq.4}$$
$$\textit{in}\text{-}\mathbf{3}$$

presumably due to the solubility of the corresponding ***in*-2** dinuclear isomer that could not be isolated. Addition of Ag(I) to ***in*-3** generates the corresponding diaqua complex ***in*-4**, that again could not be isolated because it has a strong tendency to generate the oxo-bridged derivative, ***in*-5**.

$$\textit{in,in}\text{-}\{[Ru^{II}(trpy)(H_2O)]_2(\mu\text{-}[Zn(bpp)_2])\}^{4+} \xrightarrow[\textit{in}\text{-}\mathbf{4}]{} \textit{in,in}\text{-}\{[Ru^{III}(trpy)]_2(\mu\text{-}[Zn(bpp)_2(H_2O)]\mu\text{-}(O)\}^{4+} + 2H^+ + 2e^- \qquad \textbf{Eq.5}$$
$$\textit{in}\text{-}\mathbf{5}$$

This is a consequence of the ligand architecture that in the case of the ***in*-4** complex places the two Ru-aqua groups very close to one another and favors the intramolecular [Ru-OH_2 --- H_2O-Ru] coupling, to generate the highly stable oxo bridge group, Ru-O-Ru, concomitant with oxidation of Ru(II) to Ru(III) doubly bridging the Ru centers. Formation of this group is also most likely

responsible for the five coordination of the Zn complex with an additional aqua group. Given the absence of crystal field stabilization energy for a d^{10} ion, the new structural demands imposed by the oxo-bridging group forces a distortion of the N4 coordination by the bpp^- ligands favoring a pentacoordinate geometry with an additional Ru-O bond from the aquo ligand. See below for further details of the coordination geometry of the Zn metal ion.

Monocrystals for complexes ***out*-2**, ***out*-3**, ***in*-3** and ***in*-5** were obtained and their crystal structures solved by means of X-ray diffraction analysis. Their ORTEP view is presented in Figure 1, and all the crystallographic parameters can be found in the Supporting Information. For all these complexes the coordination around the low spin d^6 Ru(II) or d^5 Ru(III) is a distorted octahedral and very similar to previously reported related Ru complexes.[10a, 11b, 24] In sharp contrast, while the bonding distances for the Zn(II) are also in agreement with previously published related complexes,[25] their geometries are radically different from one another. This is a consequence of the absence of Crystal Field Stabilization Energy (CFSE) for a d^{10} Zn(II) ion where the Zn metal center geometry is strongly dependent on the spatial effects exerted by the coordinating bridging bpp^- ligand that are in turn dependent on their geometrical arrangement around the Ru metal center.

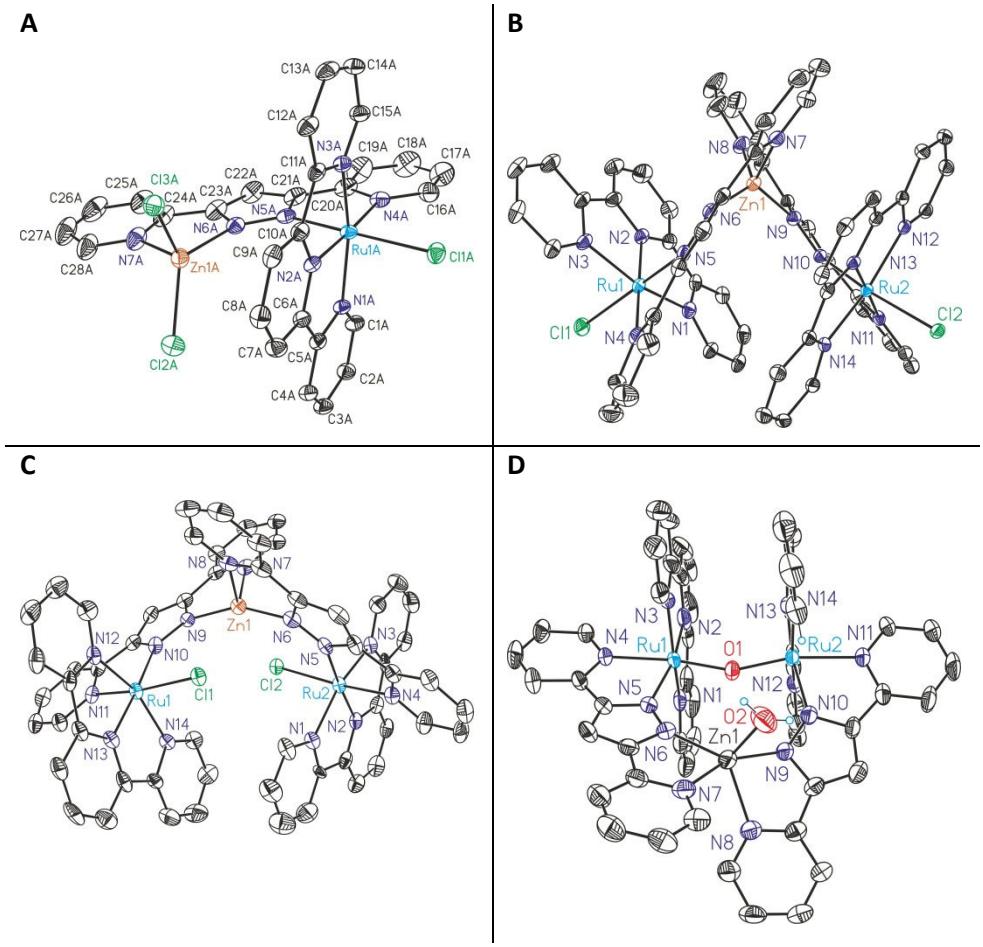

Figure 1. X-Ray structure ORTEP plots (probabilites at 50%) and labelling scheme for (A) ***out*-2**, (B) ***out*-3**, (C) ***in*-3** and (D) ***in*-5**.

For the ***out*-2** heterodinuclear complex, the Zn center is coordinated by two Cl and two N atoms from the bpp⁻ ligand in a distorted tetrahedral fashion. The dihedral angle between the planes generated by the Cl2Zn1Cl3 atoms and the N6Zn1N7 is 86.4°, close to the 90° expected for an ideal tetrahedral geometry. For the ***out*-3** heterotrinuclear complex, the geometry around the Zn metal center is again a distorted tetrahedron although now the

coordination atoms are two N atoms from a pyridyl-pyrazolyl moiety from two different bpp^- ligands. The dihedral angle between the two NZnN (N6Zn1N7 and N8Zn1N9) planes is now 78.2°. It is worth noting here that the trpy and bpp^- moieties bonded to different Ru centers are situated in a nearly parallel manner although they are too far for a potential π- π stacking interaction.

Regarding the ***in*-3** complex, the constitutional isomer of ***out*-3**, the geometry presented by Zn is now closer to a distorted octahedral geometry, where due to the new spatial arrangement of the Ru-Cl-bpp moiety their Cl atoms weakly interact with the Zn metal (d_{Zn-Cl} = 3.06 and 3.04 Å respectively). In this case the NZnN (N6Zn1N7 and N8Zn1N9) dihedral angle is 85.9°. Finally, for the ***in*-5** complex**,** which contains a Ru-O-Ru group, the Zn metal displays pentacoordination with an additional Zn-OH_2 group in a distorted square pyramidal type of geometry. Here the NZnN (N6Zn1N7 and N8Zn1N9) dihedral angle is 47.9°, which is the smallest of all the complexes described in the present work due to the special arrangement forced by the additional oxo-bridging group between the two Ru(III) centers. It is also worth mentioning here that the oxygen atom of the Zn-OH_2 groups is hydrogen bonded to a H56, of one of the trpy ligands (C56H56O2 angle, 146.6°; C56O2, 3.43 Å; H56O2, 2.60 Å).

Spectroscopic properties. The optical properties of the Ru-Cl complexes presented in this work were evaluated by means of UV-vis spectroscopy in DCM and are displayed in Figure 2. All complexes present strong ligand based π-π* bands below 340 nm and lower intensity MLCT dπ-π* transitions around 400 and 700 nm together with their vibronic components.[26] TD-DFT has been used to corroborate the nature of these transition and the results are shown in the Supporting Information (Figure S16).

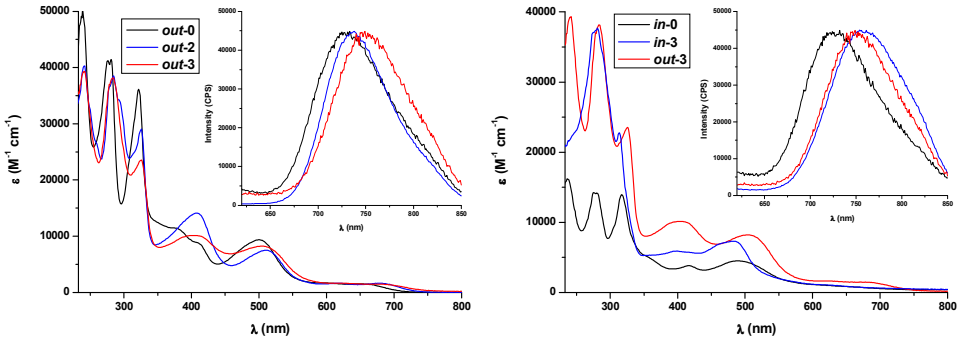

Figure 2. UV-vis and (inset) emission spectra in DCM of ***out*-0**, ***out*-2** and ***out*-3** (left) and ***in*-0, *in*-3** and ***out*-3 (**right**).**

Spectra of all complexes are very similar since the chromophores are identical. As expected, the presence in the system of a d^0 metal, such as Zn(II), does not significantly modify the overall optical properties in the visible region. A slight difference can be found from ***out*-0** and ***out*-3** on energies and extinction coefficients that might be due to the slightly geometrical distortions found in the Ru metal centers. Similar behavior is observed for the *in* complexes (Fig 2, right), where the interaction between the chlorido ligands and the zinc atom seems to produce a small shift of the dπ-π* MLCT band to higher energy.

The ***in*-5** complex was investigated in aqueous solution. At pH = 1.0, it presents the typical bands of the Ru-O-Ru transition at 610 and 680 nm as can be observed in Figure 3. These two bands are red-shifted by about 50 nm at pH = 7.0 which is indicative of the acid base properties of the oxo-bridge as had been previously observed for related oxo-bridged-Ru dimers.[27]

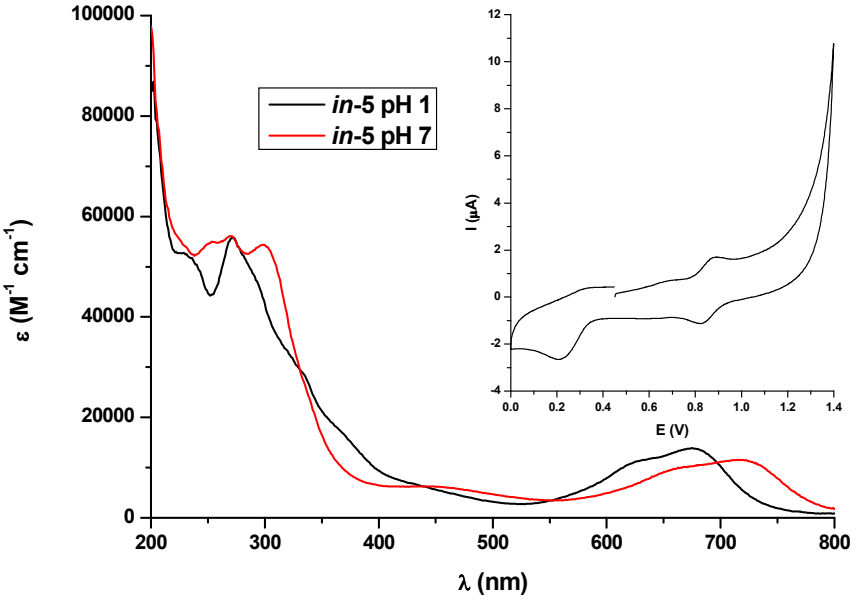

Figure 3. UV-vis at pH = 1.0 and 7.0, and (inset) CV at pH = 1.0 (*E* vs SCEE) of ***in*-5**.

Fluorescence experiments have been carried out for the complexes ***out*-2, *out*-3** and ***in*-3,** and for their mononuclear analogues ***out*-0** and ***in*-0** for comparison purposes. All these spectra are presented as insets in Figure 2. From the figure it can be clearly seen that the emission is affected by the nature of the monodentate ligand but is practically not affected by the nature of the isomer.

Redox properties. The redox properties of the Ru-Cl complexes presented in this work were analyzed by means of cyclic voltammetry in DCM containing 0.1 M TBAH [(*n*Bu_4N)(PF_6)] as supporting electrolyte, and are displayed in Figure 4. All redox potentials reported in this work are referred to the SSCE electrode, and all CV were run at a scan rate of 50 mV/s. Glassy carbon electrodes were used as working electrodes and platinum wires as auxiliary electrodes.

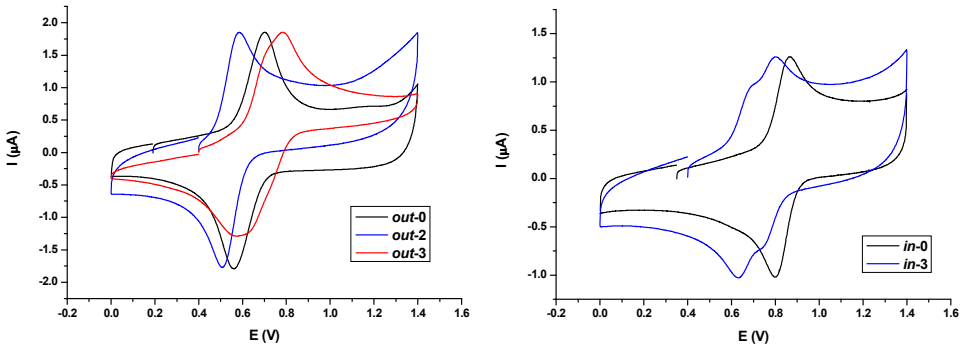

Figure 4. Cyclic voltammograms (E vs SCEE) in DCM containing 0.1 M TBAH [(nBu$_4$N)(PF$_6$)] of: left, of ***out*-0**, ***out*-2** and ***out*-3** and right, cyclic voltammograms of ***in*-0** and ***in*-3** in DCM containing 0.1 M TBAH.

The dinuclear complex ***out*-2** exhibits a chemically reversible and electrochemically quasi-reversible wave at $E_{1/2}$ = 0.54 V (ΔE_p = 76 mV), assigned to the Ru(III)/Ru(II) couple, which is 80 mV lower than ***out*-0** ($E_{1/2}$ = 0.62 V) under identical conditions. Thus, replacement of the pyrazolic-Hbpp proton by the $ZnCl_2$ group produces an enhancement of the electron density on the Ru metal center. The trinuclear complex ***out*-3** shows two waves in very close proximity at $E_{1/2}$ = 0.64 V (ΔE_p = 120 mV) and 0.69 V (ΔE_p = 150 mV), assigned to the Ru_2(III,II)/Ru_2(II/II) and Ru_2(III,III)/Ru_2(III/II) couples, respectively. The close proximity of the two couples suggests a weak electronic coupling between the two Ru centers through the {Zn(bpp)$_2$} bridging unit, as expected.[10a, 28] Comparing the redox potential for the mononuclear ***out*-0** with regard to ***out*-3** a decrease of electron density over the Ru metal centers is now observed as suggested by the anodic shift of the III/II redox potentials.

In the case of ***in*-3**, two quasi-reversible waves at $E_{1/2}$ = 0.66 V (ΔE_p = 80 mV) and 0.76 V (ΔE_p = 80 mV) assigned to the Ru_2(III,II)/Ru_2(II/II) and

Ru_2(III,III)/Ru_2(III/II) couples, respectively, indicate again a weak coupling, but now the two waves are cathodically shifted by 80-180 mV with regard to ***in*-0** ($E_{1/2}$ = 0.84 V). This effect can be associated with the Zn-Cl contacts (3.04 and 3.06 Å) that each {Ru-Cl} entity has in the *in* isomer and that do not exist in the corresponding *out* isomer. These Zn-Cl contacts that generate the difference in redox potentials are also most likely responsible for the difference in the weak electronic coupling through the two Ru metals. NIR experiments for the mixed valence III,II ***in*-3** complex were carried out in order to further characterize the electronic coupling. Unfortunately the IVCT band is so weak[29] that we were not able to properly observe it (see Figure S14-15) even working at the highest possible concentration.

The oxo-bridged complex ***in*-5** presents a completely different redox behavior. In water at pH = 1.0 a reversible wave at $E_{1/2}$ = 0.84 V ($E_{p,a}$ = 0.87 V, $E_{p,c}$ = 0.81 V; ΔE_p = 60 mV) associated with the Ru_2(IV,III)/Ru_2(III/III) couple is observed as shown in Figure 3. In addition, a chemically irreversible wave is observed at 0.25 V that is associated with the one-electron reduction of the oxo-bridged trinuclear complex to generate Ru_2(III/II). The chemical irreversibility is associated with the instability of the Ru-O-Ru bridged in the lower oxidation state where the population of antibonding orbitals[27] favors breaking of the bridging group generating the corresponding mononuclear complexes.

NMR spectroscopy. ^{1}H NMR spectra of the complexes described in this work were recorded in d_6-dmso or d_6-acetone and are assigned in the Experimental Section and their spectra are shown in Figure 5 and in the Supporting Information.

In solution complex ***out*-2** presents a symmetry plane that contains the bpp⁻ ligand and bisects the trpy moiety, thus rendering the upper and lower pyridyl of the trpy ligand magnetically equivalent. The deshielding effect produced by the Cl ligand at H16 allows one to identify the pyridyl system on the side of the Ru center. This information, together with the COSY spectra and symmetry of the complex previously mentioned, allows one to unambiguously assigning all resonances of the spectra (See Figure S1).

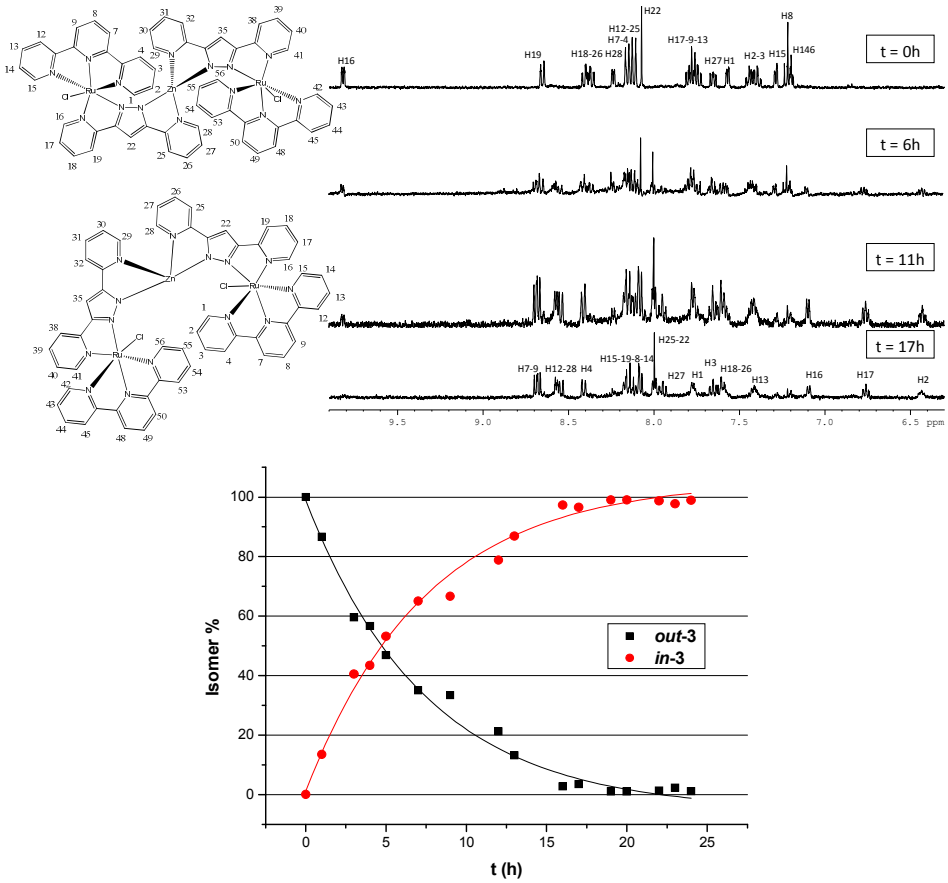

Figure 5. (Top) ^{1}H NMR spectra (400 MHz, 298 K, d_6-acetone) following the photochemical (100 W lamp) isomerization reaction from ***out*-3** to ***in*-3**. (Bottom) time profile based on the integration of resonances H16 for ***out*-3** and H12+H28 for ***in*-3.**

The ^{1}H NMR spectra of complexes ***out*-3** and ***in*-3** in d_6-acetone is depicted in Figure 5. Both exhibit a C_2 symmetry axis passing through the Zn atom but not coinciding with any bond, and thus, in both cases the two {Ru-bpp-trpy} moieties are magnetically equivalent. Symmetry together with COSY and the deshielding effect of the chlorido ligands to H16 and H41 for the ***out*-3** complex, allow to fully identify all resonances. For the case of ***in*-3,** a NOE between H14 and H29 (2.80 Å) or H28 and H42 (2.78 Å) is the key experiment that allows fully assigning the spectrum shown in Figure 5.

Reactivity. In both neutral and acidic conditions the trinuclear ***out*-4** Ru-aqua complex breaks apart and generates the corresponding mononuclear complex ***out*-1**, as indicated in the following equation

$$\underset{\textbf{\textit{out}-4}}{\textit{out,out}\text{-}\{[Ru^{II}(trpy)(H_2O)]_2(\mu\text{-}[Zn(bpp)_2])\}^{4+}} + 2\ H_2O \rightarrow 2\ \underset{\textbf{\textit{out}-1}}{\textit{out}\text{-}[Ru^{II}(Hbpp)(trpy)(H_2O)]^{2+}} + Zn(OH)_2 \qquad \textbf{Eq.6}$$

Generation of the mononuclear complex is instantaneous once the trinuclear complex is dissolved in aqueous solution, as can be clearly observed by UV-vis and CV.

On the other hand, the trinuclear ***out*-3** complex is photosensible and under irradiation with a tungsten lamp cleanly and irreversibly and quantitatively isomerizes to ***in*-3.** This isomerization process has been monitored by ^{1}H NMR spectroscopy and is shown in Figure 5. This is in sharp contrast with the photostability of the synthetic precursors, the mononuclear ***in*-** and ***out*-0** complexes.

Irreversible isomerization of the complex ***out*-3** towards ***in*-3**, is a consequence of the higher thermodynamic stability of the latter over the former. In addition, even though experimentally we could not detect any intermediate, transformation of the *out,out* complex into the *in,in* complex necessarily has to take place via the corresponding *in,out* intermediate complex, as indicated in the following equations (bpp^- and trpy ligands and overall charges have been omitted).

out,out-$\{[RuCl]_2(\mu\text{-}Zn)\}$

***out*-3**

-> *in,out*-$\{[RuCl]_2(\mu\text{-}Zn)\}$ **Eq.7**

***in, out*-3**

-> *in,in*-$\{[RuCl]_2(\mu\text{-}Zn)\}$

***in*-3**

In order to shed light on the driving force for the isomerization process, a DFT-based study was carried out, and a summary of the main results is presented in Figure 6 and in the Supporting Information. For this purpose we determined the relative stability of isomers ***out*-3**, ***in,out*-3** and ***in*-3.** As it can be observed in Figure 6, the ***in,out*-3** complex is about 12.7 kcal/mol more stable than ***out*-3** mainly due to the formation of a new Zn-Cl bond (Zn-Cl, 2.621 Å). Isomerization of the second Ru center toward the formation of ***in*-3** is 13.8 kcal/mol more stable, now due to the two Zn-Cl contacts. This is actually a structure that is very close the one observed experimentally through the X-ray diffraction analysis that is represented in Figure 1. The Zn-Cl bond length obtained from the geometry optimization process (2.920; 2.877 Å) compares fairly well with the X-ray determined parameters (3.06; 3.04 Å) although is

overestimated by approximately 0.1-0.2 Å. Including dispersion in the calculations further decrease the Zn-Cl distance by roughly 0.05 Å.

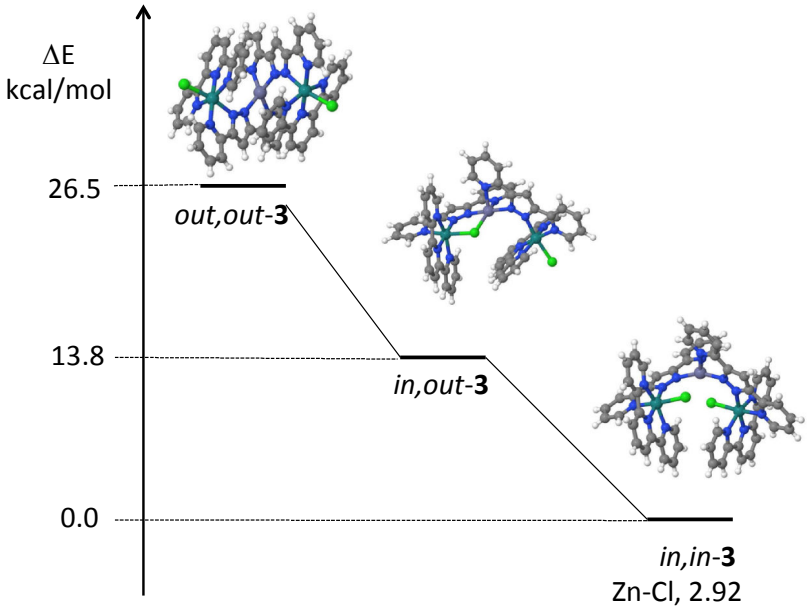

Figure 6. Energy diagram for optimized structures of three isomers of **3**, based on DFT.

3.5 Conclusions

We have prepared and thoroughly characterized a family of dinuclear and trinuclear Zn-Ru complexes containing the bpp⁻ ligand as a bridge. These include constitutional isomers that have been prepared from their corresponding *out* and *in* Ru mononuclear counterparts. The different constitutional isomers give rise not only to different solubilities but also to radically different reactivity based on the relative space disposition of the Ru-OH_2 or Ru-Cl groups. The access to through space intramolecular Ru-aqua---

aqua-Ru interactions in ***in*-4** gives rise to the oxo-bridged complex. The oxo-bridge is holding strongly and rigidly together the two Ru centers and enhances its stability so that now the trinuclear Ru complex is stable at pH = 1.0 and 7.0 whereas the trinuclear *out* complex is not. On the other hand, for the Ru-Cl case the presence of contact interactions stabilizes the *in* isomer with regard to the corresponding *out* one. The relative stability of the isomers is nicely demonstrated by the *out*->*in* photochemcial interconversion that is further supported by DFT.

The use of labile first row transition metals ion such as Zn, Fe or Mn to react with bridging dinucleating ligands such as Hbpp, generally produces oligomers[30] or grids[12a] or even coordination polymers.[12b-d] Using a substitutionally kinetically inert Ru(II) ion (at least with regard to the N-containing ligands) to coordinate first with the Hbpp ligand with subsequent addition of a substitutionally kinetically labile ion such as Zn(II) precludes the potentials oligomerization process and thus allows one to isolate the dinuclear and trinuclear complexes reported in the present work. As such these complexes can be considered as the corresponding synthetic intermediates used by first row transition metals to generate oligomers or coordination polymers.

Supporting Information content. Additional spectroscopic, electrochemical and DFT data. X-ray crystallographic data in CIF format (CCDC # 1014664-1014667). This material is available free of charge via the Internet at http://pubs.acs.org.

Acknowledgments. This research was supported by the Spanish Ministerio de Economia y Competitividad (MINECO) through projects CTQ2011-29054-C02-02, CTQ-2013-49075-R, PRI-PIBIN-2011-1278, and by the Generalitat de Catalunya (2014SGR-409 and 2014SGR-915), and the ICIQ Foundation. The Severo Ochoa Excellence Accreditation (SEV-2013-0319) is gratefully acknowledged. L.M thanks ICIQ foundation for a PhD grant.

III

I performed the synthesis, the characterization and the reactivity experiments of all the complexes presented. X-Ray structure analyses were carried out by Dr. J. Benet-Bucholz. DFT-based studies were carried out by Dr.W.R Rahman and Prof. C. Bo.

3.6 References

(1) a) Suzuki, M.; Furutachi, H.; Ōkawa, H. *Coord. Chem. Rev.* **2000,** *200–202*, 105-129; b) Gavrilova, A. L.; Bosnich, B. *Chem. Rev.* **2004,** *104*, 349-384; c) Gavrilova, A. L.; Qin, C. J.; Sommer, R. D.; Rheingold, A. L.; Bosnich, B. *J. Am. Chem. Soc.* **2002,** *124*, 1714-1722; d) Incarvito, C.; Rheingold, A. L.; Gavrilova, A. L.; Qin, C. J.; Bosnich, B. *Inorg. Chem.* **2001,** *40*, 4101-4108; e) García-Antón, J.; Bofill, R.; Escriche, L.; Llobet, A.; Sala, X. *Eur. J. Inorg. Chem.* **2012,** *2012*, 4775-4789; f) Halvagar, M. R.; Neisen, B.; Tolman, W. B. *Inorg. Chem.* **2012,** *52*, 793-799; g) Halvagar, M. R.; Tolman, W. B. *Inorg. Chem.* **2013,** *52*, 8306-8308; h) York, J. T.; Llobet, A.; Cramer, C. J.; Tolman, W. B. *J. Am. Chem. Soc.* **2007,** *129*, 7990-7999.

(2) a) Cornia, A.; Gatteschi, D.; Sessoli, R. *Coord. Chem. Rev.* **2001,** *219–221*, 573-604; b) Carlin, R. L., *Magnetochemistry*; Springer-Verlag: Berlin, 1986; c) Kahn, O., *Molecular Magnetism*; Wiley: 1993; d) Kahn, O., in *Modular Chemistry*, Michl, K. J., Ed. Kluwer Academic: Dordrecht, The Netherlands, 1997.

(3) Zhao, G.-J.; Han, K.-L. *Acc. Chem. Res.* **2011,** *45*, 404-413.

(4) a) Nieto, I.; Wooten, A. J.; Robinson, J. R.; Carroll, P. J.; Schelter, E. J.; Walsh, P. J. *Organometallics* **2013,** *32*, 7431-7439; b) Bratko, I.; Gomez, M. *Dalton Trans.* **2013,** *42*, 10664-10681.

(5) Neudeck, S.; Maji, S.; López, I.; Meyer, S.; Meyer, F.; Llobet, A. *J. Am. Chem. Soc.* **2013,** *136*, 24-27.

(6) a) Sartorel, A.; Miró, P.; Salvadori, E.; Romain, S.; Carraro, M.; Scorrano, G.; Valentin, M. D.; Llobet, A.; Bo, C.; Bonchio, M. *J. Am. Chem. Soc.* **2009,** *131*, 16051-16053; b) Gersten, S. W.; Samuels, G. J.; Meyer, T. J. *J. Am. Chem. Soc.* **1982,** *104*, 4029-4030; c) Sens, C.; Romero, I.; Rodríguez, M.; Llobet, A.; Parella, T.; Benet-Buchholz, J. *J. Am. Chem. Soc.* **2004,** *126*, 7798-7799; d) Solomon, E.

I.; Chen, P.; Metz, M.; Lee, S.-K.; Palmer, A. E. *Angew. Chem. Int. Ed.* **2001,** *40*, 4570-4590; e) Thauer, R. K.; Klein, A. R.; Hartmann, G. C. *Chem. Rev.* **1996,** *96*, 3031-3042; f) Howard, J. B.; Rees, D. C. *Chem. Rev.* **1996,** *96*, 2965-2982; g) Wallar, B. J.; Lipscomb, J. D. *Chem. Rev.* **1996,** *96*, 2625-2658; h) Belle, C.; Pierre, J.-L. *Eur. J. Inorg. Chem.* **2003,** *2003*, 4137-4146.

(7) a) Nugent, J. H. A.; Ball, R. J.; Evans, M. C. W. *Biochim. Biophys. Acta* **2004,** *1655*, 217-221; b) Wilcox, D. E. *Chem. Rev.* **1996,** *96*, 2435-2458; c) Kitajima, N.; Moro-oka, Y. *Chem. Rev.* **1994,** *94*, 737-757; d) Magnus, K. A.; Ton-That, H.; Carpenter, J. E. *Chem. Rev.* **1994,** *94*, 727-735; e) Solomon, E. I.; Sundaram, U. M.; Machonkin, T. E. *Chem. Rev.* **1996,** *96*, 2563-2606; f) Mirica, L. M.; Ottenwaelder, X.; Stack, T. D. P. *Chem. Rev.* **2004,** *104*, 1013-1046; g) Lewis, E. A.; Tolman, W. B. *Chem. Rev.* **2004,** *104*, 1047-1076; h) Karlin, K. D.; Kopf, M.-A., *Biomimetic Oxidations Catalyzed by Transition Metal Complexes*; Imperial College Press: London, UK, 2000; i) Schindler, S. *Eur. J. Inorg. Chem.* **2000,** *2000*, 2311-2326; j) Nugent, J. H. A.; Rich, A. M.; Evans, M. C. W. *Biochim. Biophys. Acta* **2001,** *1503*, 138-146; k) Renger, G. *Biochim. Biophys. Acta* **2001,** *1503*, 210-228.

(8) Cramer, C. J.; Tolman, W. B. *Acc. Chem. Res.* **2007,** *40*, 601-608.

(9) a) Roeser, S.; Maji, S.; Benet-Buchholz, J.; Pons, J.; Llobet, A. *Eur. J. Inorg. Chem.* **2013,** *2013*, 232-240; b) Sens, C.; Rodríguez, M.; Romero, I.; Llobet, A.; Parella, T.; Sullivan, B. P.; Benet-Buchholz, J. *Inorg. Chem.* **2003,** *42*, 2040-2048.

(10) a) Planas, N.; Christian, G.; Roeser, S.; Mas-Marzá, E.; Kollipara, M.-R.; Benet-Buchholz, J.; Maseras, F.; Llobet, A. *Inorg. Chem.* **2012,** *51*, 1889-1901; b) Planas, N.; Christian, G. J.; Mas-Marzá, E.; Sala, X.; Fontrodona, X.; Maseras, F.; Llobet, A. *Chem. Eur. J.* **2010,** *16*, 7965-7968.

(11) a) Sens, C.; Rodríguez, M.; Romero, I.; Llobet, A.; Parella, T.; Benet-Buchholz, J. *Inorg. Chem.* **2003,** *42*, 8385-8394; b) Roeser, S.; Farràs, P.; Bozoglian, F.; Martínez-Belmonte, M.; Benet-Buchholz, J.; Llobet, A. *ChemSusChem* **2011,** *4*, 197-207.

(12) a) Schneider, B.; Demeshko, S.; Neudeck, S.; Dechert, S.; Meyer, F. *Inorg. Chem.* **2013,** *52*, 13230-13237; b) Kim, S. B.; Pike, R. D.; Sweigart, D. A. *Acc. Chem. Res.* **2013,** *46*, 2485-2497; c) Horike, S.; Umeyama, D.; Kitagawa, S. *Acc. Chem. Res.* **2013,** *46*, 2376-2384; d) Leong, W. L.; Vittal, J. J. *Chem. Rev.* **2010,** *111*, 688-764.

(13) Data collection: APEX II, versions v2009.1-02 and v2013.4-1; Bruker AXS Inc.: Madison, WI, 2007.

(14) Data collection: APEX II, versions v2009.1-02 and v2013.4-1; Bruker AXS Inc.: Madison, WI, 2007.

(15) Data collection: APEX II, versions v2009.1-02 and v2013.4-1; Bruker AXS Inc.: Madison, WI, 2007.

(16) Blessing, R. *Acta Crystallogr. Sect. A* **1995,** *51*, 33-38.

(17) Sheldrick, G. *Acta Crystallogr. Sect. A* **2008,** *64*, 112-122.

(18) a) te Velde, G.; Bickelhaupt, F. M.; Baerends, E. J.; Fonseca Guerra, C.; van Gisbergen, S. J. A.; Snijders, J. G.; Ziegler, T. *J. Comput. Chem.* **2001,** *22*, 931-967; b) Fonseca Guerra, C.; Snijders, J. G.; te Velde, G.; Baerends, E. J. *Theor. Chem. Acc.* **1998,** *99*, 391-403.

(19) Becke, A. D. *Phys. Rev. A* **1988,** *38*, 3098-3100.

(20) a) Perdew, J. P. *Phys. Rev. B* **1986,** *33*, 8822-8824; b) Perdew, J. P. *Phys. Rev. B* **1986,** *34*, 7406-7406.

(21) a) Lenthe, E. v.; Baerends, E. J.; Snijders, J. G. *J. Chem. Phys* **1993,** *99*, 4597-4610; b) van Lenthe, E.; Baerends, E. J.; Snijders, J. G. *J. Chem. Phys* **1994,** *101*, 9783-9792.

(22) Grimme, S. *J. Comput. Chem.* **2006,** *27*, 1787-1799.

(23) Teixidor, F.; Garcia, R.; Pons, J.; Casabó, J. *Polyhedron* **1988,** *7*, 43-47.

(24) a) Maji, S.; López, I.; Bozoglian, F.; Benet-Buchholz, J.; Llobet, A. *Inorg. Chem.* **2013,** *52*, 3591-3593; b) Farràs, P.; Maji, S.; Benet-Buchholz, J.; Llobet, A. *Chem. Eur. J.* **2013,** *19*, 7162-7172; c) Romero, I.; Rodriguez, M.; Llobet, A.; Collomb-Dunand-Sauthier, M.-N.; Deronzier, A.; Parella, T.; Stoeckli-Evans, H. *J. Chem. Soc., Dalton Trans.* **2000**, 1689-1694.

(25) a) Solans, X.; Font-Altaba, M.; Briansó, J. L.; Llobet, A.; Teixidor, F.; Casabó, J. *Acta Crystallogr. Sect. C* **1983,** *39*, 1512-1514; b) Gao, C.-Y.; Qiao, X.; Ma, Z.-Y.; Wang, Z.-G.; Lu, J.; Tian, J.-L.; Xu, J.-Y.; Yan, S.-P. *Dalton Trans.* **2012,** *41*, 12220-12232; c) Trivedi, M.; Pandey, D. S.; Rath, N. P. *Inorg. Chim. Acta* **2009,** *362*, 284-290.

(26) a) Haga, M.; Dodsworth, E. S.; Lever, A. B. P. *Inorg. Chem.* **1986,** *25*, 447-453; b) Wong, C.-Y.; Che, C.-M.; Chan, M. C. W.; Leung, K.-H.; Phillips, D. L.; Zhu, N. *J. Am. Chem. Soc.* **2004,** *126*, 2501-2514; c) Kannan, S.; Ramesh, R.; Liu, Y. *J. Organomet. Chem.* **2007,** *692*, 3380-3391.

(27) a) Gilbert, J. A.; Eggleston, D. S.; Murphy, W. R.; Geselowitz, D. A.; Gersten, S. W.; Hodgson, D. J.; Meyer, T. J. *J. Am. Chem. Soc.* **1985,** *107*, 3855-3864; b) Llobet, A.; Curry, M. E.; Evans, H. T.; Meyer, T. J. *Inorg. Chem.* **1989,** *28*, 3131-3137; c) López, I.; Ertem, M. Z.; Maji, S.; Benet-Buchholz, J.; Keidel, A.; Kuhlmann, U.; Hildebrandt, P.; Cramer, C. J.; Batista, V. S.; Llobet, A. *Angew. Chem. Int. Ed.* **2014,** *53*, 205-209.

(28) a) Ahmed, H. M. Y.; Coburn, N.; Dini, D.; de Jong, J. J. D.; Villani, C.; Browne, W. R.; Vos, J. G. *Inorg. Chem.* **2011,** *50*, 5861-5863; b) Halpin, Y.; Dini, D.; Younis Ahmed, H. M.; Cassidy, L.; Browne, W. R.; Vos, J. G. *Inorg. Chem.* **2010,** *49*, 2799-2807.

(29) a) Baitalik, S.; Florke, U.; Nag, K. *J. Chem. Soc., Dalton Trans.* **1999**, 719-728; b) Brietzke, T.; Mickler, W.; Kelling, A.; Schilde, U.; Krüger, H.-J.; Holdt, H.-J. *Eur. J. Inorg. Chem.* **2012,** *2012*, 4632-4643; c) Browne, W. R.; Hage, R.; Vos, J. G. *Coord. Chem. Rev.* **2006,** *250*, 1653-1668; d) D'Alessandro, D. M.; Keene, F. R. *Chem. Soc. Rev.* **2006,** *35*, 424-440; e) D'Alessandro, D. M.; Keene, F. R. *Chem. Eur. J.* **2005,** *11*, 3679-3688; f) Das, A.; Kundu, T.; Mobin, S. M.; Priego, J. L.; Jimenez-Aparicio, R.; Lahiri, G. K. *Dalton Trans.* **2013,** *42*, 13733-13746; g) Kundu, T.; Schweinfurth, D.; Sarkar, B.; Mondal, T. K.; Fiedler, J.; Mobin, S. M.; Puranik, V. G.; Kaim, W.; Lahiri, G. K. *Dalton Trans.* **2012,** *41*, 13429-13440; h) Mandal, A.; Agarwala, H.; Ray, R.; Plebst, S.; Mobin, S. M.; Priego, J. L.; Jiménez-Aparicio, R.; Kaim, W.; Lahiri, G. K. *Inorg. Chem.* **2014,** *53*, 6082-6093; i) Mondal, P.; Agarwala, H.; Jana, R. D.; Plebst, S.; Grupp, A.; Ehret, F.; Mobin, S. M.; Kaim, W.; Lahiri, G. K. *Inorg. Chem.* **2014,** *53*, 7389-7403; j) Roeser, S.; Ertem, M. Z.; Cady, C.; Lomoth, R.; Benet-Buchholz, J.; Hammarström, L.; Sarkar, B.; Kaim, W.; Cramer, C. J.; Llobet, A. *Inorg. Chem.* **2011,** *51*, 320-327.

(30) Romain, S.; Rich, J.; Sens, C.; Stoll, T.; Benet-Buchholz, J.; Llobet, A.; Rodriguez, M.; Romero, I.; Clérac, R.; Mathonière, C.; Duboc, C.; Deronzier, A.; Collomb, M.-N. l. *Inorg. Chem.* **2011,** *50*, 8427-8436.

UNIVERSITAT ROVIRA I VIRGILI
MONONUCLEAR AND HETEROTRINUCLEAR RUTHENIUM COMPLEXES: SYNTHESIS AND WATER OXIDATION ACTIVITY.
Lorenzo Mognon
Dipòsit Legal: T 1359-2015

Supporting Information for

Ru-Zn Heteropolynuclear Complexes Containing a Dinucleating Bridging Ligand: Synthesis, Structure and Isomerism

Inorg. Chem. **2014**, *53*, 12407-12415

Lorenzo Mognon,[a] Jordi Benet-Buchholz,[a] Wahidur Rahaman,[a] Carles Bo,[a,b] and Antoni Llobet[a,c]

[a] Institute of Chemical Research of Catalonia (ICIQ), Avinguda Països Catalans 16, 43007 Tarragona, Spain

[b] Departament de Química Física i Inorgànica, Universitat Rovira i Virgili, 43007 Tarragona, Spain

[c] Departament de Química, Universitat Autònoma de Barcelona, Cerdanyola del Vallès, 08193 Barcelona, Spain

Figure S1. NMR spectra (400 MHz, 298 K, d_6-dmso) for complex *out*-{[Ru(Cl)(trpy)][$ZnCl_2$](μ-bpp))}, ***out*-2**: (a) ^{1}H NMR, (b) COSY.

(a)

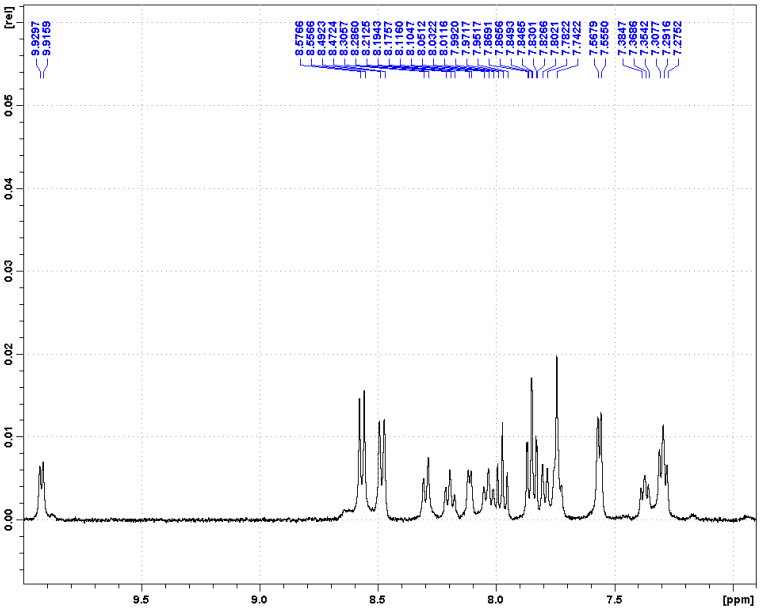

7

(b)

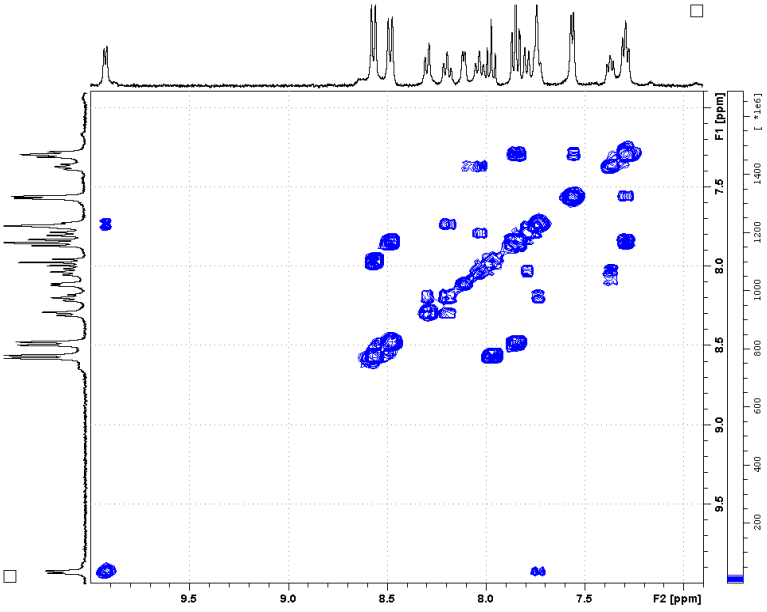

Figure S2. NMR spectra (400 MHz, 298 K, d_6-acetone) for complex *out,out*-{[Ru(Cl)(trpy)]$_2$(μ-[Zn(bpp)$_2$])}(PF$_6$)$_2$, ***out*-3**: (a) ^{1}H NMR, (b) COSY.

(a)

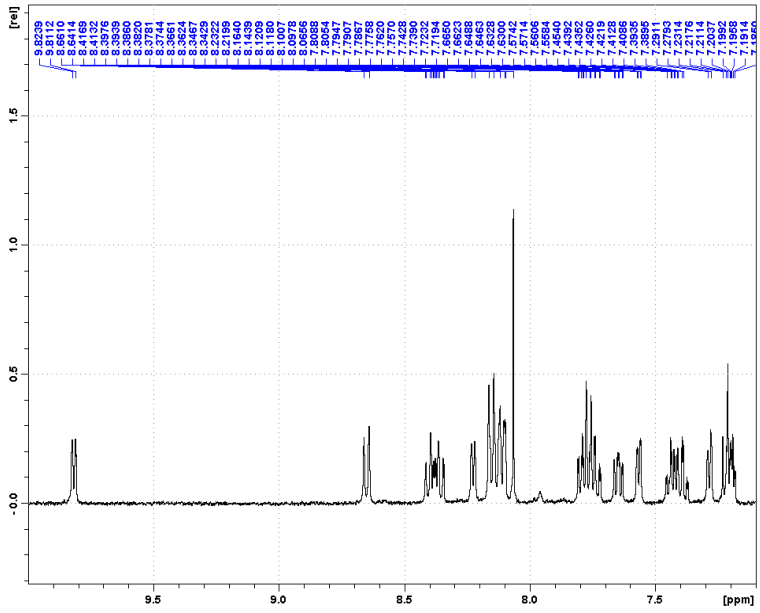

(b)

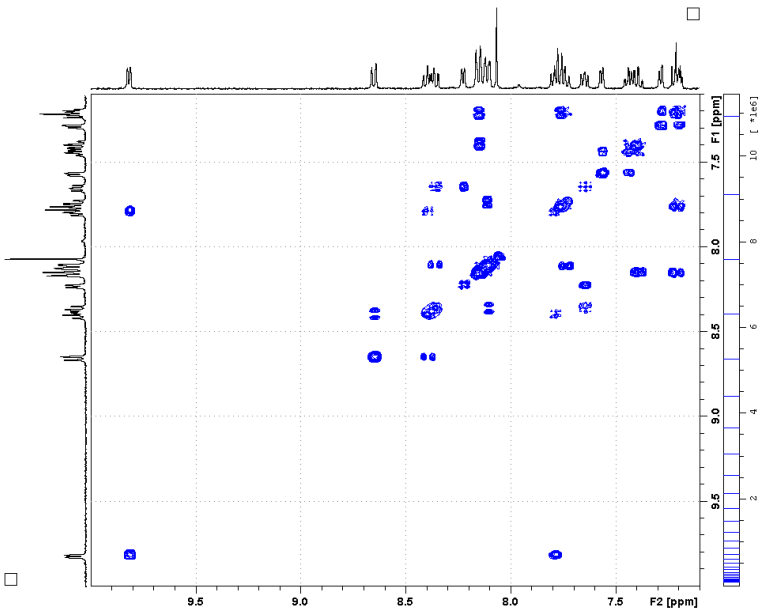

Figure S3. NMR spectra (400 MHz, 298 K, d_6-acetone) for complex *in,in*-{[Ru(Cl)(trpy)]$_2$(μ-[Zn(bpp)$_2$])}$(PF_6)_2$, ***in*-3**: (a) ^{1}H NMR, (b) COSY, (c) NOESY.

(a)

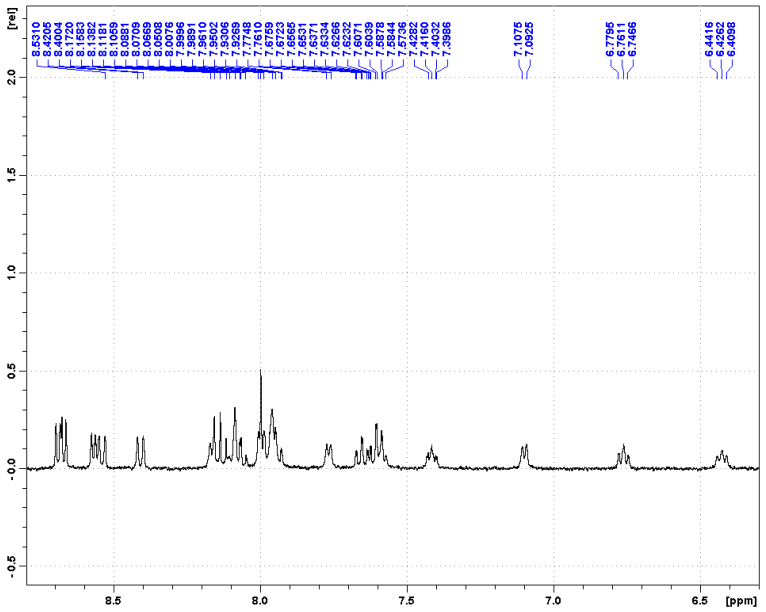

(b)

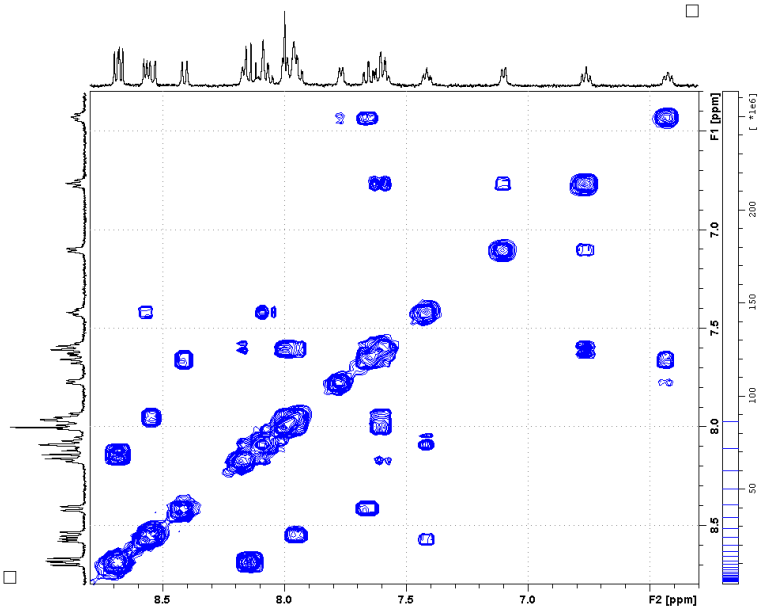

(c)

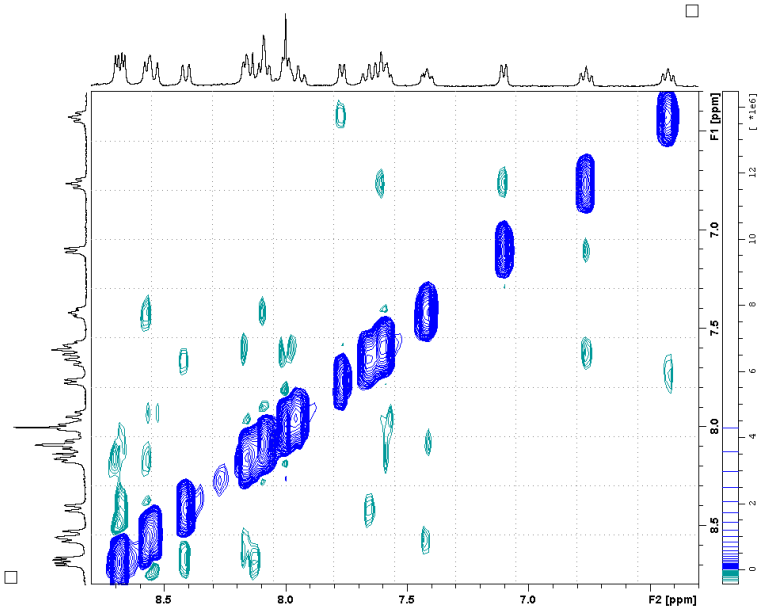

Figure S4. NMR spectra (400 MHz, 298 K, CF_3SO_3D 0.1 M in D_2O) for complex *in,in*-{[Ru^{III}(trpy)]$_2$(μ-[Zn(bpp)$_2$(H_2O)]μ-(O)}(ClO_4)]$_4$, ***in*-5**, after reduction with ZnHg: (a) ^{1}H NMR, (b) COSY. (c) ^{1}H NMR for complex *in*-[Ru(Hbpp)(H_2O)(trpy)](ClO_4)$_2$, ***in*-1**.

(a)

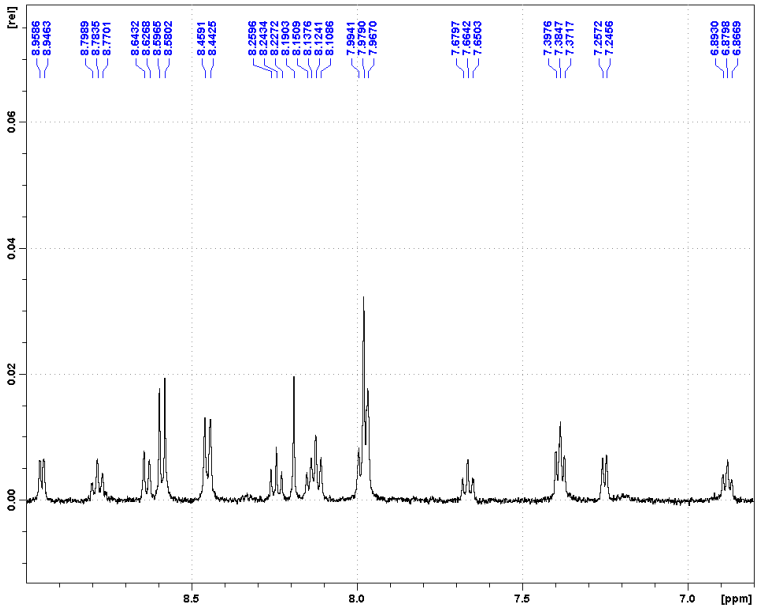

(b)

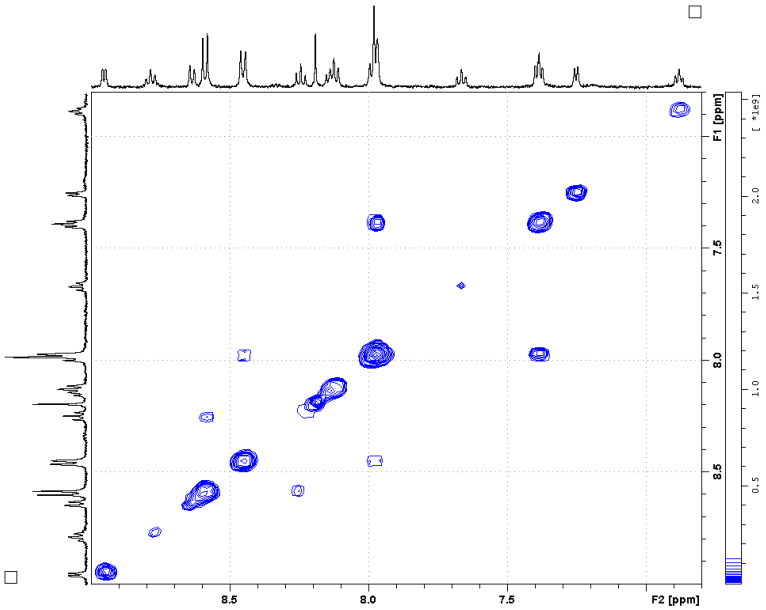

(c)

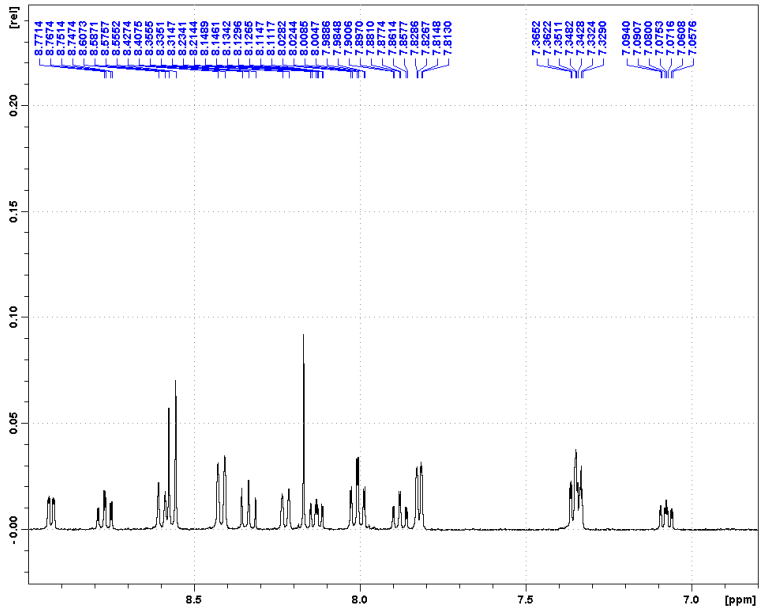

Figure S5. MALDI-MS of complex *out*-{[Ru(Cl)(trpy)][$ZnCl_2$](μ-bpp))}, ***out*-2**, in CH_2Cl_2 and the simulated cation {[Ru(Cl)(trpy)][$ZnCl_2$](μ-bpp))}$^+$.

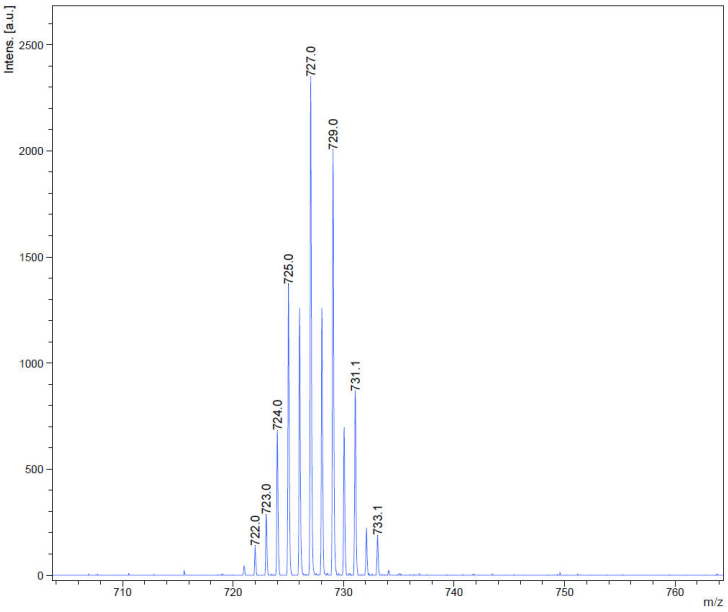

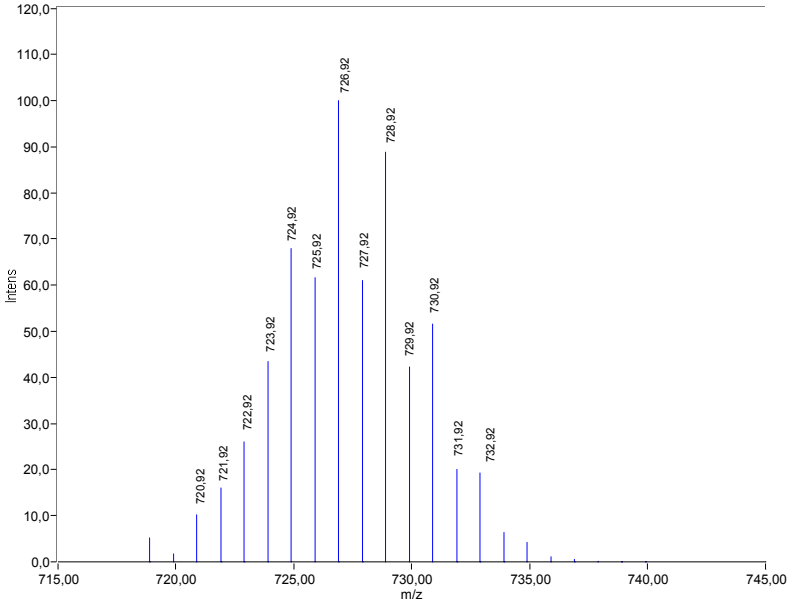

Figure S6. MALDI-MS of complex *out,out*-{[Ru(Cl)(trpy)]$_2$(μ-[Zn(bpp)$_2$])}(PF$_6$)$_2$, ***out*-3**, in acetone and the simulated cation [Ru(Cl)(Hbpp)(trpy)]$^+$.

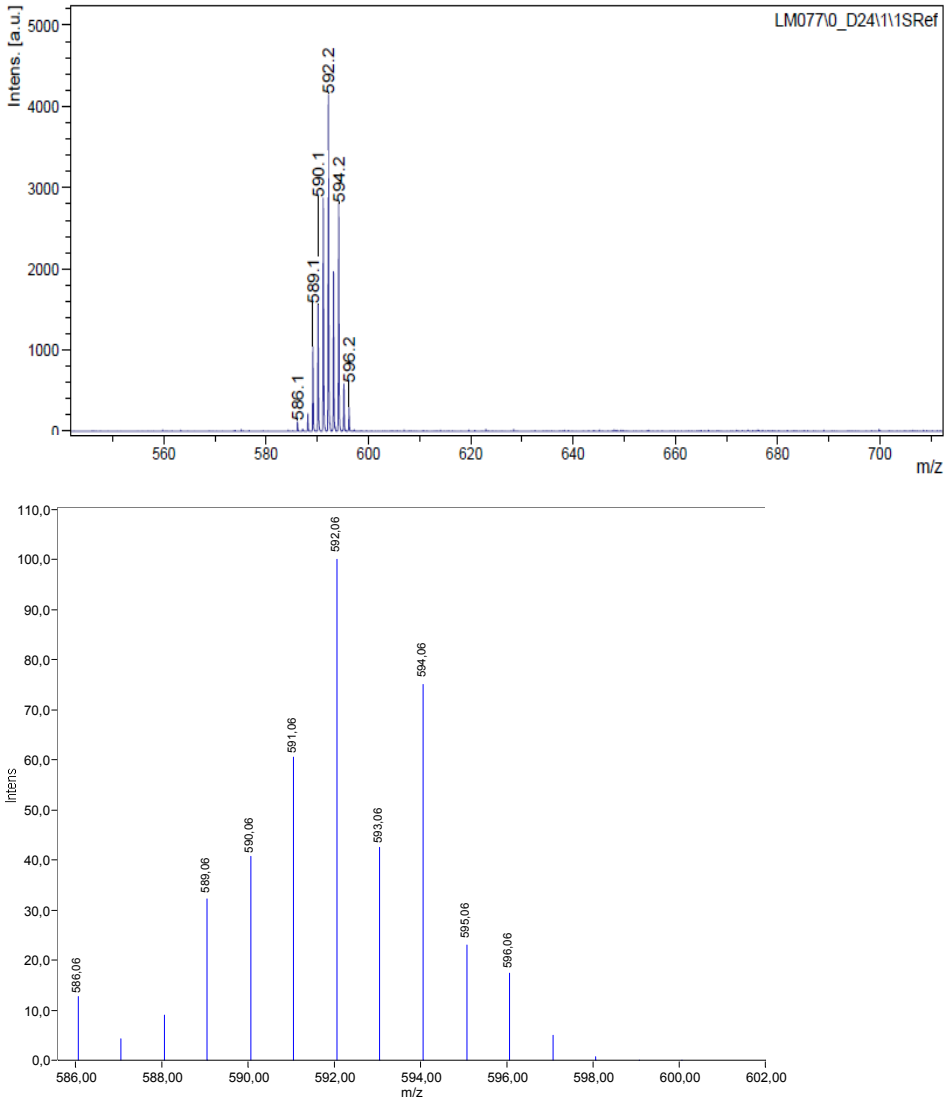

Figure S7. MALDI-MS of complex *out,out*-{[Ru (trpy)(H_2O)]$_2$(μ-[Zn(bpp)$_2$])}(ClO_4)$_4$, ***out*-4**, in H_2O and the simulated cations [Ru(bpp)(trpy)]$^+$ and [Ru(bpp)(trpy)(OH)(Na)]$^+$.

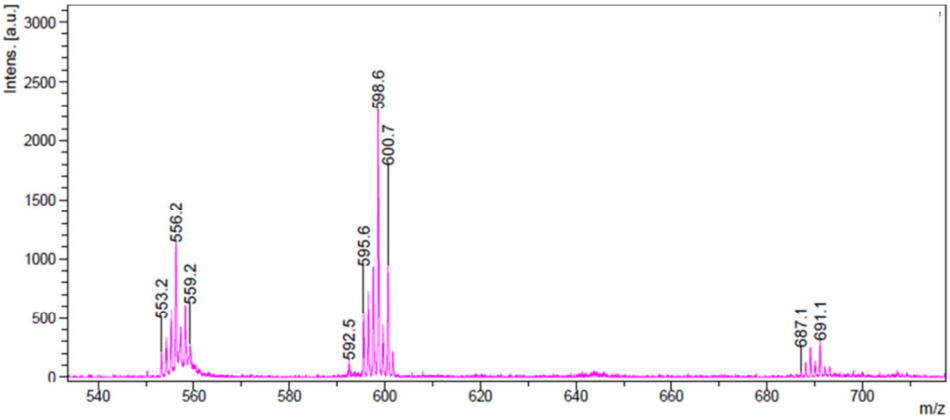

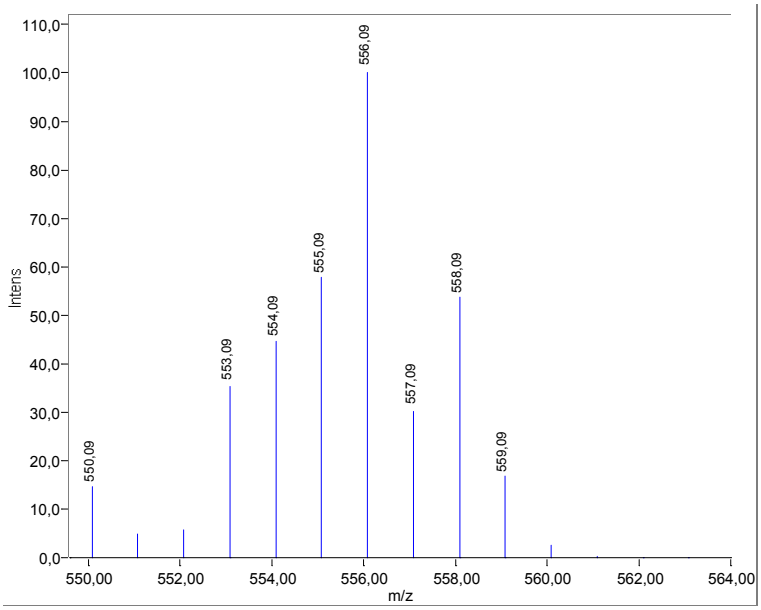

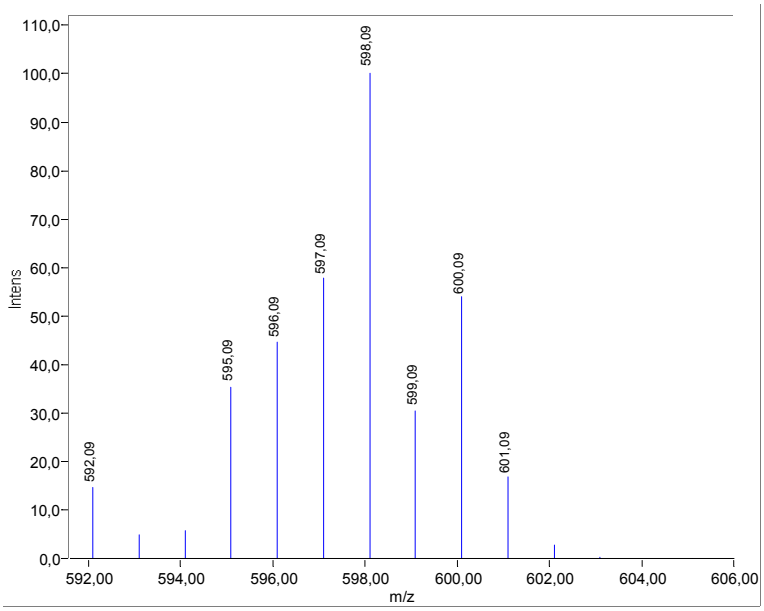
110,0
100,0
90,0
80,0
70,0
60,0
50,0
40,0
30,0
20,0
10,0
0,0
Intens
592,09
595,09
596,09
597,09
598,09
599,09
600,09
601,09
592,00
594,00
596,00
598,00
600,00
602,00
604,00
606,00
m/z

Figure S8. MALDI-MS of complex *in,in*-{[Ru(Cl)(trpy)]$_2$(μ-[Zn(bpp)$_2$])}(PF$_6$)$_2$, ***in*-3**, in acetone and the simulated cation {[Ru(Cl)(trpy)]$_2$(μ-[Zn(bpp)$_2$])}(PF$_6$)$^+$.

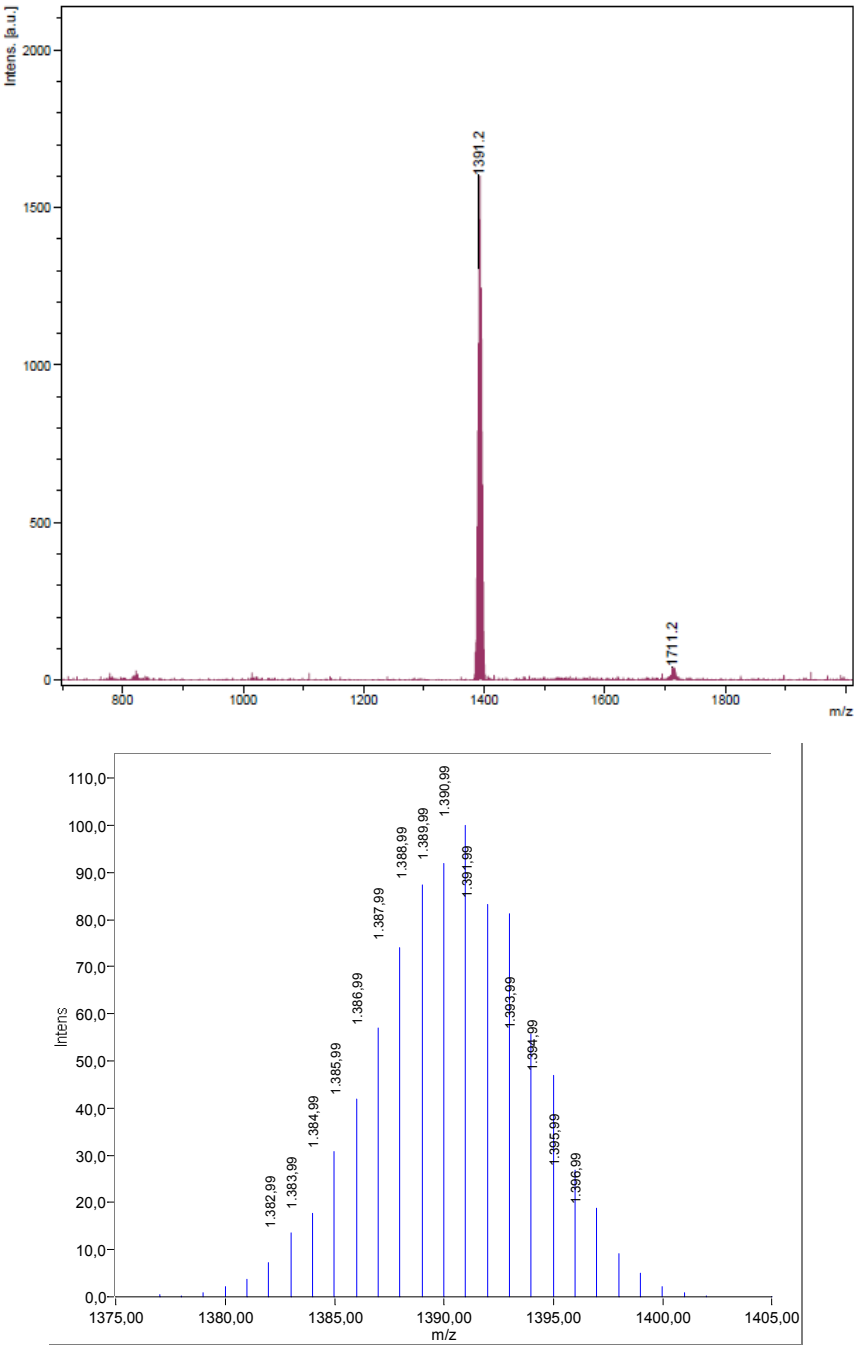

Figure S9. MALDI-MS of complex *in,in*-{[Ru (trpy)]$_2$(μ-[Zn(bpp)$_2$(H$_2$O)]μ-(O)}(ClO$_4$)$_4$, ***in*-5**, in acetone and the simulated cation [Ru(bpp)(trpy)](ClO$_4$)$^+$.

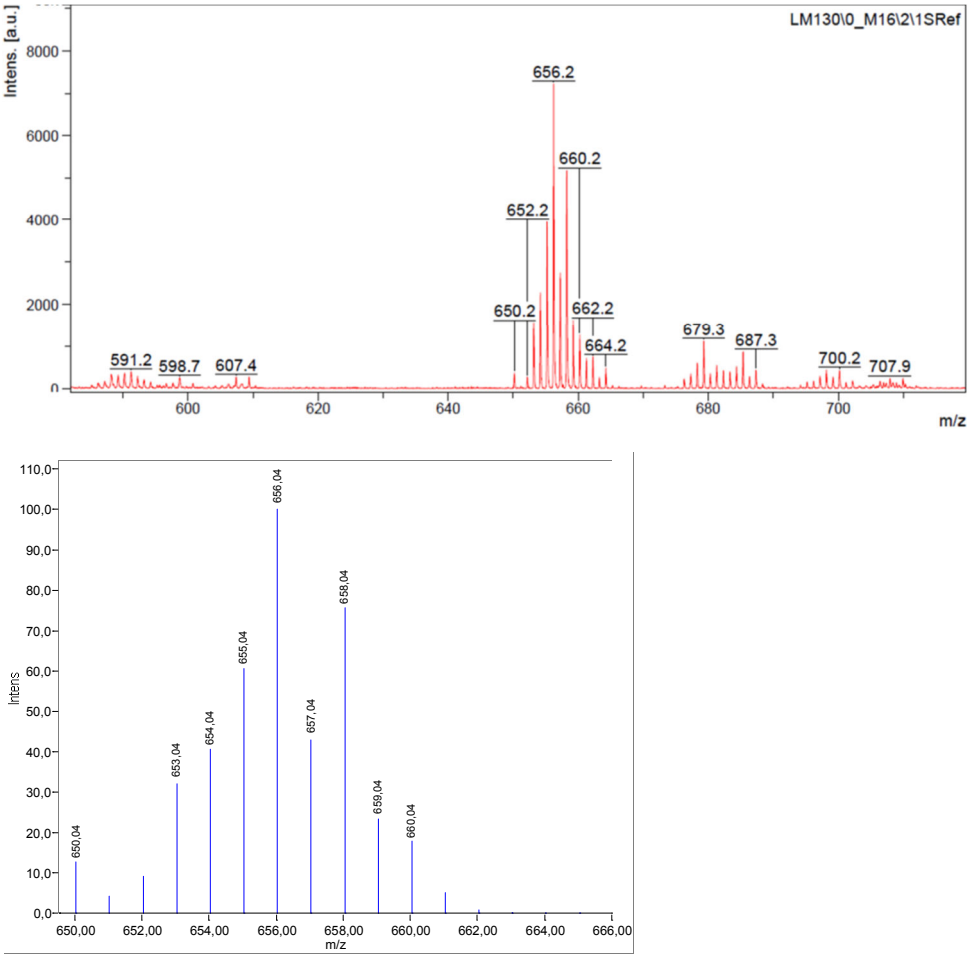

Figure S10. UV-Vis spectra in pH = 1 CF_3SO_3H for complex *in*-[Ru(Hbpp)(H_2O)(trpy)](ClO_4)$_2$, ***in*-1**.

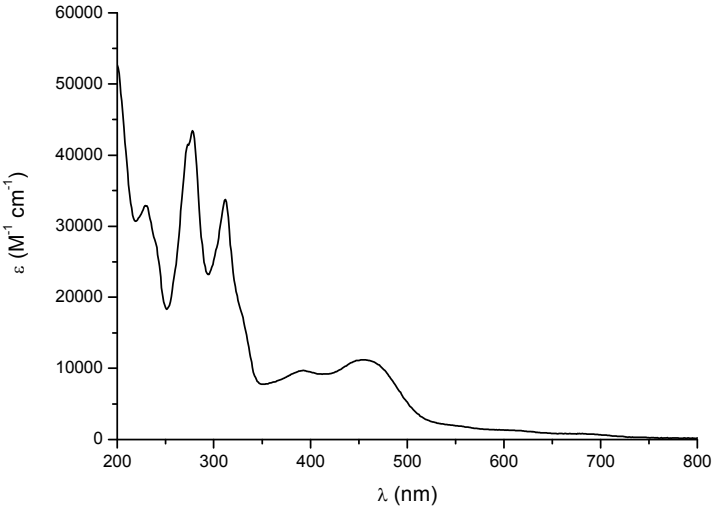

Figure S11. Uv-Vis spectra in pH = 7 phosphate buffer for complex *in*-[Ru(Hbpp)(H_2O)(trpy)](ClO_4)$_2$, ***in*-1**.

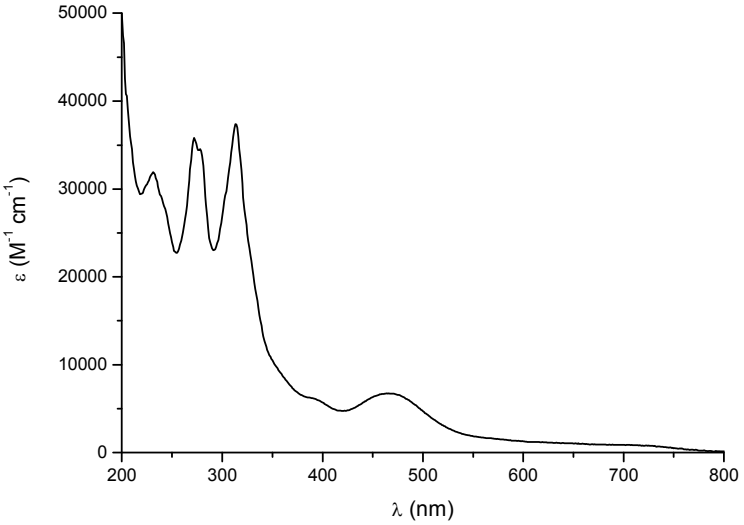

Figure S12. Cyclic voltammogram (H_2O, pH = 1 CF_3SO_3H) for complex *in*-[Ru(Hbpp)(H_2O)(trpy)](ClO_4)$_2$, ***in*-1**.

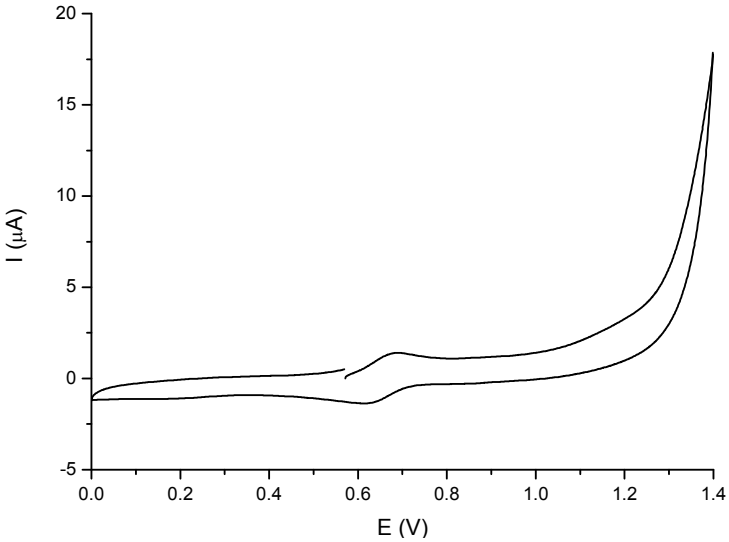

Figure S13. Cyclic voltammogram (H_2O, pH = 7 phosphate buffer) for complex *in*-[Ru(Hbpp)(H_2O)(trpy)](ClO_4)$_2$, ***in*-1**.

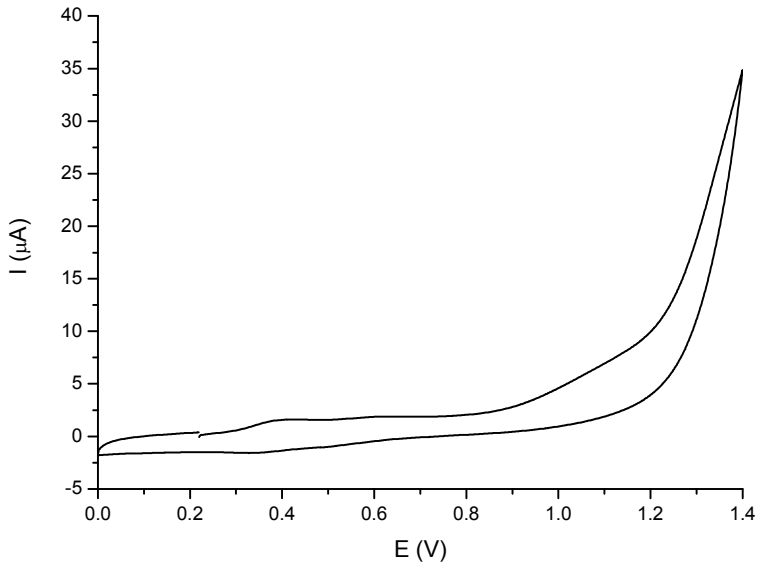

Figure S14. Left, UV-Vis spectra in DCM containing 0.1 M TBAH of ***in*-3** at oxidation states II-II, II-III and III,III. Right, Near-IR (NIR) spectrum of the III-II complex.[a]

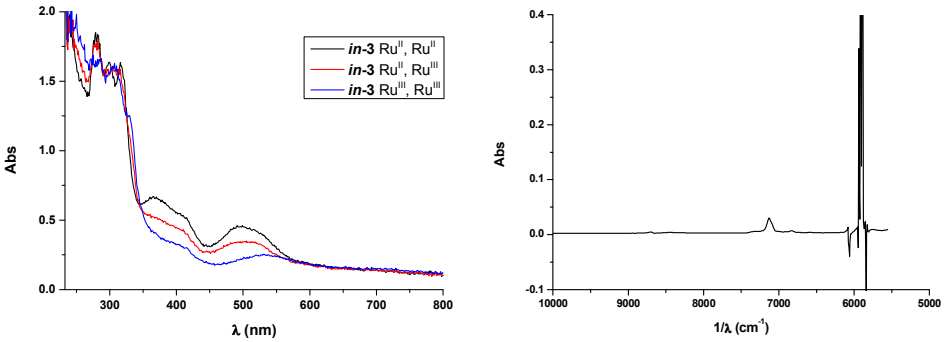

[a] Experimental details. Controlled Potential Electrolysis (CPE) were performed in a 40 mL two compartment cell (20 mL each compartment) using a Pt grid as working electrode, Ag/AgCl as reference electrode and another Pt grid as counter electrode, monitored with an Agilent UV-Vis Torlon probe with an optical path of length of 1 cm coonected to a CARY 50 Bio spectrometer. The anodic compartment contains [***in*-3**] = 0.05 mM in DCM containing 0.1 M TBAH. The NIR measurements were carried out on a Lamba 1050 PerkinElmer spectrophotometer equipped with a PMT, InGaAs and PbS detectors system, double beam optics, double monochromator and D2 and W light sources.

Figure S15. UV monitoring of a CPE of a solution of ***in*-3** in DCM containing 0.1 M TBAH. Top left, starting from a solution with OCP of 0.4 V, applying a potential of 0.71 V. Middle left, starting from a solution with OPC of 0.71 V, applying a potential of 1.00 V. Top right, CV of a solution of ***in*-3** in DCM containing 0.1 M TBAH before the applied potential. Middle left, CV after CPE at 0.71 V. Bottom left, CV after CPE at 1.00 V. The CV always starts at the open circuit potential.

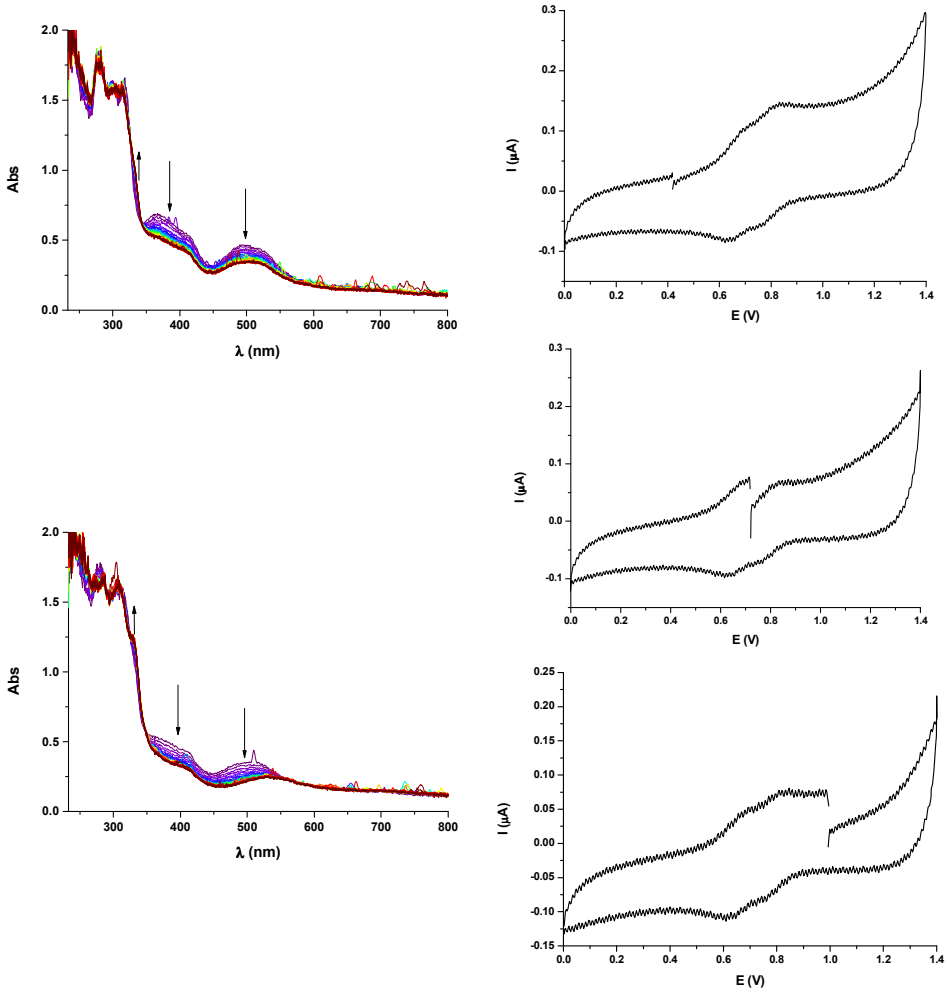

Figure S16. Left, DFT computed UV-Vis spectra for *in*-**3** and *out*-**3.**[a] Right, highest occupied and lowest unoccupied KS energy levels for *in*-**3**.

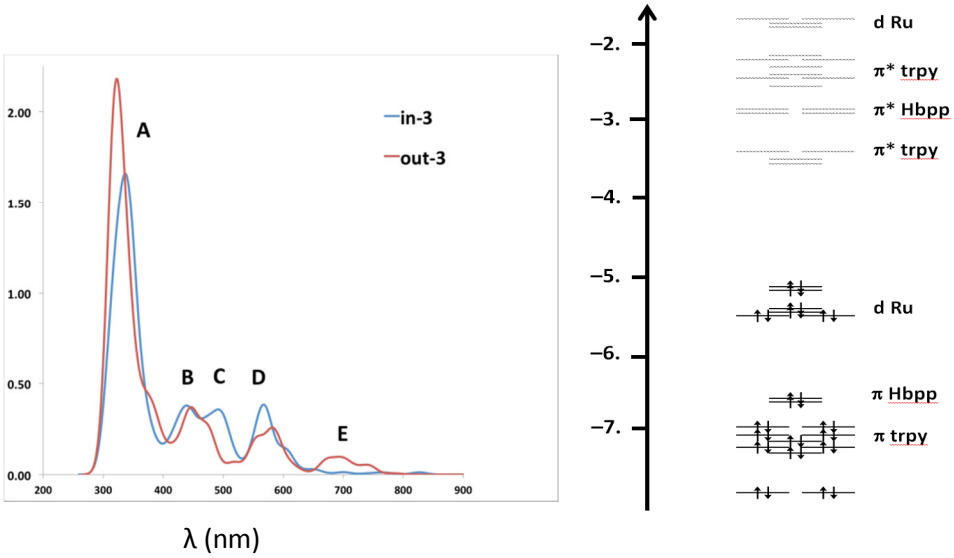

[a] UV-Vis absorption spectra were computed on the basis of TDDFT methods by including the 200 lowest singlet-singlet excitations, and using the same BP86 exchange-correlation functional used in geometry optimizations. Dichloromethane solvent effects were included by means of COSMO model. The computed spectra were simulated by fixed height sum of Gaussian functions with a peak width of 30 nm. The computed spectra of both *in*-**3** and *out*-**3** show basically five bands. The most intense band A arise from ligand-to-ligand transitions, from occupied π trpy and HBpp orbitals to their π* levels, either within the same ligand or across ligands. Bands B, C, D and E correspond all to metal-to-ligand charge transfer bands, roughly reflecting the orbitals energy ordering as plotted in the right hand side of Figure S16. Transitions in band B correspond to excitations from HOMO and HOMO–1 to the highest π* trpy orbitals; band C is build up from excitations from HOMO–2/5 to π* Hbpp orbitals, while band D is from HOMO and HOMO–1 to Hbpp too. Finally, band E corresponds to HOMOs LUMOs transitions.

Table S1a: Crystal data for compounds ***out*-2** and ***out*-3**.

Compound	***out*-2**	***out*-3**
Formula	$C_{68}H_{74}Cl_6N_{18}O_7Ru_2Zn_2$	$C_{112}H_{89.2}Cl_4F_{24}N_{28}O_{4.6}P_4Ru_4Zn_2$
Solvents	3 DMF + 3 H_2O	4.6 x H_2O
Formula weight	1801.03	3157.61
Crystal size (mm^3)	0.30 x 0.30 x 0.10	0.30 x 0.30 x 0.30
Crystal color	brown	black
Temp (K)	100	100
Crystal system	monoclinic	triclinic
Space group	$P2_1/n$	$P\bar{1}$
A (Å)	17.2373(15)	13.3567(6)
B (Å)	24.186(2)	19.7145(8)
C (Å)	18.1604(17)	23.8971(12)
α (deg)	90	79.927(2)
β (deg)	95.312(3)	82.089(2)
γ (deg)	90	75.313(2)
V ($Å^3$)	7538.5(12)	5964.3(5)
Z	4	2
ρ (g/cm^3)	1.587	1.758
μ (mm^{-1})	1.299	1.137
θ_{max} (°)	36.31	33.19
Reflec. measured	168541	132718
Unique reflections	19982 [R_{int} = 0.0532]	30739 [R_{int} = 0.0582]
Absorpt. correct.	SADABS (Bruker)	SADABS (Bruker)
Trans. min/max	0.6967/0.8811	0.7267/0.7267
Parameters	1010	1666
R1/wR2 [I>2σ(I)]	0.0537/0.1286	0.0589/0.1545
R1/wR2 [all data]	0.1009/0.1586	0.0926/0.1765
Goodness-of-fit (F^2)	1.035	1.068
Peak/hole ($e/Å^3$)	2.259/-1.526	3.778/-1.599

Table S1b: Crystal data for compounds ***in*-3 and *in*-5**.

Compound	***in*-3**	***in*-5**
Formula	$C_{60}H_{50}Cl_2F_2N_{14}O_2Ru_2Zn_1$	$C_{56}H_{45}Cl_4N_{14}O_{19.5}Ru_2Zn_1$
Solvents	1 Methanol + 1 Acetone	1 ½ H_2O
Formula weight	1627.49	1635.37
Crystal size (mm^3)	0.30 x 0.10 x 0.10	0.30 x 0.05 x 0.02
Crystal color	black	black
Temp (K)	100	100
Crystal system	triclinic	monoclinic
Space group	$P\bar{1}$	$P2_1/c$
A (Å)	13.7560(11)	21.4941(6)
B (Å)	15.4808(12)	12.5290(3)
C (Å)	16.5001(13)	24.7237(7)
α (deg)	95.233(3)	90
β (deg)	108.230(3)	113.6780(10)
γ (deg)	99.382(3)	90
V ($Å^3$)	3254.6(4)	6097.6(3)
Z	2	4
ρ (g/cm^3)	1.661	1.781
μ (mm^{-1})	1.044	1.144
θ_{max} (°)	28.15	28.027
Reflec. measured	37394	41229
Unique reflections	9235 [R_{int} = 0.0658]	10408 [R_{int}=0.0467]
Absorpt. correct.	SADABS (Bruker)	SADABS (Bruker)
Trans. min/max	0.7447/0.9028	0.91/1.00
Parameters	940	1045
R1/wR2 [I>2σ(I)]	0.0788/0.2055	0.0519/0.1489
R1/wR2 [all data]	0.1442/0.2451	0.0824/0.1741
Goodness-of-fit (F^2)	1.054	1.066
Peak/hole ($e/Å^3$)	4.006/-1.953	2.334/-1.451

Table S2. DFT Data. Cartesian Coordinates

out,out-3

C	5.467451404	17.653635454	7.649211235
H	4.647649062	16.937108513	7.650925928
C	5.543508758	18.666937877	8.596819021
H	4.763171806	18.752292297	9.352350462
C	6.609108621	19.570881054	8.543664785
H	6.689317597	20.384934658	9.263916589
C	7.556934219	19.425983025	7.536726265
H	8.389599033	20.123086073	7.460649950
C	7.423625393	18.400869655	6.593315849
C	8.312069666	18.235076499	5.440977941
C	9.363119379	19.078140222	5.067673668
H	9.643604115	19.919679073	5.698206279
C	10.009334085	18.867099047	3.848858860
H	10.808982087	19.535747799	3.533060235
C	9.582380465	17.840275868	3.003949773
H	10.027222477	17.721070098	2.017677329
C	8.540072530	17.004878527	3.414134003
C	7.903866492	15.944599203	2.627015863
C	8.349155478	15.532380344	1.365616158
H	9.218541509	16.011613848	0.918434506
C	7.670602080	14.527961416	0.681777376
H	8.002964245	14.209416989	-0.306185966
C	6.547541170	13.948898513	1.279963001
H	5.975820561	13.168385901	0.778776033
C	6.143310077	14.397851551	2.532332514

H	5.259499876	13.988537298	3.019721441
C	3.208301005	15.804722831	5.106876961
H	3.229657621	16.804917809	4.671859134
C	2.026076204	15.109058435	5.334448154
H	1.075512865	15.579516285	5.084915865
C	2.078839757	13.818384459	5.871554572
H	1.166137620	13.251445069	6.054584447
C	3.322976083	13.270667103	6.168531390
H	3.407554929	12.270295613	6.591034316
C	4.481022743	14.019157724	5.923316629
C	5.823291726	13.556450020	6.200483232
C	6.329915045	12.310205437	6.587472537
H	5.773446300	11.399847195	6.775471736
C	7.709363006	12.498979884	6.643773833
C	8.796730518	11.568291569	6.891889534
C	8.624869962	10.181290860	7.032060051
H	7.624659330	9.753024288	6.998390409
C	9.742187798	9.368705990	7.178443590
H	9.623929998	8.288431717	7.269145332
C	11.019871717	9.945259010	7.191046698
H	11.917821301	9.336929020	7.286850199
C	11.124366919	11.324846136	7.065317111
H	12.092157681	11.825557108	7.071953477
C	11.130089176	14.260342152	3.767221172
H	10.385260314	13.500552603	3.531951387
C	12.034222922	14.710058010	2.813247241
H	12.018726843	14.292876089	1.807623837

C	12.961549232	15.693520203	3.184111524
H	13.689265261	16.065360983	2.462029053
C	12.959691990	16.181513554	4.484867913
H	13.684393837	16.930063867	4.800281487
C	12.031692888	15.673781649	5.408850218
C	11.999940923	16.043570992	6.813271530
C	12.731130097	16.985338472	7.534322421
H	13.463990440	17.689751388	7.159478436
C	12.331541761	16.794160145	8.862173135
C	12.739011225	17.419136001	10.101432623
C	13.572526531	18.541994447	10.180956581
H	13.956464576	18.993771932	9.267221762
C	13.895810185	19.066626003	11.428440386
H	14.544528852	19.938502553	11.511400283
C	13.371564383	18.451381171	12.570161155
H	13.597437202	18.825281952	13.568234142
C	12.550609486	17.337678932	12.432105444
H	12.129712220	16.805610003	13.286455418
C	13.861335293	13.832313314	10.661731827
H	14.206727790	14.863216448	10.726063075
C	14.761579675	12.775484978	10.585098276
H	15.831722554	12.980403616	10.580762745
C	14.269967682	11.467726344	10.536454608
H	14.950453538	10.617488781	10.492320978
C	12.892543851	11.270070225	10.562480567
H	12.481148852	10.262241864	10.542226474
C	12.028566205	12.368907946	10.638077281

C	10.568008749	12.259517437	10.698015666
C	9.821278069	11.083464126	10.809215935
H	10.319017872	10.115709863	10.830180019
C	8.434167763	11.164093205	10.951338260
H	7.843484521	10.255070484	11.057229678
C	7.814860422	12.412307561	11.028478809
H	6.744465633	12.482454972	11.212021173
C	8.592673463	13.570249436	10.931959721
C	8.144747192	14.947126440	11.152399684
C	6.821300816	15.296611235	11.443648448
H	6.051881412	14.526577613	11.460573955
C	6.501666619	16.615948542	11.745251721
H	5.479066207	16.890446865	12.003824558
C	7.521173292	17.572995922	11.733360100
H	7.325423330	18.614946510	11.984820554
C	8.815485361	17.178848630	11.417392838
H	9.638126921	17.892092068	11.407726524
N	6.376930332	17.505414183	6.656949336
N	7.964217984	17.181329558	4.642079822
N	6.795679461	15.371169602	3.210115490
N	4.429954038	15.281259087	5.388767098
N	6.850645049	14.450173268	6.027161594
N	8.010265779	13.802119669	6.318988860
N	10.044385775	12.118384174	6.920600842
N	11.125434075	14.727223078	5.031593163
N	11.189208030	15.334085342	7.670142315
N	11.408745996	15.780341042	8.936296209

N	12.229857560	16.812089487	11.221005677
N	12.519469071	13.655039665	10.685337114
N	9.937688854	13.473575944	10.705366464
N	9.144147946	15.896870246	11.130769344
Ru	6.295249058	16.220446939	5.039639843
Ru	11.036058826	15.094893393	10.887578875
Zn	9.960069936	14.149364569	6.623202106
Cl	5.209205915	17.966040467	3.833838775
Cl	11.027139588	14.627969079	13.225491741

in, out-3

C	-2.605870722	-1.973304199	-2.354293185
H	-2.246203330	-1.014056847	-2.724054936
C	-2.557520980	-3.118537476	-3.141612252
H	-2.177329348	-3.053223916	-4.160651459
C	-3.013684670	-4.330786327	-2.614470072
H	-2.992291412	-5.243808459	-3.209120810
C	-3.514287664	-4.345373887	-1.316093480
H	-3.893145709	-5.269785610	-0.883332579
C	-3.564566016	-3.161109057	-0.572155992
C	-4.151294970	-3.065144964	0.766919664
C	-4.613815834	-4.114204072	1.566458494
H	-4.547794647	-5.144066585	1.220688024
C	-5.151481779	-3.829148212	2.823562724
H	-5.510205798	-4.637784354	3.458425168
C	-5.220191104	-2.507986419	3.270912084
H	-5.626523556	-2.284078900	4.255295413

C	-4.752554466	-1.481082301	2.445885811
C	-4.762519859	-0.043391589	2.726531783
C	-5.346157148	0.523328402	3.865019164
H	-5.785355952	-0.121531479	4.624142512
C	-5.380881639	1.906086793	4.013834360
H	-5.840715167	2.355589823	4.893463673
C	-4.829767341	2.702090960	3.005487340
H	-4.852698772	3.789546529	3.067998552
C	-4.246815283	2.089430253	1.902330610
H	-3.806344096	2.672332827	1.095279708
N	-3.102081269	-1.969056627	-1.093459469
N	-4.235546655	-1.775692293	1.214361057
N	-4.193184907	0.745335761	1.747692831
Ru	-3.431048227	-0.329775875	0.140448935
C	-6.268689355	-0.215004650	-1.083758711
H	-6.461279310	-1.000915035	-0.354864444
C	-7.268692842	0.231389826	-1.939403099
H	-8.261754401	-0.211989378	-1.879666399
C	-6.975145401	1.243971204	-2.859063279
H	-7.739108567	1.614173279	-3.542490175
C	-5.689417052	1.773583909	-2.886054567
H	-5.424258606	2.564328505	-3.586634976
C	-4.716791524	1.290518027	-2.001433626
C	-3.354239710	1.775777951	-1.926791999
C	-2.573203898	2.761400934	-2.564569996
H	-2.871930682	3.434764845	-3.359373102
C	-1.328315485	2.681073024	-1.926631100

C	-0.076456535	3.425327508	-2.031788755
C	0.140030472	4.470568941	-2.939782077
H	-0.640258890	4.753375133	-3.645184639
C	1.357357018	5.146551981	-2.912585059
H	1.541985298	5.970732217	-3.602249478
C	2.332031043	4.762552328	-1.987551403
H	3.291075907	5.275020989	-1.927568282
C	2.049887419	3.702893695	-1.126062980
H	2.777794745	3.363525714	-0.387822119
N	-5.009770663	0.288687505	-1.096264424
N	-2.593607061	1.159657220	-0.975263437
N	-1.371306178	1.701924375	-0.974969055
N	0.879667226	3.045449867	-1.141136511
C	-0.942874296	3.779868181	2.152275631
H	-1.672428907	3.928099870	1.356685444
C	-0.944374415	4.574609283	3.291407494
H	-1.680999196	5.368026675	3.407441817
C	0.026884625	4.331493628	4.271928273
H	0.054496871	4.930264839	5.182641020
C	0.967644752	3.331270925	4.066452096
H	1.744884519	3.138614209	4.803543989
C	0.924232155	2.577909700	2.880673637
C	1.910264111	1.568832559	2.536672441
C	3.000115231	1.087697885	3.260202657
H	3.304058865	1.355848980	4.264634505
C	3.619776262	0.183545080	2.392754903
C	4.805474438	-0.633880674	2.519262311

C	5.581307873	-0.722543949	3.682589513
H	5.295156191	-0.151888920	4.565002296
C	6.704363295	-1.543238109	3.694848431
H	7.319237194	-1.626263763	4.590934315
C	7.025038808	-2.258603611	2.536020897
H	7.894364725	-2.914007856	2.497561241
C	6.219940718	-2.132426918	1.409774078
H	6.421158560	-2.662529927	0.477746802
N	-0.044460367	2.798737850	1.952327695
N	1.875587687	0.977693100	1.294488950
N	2.931759788	0.129072864	1.205908213
N	5.120581440	-1.335208552	1.383410075
C	5.770547065	1.291515000	-0.758871247
H	6.176806517	1.012261499	0.212184717
C	6.330656014	2.320902455	-1.506329225
H	7.190158091	2.862999349	-1.112983696
C	5.791090496	2.620685395	-2.761592438
H	6.220370713	3.409198264	-3.379508954
C	4.702519732	1.882128542	-3.215088087
H	4.266857097	2.087886461	-4.191365509
C	4.172215631	0.857916573	-2.421994024
C	3.046795177	0.009966788	-2.823531213
C	2.396016021	0.007491479	-4.060623324
H	2.677327712	0.720486400	-4.833193116
C	1.418492123	-0.956674557	-4.315378481
H	0.921612695	-0.982511058	-5.284325447
C	1.127659335	-1.924722831	-3.351495323

H	0.425964659	-2.726827064	-3.569605244
C	1.786553198	-1.888718823	-2.119535073
C	1.677270720	-2.862954218	-1.030379611
C	0.800099050	-3.952052576	-1.039158576
H	0.145909883	-4.107498679	-1.895378368
C	0.777245247	-4.835352685	0.035126579
H	0.109525441	-5.696546059	0.029676829
C	1.633693582	-4.603363304	1.115090190
H	1.654103729	-5.267863247	1.978239423
C	2.490341364	-3.510157547	1.073303631
H	3.186764360	-3.306428134	1.884854732
N	4.712824695	0.561850799	-1.188257017
N	2.687536808	-0.892867327	-1.860294622
N	2.531918089	-2.650144514	0.028910366
Ru	3.818347478	-1.062995382	-0.266279583
Zn	0.136258009	1.484758978	0.340076261
Cl	-1.261360466	-0.549447616	1.221681538
Cl	5.178079522	-2.496984005	-1.607417183

in,in-3

Ru	11.00564498	7.52591656	4.15885008
Ru	10.04582658	14.11966483	3.55444983
Zn	8.27204865	10.43005562	2.97311326
Cl	9.73891514	9.28184758	5.22231808
Cl	10.33889243	12.22368574	2.08662655
N	11.59318520	13.45837738	4.76590259
N	11.54461179	15.15577738	2.82469265

III

N	9.08461455	15.19152853	2.05795015
N	9.43540447	15.44595055	5.05962066
N	8.45555419	13.14039756	4.41339620
N	7.84983737	11.97158556	4.17263057
N	6.44175878	9.73193061	3.99457600
N	7.44359478	10.62163799	0.94930402
N	9.20600059	8.94379436	2.01171633
N	10.12475823	8.03807812	2.37004820
N	11.90264582	6.20545786	2.80143740
N	9.68426141	6.08957252	4.86817409
N	11.93478972	6.94345749	5.78530165
N	12.68936874	8.73287039	4.08802410
C	11.53133374	12.55567113	5.77254320
H	10.58228145	12.03591473	5.89424911
C	12.61598558	12.28392153	6.60084708
H	12.49941000	11.55914972	7.40552952
C	13.82489153	12.94980165	6.38287280
H	14.68537558	12.77227032	7.02760281
C	13.91487972	13.84749958	5.32192743
H	14.84692071	14.37296543	5.12101978
C	12.79564847	14.08832759	4.51848776
C	12.78570167	15.01958266	3.38600060
C	13.86791760	15.73289862	2.86367518
H	14.85919711	15.63072921	3.30147965
C	13.66793418	16.57424053	1.76567522
H	14.50444545	17.13216825	1.34774445
C	12.39563677	16.69891650	1.20251787

H	12.23780224	17.35130862	0.34609002
C	11.33121234	15.97597434	1.74917377
C	9.92936960	15.99891039	1.32361180
C	9.44484257	16.79387381	0.27872303
H	10.13240326	17.42028811	-0.28698097
C	8.08773687	16.78808729	-0.02700810
H	7.70097753	17.40959042	-0.83460942
C	7.23393104	15.97689341	0.72673876
H	6.16241520	15.94819638	0.53073298
C	7.76639267	15.19771839	1.74736253
H	7.13782817	14.54991115	2.35668128
C	10.01573129	16.63786509	5.34284229
H	10.83685997	16.93747908	4.69408828
C	9.60540077	17.44431822	6.39694999
H	10.11541920	18.39095968	6.57605334
C	8.54636323	17.02013018	7.20645685
H	8.20611410	17.62909887	8.04342339
C	7.93492149	15.80385165	6.92419210
H	7.10675818	15.43922061	7.53194069
C	8.38625751	15.02756515	5.84962167
C	7.83667427	13.74405430	5.47306353
C	6.79266472	12.91914634	5.92892152
H	6.11115487	13.10211633	6.75013551
C	6.83924658	11.80706999	5.08026668
C	6.05850585	10.58011819	4.98626680
C	4.98304629	10.27628463	5.83265028
H	4.70201870	10.96838141	6.62644717

C	4.28584858	9.08914068	5.64255278
H	3.44685252	8.83490057	6.29231351
C	4.66851384	8.23084280	4.60689506
H	4.13581673	7.29884372	4.41745978
C	5.75258867	8.59385327	3.81322796
H	6.08772192	7.95742484	2.99272232
C	6.51560429	11.47864539	0.49178231
H	6.03845913	12.11091547	1.24127083
C	6.16306613	11.56755741	-0.85223795
H	5.40073525	12.27456685	-1.17468722
C	6.81128812	10.72956370	-1.76578474
H	6.56995091	10.77631083	-2.82843803
C	7.76593525	9.82968401	-1.30486991
H	8.28133808	9.16158965	-1.99185646
C	8.06101329	9.78997113	0.06595432
C	9.02531952	8.87190946	0.65774158
C	9.85516595	7.87655522	0.13099179
H	9.95186500	7.56675141	-0.90265887
C	10.53825044	7.36936889	1.25067248
C	11.53986372	6.35175051	1.47965044
C	12.12417907	5.56931143	0.47500582
H	11.81798204	5.71687460	-0.55850923
C	13.08818883	4.62372864	0.80774133
H	13.55401188	4.01367627	0.03392178
C	13.44794814	4.47004287	2.15141116
H	14.19362271	3.74089556	2.46155649
C	12.83738849	5.27164899	3.10829691

H	13.09403048	5.17965931	4.16250534
C	8.53350505	5.65745557	4.29994409
H	8.27170567	6.12933606	3.35439435
C	7.73150228	4.67513818	4.86970492
H	6.82153287	4.36042383	4.36011645
C	8.11304381	4.10692879	6.08923277
H	7.50435261	3.33691086	6.56246295
C	9.29265823	4.53929974	6.68689243
H	9.61736086	4.11144467	7.63343817
C	10.07038280	5.52403392	6.06656280
C	11.34793066	6.00818510	6.59510706
C	11.99131002	5.59846922	7.76659228
H	11.53230486	4.85806028	8.41832053
C	13.23218336	6.15034902	8.09418823
H	13.74274414	5.83850871	9.00410585
C	13.81817890	7.10304156	7.25593239
H	14.78297728	7.53679568	7.51064943
C	13.14880053	7.49691637	6.09388342
C	13.59222542	8.47951858	5.09992130
C	14.83796631	9.11508935	5.13127814
H	15.54368911	8.88129628	5.92656542
C	15.17340716	10.02905397	4.13576861
H	16.15055454	10.51209066	4.13904579
C	14.23623677	10.31398671	3.13904647
H	14.44345372	11.03454949	2.34900960
C	13.00979544	9.65733804	3.15243763
H	12.24439992	9.87112889	2.40756592

UNIVERSITAT ROVIRA I VIRGILI
MONONUCLEAR AND HETEROTRINUCLEAR RUTHENIUM COMPLEXES: SYNTHESIS AND WATER OXIDATION ACTIVITY.
Lorenzo Mognon
Dipòsit Legal: T 1359-2015

Chapter 4. Synthesis, Structure, Spectroscopy and Reactivity of New Heterotrinuclear Water Oxidation Catalysts

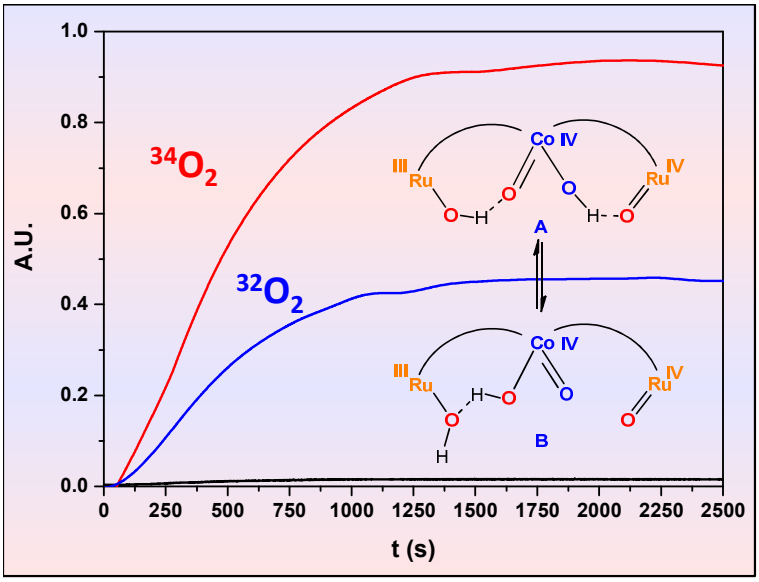

New heterotrinuclear complexes containing ruthenium and manganese or cobalt based on 2,2'-(1*H*-pyrazole-3,5-diyl)dipyridine are synthesized. Electrochemical, UV-vis and EPR experiments are carried out on different complexes. Photochemical water oxidation activity is tested with $[Ru(bpy)_3]^{2+}$ as photosensitizer and $Na_2S_2O_8$ as sacrificial electron acceptor. Oxone is used as sacrificial oxidant to study the reaction at pH = 7 and labelled water experiments shine light on the oxygen evolving mechanism.

UNIVERSITAT ROVIRA I VIRGILI
MONONUCLEAR AND HETEROTRINUCLEAR RUTHENIUM COMPLEXES: SYNTHESIS AND WATER OXIDATION ACTIVITY.
Lorenzo Mognon
Dipòsit Legal: T 1359-2015

Chapter 4. Synthesis, Structure, Spectroscopy and Reactivity of New Heterotrinuclear Water Oxidation Catalysts

UNIVERSITAT ROVIRA I VIRGILI
MONONUCLEAR AND HETEROTRINUCLEAR RUTHENIUM COMPLEXES: SYNTHESIS AND WATER OXIDATION ACTIVITY.
Lorenzo Mognon
Dipòsit Legal: T 1359-2015

Chapter 4. Synthesis, Structure, Spectroscopy and Reactivity of New Heterotrinuclear Water Oxidation Catalysts

Lorenzo Mognon,[a] Sukanta Mandal,[b] Carmen E. Castillo,[c,d] Jérôme Fortage,[c,d] Florian Molton,[c,d] Jordi Benet-Buchhlolz,[a] Carole Duboc,[c,d] Marie-Noëlle Collomb,[c,d] and Antoni Llobet[a,e]

[a] Institute of Chemical Research of Catalonia (ICIQ), Avinguda Països Catalans 16, 43007 Tarragona, Spain

[b] Department of Chemistry, Indian Institute of Technology Kharagpur,Kharagpur-721302, West Bengal, India

[c] Univ. Grenoble Alpes, DCM, F-38000 Grenoble, France

[d] CNRS, DCM, F-38000 Grenoble, France

[e] Departament de Química, Universitat Autònoma de Barcelona, Cerdanyola del Vallès, 08193 Barcelona, Spain

4.1 Abstract

Four heterotrinuclear complexes with 2,2'-(pyrazole-2,5-diyl)dipyridine (bpp^-) and 2,2':6',2''-terpyridine (trpy) ligands of general formula $\{[Ru^{II}(trpy)]_2(\mu\text{-}[M(X)_2(bpp)_2])\}(PF_6)_2$, where M = Co, Mn and X = Cl^-, AcO^- (M = Co, X = Cl^-: **$Ru_2Co\text{-}Cl_2$**; M = Mn, X = Cl^-: **$Ru_2Mn\text{-}Cl_2$**; M **=** Co, X = AcO^-: **$Ru_2Co\text{-}OAc_2$**; M = Mn, X = AcO^-: **$Ru_2Mn\text{-}OAc_2$**) are synthesized. The complexes are

characterized using different spectroscopic techniques as UV-vis and IR and mass spectrometry. X-Ray diffraction is used to characterize the complexes **Ru_2Mn-Cl_2** and **Ru_2Mn-OAc_2**. The cyclic voltammograms (CV) of all four complexes in organic solvent (CH_3CN or CH_2Cl_2) display three successive reversible oxidative waves corresponding to one-electron oxidations of each of the three metal centers. The oxidized forms of complexes **Ru_2Co-OAc_2** and **Ru_2Mn-OAc_2** are further characterized by EPR and UV-vis spectroscopy. The complexes **Ru_2Co-OAc_2** and **Ru_2Mn-OAc_2** act as pre catalysts for water oxidation reaction, as the acetato groups are easily replaced by water at pH = 7 generating the true catalysts, $\{[Ru(H_2O)(trpy)]_2(\mu\text{-}[M(H_2O)_2(bpp)_2])\}^{4+}$ (M = Co: **Ru_2Co-$(H_2O)_4$**; M = Mn: **Ru_2Mn-$(H_2O)_4$**). The photochemical water oxidation reaction is studied using $[Ru(bpy)_3]^{2+}$ as photosensitizer and $Na_2S_2O_8$ as sacrificial electron acceptor at pH = 7. The Co containing complex generates 50 TON in about 10 minutes (TOF_i = 0.21 s^{-1}) whereas the Mn containing one only generates 8 TON. The water oxidation reaction of **Ru_2Co-$(H_2O)_4$** is further investigated using Oxone as sacrificial chemical oxidant at pH = 7. Labelled water oxidation experiments suggest that a nucleophilic attack mechanism is occurring at the Co site of the trinuclear complex with cooperative involvement of the two Ru sites, via electronic coupling through the bpp^- bridging ligand and via neighboring hydrogen bonding.

4.2 Introduction

Water oxidation catalysis is a field that has been enormously expanded over the last years.[1] This development has been fueled by the interest in the topic for the achievement of new energy conversion schemes based on water and sunlight to obtain a so-called solar fuel (such as H_2), mimicking the natural photosynthesis. Water oxidation is the main reaction that occurs at the OEC-PSII,[2] yielding molecular oxygen, four protons and four electrons, which can later further react. The development of new water oxidation catalysts (WOCs) has been based mainly on mononuclear[3] and dinuclear[4] Ru complexes containing polypyridilic ligands. However, recently a number of Ir and first row transition metals complexes have also been reported to be able to oxidize water.[1c, 5]

While mononuclear complexes are in general easier to prepare, targeted polynuclear complexes can present significant synthetic challenges. Nevertheless, polynuclear complexes containing bridging ligands that can electronically couple the metal centers can attain important benefits from the perspective of a WOC. For example, multiple electronically coupled redox active metal centers can share the four electron transfers needed for the water oxidation reaction. On the other hand, non-redox active centers can be of interest to exert electronic perturbation over the redox active center.[6] They can also provide aqua/hydroxo ligands which, when strategically situated, can help to lower activation energies by hydrogen bonding with key active species bonded to the active metal, or even participate in the O-O bond formation as has been proposed for the Ca-OH_2 moiety of the OEC-PSII in a number of occasions.[7]

With these premises, we undertook the preparation of heterotrinuclear complexes where all the metal centers are redox active and possess aqua ligands, to favor the achievement of high oxidation states via Proton Coupled Electron Transfer (PCET). Here on we report the synthesis, structural, spectroscopic and electrochemical characterization of a new family of heterotrinuclear complexes containing Ru and Co or Mn as metal centers, together with their capacity to oxidize water to dioxygen.

4.3 Experimental Section

Preparations. All reagents used in the present work were obtained from Aldrich Chemical Co. and were used without further purification. Solvents were purchased from SDS, and they were purified and dried either by passing them through an activated alumina purification system (MBraun SPS-800) or by conventional distillation techniques. *Out*-[Ru(Cl)(Hbpp)(trpy)][PF_6], ***out*-0**, and [Ru(bpy)$_3$][ClO_4]$_2$ were synthesized as reported in literature.[8]

{[Ru^{II}(trpy)]$_2$(μ-[Co^{II}(Cl)$_2$(bpp)$_2$])}(PF$_6$)$_2$, Ru$_2$Co-Cl$_2$. *Out*-[Ru(Cl)(Hbpp)(trpy)][PF_6] (100 mg, 0.136 mmol) was placed in a 250 mL round-bottom flask and dissolved in 200 mL of methanol. A sample of NaOMe (8 mg, 0.142 mmol) was added and the solution stirred for 30 minutes. The reaction was then kept under 200 W light irradiation (tungsten lamp) overnight and after that 5 mL methanol/water (4:1) solution of $CoCl_2$ (25 mg, 0.190 mmol) and LiCl (57 mg, 1.344 mmol) were added. The reaction mixture was heated at 60 °C under 200 W tungsten lamp light for 5 h. It was then filtered and the volume was reduced to around 20 mL under reduced pressure. Saturated aqueous solution of KPF_6 (2 mL) was added, giving rise to a reddish-brown precipitate. The mixture was

then cooled in an ice bath for 30 minutes and the solid filtered on a frit, washed with cold water (3 times) and then with diethyl ether (3 times), and finally dried under vacuum. Yield: 60 mg (57.6 %). Anal. Calcd for $C_{56}H_{40}Cl_2CoF_{12}N_{14}P_2Ru_2 \cdot 2H_2O$: C 42.92, H 2.83, N 12.51. Found: C 42.98, H 2.88, N 12.46. MALDI (DCTB matrix, CH_2Cl_2): 1386.0 ($[M\text{-}PF_6]^+$). UV-vis [λ_{max}, nm (ε, $M^{-1}\ cm^{-1}$)]: (in CH_3CN) 510 (14470), 492 (14620), 408 (sh) (20380), 372 (25650), 315 (78330), 275 (74310), 234 (73100); (in CH_2Cl_2) 518 (sh)(12900), 495 (13340), 410 (sh) (18640), 375 (23060), 316 (68430), 276 (64500). IR (KBr, cm^{-1}, selected bands): 843 ($\nu(PF_6^-)$).

{[Ru^{II}(trpy)]$_2$(μ-[Mn^{II}(Cl)$_2$(bpp)$_2$])}(PF$_6$)$_2$, Ru$_2$Mn-Cl$_2$. *Out*-[Ru(Cl)(Hbpp)(trpy)][PF_6] (100 mg, 0.136 mmol) was placed in a 250 ml round-bottom flask and dissolved in 200 mL of methanol. A sample of NaOMe (15 mg, 0.278 mmol) was added and the solution stirred for 30 minutes. A solution of $MnCl_2 \cdot 4H_2O$ (27 mg, 0.136 mmol) and LiCl (57 mg, 1.344 mmol) in 5 mL of methanol/water (4:1) was added and the reaction mixture was heated at 60 °C for 4 hours. The solution was allowed to cool down and then stirred overnight under 200 W light irradiation (tungsten lamp) at room temperature. The resulting mixture was kept in fridge (5 °C) for 1 h and was then filtered. The volume was reduced to around 20 mL under reduced pressure. Saturated aqueous solution of KPF_6 (2 mL) was added, giving rise to a reddish-brown precipitate. The reaction mixture was then cooled in an ice bath for 30 minutes and the solid filtered on a frit, washed with cold water (3 times) and then with diethyl ether (3 times), and finally dried under vacuum. Yield: 73 mg (70.2 %). Anal. Calcd for $C_{56}H_{40}Cl_2F_{12}MnN_{14}P_2Ru_2 \cdot 2H_2O$: C 43.03, H 2.84, N 12.55. Found: C 43.13, H 2.72, N 12.15. MALDI (DCTB matrix, CH_2Cl_2): 1382.1 ($[M\text{-}PF_6]^+$). UV-vis [λ_{max}, nm (ε, $M^{-1}\ cm^{-1}$)]: (in CH_3CN) 515 (17026), 485 (18140), 408 (sh) (22830), 368 (30273),

315 (76130), 302 (78110), 276 (79180), 234 (73525); (in CH_2Cl_2) 520 (sh)(17380), 490 (19125), 410 (sh) (23330), 370 (31456), 317 (78200), 302 (84190), 282 (sh) (79700), 277 (81925). IR (KBr, cm^{-1}, selected bands): 843 ($\nu(PF_6^-)$).

General Synthetic Procedure for Ru_2Co-OAc_2 and Ru_2Mn-OAc_2. A sample of **Ru_2Co-Cl_2** (50 mg, 0.033 mmol) or **Ru_2Mn-Cl_2** (50 mg, 0.033 mmol), respectively, and NaOAc (0.030 g 0.365 mmol) was dissolved in 15 mL of an acetone/water (5:1) mixture and heated at 75°C for 3 h. After cooling at room temperature the resulting solution was filtered and few drops of saturated aqueous solution of KPF_6 were added. Upon reduction of the volume, a solid came out from the solution that was filtered and washed with cold water (3 times) and then with diethyl ether and finally dried under vacuum. The yields and characterizations of the complexes are given below:

{[Ru^{II}(trpy)]$_2$(μ-[Co^{II}(AcO)$_2$(bpp)$_2$])}(PF$_6$)$_2$, Ru_2Co-OAc_2. Yield: 0.040 g (73.4%). Anal. Calcd for $C_{60}H_{46}CoF_{12}N_{14}O_4P_2Ru_2$: C 45.67, H 2.94, N 12.43. Found: C 45.62, H 2.82, N 12.56. ESI-MS (in MeOH): 1434.1 ($[M\text{-}PF_6]^+$); 644.5 ($[M\text{-}2PF_6]^{2+}$). UV-vis [λ_{max}, nm (ε, M^{-1} cm^{-1})]: (in CH_3CN) 540 (sh) (12697), 506 (15307), 412 (sh) (16614), 368 (26614), 314 (82077), 276 (75931), 234 (67057); (in CH_2Cl_2) 540 (sh) (13587), 506 (16103), 412 (sh) (17771), 368 (27627), 314 (81785), 276 (75910), 236 (68229). IR (KBr, cm^{-1}, selected bands): 1604, 1568 ($\nu_{asym}(O_2CMe)$); 1447, 1437, 1416 ($\nu_{sym}(O_2CMe)$); 843 ($\nu(PF_6^-)$).

{[Ru^{II}(trpy)]$_2$(μ-[Mn^{II}(AcO)$_2$(bpp)$_2$])}(PF$_6$)$_2$, Ru_2Mn-OAc_2. Yield: 0.040 g (73.6%). Anal. Calcd for $C_{60}H_{46}F_{12}MnN_{14}O_4P_2Ru_2$: C 45.78, H 2.95, N 12.46. Found: C 45.90, H 2.99, N 12.51. ESI-MS (in MeOH): 1430.1 ($[M\text{-}PF_6]^+$); 642.5 ($[M\text{-}2PF_6]^{2+}$). UV-vis [λ_{max}, nm (ε, M^{-1} cm^{-1})]: (in CH_3CN) 538 (sh) (12815),

504(15384), 410 (sh) (17070), 365 (26520), 318 (71463), 306 (71388), 278 (68937), 234 (62473); (in CH_2Cl_2) 538 (sh) (13620), 504 (16069), 410 (sh) (17862), 365 (27603), 318 (71381), 306 (72999), 278 (70850), 234 (64346). IR (KBr, cm^{-1}, selected bands): 1601, 1568 ($\nu_{asym}(O_2CMe)$); 1446, 1436, 1421 ($\nu_{sym}(O_2CMe)$); 843 ($\nu(PF_6^-)$).

Instruments and measurements. *Physical methods.* Elemental analysis were performed using a CHNS-O EA-1108 elemental analyser from Fisons. IR spectra of solid samples were taken in Bruker Vector 22 FT-IR spectrophotometer (in KBr, 4000–500 cm^{-1}). UV-vis spectra were recorded either in Agilent 8453 diode-array spectrophotometer or Cary 50 scan spectrometer. The cell path length was 1 mm. MS analyses were recorded on an esquire 6000 ESI ion trap LC/MS (Bruker Daltonics) equipped with an electrospray ion source and MALDI were recorded in Bruker Autoflex.

Electrochemistry. The electrochemical measurements were run under an argon atmosphere at room temperature. When CH_3CN was used as solvent, the electrochemical measurements were performed in a dry-glove box. Cyclic voltammetry experiments were performed using an EG&G model 173 potentiostat/galvanostat equipped with a PAR model universal programmer and a PAR model 179 digital coulometer. A standard three-electrode electrochemical cell was used. Potentials were measured with an Ag/0.01 M $AgNO_3$ reference electrode in a solution 0.1 M [(nBu$_4$N)ClO_4] in CH_3CN, or with an aqueous Saturated Calomel Electrode (SCE) reference electrode in a pH = 7.0 phosphate buffer solution and CF_3CH_2OH mixture (19:1). Potentials referred to Ag/$AgNO_3$ system can be converted to the normal hydrogen electrode (NHE) by adding 548 mV. Potentials referred to SCE system can be converted to NHE electrode by adding 205 mV. The working electrodes,

polished with 2 µm diamond paste (Mecaprex Presi), were a platinum disk (5 mm in diameter) or a carbon vitreous disk (3 mm in diameter) for cyclic voltammetry. For rotating disk electrode (RDE) experiments, a carbon disk (2 mm in diameter) was used. The auxiliary electrode was a Pt wire. All the potentials are reported against NHE, unless otherwise indicated.

For experiments performed in glove box, progress of electrolysis was followed by the change in UV-Vis spectra with a MCS 501 UV-NIR (Carl Zeiss) spectrophotometer equipped with an automatic shutter. The light sources are halogen (CLH 500 20 W) and deuterium lamps (CLD 500) with optic fibers (041.002–UV SN 012105). For experiments performed in water, UV-visible spectra were recorded on a Variant Cary 300. The cell path length was 1 mm.

EPR spectroscopy. X-band EPR spectra were recorded with a Bruker EMX, equipped with the ER-4192 ST Bruker cavity.

Photochemical oxidations. The photochemical oxygen evolution was carried out under irradiation with 300 W xenon lamp (MAX 302) with band pass filter 440 nm in a custom-made glass vessel with a water jacket. The temperature of the cell was maintained at 298 K by continuous flow of water connected with a thermostat. Oxygen evolution was analysed with a gas phase Clark type oxygen electrode (Unisense Ox-N needle microsensor). Two-point calibration was performed under air saturated and nitrogen saturated conditions. The photochemical experiment involved a three component system: catalyst, sensitizer ($[Ru(bpy)_3]^{2+}$) and sacrificial electron acceptor ($Na_2S_2O_8$). The pH was maintained at 7.04 with 50 mM phosphate buffer (no salt was added to adjust the ionic strength).Three stock solutions were prepared: catalyst (1 mM in CF_3CH_2OH), $[Ru(bpy)_3](ClO_4)_2$ (1 mM in pH = 7.04 aqueous phosphate buffer) and $Na_2S_2O_8$ (44.5 mM in pH = 7.04 aqueous phosphate buffer). 1 mL $[Ru(bpy)_3](ClO_4)_2$ and 0.9 mL $Na_2S_2O_8$ from the stock were taken together in the

custom-made glass vessel and then 0.1 mL stock solution of catalyst was added under stirring conditions {$[catalyst]_f$ = 50 μM, $[[Ru(bpy)_3](ClO_4)_2]_f$ = 0.5 mM; $[Na_2S_2O_8]_f$ = 20 mM; total volume = 2 mL}. The glass vessel was sealed with rubber septum and the oxygen needle sensor was inserted through the rubber septum. The solution was thoroughly degassed and then the catalysis was initiated with irradiation of light.

Chemical water oxidation. Chemical water oxidation catalysis was performed in a jacketed vessel thermostated at 298 K. A CF_3CH_2OH solution of the catalyst was introduced in the vessel and thoroughly deaerated. Previously degassed phosphate buffer was introduced under nitrogen atmosphere and stirring. Finally a solution of oxidant was added. The headspace gaseous content was monitored with a gas-phase Clark electrode, and successively calibrated with known additions of air. On-line mass measurement of the gas evolution for labelling experiments was performed on a Pfeiffer Omnistar GSD 301C mass spectrometer, in the same conditions as the Chemical water oxidation.

X-ray Crystal Structure Determination. Crystals of **Ru_2Mn-Cl_2** were obtained by slow diffusion of diethylether into an acetonitrile solution of the complex. Crystals of **Ru_2Mn-OAc_2** were obtained by slow evaporation of a methanol solution of the complex. The measured crystals were prepared under inert conditions immersed in perfluoropolyether as protecting oil for manipulation.

Data collection: Crystal structure determination for **Ru_2Mn-Cl_2** and **Ru_2Mn-OAc_2** was carried out using a Bruker-Nonius diffractometer equipped with an APPEX 2 4K CCD area detector, a FR591 rotating anode with MoK_α radiation, Montel mirrors as monochromator and an Oxford Cryosystems low temperature device Cryostream 700 plus (T = -173 °C). Full-sphere data

collection was used with ω and φ scans. Programs used: Data collection APEX-2,[9] data reduction Bruker Saint[10] V/.60A and absorption correction SADABS.[11,12]

Structure Solution and Refinement: Crystal structure solution was achieved using direct methods as implemented in SHELXTL[13] and visualized using the program XP. Missing atoms were subsequently located from difference Fourier synthesis and added to the atom list. Least-squares refinement on F^2 using all measured intensities was carried out using the program SHELXTL. All non hydrogen atoms were refined including anisotropic displacement parameters.

Comments to the structures: **Ru_2Mn-Cl_2**: The unit cell contains one molecule of the complex, two PF_6 anions, one diethylether molecule, one acetonitrile molecule and two water molecules. One of the water molecules is disordered in two positions (ratio: 56:44). **Ru_2Mn-OAc_2**: The unit cell contains one molecule of the complex, two PF_6 anions and one molecule of methanol. One of the PF_6 anions is disordered in two orientations. The methanol molecule is also disordered in two orientations (ratio 59:31). The measured sample was formed by two crystals with a ratio of 70:30. The collected data for both crystals were processed with TWINABS taking in account overlapping reflections.[14,12]

4.4 Results and Discussion

Synthesis and solid state structure. The well-known Hbpp ligand is an asymmetric ligand which, once deprotonated, presents two equivalent coordination environments. The protonated ligand thus allows to prepare mononuclear complexes that can be used as starting materials for the preparation of homo-[15] or heterodinuclear, or heterotrinuclear[16] complexes. In the present report we use *out*-[Ru(Cl)(Hbpp)(trpy)]$^+$, ***out*-0**, as the starting material for the preparation of heterotrinuclear complexes containing redox active metals, as displayed in Scheme 1.

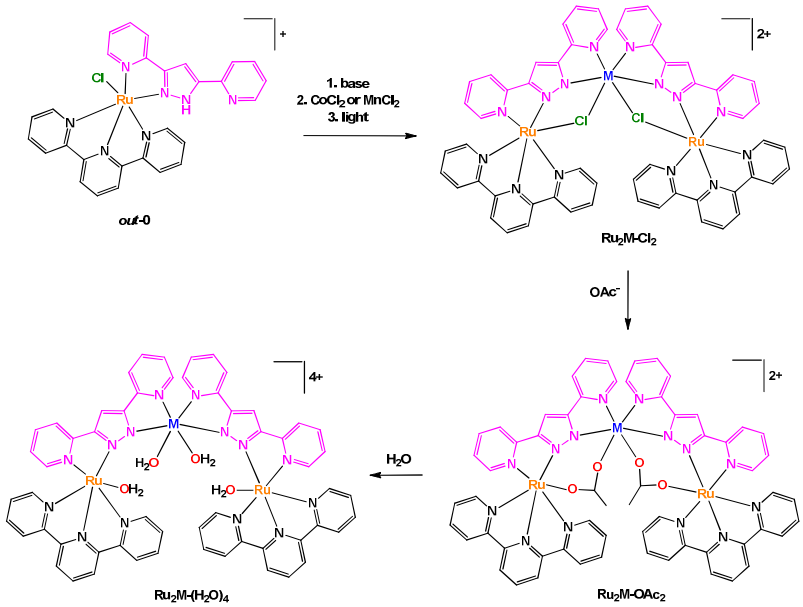

Scheme 1. Synthetic strategy followed for the preparation of trinuclear complexes and their labelling

The pyrazolato proton of ***out*-0** is removed using NaOMe as a base, then $MnCl_2$ or $CoCl_2$ salts are used to react with the vacant coordination sites of the bpp^- ligand as shown in Equation 1 for the cobalt case

$$2\ \textit{out}\text{-}[Ru(Cl)(Hbpp)(trpy)]^+ + 2\ MeO^- + CoCl_2 \xrightarrow[\textbf{out-0}]{} \underset{\textbf{Ru}_2\textbf{Co-Cl}_2}{\{[Ru(trpy)]_2(\mu\text{-}[Co(bpp)_2][(\mu\text{-}Cl)_2])\}^{2+}} + 2\ Cl^- + 2\ MeOH \qquad \textbf{Eq.1}$$

Complex $\mathbf{Ru_2Co\text{-}Cl_2}$ is obtained in 58% yield, whereas a 70% yield is obtained for $\mathbf{Ru_2Mn\text{-}Cl_2}$ following a similar synthetic strategy. Light exposure via tungsten lamp is employed to favor the isomerization of the *out* isomers to the corresponding *in*, in order to avoid the formation of different isomers of the intramolecular bridged trinuclear complex.[16]

Treatment of these trinuclear complexes with sodium acetate at 75°C in an acetone:water 5:1 solution replaces the chlorido bridging ligands by the more labile acetato ligands, as indicated in the following equation.

$$\underset{\textbf{Ru}_2\textbf{Co-Cl}_2}{\{[Ru(trpy)]_2(\mu\text{-}[Co(bpp)_2][(\mu\text{-}Cl)_2])\}^{2+}} + 2\ OAc^- \xrightarrow{} \underset{\textbf{Ru}_2\textbf{Co-AcO}_2}{\{[Ru(trpy)]_2(\mu\text{-}[Co(bpp)_2][(\mu\text{-}OAc)_2])\}^{2+}} + 2\ Cl^- \qquad \textbf{Eq.2}$$

Finally, substitution of the acetato bridges by the monodentate aqua ligands leads to the formation of the corresponding tetra-aqua complex in neutral pH (Eq. 3).

$$\{[Ru(trpy)]_2(\mu\text{-}[Co(bpp)_2][(\mu\text{-}OAc)_2])\}^{2+} + 4\ H_2O$$

Ru_2Co-OAc_2

$$\rightarrow \{[Ru(H_2O)(trpy)]_2(\mu\text{-}[Co(H_2O)_2(bpp)_2])\}^{4+} + 2\ OAc^-$$ **Eq.3**

Ru_2Co-$(H_2O)_4$

In contrast, under acidic conditions the trinuclear complexes decompose to the corresponding mononuclear ***in*-1** and free Co(II) (Figure S23).

The synthetic strategies used for the preparation of **Ru_2Mn-OAc_2**, and **Ru_2Mn-$(H_2O)_4$** are analogous to those of the cobalt counterparts.

All these new complexes have been characterized by analytic, spectroscopic or electrochemical techniques. Further, X-ray diffraction analysis has been carried out for the Mn complexes, **Ru_2Mn-Cl_2** and **Ru_2Mn-OAc_2**, and the ORTEP view of their cationic moiety is presented in Figure 1.

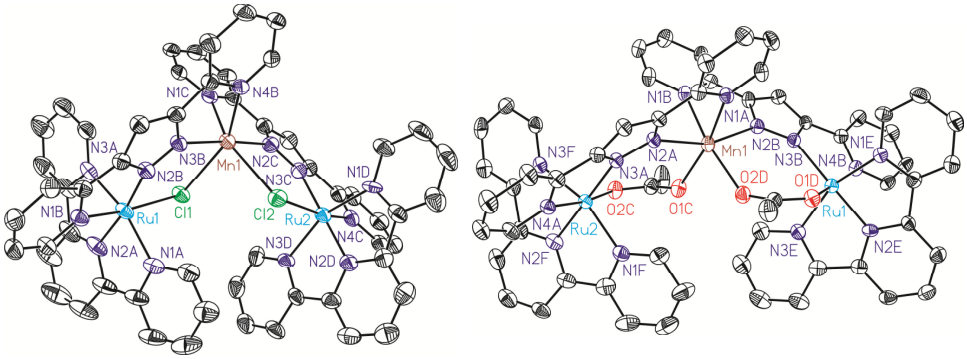

Figure 1. ORTEP plots (50% probability) for the cationic structures of complexes **Ru_2Mn-Cl_2** (left) and **Ru_2Mn-$(OAc)_2$** (right). Hydrogen atoms have been omitted.

All the metal centers present pseudo-octahedral symmetry around the first coordination sphere. In the **Ru_2Mn-Cl_2** case the ruthenium atoms are

coordinated by five N-atoms, three from a meridional trpy ligand and two from a bpp^-, while the sixth coordination position is occupied by a chlorido ligand. The manganese center is coordinated by the same two bridging chlorido moieties, in a *cis* fashion, and by the two chelating bpp^- ligands. The "$Mn(bpp)_2$" moiety can thus be considered as a bridge between the two Ru centers (see Figure 1 and Scheme 1). A very similar structure is obtained for **$Ru_2Mn\text{-}OAc_2$** where the bridging chlorido ligands have been substituted by the bridging acetato ligands. For both structures the bonding distances and angles presented by the Ru(II) and Mn(II) centers are unremarkable.[17]

Redox properties and UV-vis spectroscopy in organic solvents for $Ru_2M\text{-}OAc_2$. The cyclic voltammogram of **$Ru_2Co\text{-}OAc_2$** in CH_3CN (Figure 2) displays three successive reversible oxidation waves at $E_{1/2}$ = 0.70 (ΔE_p = 75 mV), 1.08 (ΔE_p = 60 mV), and 1.22 V (ΔE_p = 60 mV), and one reversible reduction wave at $E_{1/2}$ = -1.23 V (ΔE_p = 80 mV). Each of the three oxidation processes corresponds to the exchange of one electron per molecule of complex as evidenced by rotating disk electrode experiments (Figure S19). The first process is assigned to the oxidation of the cobalt Co(III)/Co(II) and the two last ones to the oxidation of the two Ru sites, $Ru_2(II,III)/Ru_2(II,II)$ and $Ru_2(III,III)/Ru_2(II,III)$. The presence of two distinct one-electron redox processes, close in potential (ΔE = 140 mV), instead of a two-electron single wave, is in agreement with two identical electroactive centers in the molecule that can electronically communicate. This is the case of the two Ru sites that can interact through the conjugation of the bridging bpp^- ligands, the acetato bridge and the central Co^{3+} core. The two electron reduction wave at -1.23 V is assigned to the reduction of the terpyridine units of the Ru(II) centers. The shoulder observed

at -1.18 V indicates that the two terpyridine ligands are not fully equivalent in accordance with a weak electronically coupling between the two Ru subunits.

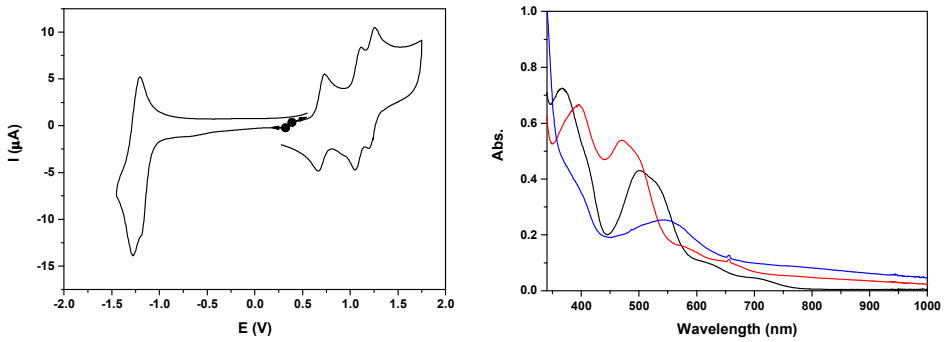

Figure 2. (Left) Cyclic voltammogram of a 0.25 mM solution of **Ru_2Co-OAc_2** in 0.1 M [(nBu$_4$N)ClO$_4$] in CH_3CN, at a scan rate of 100 mV s^{-1}. (Right) UV-visible absorption spectra of a 0.25 mM solution of **Ru_2Co-OAc_2** in 0.1 M [(nBu$_4$N)ClO$_4$] in CH_3CN, in oxidation states (black) Ru_2(II)Co(II), (red) Ru_2(II)Co(III) and (blue) Ru_2(III)Co(III).

The two oxidized forms of the complex, Ru_2(II)Co(III) and Ru_2(III)Co(III) are stable in CH_3CN, as tested by successive electrolysis at E = 0.85 V and E = 1.40 V, which consume, respectively, one and two electrons (Figure S18). Rotating disk electrode experiments confirm the quantitative formation of these species (Figure S19). The electrogenerated solutions have been analyzed also by UV-visible (Figure 2) and EPR spectroscopy (Figure 4, see below).

The three stable oxidation states, Ru_2(II)Co(II), Ru_2(II)Co(III) and Ru_2(III)Co(III), have distinct UV-visible signature. The initial orange Ru_2(II)Co(II) solution exhibits two intense visible bands at 366 and 500 nm (with a shoulder at 530 nm) and two less intense shoulders at 620 and 710 nm. The oxidation of the central Co(II) unit into Co(III) leads to a shift of the intense visible bands at 396 and 473 nm (shoulder at 500 nm) and of the two shoulders at 580 and 655

nm. A more pronounced color change of the solution is observed when the two Ru(II) species are oxidized into Ru(III), as indicated by the replacement of all the previous visible bands by new ones at 390 (shoulder) and 545 nm. An increase of the absorption is also observed between 600 and 1000 nm. As the more evident changes occur after the oxidation from Ru_2(II)Co(III) to Ru_2(III)Co(III), the intense visible absorption bands originate from the ruthenium units.

Back electrolysis of the final solution conducted at 0.35 V (three electrons exchanged) restores quantitatively the initial complex, Ru_2(II)Co(II) (Figure S20). This demonstrates the perfect stability of the different oxidation states of the trinuclear compound, and the reversibility of the processes.

The cyclic voltammogram of **Ru_2Mn-OAc$_2$** in CH_3CN (Figure 3 and S21) also displays three successive one-electron reversible oxidation waves at $E_{1/2}$ = 0.85 V (ΔE_p = 60 mV), 0.96 V (ΔE_p = 70 mV) and 1.47 V (ΔE_p = 100 mV) at a scan rate of 50 mV s^{-1} and a reversible two-electron terpyridine-centered reduction wave at $E_{1/2}$ = -1.23 V (ΔE_p = 80 mV). The two first oxidation waves, very close in potential (ΔE = 110 mV), are thus assigned to the oxidation of the Ru sites, Ru_2(II,III)/Ru_2(II,II) and Ru_2(III,III)/Ru_2(II,III) and the last one to the Mn central unit, Mn(III)/Mn(II).

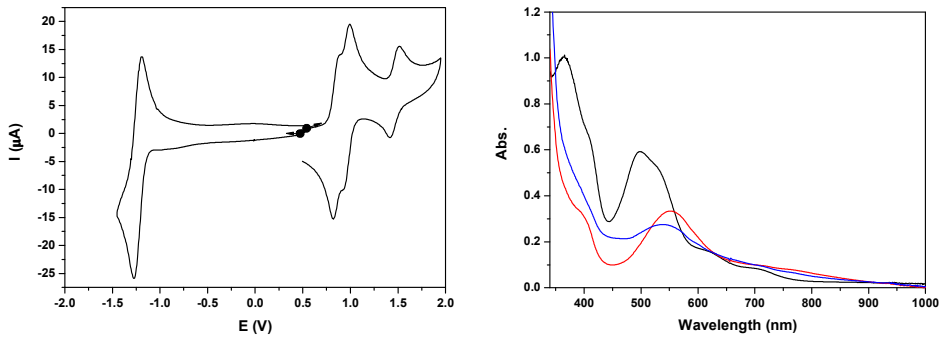

Figure 3. (Left) Cyclic voltammogram of a 0.41 mM solution of **Ru_2Mn-OAc_2** in 0.1 M [(nBu$_4$N)ClO$_4$] in CH_3CN, at a scan rate of 50 mV s^{-1}. (Right) UV-visible absorption spectra of a 0.41 mM solution of **Ru_2Mn-OAc_2** in 0.1 M [(nBu$_4$N)ClO$_4$] in CH_3CN, in oxidation states, (black) Ru_2(II)Mn(II), (red) Ru_2(III)Mn(II) and (blue) Ru_2(III)Mn(III).

The stability of the two oxidized states, Ru_2(III)Mn(II) and Ru_2(III)Mn(III), has been evaluated by two successive electrolysis at E = 1.11 V and 1.69 V. The first electrolysis at 1.11 V consumed two electrons per molecule of initial complex and leads to the quantitative formation of the Ru_2(III)Mn(II) species. An additional one electron oxidation carried out at 1.69 V leads to the formation of the fully oxidized form, Ru_2(III)Mn(III). At this stage, it should be pointed out the presence of an additional reversible process at $E_{1/2}$ = 1.23 V with very small intensity, probably related to a minor decomposition of the complex by decoordination of the Mn ion (less than 5%, Figure S21). Indeed, the potential of this new process is similar to that of a RuN_6 mononuclear complex such as *in*-[Ru(Hbpp)(trpy)(CH_3CN)]$^{2+}$. Both electrolysis have been monitored by UV-vis and X-band EPR spectroscopy (Figures 3 and 4, respectively).

The UV-vis absorption spectrum of **Ru_2Mn-OAc_2** with two intense visible bands at 365 and 497 nm (with a shoulder at 530 nm) and two less intense

shoulders at 620 and 710 nm, is nearly identical to that of **$Ru_2Co\text{-}OAc_2$** (see Figure S9 for a comparison of the spectra). These observations confirm that the visible absorption bands originate mainly from the Ru units. Once the two Ru(II) units have been oxidized, formation of the Ru_2(III)Mn(II) species leads to significant changes with the replacement of the initial visible bands by new ones at 400 (shoulder) and 553 nm and two shoulders at 710 and 764 nm. For the fully oxidized solution, the oxidation of the central Mn(II) unit into Mn(III) leads to minor changes, with a shift of the band at 553 nm to 538 nm and a small increase of the absorption around 450 nm (Figure 3).

The initial reduced state of the complex **$Ru_2Mn\text{-}OAc_2$** is restored almost quantitatively by a back electrolysis of the final solution at 0.35 V (Figure S22).

Magnetic properties. The X-band EPR spectra of the initial and electrochemically oxidized solutions of **$Ru_2Co\text{-}OAc_2$** (see above) have been recorded at low temperature (13 K) (Figure 4). The initial solution of **$Ru_2Co\text{-}OAc_2$** shows an EPR signal characteristic of a Co(II) ion (d^7) in the high spin state (S = 3/2), arising from the central Co(II) unit, as both Ru units (Ru(II), d^6) are diamagnetic and thus EPR silent. The analysis of high spin Co(II) centers is difficult because the zero field splitting (ZFS) energy is usually greater than the Zeeman interaction, leading to spectra insensitive to the magnitude of the axial term (D) of the ZFS. Consequently, only the real g-values (g_{real}) and the rhombicity (E/D ratio) of the system can be extracted from the simulation of the EPR spectra. Simulation of the experimental data provides the following spin-Hamiltonian parameters for the Ms = $|\pm 1/2\rangle$: $g_{real(x,y)}$ = 2.42, $g_{real(z)}$ = 2.31, and E/D =0.23.

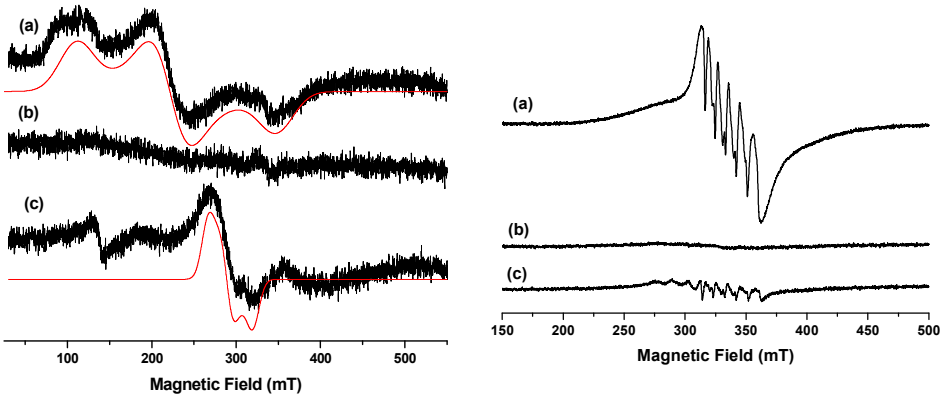

Figure 4. (Left) X-band EPR spectra recorded at 13 K of a 0.25 mM solution of **$Ru_2Co\text{-}OAc_2$** in 0.1 M [(nBu$_4$N)ClO$_4$] in CH_3CN, in oxidation states (a) Ru_2(II)Co(II), (b) Ru_2(II)Co(III) and (c) Ru_2(III)Co(III), (black) and corresponding simulated spectra(red). (Right) X-band EPR at 100 K of a 0.41 mM solution of **$Ru_2Mn\text{-}OAc_2$** in 0.1 M [(nBu$_4$N)ClO$_4$] in CH_3CN, in oxidation states, (a) Ru_2(II)Mn(II), (b) Ru_2(III)Mn(II) and (c) Ru_2(III)Mn(III).

After the one-electron oxidation into Ru_2(II)Co(III), the solution becomes EPR silent, in accordance with the formation of the EPR silent low-spin Co(III) species (d^6) (S = 0). For the fully oxidized solution of Ru_2(III)Co(III), an EPR signal characteristic of an S = 1/2 species is observed that can be attributed to the signature of two low spin Ru(III) ions (d^5). The g-values have been determined by simulating the experimental data: g_1 = 2.58, g_2 = 2.38 and g_3 = 2.15 leading to a g_{iso} value of 2.38 that lies in the range 2.07-2.48, expected for such systems. The presence of three g-values is indicative of a rhombic distortion around the Ru(III) ions in the complex. This unique signal points out that the two Ru(III) units are not magnetically coupled through the diamagnetic central Co(III) ion. The EPR transition observed at 1300 G (130 mT) is assigned to an impurity of a high spin Co(II) species.

The EPR signal of the initial **Ru_2Mn-OAc_2** solution at 100 K exhibits a 6-lines signal characteristic of a high-spin Mn(II) ion ($3d^5$, S = 5/2), and is related to the central Mn(II) unit of the complex (Figure 4). This signal fully disappears after oxidation of the two diamagnetic Ru(II) units into Ru(III). The resulting spectrum displays no EPR signal whichever the temperature (between 13 K and 200 K). The absence of an X-band EPR signal for the Ru_2(III)Mn(II) species is consistent with the formation of a trinuclear complex in which the metallic ions (the Ru(III) (S = 1/2) and the Mn(II) (S = 5/2) ions) are magnetically coupled through the pyrazolate and acetato bridges. The fully oxidized solution of Ru_2(III)Mn(III) is also EPR silent in agreement with a magnetic coupling between the two Ru(III) (S = 1/2) and the Mn(III) (d^4, S = 2) ions. The low-intensity signals observed around g = 2 is attributed to some decomposition of the trinuclear Ru_2(III)Mn(III) $(OAc)_2$ complex (less than 5 %, as shown by electrochemistry) into "free" Mn(II) (six lines feature centered at g = 2.0, 339 mT) and the mononuclear $[Ru^{III}(bpp)(trpy)(CH_3CN)]^{3+}$ complex (S = 1/2) (the two features at low field compared to the six lines feature).

Redox properties in aqueous solutions. The redox properties of the trinuclear complexes **Ru_2Co-$(H_2O)_4$** and **Ru_2Mn-$(H_2O)_4$** were investigated by means of CV and DPV in a mixture of pH = 7.0 phosphate buffer (50 mM) and CF_3CH_2OH (19:1), the latter due to poor solubility of the complexes in water. While very nicely defined waves were observed in organic solvents for their acetato counterparts as shown previously, in aqueous solution the waves are very wide (Figure S24). Nevertheless, the DPVs in Figure 5 allow to observe three faradaic processes situated at approximately 0.6, 0.7 and 1.0 V for both **Ru_2Co-$(H_2O)_4$** and **Ru_2Mn-$(H_2O)_4$**, which are plotted together with the mononuclear aqua complex ***in*-1** for comparative purposes. However, the most

important feature is the large electrocatalytic wave displayed by these complexes, starting at 1.3 V for **Ru_2Co-$(H_2O)_4$** and at around 1.5 V for **Ru_2Mn-$(H_2O)_4$** and ***in*-1**, and that is associated to water oxidation catalysis.

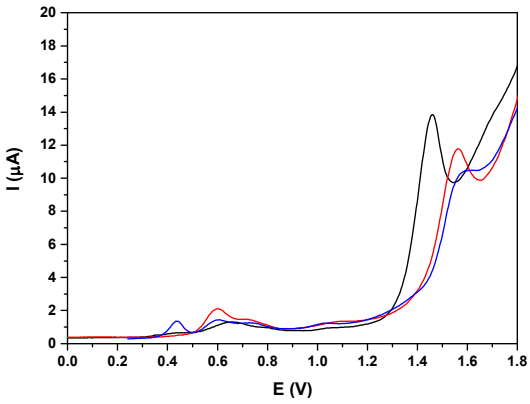

Figure 5. DPV of (black) **Ru_2Co-$(H_2O)_4$**, (red) **Ru_2Mn-$(H_2O)_4$** and (blue) ***in*-1** in a pH = 7.0 (50 mM) phosphate buffer solution and CF_3CH_2OH mixture (19:1).

Water oxidation catalysis. Photochemically driven water oxidation catalysis has been carried out through the photogeneration of $[Ru(bpy)_3]^{3+}$ as chemical oxidant (Eq. 4-6).

$$[Ru^{II}(bpy)_3]^{2+} + h\nu \rightarrow [Ru^{II}(bpy)_3]^{2+*} \quad \textbf{Eq. 4}$$

$$[Ru^{II}(bpy)_3]^{2+*} + S_2O_8^{2-} \rightarrow [Ru^{III}(bpy)_3]^{3+} + SO_4^{2-} + SO_4^{-}\cdot \quad \textbf{Eq. 5}$$

$$[Ru^{II}(bpy)_3]^{2+} + SO_4^{-}\cdot \rightarrow [Ru^{III}(bpy)_3]^{3+} + SO_4^{2-} \quad \textbf{Eq. 6}$$

The oxygen generation profile as a function of time is presented in Figure 6 for the systems Cat 50 μM/$[Ru(bpy)_3]^{2+}$ 0.5 mM/$Na_2S_2O_8$ 20 mM/pH = 7.0 (50 mM phosphate buffer), with total volume of 2.0 mL (H_2O:CF_3CH_2OH = 19:1) using a 300 W Xenon lamp with band pass filter of 440 nm and thermostated

at 298 K. Under these conditions **Ru_2Co-$(H_2O)_4$** generates 50 TON in about 10 minutes (TOF_i = 0.21 s^{-1}) whereas **Ru_2Mn-$(H_2O)_4$** only generates 8 TON and the mononuclear complex ***in*-1** does not generate any molecular oxygen within this time frame. These results are consistent with the electrochemical analysis, as the potentials for the catalysis for **Ru_2Mn-$(H_2O)_4$** and ***in*-1** are too high for the redox couple Ru(III)/Ru(II) of [Ru(bpy)$_3$] (E = 1.26 V).

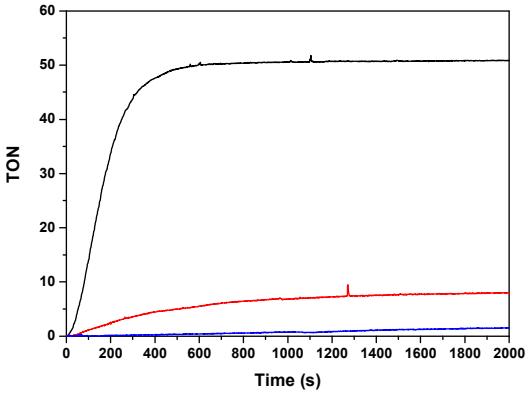

Figure 6. Photochemically induced oxidation of (black) **Ru_2Co-$(H_2O)_4$**, (red) **Ru_2Mn-$(H_2O)_4$**) and (blue) ***in*-1.** Reaction conditions: $[catalyst]_f$ = 50 µM, $[[Ru(bpy)_3](ClO_4)_2]_f$ = 0.5 mM; $[Na_2S_2O_8]_f$ = 20 mM; total volume = 2 mL in a pH = 7.0 (50 mM) phosphate buffer solution and CF_3CH_2OH mixture (19:1). A 300 W Xenon lamp was used to illuminate the sample through a band pass filter of 440 nm at 298 K.

In light of the good results obtained in the photoactivated experiment, water oxidation catalysis with **Ru_2Co-$(H_2O)_4$**, and with the mononuclear ***in*-1** for comparison, was also investigated using oxone ($KHSO_5$) as chemical oxidant. The oxygen evolution profiles as a function of time are presented in Figure 6. The Co containing complex generates 1.0 µmol of oxygen (0.41 µmols are subtracted due to the activity of the blank under the same conditions) that correspond to about 13 TON.

Labelling experiments using $H_2{}^{18}O$ were also carried out in order to extract mechanistic information regarding the O-O bond formation event when using oxone as a chemical oxidant. The O_2 36/34/32 isotope ratio was followed by on-line Mass Spectrometry. Two different degrees of H_2O labelling were employed, and the results obtained are showed in Figure 7.

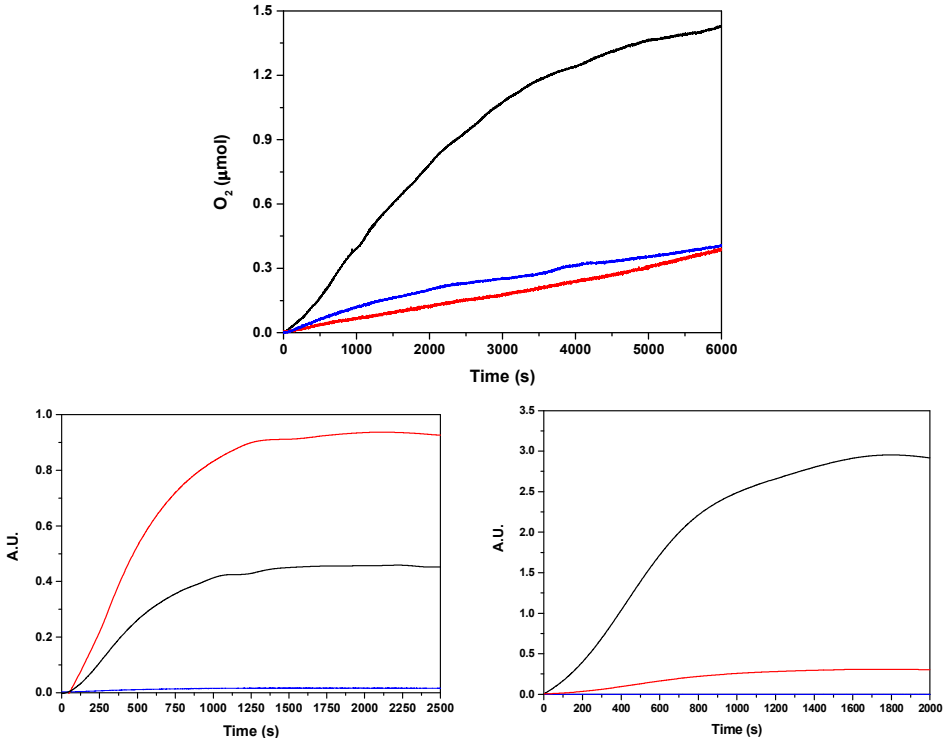

Figure 7. (Top) Oxygen evolution profile using oxone (4.7 mM) as chemical oxidant for (black) 40 µM **Ru_2Co-$(H_2O)_4$**, (blue) 80 µM ***in*-1** and (red) a solution without complexes, using a pH= 7.0 (50 mM) phosphate buffer up to a total volume of 2.0 mL (H_2O:CF_3CH_2OH = 19:1) in a 298 K thermostated cell. (Bottom) Isotopic oxygen generation profile monitored by on-line MS for the **Ru_2Co-OAc_2** using oxone in the same conditions. Bottom left using 97% $H_2{}^{18}O$, and bottom right using 15% $H_2{}^{18}O$. Color code: black $^{32}O_2$, red $^{34}O_2$, blue $^{36}O_2$.

These labelling experiments together with the experiments previously described are in agreement with the mechanism proposed in Scheme 2, based on the following assumptions, evidences and related deductions. For this discussion we initially consider only the experiment with 97% of $H_2{}^{18}O$.

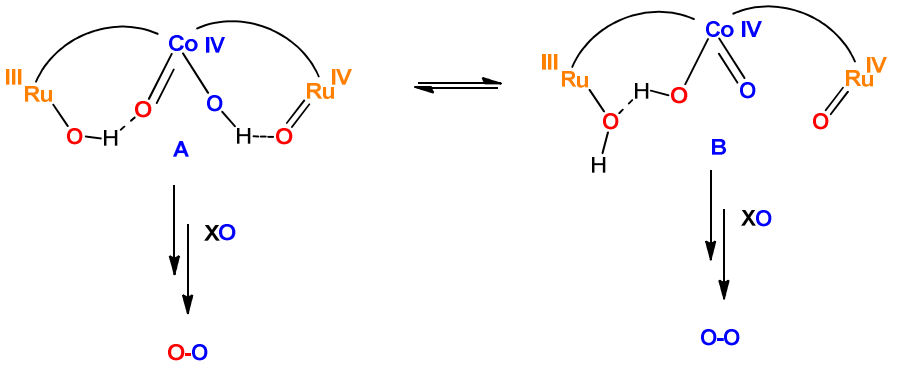

Scheme 2. Fast tautomeric equilibrium proposed for the active species of the trinuclear **$Ru_2Co(H_2O)_4$** complex just before the O-O bond formation step. The bpp^- ligand is represented by an arc and the trpy ligands are omitted for clarity purposes. XO represent the oxidant oxone ($KHSO_5$). The blue oxygens are ^{16}O and the red oxygens are ^{18}O.

a. rRaman experiments under the same conditions as the labelling experiments showed that no ^{18}O exchange occurs at all between water and oxone during at least 10 h (Figure S25).[18]
b. Substitution reactions of aqua ligands at low oxidation states (II) for Ru and Co complexes occur rapidly, so all the aqua ligands are initially present as $H_2{}^{18}O$.
c. Peroxide oxidations of Ru-aqua polypyridyl complexes occur through dehydrogenation pathways.[19] Thus oxone will react with low oxidation states of Ru-aqua as follows:

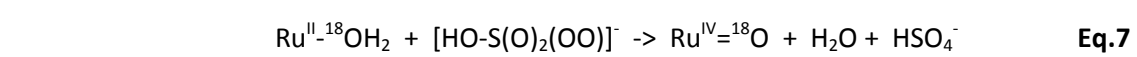

Eq.7

d. Oxidation of cobalt polyridylic complexes with peroxides occurs primarily via nucleophilic substitution.[20]

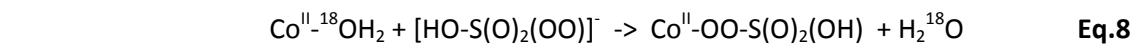

Eq.8

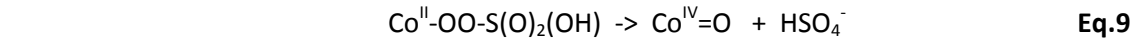

Eq.9

e. Tautomeric equilibrium between the oxo-hdyroxo complexes as described in Equation 10 would produce labelling scrambling and has been earlier proposed for related complexes.[21]

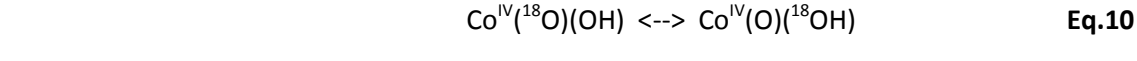

Eq.10

f. The practically negligible amount of $^{36}O_2$ in the 97% $H_2{}^{18}O$ experiment indicates the inexistence of intramolecular pathways between Ru=O and Co=O moieties. In addition, it also precludes the existence of bimolecular pathways involving only Ru=O groups. On the other hand potential bimolecular pathways involving only Co centers is sterically highly disfavored.

g. The mononuclear complex ***in*-1** does not generate sufficient oxygen to be significant in the applied conditions and thus manifests the inexistence of O_2 coming independently from Ru-aqua/Ru-oxo moieties.

h. *Cis* O-O coupling within the same Co metal center would be compatible with the ratios of isotopic labelling obtained, although

this mechanism has been discarded based on DFT in a number of examples.[22]

i. The 97% labelling experiment (Figures 7 and S26) is consistent with the existence of a very fast tautomeric equilibrium where species A and B exists in a 2:1 ratio respectively (See Scheme 2).

   The origin of the higher stabilization of species A is proposed to come from the higher hydrogen bond capacity of isomer A with regard to that of B. Oxidation states of Ru and Co are tentatively assigned from the apparent removal of 4/5 electrons from the oxidation state II,II,II as judged from the electrocatalytic wave displayed by the complex.

   Assuming this equilibrium, the reaction of oxone (XO) with A and B would generate molecular oxygen with a ratio of isotopes of $^{34}O_2/^{32}O_2 = 2/1$.

j. Finally, changing the ratio of labelled water to 15% ^{18}O (Figures 7 and S26), will generate molecular oxygen with a ratio of $^{34}O_2/^{32}O_2 = 1/9$. Experimentally we find a ratio of 1/10 with a very good agreement with the proposed mechanism.

Overall the labelling experiments carried out together with the rest of the electrochemical and spectroscopic properties are in agreement with the presence of a nucleophilic attack mechanism occurring at the Co site of the trinuclear complex, with cooperative interaction of the two Ru sites via electronic coupling through the bpp^- bridging ligand and via neighboring hydrogen bonding.

4.5 Conclusions

We have prepared and isolated a family of trinuclear complexes, $Ru_2M\text{-}X_2$ (M=Co or Mn; X = Cl or OAc), where the central Co or Mn atom, together with two bpp^- ligands, acts as a bridge between the two external Ru moieties. These complexes have been characterized in the solid state by X-ray diffraction analysis and in solution by spectroscopic (EPR, UV-vis) and by electrochemical (CV, DPV) techniques. Overall, all these experiments for the chlorido or acetato bridge complexes show the presence of a relatively weak electronic coupling among the metal centers, transmitted through the bridging ligands. In addition it is very interesting to see how the redox pattern radically changes from the Mn complexes with regard to the Co complexes manifesting the intrinsically different electronic properties of the two transition metals. In aqueous acidic media the trinuclear complexes revert to the Ru mononuclear counterparts and free Co(II) or Mn(II). However at pH = 7.0 the integrity of the trinuclear complex is fully retained. Particularly interesting is the heterotrinuclear **$Ru_2Co\text{-}(H_2O)_4$** complex that at this pH is capable of catalytically oxidizing water to molecular dioxygen chemically, electrochemically and photochemically. In addition $H_2{}^{18}O$ labelled experiments nicely allow to elucidate the mechanism of the O-O bond formation, which is one of the crucial steps in oxygen evolution systems from a mechanistic perspective, and that has never been done up to now with first row transition metal complexes.

Acknowledgements. We thank MINECO (CTQ-2013–49075-R, SEV-2013-0319, CTQ2014-52974-REDC), the EU COST actions CM1202 and CM1205. L. M. thanks “ICIQ-Foundation” for a Ph.D. grant. C.E.C’s acknowledges the MICINN for a postdoctoral grant. The authors wish to thank for financial supports the LABEX ARCANE (ANR-11-LABX-0003-01) for the project H_2Photocat including

the C. E. C.'s post-doctoral fellowship. This work was also supported by ICMG FR 2067 and COST CM1202 program (PERSPECT H_2O).

IV

I performed the chemical oxidation experiments, the water labelling experiments and actively participated in the elaboration of the oxygen evolution mechanism.

4.6 References

(1) a) Berardi, S.; Drouet, S.; Francas, L.; Gimbert-Surinach, C.; Guttentag, M.; Richmond, C.; Stoll, T.; Llobet, A. *Chem. Soc. Rev.* **2014,** *43*, 7501-7519; b) López, I.; Ertem, M. Z.; Maji, S.; Benet-Buchholz, J.; Keidel, A.; Kuhlmann, U.; Hildebrandt, P.; Cramer, C. J.; Batista, V. S.; Llobet, A. *Angew. Chem. Int. Ed.* **2014,** *53*, 205-209; c) Rigsby, M. L.; Mandal, S.; Nam, W.; Spencer, L. C.; Llobet, A.; Stahl, S. S. *Chem. Sci.* **2012,** *3*, 3058-3062.

(2) Karlsson, S.; Boixel, J.; Pellegrin, Y.; Blart, E.; Becker, H.-C.; Odobel, F.; Hammarstrom, L. *Faraday Discuss.* **2012,** *155*, 233-252.

(3) Duan, L.; Bozoglian, F.; Mandal, S.; Stewart, B.; Privalov, T.; Llobet, A.; Sun, L. *Nat. Chem.* **2012,** *4*, 418-423.

(4) a) Neudeck, S.; Maji, S.; López, I.; Meyer, S.; Meyer, F.; Llobet, A. *J. Am. Chem. Soc.* **2013,** *136*, 24-27; b) Sander, A. C.; Maji, S.; Francàs, L.; Böhnisch, T.; Dechert, S.; Llobet, A.; Meyer, F. *ChemSusChem* **2015,** *8*, 1697-1702.

(5) a) Garrido-Barros, P.; Funes-Ardoiz, I.; Drouet, S.; Benet-Buchholz, J.; Maseras, F.; Llobet, A. *J. Am. Chem. Soc.* **2015,** *137*, 6758-6761; b) Karlsson, E. A.; Lee, B.-L.; Åkermark, T.; Johnston, E. V.; Kärkäs, M. D.; Sun, J.; Hansson, Ö.; Bäckvall, J.-E.; Åkermark, B. *Angew. Chem. Int. Ed.* **2011,** *50*, 11715-11718.

(6) Yoon, H.; Lee, Y.-M.; Wu, X.; Cho, K.-B.; Sarangi, R.; Nam, W.; Fukuzumi, S. *J. Am. Chem. Soc.* **2013,** *135*, 9186-9194.

(7) a) Ferreira, K. N.; Iverson, T. M.; Maghlaoui, K.; Barber, J.; Iwata, S. *Science* **2004,** *303*, 1831-1838; b) Dau, H.; Limberg, C.; Reier, T.; Risch, M.; Roggan, S.; Strasser, P. *ChemCatChem* **2010,** *2*, 724-761.

(8) Sens, C.; Rodríguez, M.; Romero, I.; Llobet, A.; Parella, T.; Benet-Buchholz, J. *Inorg. Chem.* **2003,** *42*, 8385-8394.

(9) Data collection: APEX II, versions v2009.1-02 and v2013.4-1; Bruker AXS Inc.: Madison, WI, 2007.

(10) Data reduction: SAINT, versions V7.60A and V8.30c; Bruker AXS Inc.: Madison, WI, 2007.

(11) SADABS, V2008/1 and V2012/1; Bruker AXS Inc.: Madison, WI, 2001.

(12) Blessing, R. *Acta Crystallogr. Sect. A* **1995,** *51*, 33-38.

(13) Sheldrick, G. *Acta Crystallogr. Sect. A* **2008,** *64*, 112-122.

(14) TWINABS, version 2008/4 Bruker AXS Inc.: Madison, WI.

(15) Sens, C.; Romero, I.; Rodríguez, M.; Llobet, A.; Parella, T.; Benet-Buchholz, J. *J. Am. Chem. Soc.* **2004,** *126*, 7798-7799.

(16) Mognon, L.; Benet-Buchholz, J.; Rahaman, S. M. W.; Bo, C.; Llobet, A. *Inorg. Chem.* **2014,** *53*, 12407-12415.

(17) a) Roeser, S.; Ertem, M. Z.; Cady, C.; Lomoth, R.; Benet-Buchholz, J.; Hammarström, L.; Sarkar, B.; Kaim, W.; Cramer, C. J.; Llobet, A. *Inorg. Chem.* **2011,** *51*, 320-327; b) Romain, S.; Rich, J.; Sens, C.; Stoll, T.; Benet-Buchholz, J.; Llobet, A.; Rodriguez, M.; Romero, I.; Clérac, R.; Mathonière, C.; Duboc, C.; Deronzier, A.; Collomb, M.-N. l. *Inorg. Chem.* **2011,** *50*, 8427-8436.

(18) Limburg, J.; Vrettos, J. S.; Chen, H.; de Paula, J. C.; Crabtree, R. H.; Brudvig, G. W. *J. Am. Chem. Soc.* **2001,** *123*, 423-430.

(19) Gilbert, J.; Roecker, L.; Meyer, T. J. *Inorg. Chem.* **1987,** *26*, 1126-1132.

(20) Sawyer, D. T.; Sobkowiak, A.; Matsushita, T. *Acc. Chem. Res.* **1996,** *29*, 409-416.

(21) Bernadou, J.; Fabiano, A.-S.; Robert, A.; Meunier, B. *J. Am. Chem. Soc.* **1994,** *116*, 9375-9376.

(22) Wang, L.-P.; Van Voorhis, T. *J. Phys. Chem. Lett.* **2011,** *2*, 2200-2204.

Supporting Information for

Synthesis, Structure, Spectroscopy and Reactivity of New Heterotrinuclear Water Oxidation Catalysts

Lorenzo Mognon,[a] Sukanta Mandal,[b] Carmen E. Castillo,[c,d] Jérôme Fortage,[c,d] Florian Molton,[c,d] Jordi Benet-Buchhlolz,[a] Carole Duboc,[c,d] Marie-Noëlle Collomb,[c,d] and Antoni Llobet[a,e]

[a] Institute of Chemical Research of Catalonia (ICIQ), Avinguda Països Catalans 16, 43007 Tarragona, Spain

[b] Department of Chemistry, Indian Institute of Technology Kharagpur,Kharagpur-721302, West Bengal, India

[c] Univ. Grenoble Alpes, DCM, F-38000 Grenoble, France

[d] CNRS, DCM, F-38000 Grenoble, France

[e] Departament de Química, Universitat Autònoma de Barcelona, Cerdanyola del Vallès, 08193 Barcelona, Spain

Table S1. Crystal data and structure refinement for **Ru_2Mn-Cl_2**.

Empirical formula	C62 H57 Cl2 F12 Mn N15 O3 P2 Ru2
Formula weight	1678.15
Temperature	100(2) K
Wavelength	0.71073 Å
Crystal system	Triclinic
Space group	P-1
Unit cell dimensions	a = 14.6868(18) Å α= 69.889(3) °.
	b = 15.5818(14) Å β = 66.513(2) °.
	c = 17.997(2) Å γ = 67.869(2) °.
Volume	3406.8(7) $Å^3$
Z	2
Density (calculated)	1.636 Mg/m^3
Absorption coefficient	0.836 mm^{-1}
F(000)	1686
Crystal size	0.10 x 0.05 x 0.05 mm^3
Theta range for data collection	1.45 to 32.93 °.
Index ranges	-22<=h<=22 ,-23 <=k<=23 ,-27<=l<=27
Reflections collected	24640
Independent reflections	13360 [R(int) = 0.0934]
Completeness to theta = 32.93°	0.964 %
Absorption correction	Empirical
Max. and min. transmission	0.9594 and 0.9211
Refinement method	Full-matrix least-squares on F^2
Data / restraints / parameters	24640 / 12 / 905
Goodness-of-fit on F^2	1.019
Final R indices [I>2sigma(I)]	R1 = 0.0741 , wR2 = 0.1992
R indices (all data)	R1 = 0.1549 , wR2 = 0.2546
Largest diff. peak and hole	3.138 and -1.357 $e.Å^{-3}$

Table S2. Crystal data and structure refinement for **Ru_2Mn-OAc_2**.

Empirical formula	C61 H50 F12 Mn N14 O5 P2 Ru2
Formula weight	1606.17
Temperature	100(2) K
Wavelength	0.71073 Å
Crystal system	Triclinic
Space group	P-1
Unit cell dimensions	a = 14.471(3) Å α= 114.334(5) °.
	b = 15.501(4) Å β = 112.431(4) °.
	c = 16.913(4) Å γ = 91.203(5) °.
Volume	3123.0(13) $Å^3$
Z	2
Density (calculated)	1.708 Mg/m^3
Absorption coefficient	0.827 mm^{-1}
F(000)	1610
Crystal size	0.10 x 0.10 x 0.01 mm^3
Theta range for data collection	2.36 to 30.66 °
Index ranges	-20 <=h<=18 ,-21 <=k<=20 ,0 <=l<=24
Reflections collected	17781
Independent reflections	17781 [R(int) = 0.0000]
Completeness to theta = 30.66°	92.0%
Absorption correction	Empirical
Max. and min. transmission	0.9918 and 0.9219
Refinement method	Full-matrix least-squares on F^2
Data / restraints / parameters	17781 / 32 / 937
Goodness-of-fit on F^2	1.036
Final R indices [I>2sigma(I)]	R1 = 0.0696 , wR2 = 0.1485
R indices (all data)	R1 = 0.1433 , wR2 = 0.1785
Largest diff. peak and hole	1.857 and -1.081 $e.Å^{-3}$

Figure S1. Mass spectra (MALDI+) of $\{[Ru^{II}(trpy)]_2(\mu\text{-}[Co^{II}(Cl)_2(bpp)_2])\}(PF_6)_2$, **$Ru_2Co\text{-}Cl_2$**, in dctb-$CH_2Cl_2$. The peak at 1386.0 corresponds to cation $[M\text{-}PF_6]^+$; experimental (left) and simulated (right).

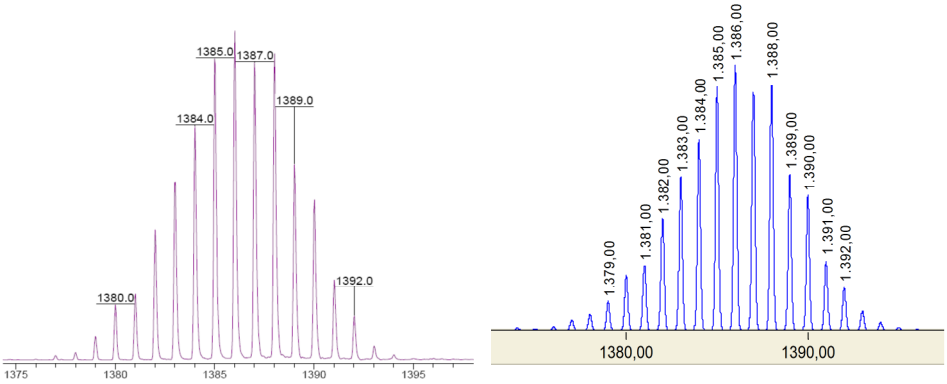

Figure S2. Mass spectra (MALDI+) of $\{[Ru^{II}(trpy)]_2(\mu\text{-}[Mn^{II}(Cl)_2(bpp)_2])\}(PF_6)_2$, **$Ru_2Mn\text{-}Cl_2$**, in dctb-$CH_2Cl_2$. The peak at 1382.1 corresponds to cation $[M\text{-}PF_6]^+$; experimental (left) and simulated (right).

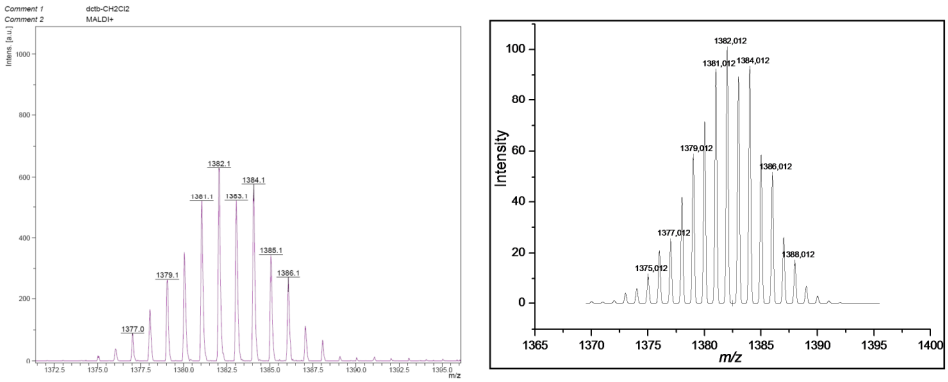

Figure S3. ESI Mass spectra of {[Ru^{II}(trpy)]$_2$(μ-[Co^{II}(AcO)$_2$(bpp)$_2$])}$(PF_6)_2$, **Ru_2Co-OAc_2**, in MeOH. (a) the peak at 1434 corresponds to cation [M-PF_6]+;Experimental (left) and simulated (right); the peak at 644.5 corresponds to cation [M-2PF_6]$^{2+}$;Experimental (left) and simulated (right).

(a)

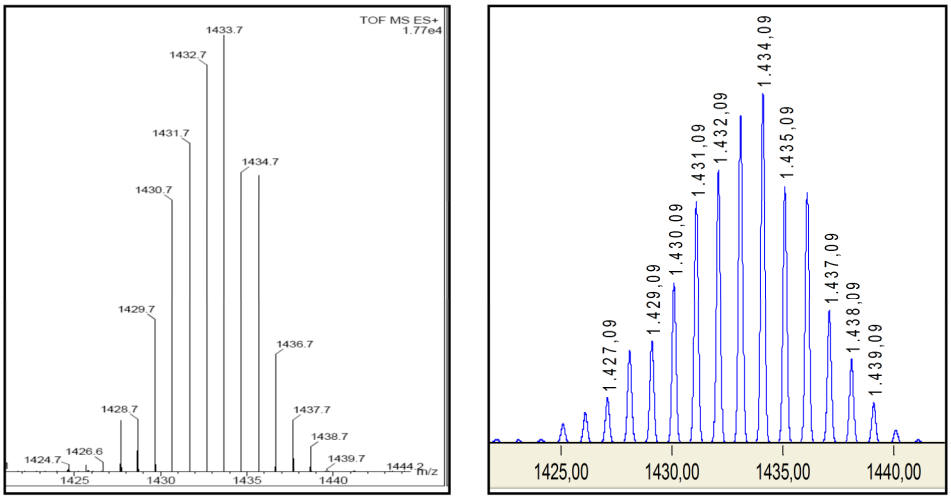

(b)

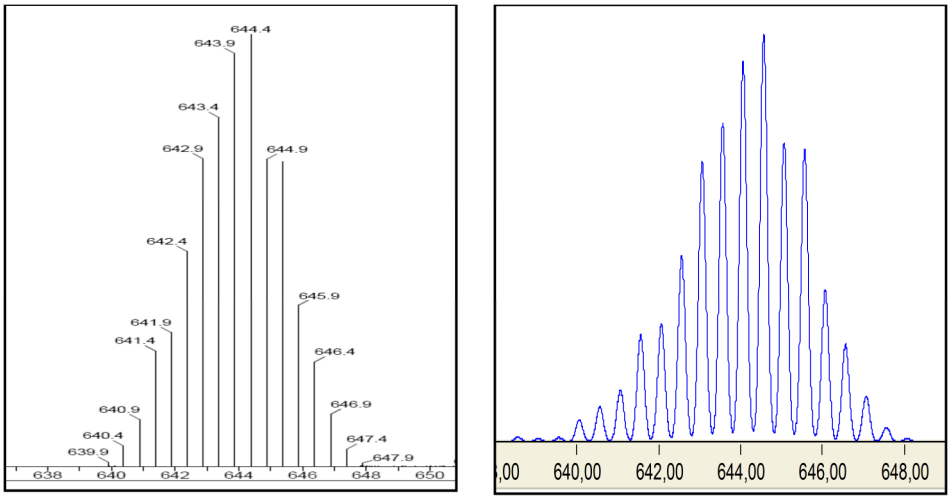

Figure S4. ESI Mass spectra of $\{[Ru^{II}(trpy)]_2(\mu\text{-}[Mn^{II}(AcO)_2(bpp)_2])\}(PF_6)_2$, **$Ru_2Mn\text{-}OAc_2$**, in MeOH. (a) The peak at 1430 corresponds to cation $[M\text{-}PF_6]^+$; Experimental (left) and simulated (right); (b) the peak at 642.5 corresponds to cation $[M\text{-}2PF_6]^{2+}$;Experimental (left) and simulated (right).

(a)

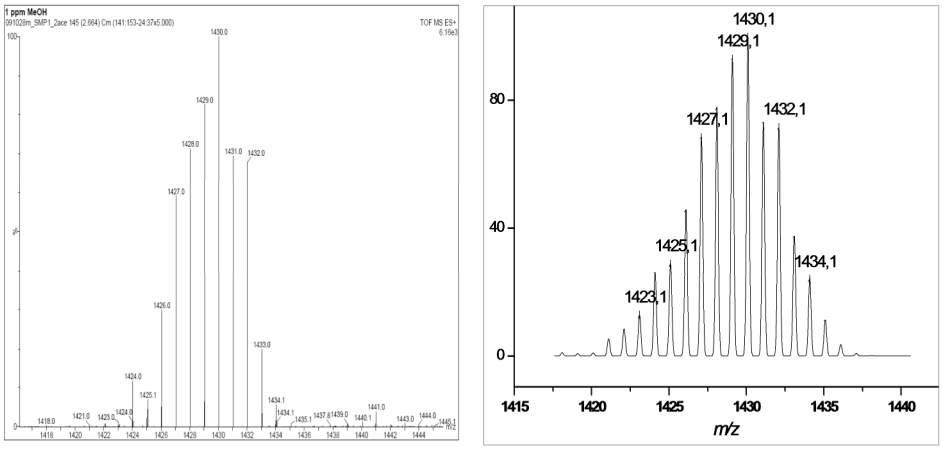

(b)

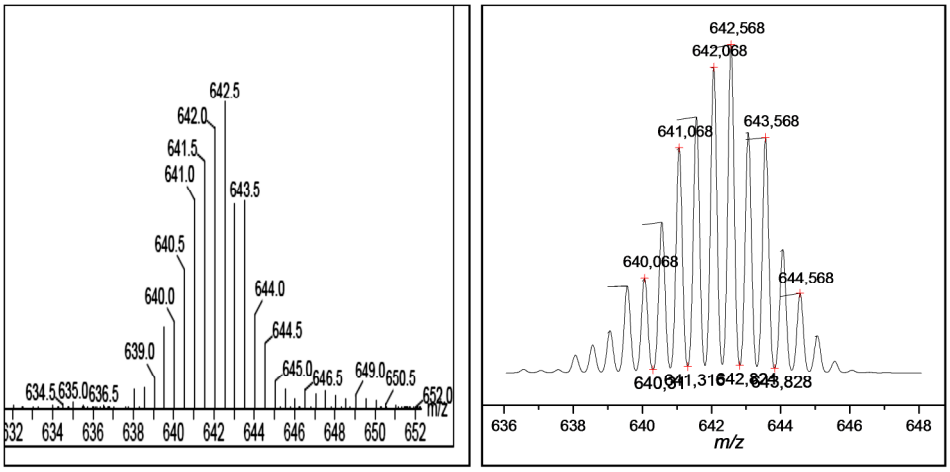

Figure S5. UV-vis spectra of {[Ru^{II}(trpy)]$_2$(μ-[Co^{II}(Cl)$_2$(bpp)$_2$])}$(PF_6)_2$, **Ru_2Co-Cl_2**, in (a) CH_3CN and (b) CH_2Cl_2.

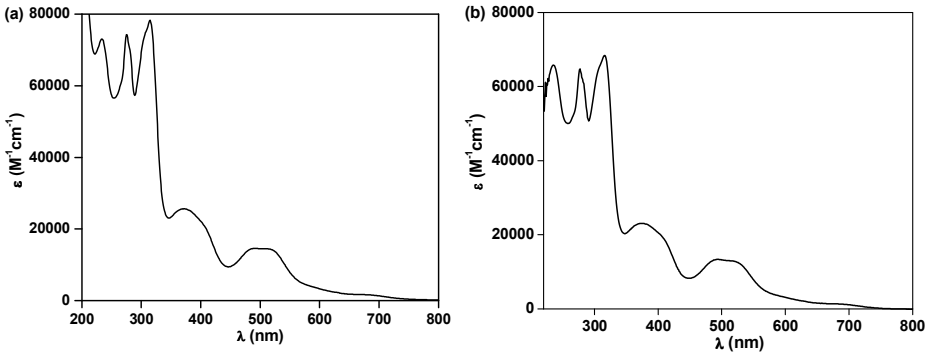

Figure S6. UV-vis spectra of {[Ru^{II}(trpy)]$_2$(μ-[Mn^{II}(Cl)$_2$(bpp)$_2$])}$(PF_6)_2$, **Ru_2Mn-Cl_2**, in (a) CH_3CN and (b) CH_2Cl_2.

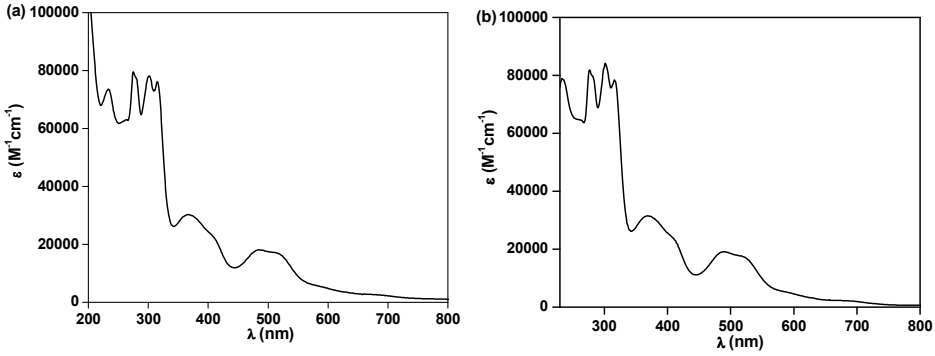

Figure S7. UV-vis spectra of $\{[Ru^{II}(trpy)]_2(\mu\text{-}[Co^{II}(AcO)_2(bpp)_2])\}(PF_6)_2$, **$Ru_2Co$-$OAc_2$**, in (a) CH_3CN and (b) CH_2Cl_2.

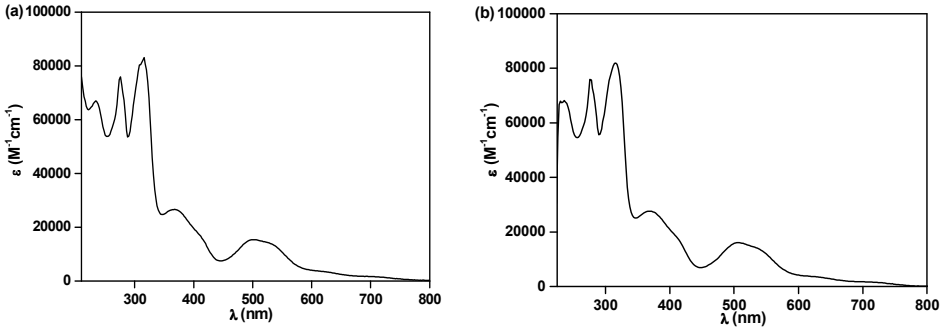

Figure S8. UV-vis spectra of $\{[Ru^{II}(trpy)]_2(\mu\text{-}[Mn^{II}(AcO)_2(bpp)_2])\}(PF_6)_2$, **$Ru_2CMn$-$OAc_2$**, in (a) CH_3CN and (b) CH_2Cl_2.

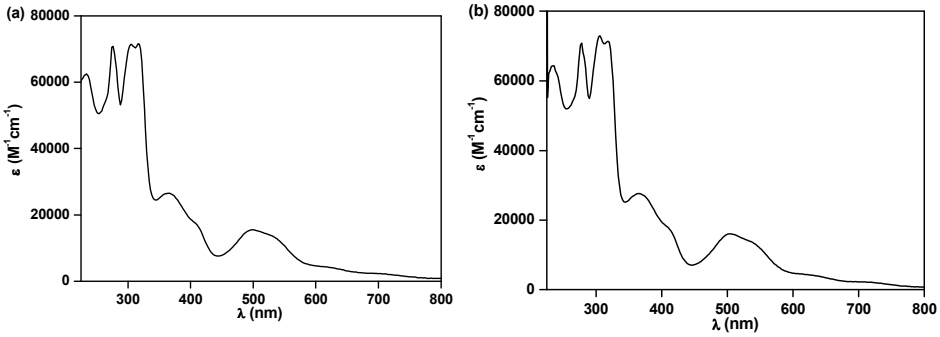

Figure S9. UV-visible absorption spectra of a 0.25 mM solution of **Ru_2Co-OAc_2** (red) in CH_3CN and of a 0.41 mM solution of **Ru_2Mn-OAc_2** (black) in CH_3CN.

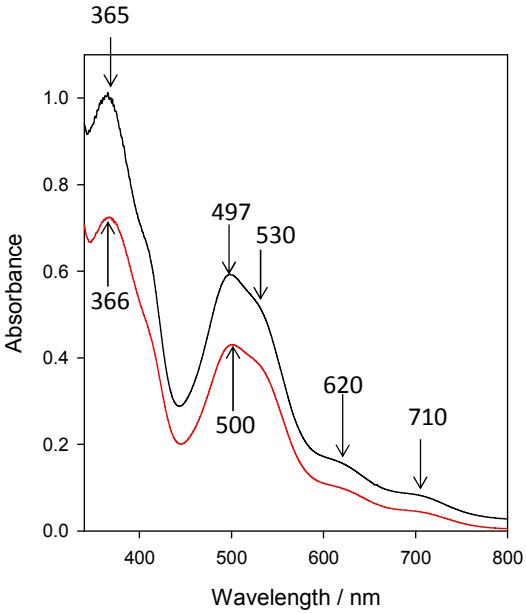

Figure S10. IR spectra (KBr) of $\{[Ru^{II}(trpy)]_2(\mu\text{-}[Co^{II}(Cl)_2(bpp)_2])\}(PF_6)_2$, **$Ru_2Co\text{-}Cl_2$**.

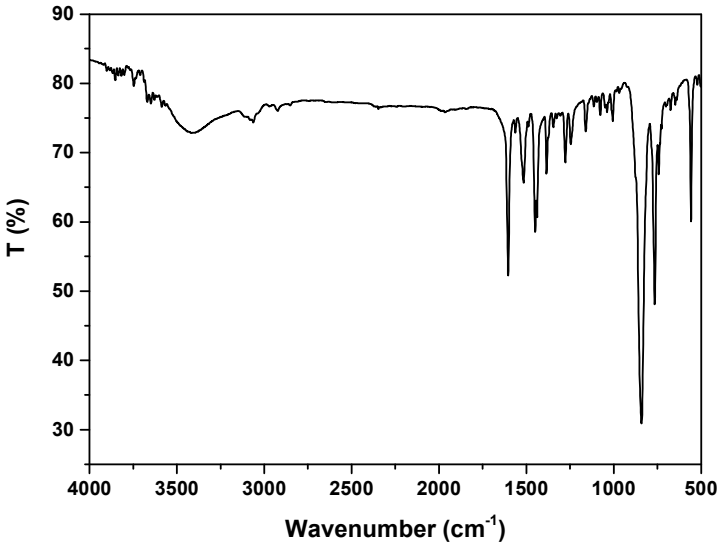

Figure S11. IR spectra (KBr) of $\{[Ru^{II}(trpy)]_2(\mu\text{-}[Mn^{II}(Cl)_2(bpp)_2])\}(PF_6)_2$, **$Ru_2Mn\text{-}Cl_2$**.

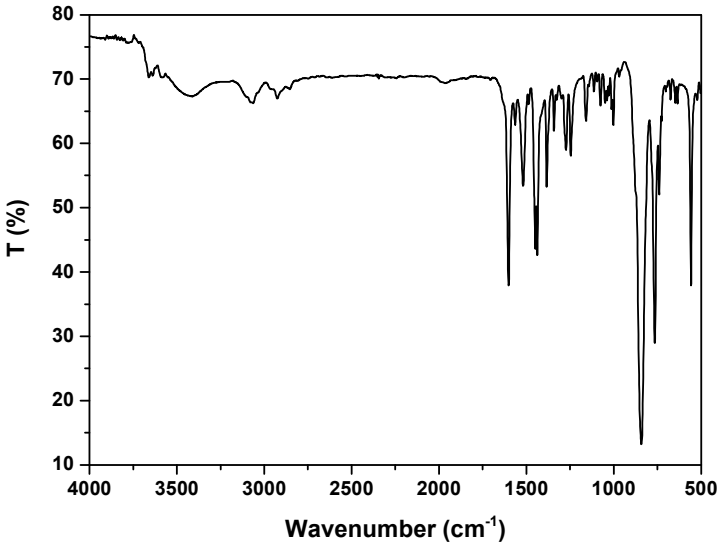

Figure S12. IR spectra (KBr) of {[Ru^{II}(trpy)]$_2$(μ-[Co^{II}(OAc)$_2$(bpp)$_2$])}$(PF_6)_2$, **Ru_2Co-OAc_2**.

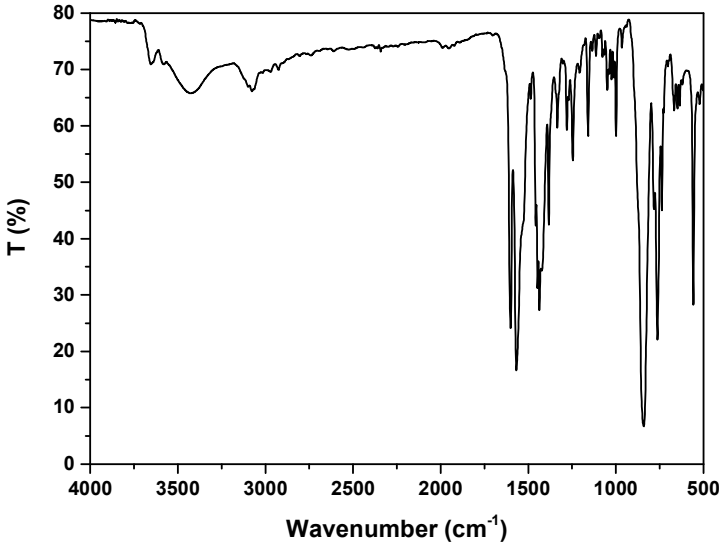

Figure S13. IR spectra (KBr) of {[Ru^{II}(trpy)]$_2$(μ-[Mn^{II}(OAc)$_2$(bpp)$_2$])}$(PF_6)_2$, **Ru_2Mn-OAc_2**.

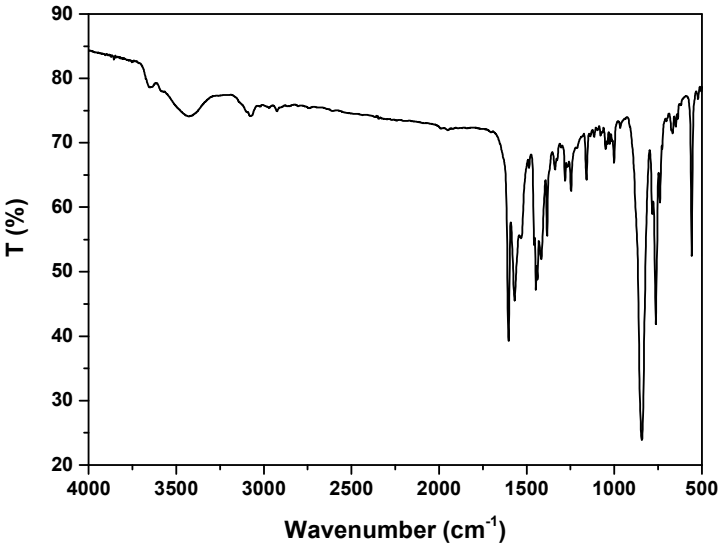

Figure S14. CV (black) and DPV (red) of $\{[Ru^{II}(trpy)]_2(\mu\text{-}[Co^{II}(Cl)_2(bpp)_2])\}(PF_6)_2$, **$Ru_2Co\text{-}Cl_2$**, in CH_2Cl_2.

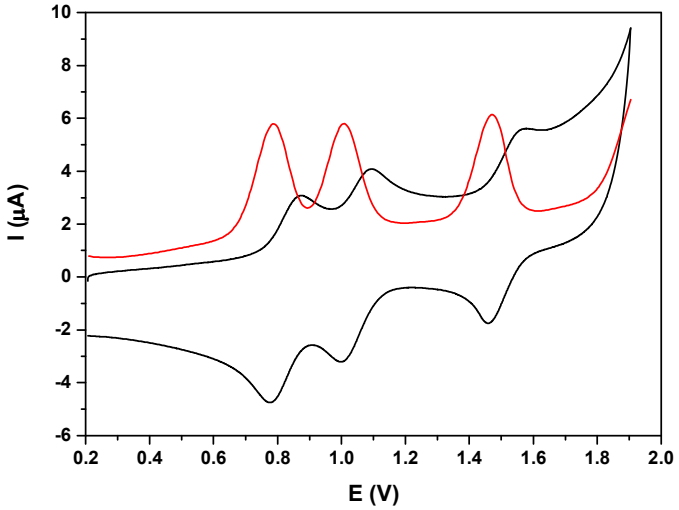

Figure S15. CV (black) and DPV (red) of $\{[Ru^{II}(trpy)]_2(\mu\text{-}[Mn^{II}(Cl)_2(bpp)_2])\}(PF_6)_2$, **$Ru_2Mn\text{-}Cl_2$**, in CH_2Cl_2.

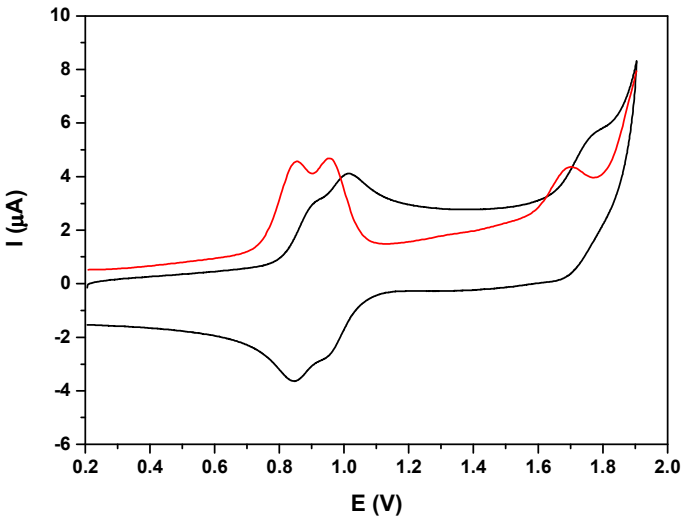

Figure S16. CV (black) and DPV (red) of {[Ru^{II}(trpy)]$_2$(μ-[Co^{II}(AcO)$_2$(bpp)$_2$])}$(PF_6)_2$, **Ru_2Co-OAc_2**, in CH_3CN.

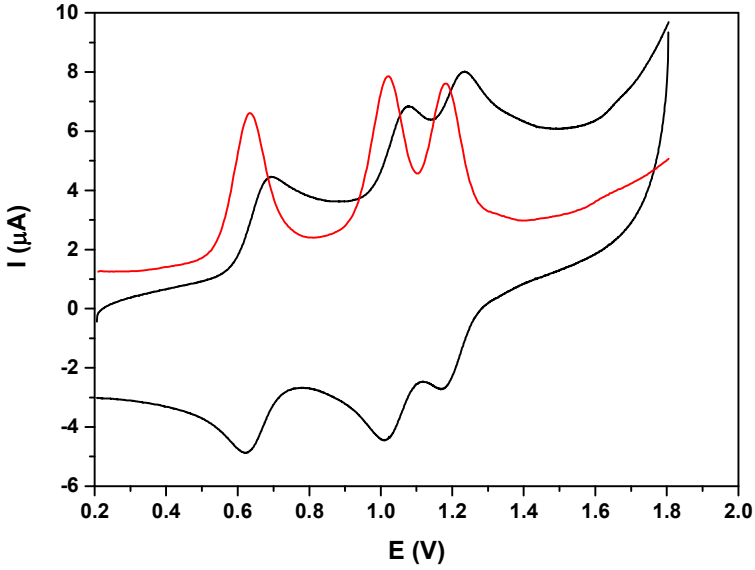

Figure S17. CV (black) and DPV (red) of {[Ru^{II}(trpy)]$_2$(μ-[Mn^{II}(AcO)$_2$(bpp)$_2$])}$(PF_6)_2$, **Ru_2Mn-OAc_2**, in CH_3CN.

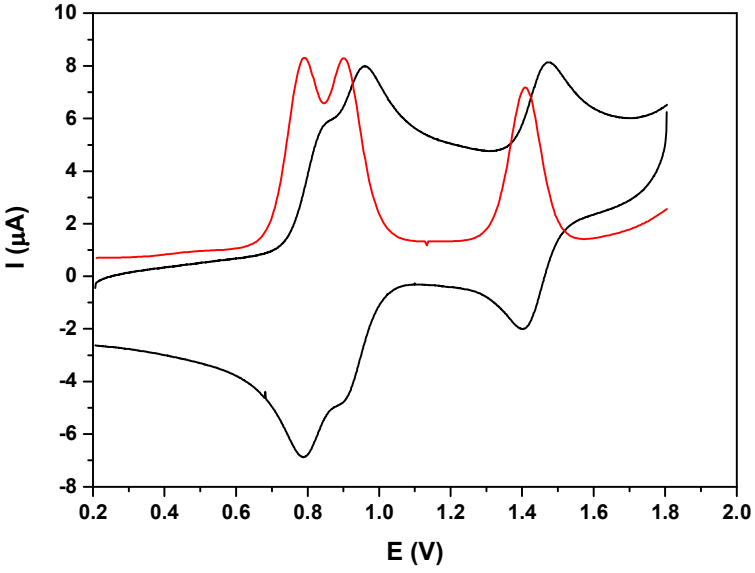

Figure 18. Cyclic voltammograms at a vitreous carbon electrode (diameter 3 mm) in CH_3CN, 0.1 M [(nBu$_4$N)ClO$_4$] of (A) a 0.25 mM solution of **Ru$_2$Co-OAc$_2$**, (B) after exhaustive oxidation at 0.85 V vs NHE (0.30 vs Ag/Ag$^+$) of the previous solution (formation of Ru$_2$(II)Co(III)), (C) after exhaustive oxidation at 1.40 vs NHE (0.85 vs Ag/Ag$^+$) of the previous solution (formation of Ru$_2$(III)Co(III)); scan rate 100 mV·s^{-1}.E vs NHE = E vs Ag/Ag$^+$ + 0.548.

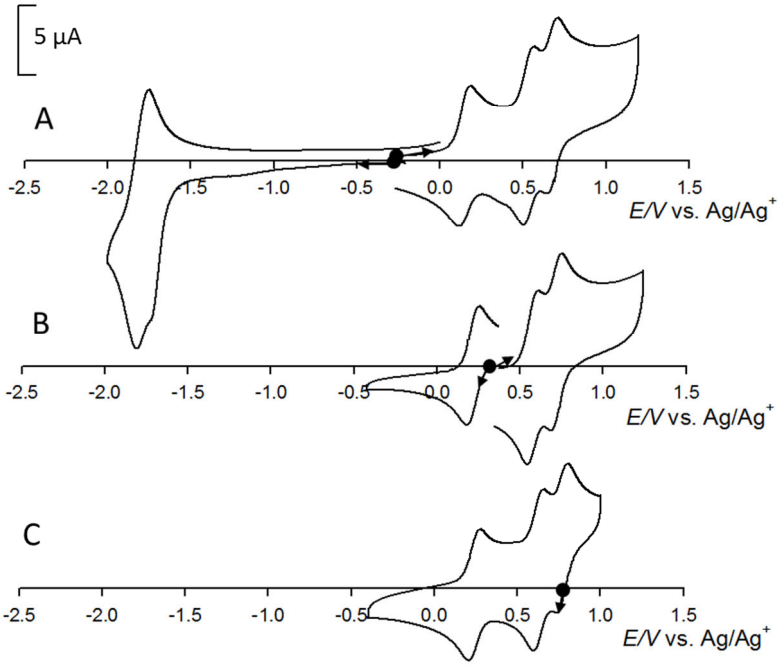

Figure S19. Voltammograms at a carbon Rotating Disk Electrode (2 mm diameter) of a 0.25 mM solution of **Ru_2Co-OAc_2** in CH_3CN, 0.1 M [(nBu$_4$N)ClO$_4$],: (A) initial solution, (B) after oxidation at 0.85 V vs NHE (0.30 vs Ag/Ag$^+$), (C) after oxidation at 1.40 vs NHE (0.85 vs Ag/Ag$^+$), rotation rate: ω = 600 rot/min, scan rate: v = 10 mVs^{-1}. *E* vs NHE = *E* vs Ag/Ag$^+$ + 0.548.

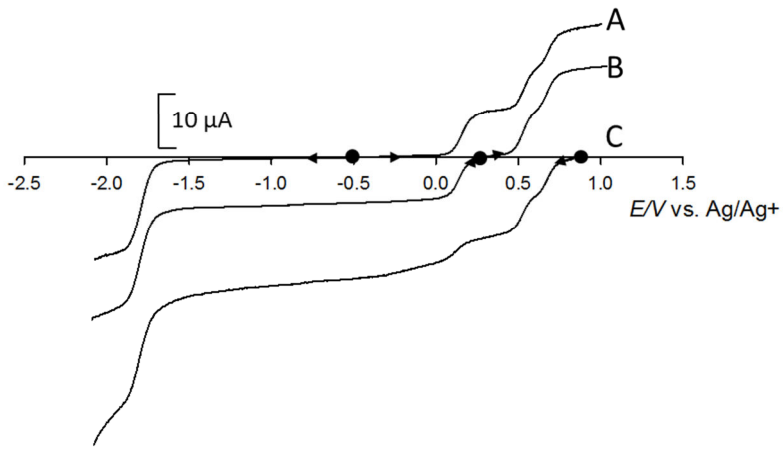

Figure S20. Cyclic voltammograms at a vitreous carbon electrode (diameter 3 mm) in CH_3CN, 0.1 M [(nBu$_4$N)ClO$_4$] of a 0.25 mM solution of **Ru_2Co-OAc_2** (black) and after two successive oxidations at 0.85 and 1.40 V vs NHE(0.30 and 0.85 V vs Ag/Ag$^+$), respectively, and one reduction at 0.35 V vs NHE(-0.20 V vs Ag/Ag$^+$) (red). *E* vs NHE = *E* vs Ag/Ag$^+$ + 0.548.

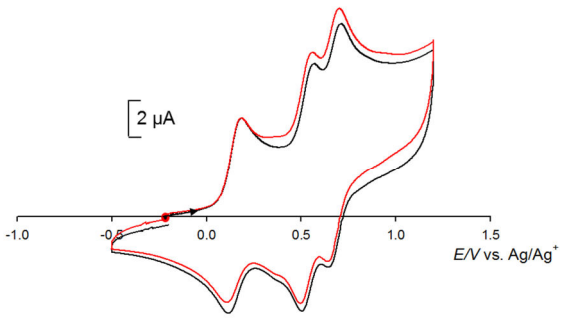

Figure S21. Cyclic voltammograms at a vitreous platinum electrode (diameter 5 mm) in CH_3CN, 0.1 M [(nBu$_4$N)ClO_4]of (A) a 0.41 mM solution of **Ru_2Mn-OAc_2**, (B) after exhaustive oxidation at 1.11 V vs NHE (0.56 vs Ag/Ag^+) of the previous solution (formation of Ru_2(III)Mn(II)), (C) after exhaustive oxidation at 1.69 vs NHE (1.14 vs Ag/Ag^+) of the previous solution (formation of Ru_2(III)Mn(III)); scan rate 50 $mV{\cdot}s^{-1}$.E vs NHE = E vs Ag/Ag^+ + 0.548.

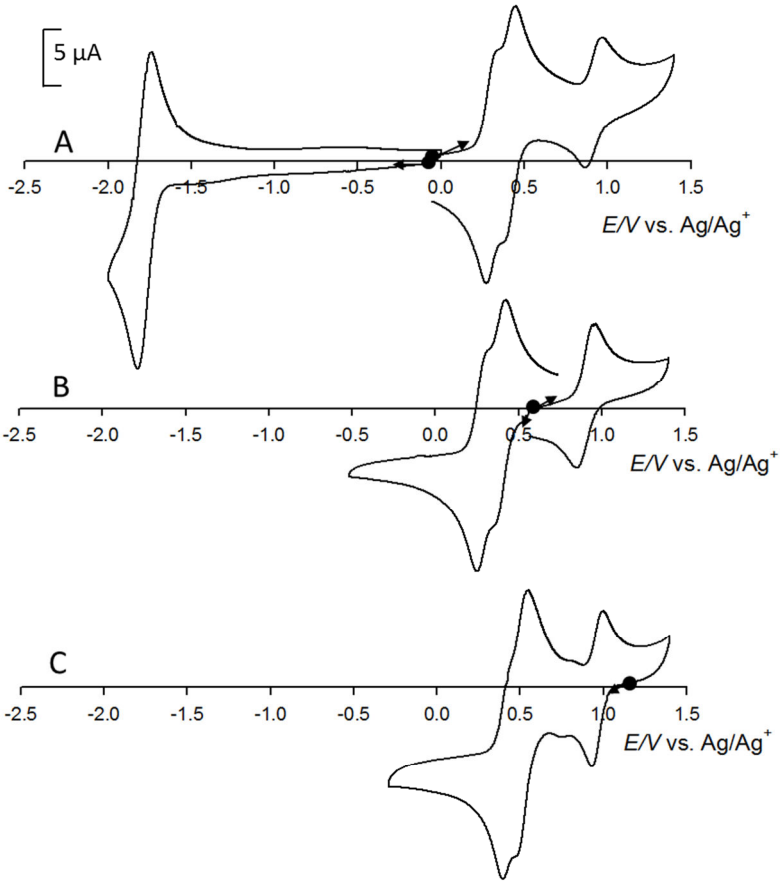

Figure S22. Cyclic voltammograms at a vitreous platinum electrode (diameter 5 mm) in CH_3CN, 0.1 M [(nBu$_4$N)ClO_4] of a 0.41 mM solution of **Ru_2Mn-OAc_2** (black) and after two successive oxidations at 1.11 and 1.69 V vs NHE(0.56 and 1.14 V vs Ag/Ag^+), respectively, and one reduction at 0.35 V vs NHE(-0.20 V vs Ag/Ag^+) (red). E vs NHE = E vs Ag/Ag^+ + 0.548

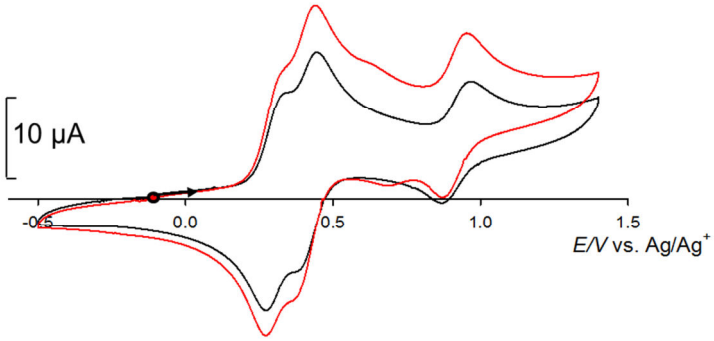

Figure S23. CV in a mixture (19:1) of pH = 1 CF_3SO_3H and CF_3CH_2OH, of (red) **Ru_2Co-OAc$_2$**, (black) **Ru_2Mn-OAc$_2$**, and (blue) ***in*-1**.

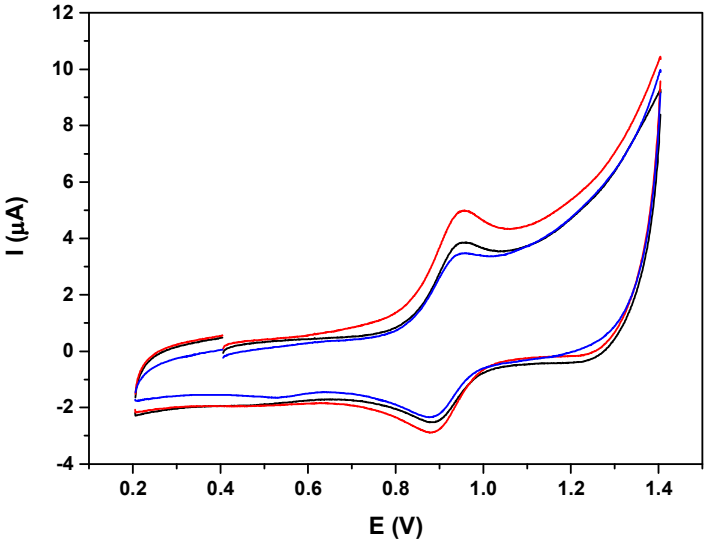

Figure S24. CV in a mixture (19:1) of pH = 7.0 (50 mM) phosphate buffer and CF_3CH_2OH, of (red) **Ru_2Co-OAc$_2$**, (black) **Ru_2Mn-OAc$_2$**, and (blue) ***in*-1**.

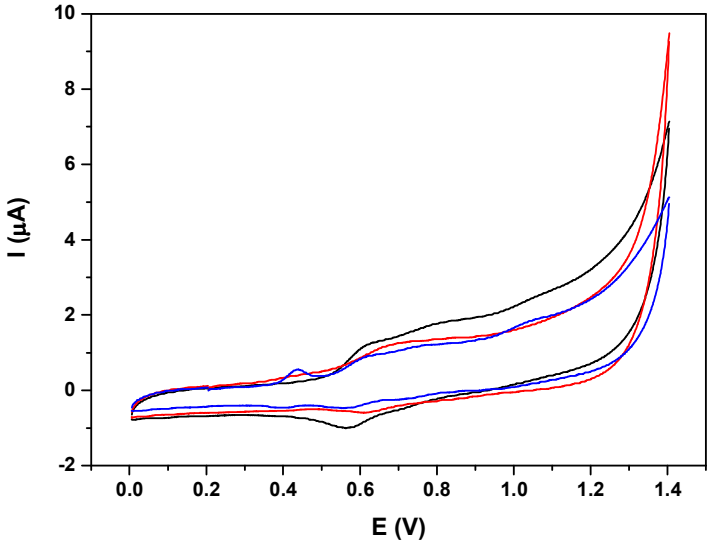

Figure S25. rRaman spectra of a mixture of 400 µLof a 0.5 M solution of Oxone in pH = 7.0 phosphate buffer mixed with 400 µL of $H_2{}^{16}O$ (red) and mixed with 400 µL of $H_2{}^{18}O$ (orange), after 30minutes (yellow), 1 hour (green), 2 hours (blue) and 10 hours (purple).

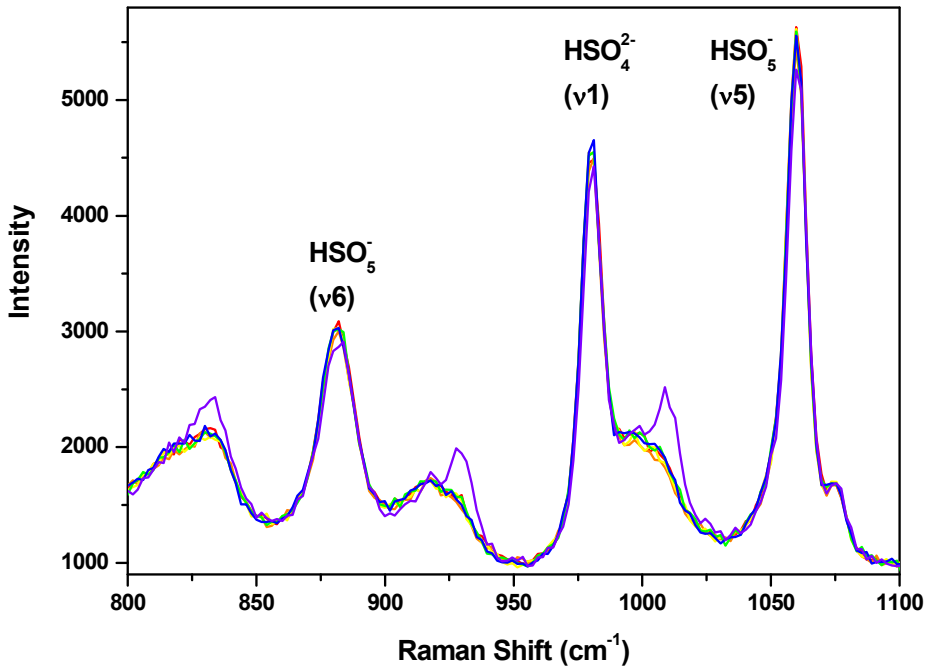

Figure S26. Ratios $^{32}O_2/^{34}O_2$ obtained from the on-line mass analysis. Top: isotopic labelling at 97% of $H_2{}^{18}O$. Bottom: isotopic labelling at 15% of $H_2{}^{18}O$.

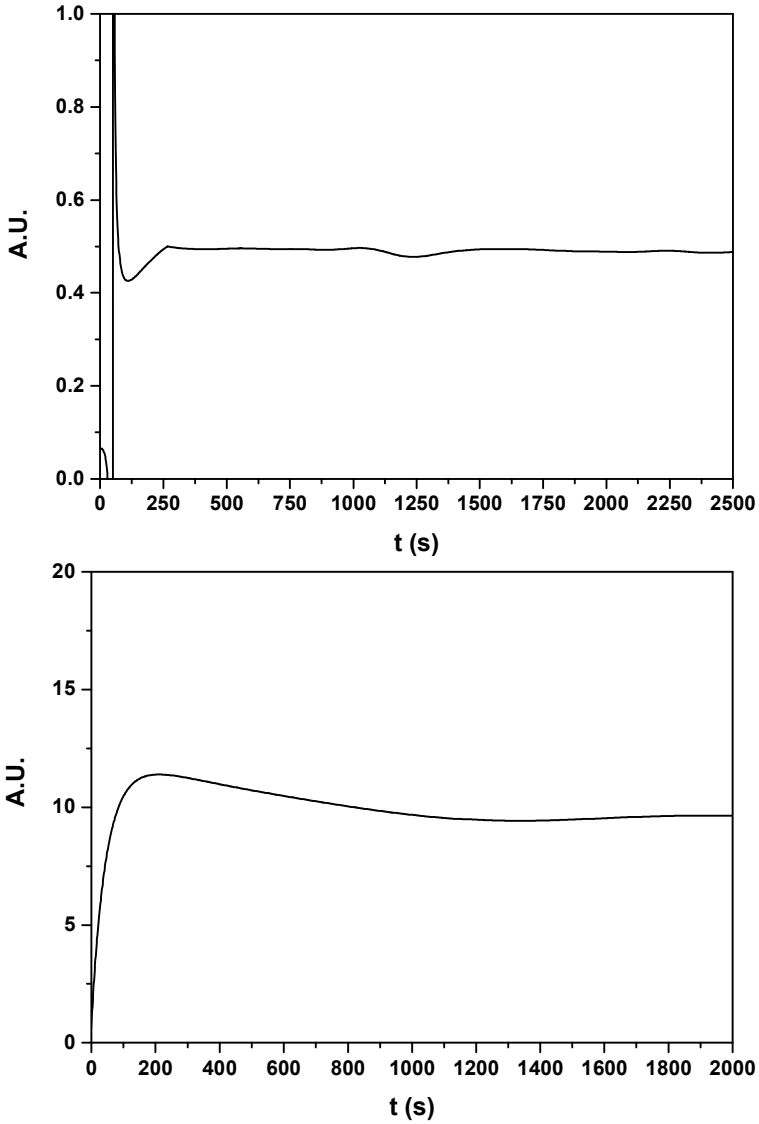

UNIVERSITAT ROVIRA I VIRGILI
MONONUCLEAR AND HETEROTRINUCLEAR RUTHENIUM COMPLEXES: SYNTHESIS AND WATER OXIDATION ACTIVITY.
Lorenzo Mognon
Dipòsit Legal: T 1359-2015

UNIVERSITAT ROVIRA I VIRGILI
MONONUCLEAR AND HETEROTRINUCLEAR RUTHENIUM COMPLEXES: SYNTHESIS AND WATER OXIDATION ACTIVITY.
Lorenzo Mognon
Dipòsit Legal: T 1359-2015

Chapter 5. Single Site Isomeric Ru WOCs with Electron Withdrawing Groups: Synthesis, Electrochemical Characterization and Reactivity

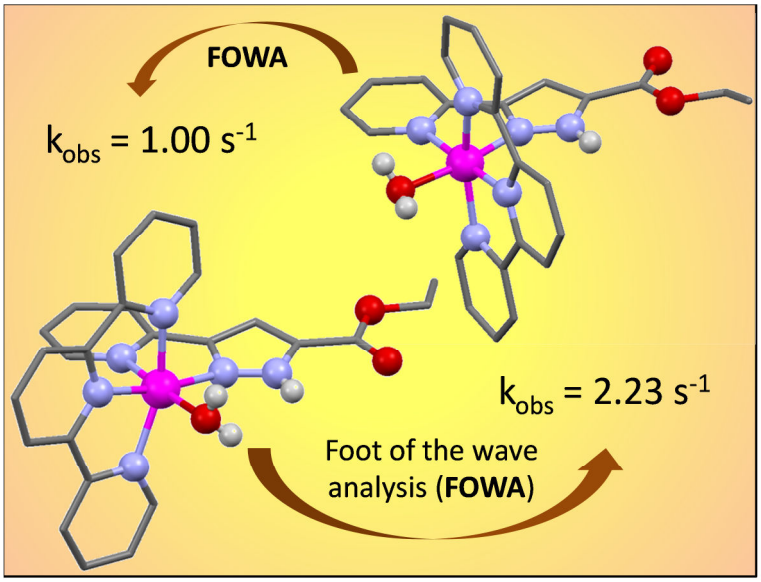

New mononuclear ruthenium complexes based on 1*H*-Pyrazole-3-Carboxylic Acid, 5-(2-pyridinil)-, ethyl ester are synthesized and extensively characterized. A linkage isomerism is identified and analyzed by electrochemical methods. Foot-of-the-wave analysis is applied to the electrocatalytic water oxidation and kinetic constants are obtained. Ce(IV) is used as sacrificial oxidant to study chemically driven water oxidation.

UNIVERSITAT ROVIRA I VIRGILI
MONONUCLEAR AND HETEROTRINUCLEAR RUTHENIUM COMPLEXES: SYNTHESIS AND WATER OXIDATION ACTIVITY.
Lorenzo Mognon
Dipòsit Legal: T 1359-2015

Chapter 5. Single Site Isomeric Ru WOCs with Electron Withdrawing Groups: Synthesis, Electrochemical Characterization and Reactivity.

UNIVERSITAT ROVIRA I VIRGILI
MONONUCLEAR AND HETEROTRINUCLEAR RUTHENIUM COMPLEXES: SYNTHESIS AND WATER OXIDATION ACTIVITY.
Lorenzo Mognon
Dipòsit Legal: T 1359-2015

Chapter 5. Single Site Isomeric Ru WOCs with Electron Withdrawing Groups: Synthesis, Electrochemical Characterization and Reactivity

Lorenzo Mognon,[a] Jordi Benet-Buchholz,[a] and Antoni Llobet[a,b]

[a] Institute of Chemical Research of Catalonia (ICIQ), Avinguda Països Catalans 16, 43007 Tarragona, Spain

[b] Departament de Química, Universitat Autònoma de Barcelona, Cerdanyola del Vallès, 08193 Barcelona, Spain

5.1 Abstract

The synthetic intermediate *cis(out), cis*-[Ru(Cl)$_2$(HL)(dmso)$_2$], **1**, and four new mononuclear ruthenium complexes with general formula *out/in*-[Ru(HL)(trpy)(X)]$^{m+}$ (X = Cl$^-$, m = 1, **2a**$^+$ and **2b**$^+$; X = H_2O, m = 2, **3a**$^{2+}$ and **3b**$^{2+}$) based on the never used before ligand 1*H*-Pyrazole-3-Carboxylic Acid, 5-(2-pyridinil)-, ethyl ester (HL), are synthesized and characterized by analytical, spectroscopic and electrochemical methods. A linkage isomerism is observed for a dmso moiety of **1**, and relevant thermodynamic and kinetic values are obtained through electrochemical experiments and compared to literature. Different synthetic routes are developed to obtain isomeric **2a**$^+$ and **2b**$^+$, with

different relative yields. Water oxidation activity of **3a**$^{2+}$ and **3b**$^{2+}$ is analyzed by means of electrochemical methods, through foot-of-the-wave analysis, yielding k_{obs} values of 1.00 and 2.23 s^{-1}, respectively. Chemically driven water oxidation activity is tested using $[(NH_4)_2Ce(NO_3)_6]$ as sacrificial electron acceptor, and values of TON = 10.8 and $TOF_i = 58.2 \times 10^{-3}$ s^{-1} for **3a**$^{2+}$ and TON = 4.2 and $TOF_i = 15.4 \times 10^{-3}$ s^{-1} for **3b**$^{2+}$ are obtained.

5.2 Introduction

Since the discovery by Thummel et al.[1] that mononuclear Ru complexes were active as water oxidation catalysts, there has been a large development of the field based on this type of complexes. A number of examples exist in the literature which are mainly based on the bimpy[2] and trpy-bpy systems. In 2008 Meyer et al.[3] offered a mechanistic description of how the water oxidation occurred at a molecular level: the O-O bond formation is proposed to occur based on the water nucleophilic attack pathway (WNA). This description has now been adapted to many other mononuclear Ru complexes, and also to some Ir or first row transition metals, where the water oxidation catalysis is claimed to proceed through a molecular pathway.[4]

Later on, Berlinguette and coworkers[5] studied the strong influence that electronic perturbation of the metal center exerted through remote positions of the ligands over the whole water oxidation catalytic process. Our group have recently reported examples of mononuclear ruthenium terpy-bpy complexes having bpy substituted with fluoro groups at different positions, in order to observe the effect of electron withdrawing groups on the overall water oxidation process.[6] Finally, recent reports by Yagi and coworkers[7] have

shown how the presence of a N-lone pair can influence reactivity in isomeric 2-(2-pyridyl)-1,8-naphthyridine complexes.

In the present chapter we report the full spectroscopic and electrochemical characterization of a new family of complexes of general formula *out/in*-[Ru(HL)(trpy)(X)]$^{m+}$ (HL = 1*H*-Pyrazole-3-Carboxylic Acid, 5-(2-pyridinil)-, ethyl ester; X = Cl^-, m = 1, **2a**$^+$ and **2b**$^+$; X = H_2O, m = 2, **3a**$^+$ and **3b**$^+$), that allows to observe the subtle differences produced by the *out* and *in* constitutional isomers. These include specific intrinsic electronic *trans* and acid/base effects. Moreover, the electron withdrawing nature of the ester will allow us to compare their performances with related complexes previously reported in the literature.

In addition we also report a synthetic intermediate with formula *cis(out), cis*-[Ru(Cl)$_2$(HL)(dmso)$_2$], **1**, that represents a new example of Ru-dmso linkage isomerization phenomena prompted by a change in oxidation state of the Ru(II) metal center.

5.3 Experimental Section

Preparations. *1*H-Pyrazole-3-Carboxylic Acid, 5-(2-pyridinil)-, ethyl ester (HL),[8] [RuCl$_2$(dmso)$_4$][9] and *cis*-[Ru(Cl)$_2$(trpy)(dmso)][10] were prepared accordingly to literature procedures.

***cis(out), cis*-[Ru(Cl)$_2$(HL)(dmso)$_2$]·H$_2$O, 1·H$_2$O.** In a 250 mL round-bottom flask, HL (1.5 g, 6.91 mmol) and RuCl$_2$(dmso)$_4$ (3.35 g, 6.91 mmol) are refluxed overnight in methanol (180 mL). The solution is then cooled to room temperature and a yellow solid is filtered. The solid is washed with cold

methanol and with diethyl ether and then dried under vacuum. Yield: 2.525 g (67.0%). Anal. Found (calcd) for $C_{15}H_{23}Cl_2N_3O_4RuS_2 \cdot H_2O$; C, 32.23 (31.97); H,4.21 (4.47); N, 7.32 (7.46); S, 11.48 (11.38). ^{1}H NMR (400 MHz, d_6-dmso): δ = 9.23 (d, $^3J_{1\text{-}2}$ = 5.24 Hz, H1), 8.38 (d, $^3J_{4\text{-}3}$ = 7.74 Hz, H4), 8.21 (dd, $^3J_{3\text{-}4}$ = 7.74 Hz, $^3J_{3\text{-}2}$ = 7.74 Hz, H3), 7.97 (s, H7), 7.70 (dd, $^3J_{2\text{-}3}$ = 7.74 Hz, $^3J_{2\text{-}1}$ = 5.24 Hz, H2), 4.40 (m, H10), 3.47 (s, CH_3 of C14 and C15), 3.44 (s, H12), 2.54 (s, H13), 1.34 (t, $^3J_{11\text{-}10}$ = 7.11 Hz, H11). Cyclic voltammetry (CH_2Cl_2, TBAH): $E_{1/2}$ = 1.39 V (ΔE_p = 121 mV).

***out*-[Ru(Cl)(HL)(trpy)](PF$_6$)·CH$_3$OH, 2a(PF$_6$)·MeOH, and *in*-[Ru(Cl)(HL)(trpy)](PF$_6$)·H$_2$O, 2b(PF$_6$)·H$_2$O. Route A.** In a 250 mL round bottom flask, **1** (200 mg, 0.367 mmol) and terpyridine (86 mg, 0.369 mmol) are dissolved in methanol (150 mL). The solution is refluxed overnight. The mixture is then evaporated to dryness, and the resulting solid dissolved in CH_2Cl_2 and purified over neutral alumina using a mixture CH_2Cl_2/CH_3CN (1:1, v/v) as eluent. The first pink fraction, corresponding to the *out* isomer, is added to 1 mL of a saturated aqueous NH_4PF_6 solution and then dried at the rotary evaporator. The residue thus obtained is dissolved in acetone and water is added. The acetone is evaporated until a brown solid precipitates. The solid is filtered on a frit, washed with cold water and diethyl ether and dried under vacuum. Yield: 161 mg (59.9%). Anal. Calcd for $C_{26}H_{22}ClF_6N_6O_2PRu \cdot MeOH$: C, 42.45; H, 3.43; N, 11.00. Found: C, 42.29; H, 3.15; N, 10.80. ^{1}H NMR (500 MHz, d_6-acetone): δ = 10.18 (d, $^3J_{16\text{-}17}$ = 5.02 Hz, H16), 8.66 (d, $^3J_{7\text{-}8}$ = $^3J_{9\text{-}8}$ = 8.01 Hz, H7, H9), 8.63 (d, $^3J_{19\text{-}18}$ = 7.90 Hz, H19), 8.60 (d, $^3J_{4\text{-}3}$ = $^3J_{12\text{-}13}$ = 7.79 Hz, H4, H12), 8.35 (dd, $^3J_{18\text{-}19}$ = 7.90 Hz, $^3J_{18\text{-}17}$ = 7.66 Hz, H18), 8.15 (t, $^3J_{8\text{-}7}$ = $^3J_{8\text{-}9}$ = 8.01 Hz, H8), 8.01 (dd, $^3J_{3\text{-}4}$ = $^3J_{13\text{-}12}$ = 7.79 Hz, $^3J_{3\text{-}2}$ = $^3J_{13\text{-}14}$ = 7.57 Hz, H3, H13), 7.93 (dd, $^3J_{17\text{-}18}$ = 7.66 Hz, $^3J_{17\text{-}16}$ = 5.02 Hz, H17), 7.83 (d, $^3J_{1\text{-}2}$ = $^3J_{15\text{-}14}$ = 5.14 Hz, H1, H15), 7.80 (s, H22), 7.42(dd, $^3J_{2\text{-}3}$ = $^3J_{14\text{-}13}$ = 7.57 Hz, $^3J_{2\text{-}1}$ = $^3J_{14\text{-}15}$ = 5.14 Hz, H2, H14),

4.40 (q, $^3J_{25\text{-}26}$ = 7.05 Hz, H25) , 1.34 (t, $^3J_{26\text{-}25}$ = 7.05 Hz, H26). ESI-MS (MeOH): *m/z* = 587.0 ([Ru(Cl)(HL)(trpy)]$^+$). Cyclic Voltammetry (CH_2Cl_2, TBAH): $E_{1/2}$ = 1.04 V (ΔE_p = 95 mV).

The fraction remaining on the column, which corresponds to the *in* isomer together with $[Ru(trpy)_2]^{2+}$ and other secondary products, is eluted with methanol and purified over a silica column using a solution 0.05 % of NH_4OH in methanol as eluent. The first yellow eluted fraction from this second column is discarded and the second one (purple) corresponds to the deprotonated *in* complex. This solution is evaporated to dryness and afterward dissolved in acetone containing a few drops of 0.5 M HCl and 1 mL of a saturated NH_4PF_6 aqueous solution. Traces of silica are removed by filtration over cotton. The volume is then again reduced on a rotary evaporator until a solid precipitates out of the solution. The mixture is then cooled in a fridge overnight and the solid filtered on a frit, washed with cold water and diethyl ether, and dried under vacuum. Yield: 16 mg (6.0%) Anal. Calcd for $C_{26}H_{22}ClF_6N_6O_2PRu\cdot H_2O$: C, 41.64; H, 3.23; N, 11.21. Found : C, 41.59; H, 3.14; N, 11.15. ^{1}H NMR (500 MHz, d_6-acetone): δ = 8.74 (d, $^3J_{7\text{-}8}$ = $^3J_{9\text{-}8}$ = 8.05 Hz, H7, H9), 8.62 (d, $^3J_{4\text{-}3}$ = $^3J_{12\text{-}13}$ = 7.98 Hz, H4, H12), 8.35 (d, $^3J_{19\text{-}18}$ = 7.75 Hz, H19), 8.22 (t, $^3J_{8\text{-}7}$ = $^3J_{8\text{-}9}$ = 8.05 Hz, H8), 8.21 (s, H22), 8.02 (d, $^3J_{1\text{-}2}$ = $^3J_{15\text{-}14}$ = 5.39 Hz, H1, H15), 8.01 (dd, $^3J_{3\text{-}4}$ = $^3J_{13\text{-}12}$ = 7.98 Hz, $^3J_{3\text{-}2}$ = $^3J_{13\text{-}14}$ = 7.90 Hz, H3, H13), 7.79 (dd, $^3J_{18\text{-}19}$ = 7.75 Hz, $^3J_{18\text{-}17}$ = 7.60 Hz, H18), 7.74 (dd, $^3J_{2\text{-}3}$ = $^3J_{14\text{-}13}$ = 7.90 Hz, $^3J_{2\text{-}1}$ = $^3J_{14\text{-}15}$ = 5.39 Hz, H2, H14), 7.45 (d, $^3J_{16\text{-}17}$ = 5.84 Hz, H16), 7.02(dd, $^3J_{17\text{-}18}$ = 7.60 Hz, $^3J_{17\text{-}16}$ = 5.84 Hz, H17), 4.55 (q, $^3J_{25\text{-}26}$ = 7.03 Hz, H25), 1.47 (t, $^3J_{26\text{-}25}$ = 7.03 Hz, H26). ESI-MS (MeOH): *m/z* = 587.1 ([Ru(Cl)(HL)(trpy)]$^+$). Cyclic Voltammetry (CH_2Cl_2, TBAH): $E_{1/2}$ = 1.13 V (ΔE_p = 144 mV).

Route B. In a 250 mL round-bottom flask, *cis*-[Ru(Cl)$_2$(dmso)(trpy)] (177.4 mg, 0.367 mmol) and HL (80.0 mg, 0.368 mmol) are dissolved in methanol (150 mL) and the solution is refluxed for 5 days. The purification method is the same as route A. Yields: 32 mg of **2a** (11.9%) and 65 mg of **2b** (24.2%).

***out*-[Ru(HL)(trpy)(H$_2$O)](ClO$_4$)$_2$·2H$_2$O, 3a(ClO$_4$)$_2$·2H$_2$O.** In a 25 mL round-bottom flask, 50 mg (0.068 mmol) of *out*-[Ru(Cl)(HL)(trpy)](PF$_6$) and 15 mg (0.072 mmol) of AgClO$_4$ are dissolved in 20 mL of a water/acetone 1:3 mixture and refluxed for 2 h away from light. The solution is then cooled in the fridge for 1h. The precipitated AgCl is filtered over Celite. A few drops of a saturated LiClO$_4$ aqueous solution are added to the filtrate, and then the volume is reduced until the formation of a precipitate. The solution is then cooled in fridge overnight, filtered and the solid washed with cold water and diethyl ether and then vacuum dried. Yield: 41 mg (78.5%). Anal. Calcd for C$_{26}$H$_{24}$Cl$_2$N$_6$O$_{11}$Ru·0.5H$_2$O: C, 40.17; H, 3.24; N, 10.81. Found: C, 40.05; H, 2.91; N, 10.62.^{1}H NMR (500 MHz, pD = 1.0 in 0.1 M CF$_3$SO$_3$D in D$_2$O): δ = 9.38 (d, $^3J_{16\text{-}17}$ = 5.52 Hz, H16), 8.50 (d, $^3J_{7\text{-}8}$ = $^3J_{9\text{-}8}$ = 8.15 Hz, H7, H9), 8.39 (d, $^3J_{12\text{-}13}$ = $^3J_{4\text{-}3}$ = 8.03 Hz, H12, H4), 8.36 (d, $^3J_{19\text{-}18}$ = 7.93 Hz, H19), 8.25 (dd, $^3J_{18\text{-}19}$ = 7.93 Hz, $^3J_{18\text{-}17}$ = 7.67 Hz, H18), 8.16 (t, $^3J_{8\text{-}7}$ = $^3J_{8\text{-}9}$ = 8.15 Hz, H8), 7.94 (dd, $^3J_{3\text{-}4}$ = $^3J_{13\text{-}12}$ = 8.03 Hz, $^3J_{3\text{-}2}$ = $^3J_{13\text{-}14}$ = 7.75 Hz, H3, H13), 7.86 (dd, $^3J_{17\text{-}18}$ = 7.67 Hz, $^3J_{17\text{-}16}$ = 5.52 Hz, H17), 7.75 (d, $^3J_{1\text{-}2}$ = $^3J_{15\text{-}14}$ = 5.55 Hz, H1, H15), 7.54 (s, H22), 7.29 (dd, $^3J_{2\text{-}3}$ =$^3J_{14\text{-}13}$ = 7.75 Hz, $^3J_{2\text{-}11}$ = $^3J_{14\text{-}15}$ = 5.55 Hz, H2, H14), 4.16 (q, $^3J_{25\text{-}26}$ = 7.15 Hz, H25), 1.15 (t, $^3J_{26\text{-}25}$ = 7.15 Hz, H26). ESI-MS (MeOH): *m/z* = 568.0 [Ru(OH)(HL)(trpy)]$^+$). Cyclic Voltammetry (pH = 1.0 in CF$_3$SO$_3$H): $E_{1/2}$ = 0.93 V (ΔE_p = 59 mV), $E_{1/2}$ = 1.26 V (ΔE_p = 165 mV); Cyclic Voltammetry (pH = 7.0 phosphate buffer): $E_{1/2}$ = 0.52 V (ΔE_p = 59 mV).

***in*-[Ru(HL)(trpy)(H_2O)](ClO_4)$_2$, 3b(ClO_4)$_2$.** This compound is prepared following the same procedure as **3a**, but using complex **2b** instead of **2a** as reagent. Yield: 35.0 mg (67.0%). Anal. Calcd for $C_{26}H_{24}Cl_2N_6O_{11}Ru$: C, 40.64; H, 3.15; N, 10.94. Found: C, 40.52; H, 2.89; N, 10.66. ^{1}H NMR (500 MHz, pD = 1.0 in 0.1 M CF_3SO_3D in D_2O): δ = 8.54 (d, $^3J_{19\text{-}18}$ = $^3J_{19\text{-}20}$ = 8.15 Hz, H19), 8.40 (d, $^3J_{15\text{-}14}$ = $^3J_{23\text{-}24}$ = 7.87 Hz, H15, H23), 8.20 (t, $^3J_{19\text{-}18}$ = $^3J_{19\text{-}20}$ = 8.15 Hz, H19), 7.99 (d, $^3J_{4\text{-}3}$ = 7.68 Hz, H4), 7.97 (s, H7), 7.94 (dd, $^3J_{14\text{-}13}$ = $^3J_{24\text{-}25}$ = 7.89 Hz, $^3J_{14\text{-}15}$ = $^3J_{24\text{-}23}$ = 7.68 Hz, H14, H24), 7.86 (d, $^3J_{12\text{-}13}$ = $^3J_{26\text{-}25}$ = 5.14 Hz, H12, H26), 7.59 (dd, $^3J_{3\text{-}4}$ = 7.68 Hz, $^3J_{3\text{-}2}$ = 7.56 Hz, H3), 7.35 (dd, $^3J_{13\text{-}14}$ = $^3J_{25\text{-}24}$ = 7.89 Hz dd, $^3J_{13\text{-}12}$ = $^3J_{25\text{-}26}$ = 5.49 Hz, H13, H25), 7.18 (d, $^3J_{1\text{-}2}$ = 5.49 Hz, H1), 6.81 (dd, $^3J_{2\text{-}3}$ = 7.56 Hz, $^3J_{2\text{-}1}$ = 5.49 Hz, H2), 4.56 (q, $^3J_{10\text{-}11}$ = 7.10 Hz, H10), 1.47 (t, $^3J_{11\text{-}10}$ = 7.10 Hz, H11). ESI-MS (MeOH): *m/z* = 569.1 ([Ru(OH)(HL)(trpy)]$^+$). Cyclic Voltammetry (pH = 1.0 in 0.1 M CF_3SO_3H): $E_{1/2}$ = 1.00 V (ΔE_p = 63 mV); cyclic voltammetry (pH = 7.0 in phosphate buffer): $E_{1/2}$ = 0.60 V (ΔE_p = 60 mV).

Instruments and measurements. Electrochemical experiments were performed in a one-compartment three electrode cell, using glassy carbon working electrode (ø = 3 mm), platinum counter electrode (ø = 2 mm) and SSCE or Hg/$HgSO_4$ as reference electrodes in organic or aqueous solvents, respectively. All the potentials reported are referred to NHE.

UV–vis spectroscopy was performed on a Cary 50 (Varian) UV–vis spectrometer using 1 cm quartz cells.

Online manometric measurements were carried out on a Testo 521 differential pressure manometer with an operating range of 0.1–10 kPa and accuracy within 0.5% of the measurements. The manometer was coupled to thermostatic reaction vessels for dynamic monitoring of the headspace pressure above each reaction solution. The manometer's secondary ports were

connected to thermostatic reaction vessels containing the same solvents and headspace volumes as the sample vials. Each measurement for a reaction solution (2.0 mL) was performed at 298 K.

The NMR spectroscopy experiments were performed on Bruker Avance 400 and 500 Ultrashield NMR spectrometers.

X-ray Crystal Structure Determination. Crystals of **1** were obtained by slow cooling of a saturated methanol solution of the complex. Crystals of both **3a**$^{2+}$ and **3b**$^{2+}$ were obtained by slow cooling of saturated aqueous solutions. The measured crystals were prepared under inert conditions immersed in perfluoropolyether as protecting oil for manipulation.

Data collection: Crystal structure determination for **1** was carried out using a Bruker-Nonius diffractometer equipped with an APPEX 2 4K CCD area detector, a FR591 rotating anode with MoK_α radiation, Montel mirrors as monochromator and an Oxford Cryosystems low temperature device Cryostream 700 plus (T = -173 °C). Crystal structure determinations for **3a**$^{2+}$ and **3b**$^{2+}$ were carried out using a Apex DUO diffractometer equipped with a Kappa 4-axis goniometer, an APEX II 4K CCD area detector, a Microfocus Source E025 IuS using MoK_α radiation, Quazar MX multilayer Optics as monochromator and an Oxford Cryosystems low temperature device Cryostream 700 plus (T = -173 °C). Full-sphere data collection was used with ω and φ scans. Programs used: Data collection APEX-2,[11] data reduction Bruker Saint[12] V/.60A and absorption correction SADABS.[13,14]

Structure Solution and Refinement: Crystal structure solution was achieved using direct methods as implemented in SHELXTL[15] and visualized using the program XP. Missing atoms were subsequently located from difference Fourier synthesis and added to the atom list. Least-squares refinement on F^2 using all

measured intensities was carried out using the program SHELXTL. All non hydrogen atoms were refined including anisotropic displacement parameters.

Comments to the structures: **1:** The asymmetric unit contains one molecule of the metal complex and one molecule of methanol. The methanol molecule is disordered in three orientations (ratio: 45:40:15). **3a**$^{2+}$**:** The asymmetric unit contains one molecule of the ruthenium metal complex, two ClO_4 anions and two non-coordinated water molecules. One of the ClO_4 anions is disordered in two orientations (ratio: 60:40). **3b**$^{2+}$**:** The asymmetric unit contains one molecule of the cationic metal complex and two ClO_4 anions.

5.4 Results and Discussion

Synthesis and solid state structure. The synthesis of the chlorido complexes **2a**$^{+}$ and **2b**$^{+}$ described in this work has been carried out by two different synthetic routes outlined in Scheme 1, that use $[Ru(Cl)_2(dmso)_4]$, as the starting material.

These two routes differ in the sequential substitution of the Cl and dmso ligands by trpy and HL. In Route A, HL is refluxed in methanol together with $[Ru(Cl)_2(dmso)_4]$ to generate *cis(out), cis*-$[Ru(Cl)_2(HL)(dmso)_2]$, **1**, which has an intense yellow color and where two dmso ligands have been replaced by HL with a good isolated yield of over 67%. This substitution can potentially lead to the formation of six different stereoisomers, with two pairs of enantiomers, depending on the different relative coordination position of the chlorido and dmso ligands.[16]

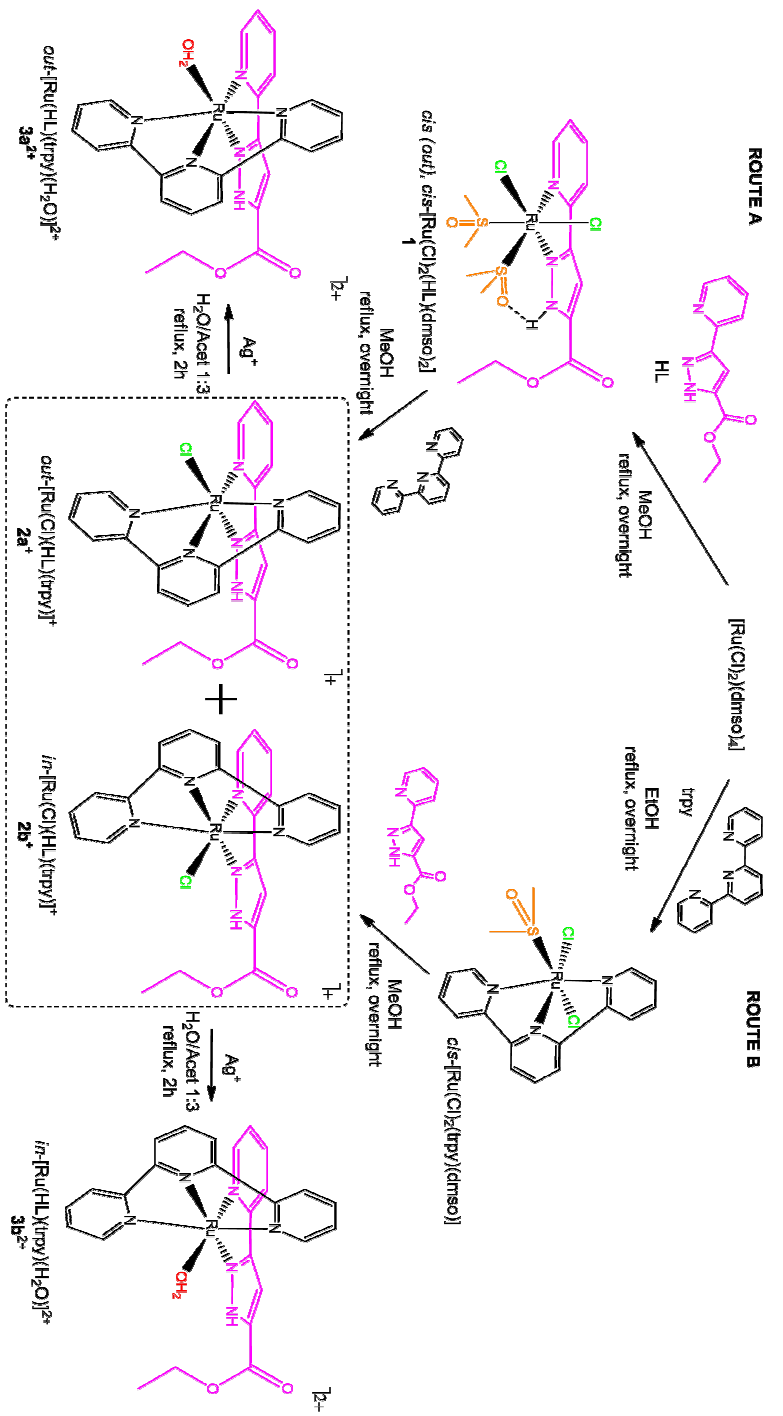

Scheme 1. Synthetic strategy and labelling scheme used for the ligands and complexes described in this work.

The predominance of **1** can be rationalized based on the synergic π-donor and π–acceptor capacities of the Cl and dmso ligands when they are *trans* to one another, and the stabilization provided by the hydrogen bond between the pyrazole N-H and the oxygen atom of the equatorial dmso ligand (see X-ray structure in Figure 1). Further reaction of **1** with trpy replaces one chlorido and two dmso ligands to form a mixture of the *in* and *out* isomers $[Ru(Cl)(HL)(trpy)]^+$, $\mathbf{2a}^+$ and $\mathbf{2b}^+$ in a 10:1 ratio. The two isomers can be easily separated by column chromatography first in alumina and then in silica, giving highly pure $\mathbf{2a}^+$ and $\mathbf{2b}^+$ with isolated yields of 60% and 6% respectively. In Route B, the trpy ligand is used in the first step, and upon reacting with $[Ru(Cl)_2(dmso)_4]$ generates *cis*-$[Ru(Cl)_2(trpy)(dmso)]$ (that has been previously described),[10] and further addition of HL generates a mixture of the Ru-Cl isomer $\mathbf{2a}^+$ and $\mathbf{2b}^+$ in 12% and 24% yields respectively that represents a 1:2 ratio.

The different relative ratios of $\mathbf{2a}^+$ and $\mathbf{2b}^+$ obtained depending on the synthetic route clearly point out to the existence of strongly differentiating factors. In route A, it is clear that the replacement of 2 dmso and 1 Cl^- of **1** by trpy takes place easily, forming directly $\mathbf{2a}^+$. On the other hand, for the $\mathbf{2b}^+$ case, an additional ligand reorganization is need, otherwise the simple meridional substitution would generate *in*-$[Ru(HL)(trpy)(dmso)]^{2+}$, that is not even detected. In sharp contrast, *cis*-$[Ru(Cl)_2(trpy)(dmso)]$ shows a symmetry plane perpendicular to the trpy, and thus the differentiating factor comes from the relative orientation of the incoming HL ligand that will form a geometry with the chlorido ligand trans to the pyridyl nitrogen, thus favoring $\mathbf{2b}^+$, or to the pyrazolyl nitrogen, thus favoring $\mathbf{2a}^+$.

A 2 hours reflux of **2a**$^{+}$, or **2b**$^{+}$, in an acetone/water mixture in presence of $AgClO_4$ yields the aquo compounds **3a**$^{2+}$ and **3b**$^{2+}$, respectively, in good yields (79% and 67%). Light exposure (100 W tungsten lamp) of pure **3a**$^{2+}$ or **3b**$^{2+}$ in a 0.1 M CF_3SO_3D in D_2O for 14 hours produces an isomerization phenomena that generates a 1:1 mixture of **3a**$^{2+}$ and **3b**$^{2+}$. This isomerization reaction was monitored by NMR spectroscopy and a 1:1 mixture is always obtained irrespectively of the starting material used, manifesting that both isomers have comparable stabilities (Figure S6).

Monocrystals for complexes **1**, **3a**$^{2+}$ and **3b**$^{2+}$ were obtained and their crystal structures solved by means of X-ray diffraction analysis. An ORTEP drawing for **1**, **3a**$^{2+}$ and **3b**$^{2+}$ is shown in Figure 1. In all the structures the geometry around the metal center consists of a distorted octahedron as expected for a low-spin d^6 Ru(II), similar to previously reported complexes.[6, 17] It is interesting to mention that complex **1** presents a strong hydrogen bonding between H3A and O4 (N(3)-H(3A) = 0.0881(3) Å, H(3A)-O(4) = 2.044(3) Å, N(3)-O(4) = 2.746(5) Å, N(3)-H(3A)-O(4) = 135.9(2)°).

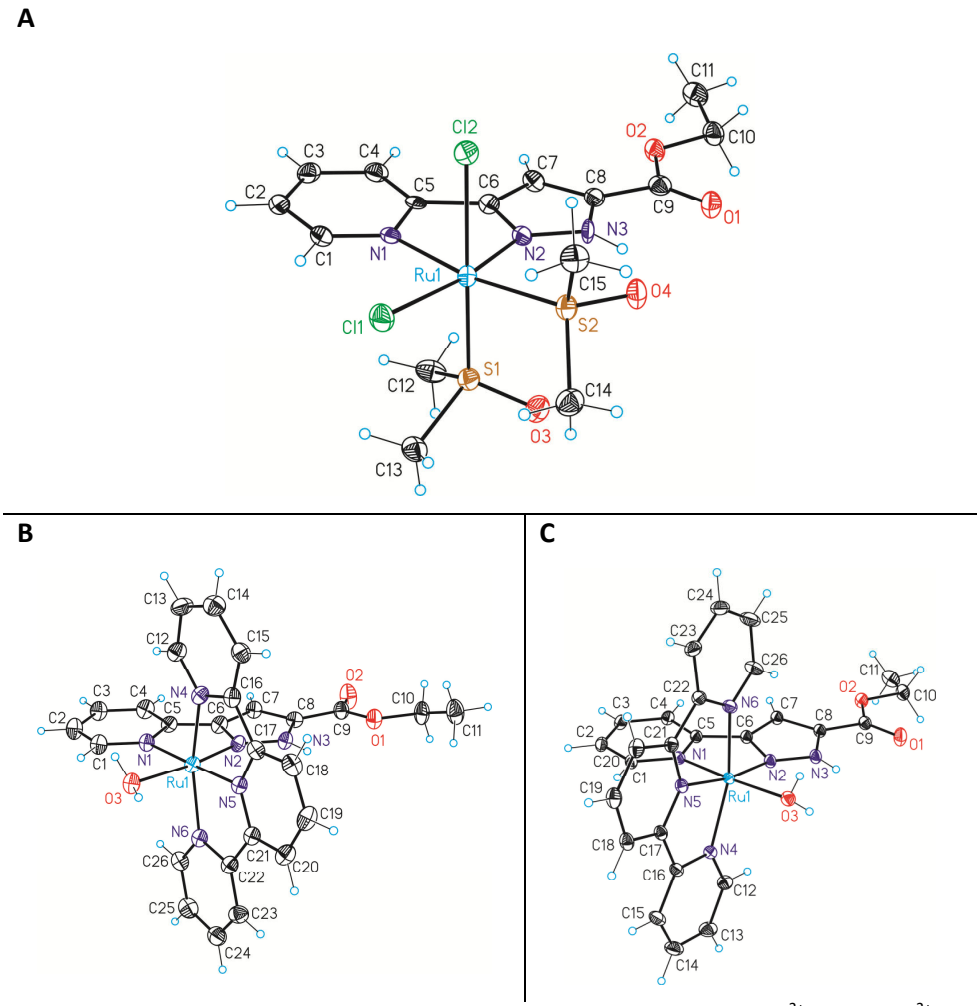

Figure 1. ORTEP drawing (thermal ellipsoids 50 %) of complexes: (A) **1**, (B) **3a**$^{2+}$, and (C) **3b**$^{2+}$.

Spectroscopic properties. ^{1}H NMR, COSY and NOESY of all the complexes were registered in d_6-dmso, d_6-acetone or in pD = 1.0 CF_3SO_3D in D_2O, and are presented in Figure 2 and in the Supporting Information. All the resonances could be identified based on symmetry, integrations and thanks to bidimensional experiments and show that the structures described in the solid state are maintained in solution.

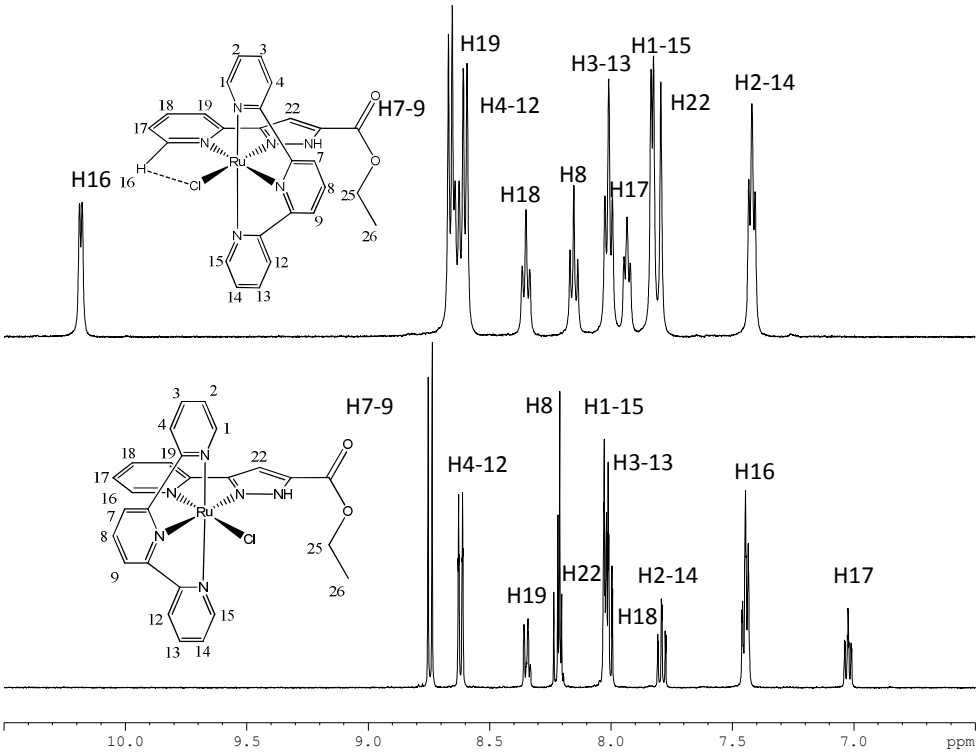

Figure 2. ^{1}H-NMR spectra in d_6-acetone (500 MHz, 298 K) and assignment for complexes (top) **2a**$^{+}$ and (bottom) **2b**$^{+}$.

Complexes **2a**$^{+}$, **2b**$^{+}$, **3a**$^{2+}$ and **3b**$^{2+}$ possess a symmetry plane that contains the HL ligand and bisects the trpy ligand thus rendering the lower and upper protons of the pyridyl-trpy moieties magnetically equivalent. It is worth mentioning here that complex **2a**$^{+}$ shows the typical signal at low field (δ = 10.18) for a proton deshielded due to the diamagnetic anisotropy generated by the chlorido ligand,[18] allowing one to fully assign the signals. A further clue in this direction is given by the NOE signal between H19 and H22 (2.30 Å, see Figure S2). None of these features are present in **2b**$^{+}$ spectra, so its assignment is based on intensities of the integrals and experimental considerations on the

coupling constants of pyridyl systems: the closer the proton to the nitrogen, the smaller the coupling constant. For complexes **3a**$^{2+}$ and **3b**$^{2+}$ the NMR was run in presence of ascorbic acid to avoid complex oxidation, and the same deshielding due to anisotropic effects, this time coming from the aqua ligand, can be seen in **3a**$^{2+}$ for the signal of H16 (δ = 9.38, Figure S4).

The optical properties of the Ru-Cl complexes **1**, **2a**$^{+}$ and **2b**$^{+}$ were investigated by UV-vis spectroscopy in CH_2Cl_2 and those of the Ru-aqua complexes **3a**$^{2+}$ and **3b**$^{2+}$ were recorded in 0.1 M triflic acid aqueous solution and are displayed in Figure 3 and in the SI.

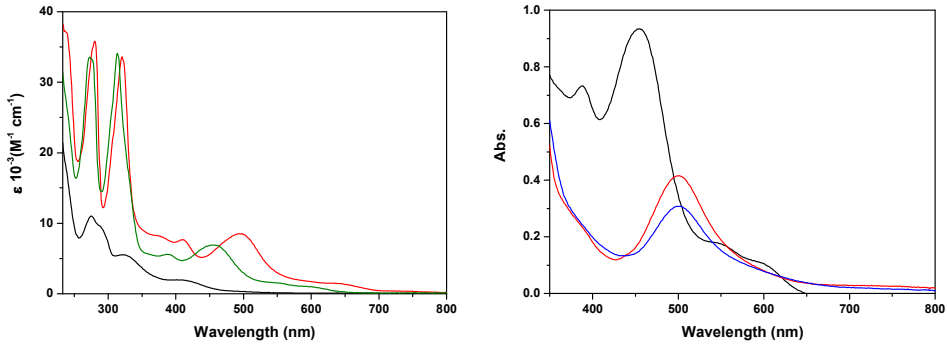

Figure 3. UV-vis spectra of (left) **1** (black) and **2a**$^{+}$ (red) in CH_2Cl_2 and **3a**$^{2+}$ (green) in a pH = 1 CF_3SO_3H solution.; and (right) different oxidation states of **3a**$^{2+}$ in a pH = 1 CF_3SO_3H solution: Ru(II) (black),Ru(III) (red) and Ru(IV) (blue).

All the spectra show the typical π-π* transitions due to the aromatic ligands below 350 nm, and weaker MLCT dπ-π* between 400 and 650 nm. It is interesting to see the shift to lower energies of the Ru-Cl MLCT with regard to those of the Ru-OH_2 complexes due to a destabilization of the Ru dπ orbitals exerted by the chlorido ligand.[17b, 19] The spectra of *out* and *in* isomers both in case of the chlorido and the aqua complexes are practically identical.

Spectrophotometric redox titrations were also carried using Ce(IV) as oxidant for **3a**$^{2+}$ and **3b**$^{2+}$ and are displayed in Figure 3 and in the SI, respectively.

Redox properties of Ru-Cl complexes and linkage isomerization. The redox properties of the Ru-Cl complexes **1**, **2a**$^{+}$ and **2b**$^{+}$ presented in this work were analyzed by means of cyclic voltammetry in a solution 0.1 M of TBAH [(*n*Bu_4N)(PF_6)] in CH_2Cl_2 and their redox potentials are referred to the NHE electrode. All CVs were run at a scan rate of 50 mV/s, unless explicitly stated. Glassy carbon electrodes were used as working electrodes and platinum electrodes as auxiliary electrodes.

The electrochemistry of complex **1** shows the typical behavior associated with a dmso ligand isomerization.[16, 20] In the anodic scan, a wave (i_{a1}) can be seen at $E_{p,a}$ = 1.42 V, with a cathodic wave (i_{c1}) at $E_{p,c}$ = 1.33 V much less intense. A second cathodic wave i_{c2} is seen at $E_{p,c}$ = 0.65 V. To fully understand this redox behavior, we performed quick Controlled Potential Electrolysis (CPE) at 0.24 V and at 1.84 V, followed by CVs at different scan rates. As can be seen in Figure 4, upon oxidation of the complex the waves at higher potentials diminishes in intensity, while a new anodic wave i_{a2} rises at a lower potential of $E_{p,a}$ = 0.76 V. The ratios [i_{c1}]/[i_{a1}] and [i_{c2}]/[i_{a2}] depend strongly on the scan rate. We associate this behavior with a different coordination mode of a dmso ligand, either S or O bond. The higher potential redox wave is associated to the Ru(III)/Ru(II) couple when the dmso is bonded through the S atom; when in oxidation state Ru(III), the metal center shows more affinity for the oxygen atom of the ligand, thus promoting the ligand isomerization. The O bonded dmso is a worse π-accepting ligand than the S bonded, so the redox potential for the Ru(III)/Ru(II) couple of the O bonded complex is lower. This equilibrium upon the one electron oxidation of **1** can be described as:

$$Ru^{III}-O \underset{k^{III}_{S\rightarrow O}}{\overset{k^{III}_{O\rightarrow S}}{\rightleftarrows}} Ru^{III}-S \qquad K^{III}_{O\rightarrow S} \qquad \textbf{Eq.1}$$

The equilibrium constant $K^{III}_{O->S}$ for the Ru^{III}-O/Ru^{III}-S reaction can be obtained from the CVs starting at 1.84 V, plotting the ratio $[i_{c1}]/[i_{c2}]$ versus the inverse of the scan rate (v^{-1}, see Figure S13c) and extrapolating for v->∞, where the intensities of the waves correspond to the concentrations at the equilibrium. This mathematical treatment results in $K^{III}_{O->S}$ = 0.41.

The kinetic constants for the isomerization were calculated using the working curves proposed by Shain and co-workers[21] for the case of a reversible chemical reaction preceding an electron transfer. The ratio i_k/i_d was calculated by measuring i_k (i_k is the measured peak current, i_{c1}) starting at 1.84 V after a CPE of 2 minutes, and i_d (i_d is the corresponding diffusion current in the absence of a chemical reaction, i_{a1}) starting at 0.24 V after a CPE of 2 minutes;. The values thus obtained are: $k^{III}_{O->S} = 2.0 \times 10^{-1}\ s^{-1}$ and $k^{III}_{S->O} = 4.9 \times 10^{-1}\ s^{-1}$.

Assuming $E^0 = E_{1/2}$ and knowing the value of $K^{III}_{O->S}$, the thermodynamic cycle in the inset of Figure 4 can be derived and used to calculate $K^{II}_{S->O} = 2.1 \times 10^{+11}$.

The kinetic isomerization constant $k^{II}_{O->S}$ can be extrapolated from the dependency of $\ln(i_{a2}/v^{1/2})$ *vs*. time[22] and yields a value of $9.3 \times 10^{-2}\ s^{-1}$. The remaining constant can be obtained from the value of $K^{II}_{S->O}$, resulting in $k^{II}_{S->O} = 4.5 \times 10^{-13}\ s^{-1}$.

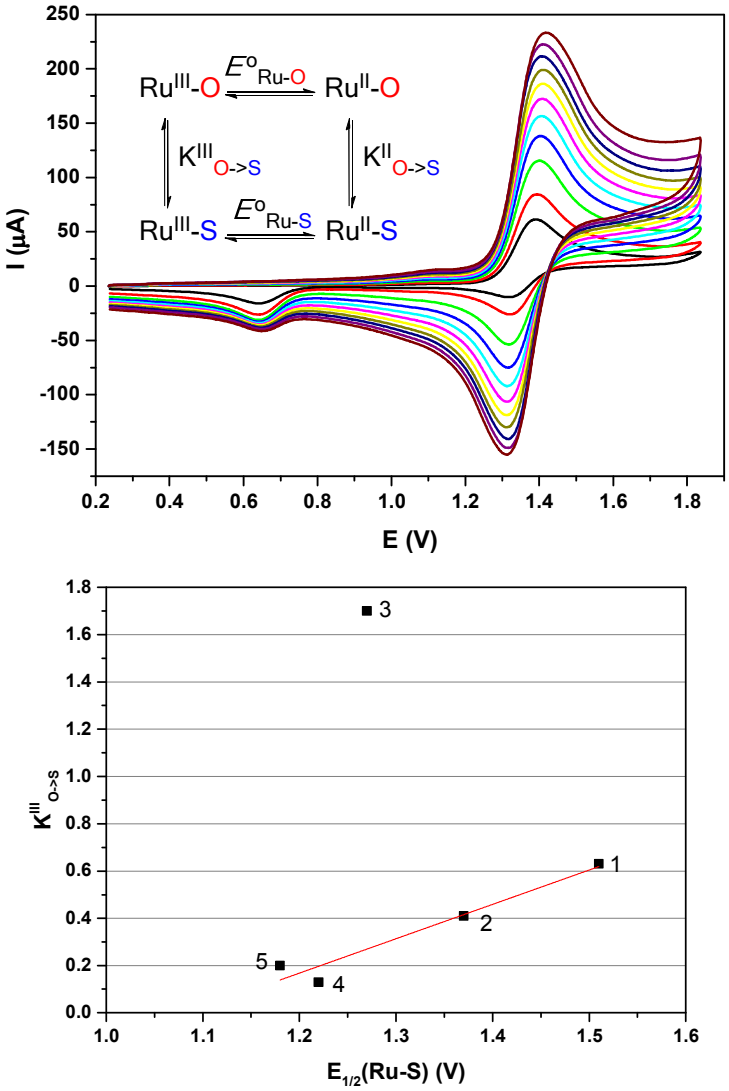

Figure 4. (Top) Cyclic voltammograms at different scan rates obtained after 2 minutes CPE at an E_{app} = 0.24 V for a solution of **1** 0.1M TBAH in CH_2Cl_2. Black: 50 mV/s, red: 100 mV/s, green: 200 mV/s, blue: 300 mV/s, light blue: 400 mV/s, pink: 500 mV/s, yellow: 600 mV/s, dark yellow: 700 mV/s, dark blue: 800 mV/s, purple: 900 mV/s and brown: 1000 mV/s. Inset: linkage isomerization cycle for the Ru-dmso system, only the dmso atom bonded to the Ru metal center is shown. (Bottom) Plot of $K^{III}_{O->S}$ versus $E_{1/2}$(Ru-S) for a series of complexes reported in Table 1; the numbers correspond to the entry of Table 1.

Table 1. Thermodynamic and kinetic data of selected complexes for comparison with complex **1**.

Entry	Complex	$K^{III}_{O->S}$	$k^{III}_{O->S}$ [s^{-1}]	$k^{III}_{S->O}$ [s^{-1}]	$K^{II}_{(O->S)}$	$k^{II}_{O->S}$ [s^{-1}]	$k^{II}_{S->O}$ [s^{-1}]	$E_{1/2}$ (Ru-S) [V]	$E_{1/2}$ (Ru-O) [V]	Solv
1[22]	*cis, cis, cis*-$[Ru(Cl)_2(tbpy)_2(dmso)_2]$	0.63	1.2	1.9	$2.1 \times 10^{+12}$	1.0×10^{-2}	5.0×10^{-14}	1.51	0.79	CH_3CN
2	**1**	0.41	2.0×10^{-1}	4.9×10^{-1}	$2.1 \times 10^{+11}$	9.3×10^{-2}	4.5×10^{-13}	1.37	0.69	CH_2Cl_2
3[20]	*cis(out), cis*-$[Ru(Cl)_2(H3p)(dmso)_2]$	1.7	2.8×10^{-1}	1.7×10^{-1}	$5.2 \times 10^{+11}$	4.9×10^{-1}	9.3×10^{-14}	1.27	0.70	CH_2Cl_2
4[23]	*out*-$[Ru(bpp)(trpy)(dmso)]^+$	0.13	7.7×10^{-2}	6.0×10^{-1}	$5.5 \times 10^{+8}$	2.5×10^{-1}	4.6×10^{-10}	1.22	0.65	CH_2Cl_2
5[20]	*trans, cis*-$[Ru(Cl)_2(H3p)(dmso)_2]$	0.20	5.7×10^{-2}	2.2×10^{-1}	$5.3 \times 10^{+8}$	8.7×10^{-2}	1.6×10^{-10}	1.22	0.63	CH_2Cl_2

The acronyms tbpy, bpp and H3p stand for the 4-*tert*-butylpyridine, the 2,2′-(pyrazolate-3,5-diyl)dipyridine and the 5-phenyl-3-(2-pyridyl)-1Hpyrazole ligands respectively.

Table 1 compiles similar data for related Ru-dmso complexes reported in the literature that also undergo linkage isomerization processes as described by the square cycle shown in the inset of Figure 4. In general $K^{II}_{O->S}$ are extremely high, meaning that once formed the Ru^{II}-O species immediately isomerizes towards Ru^{II}-S. On the other hand the tendency to isomerize for the Ru^{III}-S to the corresponding Ru^{III}-O, although generally favored, is much lower. It is interesting to observe in Table 1 that the K^{III} value nicely correlates with $E_{1/2}$(Ru-S) redox potential except for complex in entry 3 as can be seen graphically in Figure 4. This phenomenon can be rationalized in terms of the Pearson theory for HSAB, where the higher the HOMO-LUMO gap the higher the hardness of a particular transition metal Lewis acid. In this sense the higher redox potential for the Ru(III)/Ru(II) couple would imply a lower energy for the dπ orbitals and thus a larger HOMO-LUMO gap.

In CH_2Cl_2, complex **2a**$^+$ shows a chemically reversible and electrochemically quasi-reversible wave at 1.04 V (ΔE_p = 95 mV), while **2b**$^+$ shows a chemically reversible and electrochemically irreversible wave at 1.13 V (ΔE_p = 144 mV). Both waves can be assigned to the Ru(III)/Ru(II) couple, and the 90 mV potential difference between the two isomers is attributed to the different *trans* organization in the first coordination sphere of the metal center:[17b] while the Ru-Cl bond is *trans* to N-pyrazole in **2a**$^+$, in **2b**$^+$ the Ru-Cl is *trans* to the N-pyridil of the HL ligand.

Redox properties of Ru-H_2O complexes and water oxidation catalysis. The redox properties of the Ru-H_2O complexes **3a**$^{2+}$ and **3b**$^{2+}$ were analyzed by means of cyclic voltammetry and differential pulse voltammetry in aqueous solutions, using 0.1 M CF_3SO_3H for the measurement at pH = 1.0 or the

appropriate phosphate buffer for measurement at other pHs. Their redox potentials are referred to the NHE electrode.

At pH = 1 complex **3a**$^{2+}$ shows a chemical and electrochemical reversible wave at 0.93 V (ΔE_p = 59 mV), assigned to the Ru(III)/Ru(II) couple as can be seen in Figure 5. A second anodic waves assigned to the IV/III couple is observed at 1.35 V that has a very broad cathodic wave. The full recovery of the III/II wave in the cathodic region (i_a/i_c = 1.01) indicates the presence of slow ET process rather than a decomposition pathway. Further in the anodic region, a large electrocatalytic current intensity is observed whose foot of the wave is approximately at 1.5 V. After catalysis, in the reverse scan the IV/III wave is not observed at all and a small amount of the III/II is found (i_a/i_c= 2.42), clearly pointing out towards the existence of decomposition pathways coupled to the water oxidation reaction. Indeed further scanning in the cathodic region shows the presence of a new redox process with potential close to 0.65 V whose nature is unknown.

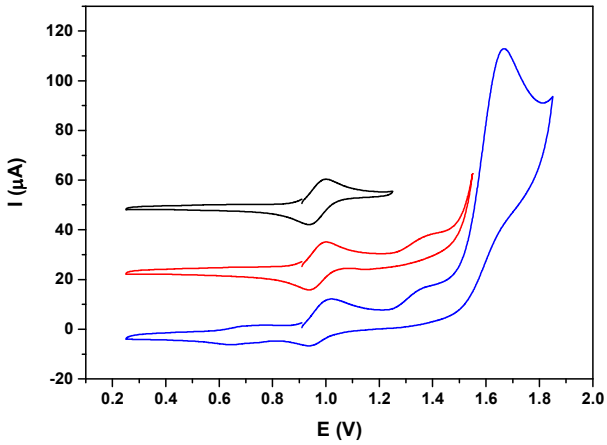

Figure 5. iR compensated CV of **3a**$^{2+}$ in an aqueous pH = 1.0 CF_3SO_3H at a scan rate of 50 mV/s on glassy carbon electrode.

All the redox waves observed are pH dependent except for the V/IV wave as can be observed in the Pourbaix diagram displayed in Figure 6, where the zones of stability of the different species with different degree of oxidation and protonation derived from **3a**$^{2+}$ are reported.

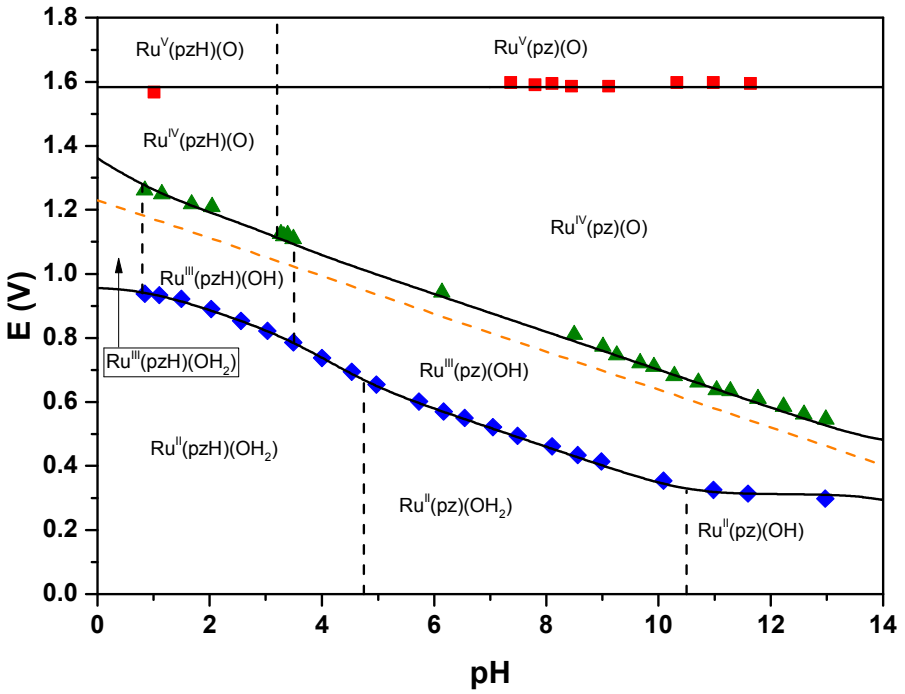

Figure 6. Pourbaix diagram for complex **3a**$^{2+}$.pzH stands for the pyrazolic proton.

The pH dependency of the III/II and IV/III waves arises from the capacity of the aqua ligand directly bonded to Ru to undergo up to two proton losses and from the pyrazolato moiety of the HL ligand. All pK_a are represented with vertical lines in the Pourbaix diagram. For the III/II redox couple the evolution of the redox potential as function of pH is influenced by two pK_a at oxidation state II and two at oxidation state III and thus is rather complex. For this reason mathematical simulation was carried out using Equation 2:

$$E(\mathrm{III/II}) = \left[E(\mathrm{III/II})_{\mathrm{pH=0}}\right] + \left(0.05916 * \log\left(\frac{[\mathrm{H^+}]^3 + [\mathrm{H^+}]^2\mathrm{K^{II}_{a1}} + [\mathrm{H^+}]\mathrm{K^{II}_{a1}K^{II}_{a2}} + \mathrm{K^{II}_{a1}K^{II}_{a2}K^{II}_{a3}}}{[\mathrm{H^+}]^3 + [\mathrm{H^+}]^2\mathrm{K^{III}_{a1}} + [\mathrm{H^+}]\mathrm{K^{III}_{a1}K^{III}_{a2}} + \mathrm{K^{III}_{a1}K^{III}_{a2}K^{III}_{a3}}}\right)\right) \quad \textbf{Eq.2}$$

where $E(III/II)_{pH=0}$ is the potential for the III/II couple at pH = 0 and K^{X}_{an} is the n^{th} acid –base constant for the specie in oxidation state X.

This allowed us to extract the correct pK_a that are reported in Table 2, along with other relevant thermodynamic and kinetic properties of complex **3a**$^{2+}$ and other related complexes for comparison purposes. Although much simpler because of the lower number of pK_a involved the IV/III redox waves was also simulated and is also exhibited in the Pourbaix diagram.

For the case of the **3b**$^{2+}$ isomer the electrochemical properties are relatively similar and the CVs and Pourbaix diagram are reported in the Supporting Information. One of the most striking features when comparing the two constitutional isomers is the value of ΔE, defined as the difference between the IV/III and III/II redox potentials which is 360 mV for **3a**$^{2+}$ and 240 for **3b**$^{2+}$ at pH = 7.0. This manifests that for **3a**$^{2+}$ the zone of stability of oxidation state III is much more favored than in the case of **3b**$^{2+}$. This is necessarily an electronic effect produced by the different relative *trans* coordination of the HL ligand, as discussed in the structural section, and highlights how very small variations of the complex structure can strongly influence the electronic properties of the Ru metal center.

Comparing the redox potential of complex ***out*-1** (Table 2, entry 1) with **3a**$^{2+}$, the electron withdrawing effect exerted by the carboxylate group can be clearly seen in an increment of 30 mV of the IV/III couple and of 40 mV for the III/II couple. In sharp contrast comparing it with **3b**$^{2+}$, the latter increases the III/II by 130 mV but does not modify the IV/III redox potentials, again showing the difficulty of predicting beforehand the redox potentials of a particular redox couple. It is important to mention here that correlations have been reported in the literature between redox potentials based on ligand electron donating and/or electron withdrawing effects, such as the ones proposed by Lever et al.[24] Those correlations are certainly useful and give a rough estimate of the potentials especially for those cases where only one oxidative ET is found within the limits of the solvent stability. In this case however, the calculations do not differentiate between isomers and thus manifest once more the need to prepare, separate and purify complexes undergoing multiple ET processes to measure their redox couples. As further example, it is interesting to see how electronic perturbation on the Ru(H_2O)-trpy-substituted-bpy system influence redox potentials when compared with unsubstituted bpy ligands (See entries 4-7 in Table 2). In particular, entry 5 presents an electron donating group, which should decrease the IV/III and III/II redox potentials, while entry 6 presents an electron withdrawing group, which in turn should increase the potentials. The effects are the expected ones, but to different extents on different redox couples, so that they generate in both cases an unexpected increase of the zone of stability of oxidation state III. In sharp contrast the electron withdrawing F-group in entry 7 produces just the opposite effect, wiping out the stability zone of the oxidation state II, and only a two-electron wave for the IV/II couple is found.

Table 2. Thermodynamic and catalytic data for **3a**$^{2+}$ and **3b**$^{2+}$ and for related Ru-aqua complexes described in the literature at pH = 7.0.

Entry	Complex[a]	$E_{1/2}$(V) *vs.* NHE				ΔE[c]	$pK_{a,II}$[d]	$pK_{a,III}$[d]	$pK_{a,III}$[e] pyrazole	$TOF_i \cdot 10^3$ (TON)[f]
		IV/III	III/II	IV/II[b]	V/IV					
1[19]	*out*-[Ru(Hbpp)(trpy)(H_2O)]$^{2+}$, ***out*-1**	0.85	0.48	0.67		370	11.1	2.8	6.88/5.43	
2	*out*-**3a**$^{2+}$	0.88	0.52	0.70	1.59	360	10.5	0.8	4.75/3.5/3.2	58.2 (10.8)
3	*in*-**3b**$^{2+}$	0.85	0.61	0.73	1.54	240	10.8	1.0	5.6/4.5/4.0	15.4 (4.2)
4[6]	[Ru(bpy)(trpy)(H_2O)]$^{2+}$	0.83	0.72	0.78	1.86	110	9.8	1.7		15.1 (18.3)
5[5]	[Ru(4,4'-$(MeO)_2$-bpy)(trpy)(H_2O)]$^{2+}$	0.82	0.64	0.76		240	11.2	3.2		
6[5]	[Ru(4,4'-$(HOOC)_2$-bpy)(trpy)(H_2O)]$^{2+}$	0.89	0.75	0.82		140	10.4	1.2		
7[6]	[Ru(6,6'-F_2-bpy)(trpy)(H_2O)]$^{2+}$	--	--	0.80[g]	1.93	--	10.4	--		1.7 (7.8)

[a]Ligand abbreviations: 4,4'-$(MeO)_2$-bpy is 4,4'-dimethoxy-2,2'-bipyridine; 4,4'-$(HOOC)_2$-bpy is 4,4'-dicarboxy-2,2'-bipyridine. [b]Calculated as $[E_{1/2}(IV/III)+E_{1/2}(III,II)]/2$. [c]$\Delta E = E_{1/2}(IV/III)-E_{1/2}(III,II)$ in mV. [d]$pK_{a,II}$ and $pK_{a,III}$ represent the pK_a of the corresponding Ru^{II}-OH_2 and Ru^{III}-OH_2 species, respectively. [e]pKa for the pyrazole proton, at the different oxidation states II/III/IV. [f]TOF_i stands for initial Turn Over Frequencies in cycles per second and TON for Turn Over Numbers. This values are extracted for the catalytic reactions involving 1.0 mM Cat/100 mM Ce(IV) in a 0.1 M triflic acid solution with a total volume of 2 mL. [g]Two electron process.

The electron withdrawing perturbation exerted by the carboxylate group is also obviously transmitted to the pK_a values of all the acid-base moieties of the complexes, namely the Ru-H_2O/Ru-OH couple and the pyrazolate/pyrazolato couple. Comparing ***out*-1** with **3a**$^{2+}$ a decrease of all pK_a values is observed, as expected. On the other hand, the potential hydrogen bonding between the Ru-OH_2, the proton from the pyrazolate moiety and a free water (See Chapter 6) that could take place for the **3b**$^{2+}$ isomer, but that cannot occur in **3a**$^{2+}$, produces an increase of all the related pK_a values meaning that all the conjugated bases are stabilized by hydrogen bonding.

In order to obtain kinetic information about the catalytic process, a foot-o-the-wave analysis was carried out to calculate apparent rate constant k_{obs}. We followed the methodology described by Saveant et al.[25] which assumes that the rate determining step (rds) is the last electron transfer. Under catalytic conditions Equation 3 is operative,

$$\frac{i}{i_p^0} = \frac{8.96\sqrt{\frac{RT}{Fv}k_{obs}}}{1+\exp\left[\frac{F}{RT}(E_{PQ}^0 - E)\right]} \qquad \textbf{Eq.3}$$

where E^0_{PQ} is the standard potential for the catalysis-initiating redox couple (1.56 V for **3a**$^{2+}$ and 1.64 V for **3b**$^{2+}$, extracted from the DPVs in Figure S16), *i* is the current intensity in the presence of substrate, i^0_p is the current intensity in the absence of substrate (we approximate this current to the current associated with the Ru(III)/Ru(II) couple), *F* is the faraday constant, *v* is the scan rate and *R* is 8.314 J $mol^{-1}K^{-1}$. CVs of **3a**$^{2+}$ at different scan rates (100 – 1000 mV/s) are shown in Figure 7 (left, top). k_{obs} can be extracted from the plot of

i/i^0_p vs. $1/\{1+\exp[(F/RT)(E^0_{PQ}-E)]\}$ as shown in Figure 7 (left, bottom) and in Figure S25 in the Supporting Information.

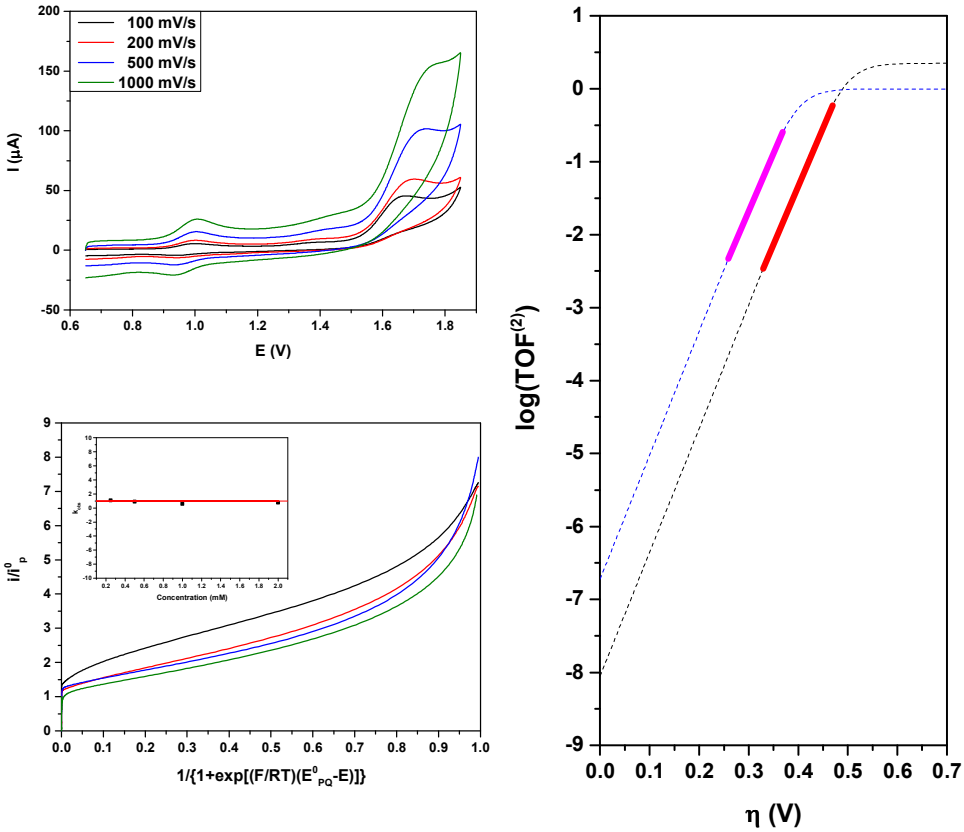

Figure 7. (Left, top) Background corrected CVs in H_2O/CF_3SO_3H (pH = 1.0) at 100-1000 mV/s scan rates. Black: 100 mV/s, red: 200 mV/s, blue: 500 mV/s, green: 1000 mV/s. (Left, bottom) Foot Of the Wave analysis plotting i/i^0_p vs. $1/\{1+\exp[(F/RT)(E^0_{PQ}-E)]\}$ at each scan rate (same color code). Inset: plot of the different k_{obs} values extracted from the foot of the wave analysis at each scan rate. The red line represents the average k_{obs} value. (Right) Catalytic Taffel plots for **3a**$^{2+}$ (blue) and **3b**$^{2+}$ (black).The magenta and red line represent the scanned potentials.

The largest slope at the very beginning of the catalytic process (which translates to the foot of the wave in the original CVs) gives a values of k_{obs} =

1.00 s^{-1} for **3a**$^{2+}$ and 2.23 s^{-1} for **3b**$^{2+}$. The relationship between the turnover frequency $TOF^{(2)}$ and the overpotential η, defined as the difference between the applied potential *E* and the thermodynamic potential of the catalyzed reaction E^0_{AC}, in this case water oxidation, is governed by Equation 4 and plotted in Figure 7 (right).

$$TOF^{(2)} = \frac{k_{obs}}{1 + \exp\left[\frac{F}{RT}(E^0_{PQ} - E^0_{AC} - \eta)\right]} \qquad \textbf{Eq.4}$$

The graph shows how the lower value of E^0_{PQ} for **3a**$^{2+}$ translates in higher turnover frequencies when the overpotential is under 0.5 V. It should be noted that kinetic parameters for catalytic reactions derived from electrochemical measurements depend on various details of the experimental procedures, and values from different studies should be compared only with caution.[26]

Complexes **3a**$^{2+}$ and **3b**$^{2+}$ were tested for chemical water oxidation at pH = 1 with $[(NH_4)_2Ce(NO_3)_6]$ (CAN). As shown in Figure S20, manometric measurements of both complexes show activity and the reaction is finished after 20 minutes. As expected by the electrochemical characterization, **3a**$^{2+}$ is more reactive than the corresponding *in* isomer, yielding a 12.1 TON activity and a maximum TOF_i of 64.6 × 10^{-3} s^{-1}, with an oxidative efficiency of 49%. On the other hand **3b**$^{2+}$ exhibits lower activity (5.6 TON), TOF_i (20.7 × 10^{-3} s^{-1}) and oxidative efficiency (23%). To investigate the nature of the measured gas, on-line mass experiments were conducted under the same conditions as the manometry experiments, and the results are shown in Figure 8. The ratios O_2/CO_2 are in both cases favorable to oxygen: 9.1 for **3a**$^{2+}$ and 2.9 for **3b**$^{2+}$ (See

Figure S20c). CO_2 production indicates oxidative degradation of the ligands, and is the probable responsible for the general low oxidative efficiency and in particular of the lower performances of the *in* isomer. The corrected values of the manometric experiments are consequently TON = 10.8 and TOF_i = 58.2 × 10^{-3} s^{-1} for **3a**$^{2+}$ and TON = 4.2 and TOF_i = 15.4 × 10^{-3} s^{-1} for **3b**$^{2+}$.

The higher generation of CO_2 by **3b**$^{2+}$ could be attributed to a different impact of the electronic effects discussed through the chapter on the two competing reactions: *e.g.* while favoring the water oxidation reaction for **3a**$^{2+}$, they disfavor the competitive ligand oxidation reaction; and the opposite is true for **3b**$^{2+}$.

5.5 Conclusions

We prepared and thoroughly characterized a new family of ruthenium complexes, based on the never before used 1*H*-Pyrazole-3-Carboxylic Acid, 5-(2-pyridinil)-, ethyl ester ligand. Extensive electrochemical studies shone light on different reactions for different complexes: complex **1** showed dmso ligand isomerization, and a number of kinetic and thermodynamic values were calculated; while **3a**$^{2+}$ and **3b**$^{2+}$ showed water oxidation properties. The latter were investigated both electrochemically through foot-of-the-wave analysis, and chemically, through reaction with CAN as sacrificial electron acceptor for water oxidation. The higher activity of **3a**$^{2+}$ is explained as consequence of the electronic effects analyzed by electrochemical experiments and the construction of Pourbaix diagrams.

The present work constitutes an extensive study on the properties of ruthenium complexes and their dependence on the ligand modification, both

through characterization of new compounds and by comparison with relevant literature data. It also represents a solid starting point for further modification of the backbone of the hereby synthesized complexes, an example of which will be presented in the next chapter.

Acknowledgments. This research was supported by the Spanish Ministerio de Economia y Competitividad (MINECO) through projects CTQ-2013-49075-R, CTQ2014-52974-REDC, and by the EU COST actions CM1202 and CM1205. L. M. thanks "ICIQ-Foundation" for a Ph.D. grant. The Severo Ochoa Excellence Accreditation (SEV-2013-00319) is gratefully acknowledged.

V

I performed the synthesis, the characterization, the electrochemical experiments and reactivity experiments of all the complexes presented. X-Ray structure analyses were carried out by Dr. J. Benet-Bucholz.

5.6 References

(1) Tseng, H.-W.; Zong, R.; Muckerman, J. T.; Thummel, R. *Inorg. Chem.* **2008,** *47*, 11763-11773.

(2) Concepcion, J. J.; Jurss, J. W.; Brennaman, M. K.; Hoertz, P. G.; Patrocinio, A. O. T.; Murakami Iha, N. Y.; Templeton, J. L.; Meyer, T. J. *Acc. Chem. Res.* **2009,** *42*, 1954-1965.

(3) Concepcion, J. J.; Jurss, J. W.; Templeton, J. L.; Meyer, T. J. *J. Am. Chem. Soc.* **2008,** *130*, 16462-16463.

(4) a) Blakemore, J. D.; Schley, N. D.; Balcells, D.; Hull, J. F.; Olack, G. W.; Incarvito, C. D.; Eisenstein, O.; Brudvig, G. W.; Crabtree, R. H. *J. Am. Chem. Soc.* **2010,** *132*, 16017-16029; b) Wasylenko, D. J.; Ganesamoorthy, C.; Borau-Garcia, J.; Berlinguette, C. P. *Chem. Commun.* **2011,** *47*, 4249-4251.

(5) Wasylenko, D. J.; Ganesamoorthy, C.; Henderson, M. A.; Koivisto, B. D.; Osthoff, H. D.; Berlinguette, C. P. *J. Am. Chem. Soc.* **2010,** *132*, 16094-16106.

(6) Maji, S.; López, I.; Bozoglian, F.; Benet-Buchholz, J.; Llobet, A. *Inorg. Chem.* **2013,** *52*, 3591-3593.

(7) Yamazaki, H.; Hakamata, T.; Komi, M.; Yagi, M. *J. Am. Chem. Soc.* **2011,** *133*, 8846-8849.

(8) Dubs, C.; Yamamoto, T.; Inagaki, A.; Akita, M. *Organometallics* **2006,** *25*, 1344-1358.

(9) Evans, I. P.; Spencer, A.; Wilkinson, G. *J. Chem. Soc., Dalton Trans.* **1973**, 204-209.

(10) Ziessel, R.; Grosshenny, V.; Hissler, M.; Stroh, C. *Inorg. Chem.* **2004,** *43*, 4262-4271.

(11) Data collection: APEX II, versions v2009.1-02 and v2013.4-1; Bruker AXS Inc.: Madison, WI, 2007.

(12) Data reduction: SAINT, versions V7.60A and V8.30c; Bruker AXS Inc.: Madison, WI, 2007.

(13) SADABS, V2008/1 and V2012/1; Bruker AXS Inc.: Madison, WI, 2001.

(14) Blessing, R. *Acta Crystallogr. Sect. A* **1995,** *51*, 33-38.

(15) Sheldrick, G. *Acta Crystallogr. Sect. A* **2008,** *64*, 112-122.

(16) Sens, C.; Rodríguez, M.; Romero, I.; Llobet, A.; Parella, T.; Sullivan, B. P.; Benet-Buchholz, J. *Inorg. Chem.* **2003,** *42*, 2040-2048.

(17) a) Planas, N.; Christian, G.; Roeser, S.; Mas-Marzá, E.; Kollipara, M.-R.; Benet-Buchholz, J.; Maseras, F.; Llobet, A. *Inorg. Chem.* **2012,** *51*, 1889-1901; b) Roeser, S.; Farràs, P.; Bozoglian, F.; Martínez-Belmonte, M.; Benet-Buchholz, J.; Llobet, A. *ChemSusChem* **2011,** *4*, 197-207; c) Farràs, P.; Maji, S.; Benet-Buchholz, J.; Llobet, A. *Chem. Eur. J.* **2013,** *19*, 7162-7172; d) Romero, I.; Rodriguez, M.; Llobet, A.; Collomb-Dunand-Sauthier, M.-N.; Deronzier, A.; Parella, T.; Stoeckli-Evans, H. *J. Chem. Soc., Dalton Trans.* **2000**, 1689-1694.

(18) Mognon, L.; Benet-Buchholz, J.; Rahaman, S. M. W.; Bo, C.; Llobet, A. *Inorg. Chem.* **2014,** *53*, 12407-12415.

(19) Sens, C.; Rodríguez, M.; Romero, I.; Llobet, A.; Parella, T.; Benet-Buchholz, J. *Inorg. Chem.* **2003,** *42*, 8385-8394.

(20) Roeser, S.; Maji, S.; Benet-Buchholz, J.; Pons, J.; Llobet, A. *Eur. J. Inorg. Chem.* **2013,** *2013*, 232-240.

(21) Nicholson, R. S.; Shain, I. *Anal. Chem.* **1964,** *36*, 706-723.

(22) Silva, D. O.; Toma, H. E. *Can. J. Chem.* **1994,** *72*, 1705-1708.

(23) Benet-Buchholz, J.; Comba, P.; Llobet, A.; Roeser, S.; Vadivelu, P.; Wiesner, S. *Dalton Trans.* **2010,** *39*, 3315-3320.

(24) Lever, A. B. P. *Inorg. Chem.* **1990,** *29*, 1271-1285.

(25) Costentin, C.; Drouet, S.; Robert, M.; Savéant, J.-M. *J. Am. Chem. Soc.* **2012,** *134*, 11235-11242.

(26) Rountree, E. S.; McCarthy, B. D.; Eisenhart, T. T.; Dempsey, J. L. *Inorg. Chem.* **2014,** *53*, 9983-10002.

UNIVERSITAT ROVIRA I VIRGILI
MONONUCLEAR AND HETEROTRINUCLEAR RUTHENIUM COMPLEXES: SYNTHESIS AND WATER OXIDATION ACTIVITY.
Lorenzo Mognon
Dipòsit Legal: T 1359-2015

Supporting Information for

Single Site Isomeric Ru WOCs with Electron Withdrawing Groups: Synthesis, Electrochemical Characterization and Reactivity

Lorenzo Mognon,[a] Jordi Benet-Buchholz,[a] and Antoni Llobet[a,b]

[a] Institute of Chemical Research of Catalonia (ICIQ), Avinguda Països Catalans 16, 43007 Tarragona, Spain

[b] Departament de Química, Universitat Autònoma de Barcelona, Cerdanyola del Vallès, 08193 Barcelona, Spain

Table S1. Crystal data and structure refinement for **1**.

Empirical formula	C16 H27 Cl2 N3 O5 Ru S2
Formula weight	577.49
Temperature	100(2) K
Wavelength	0.71073 Å
Crystal system	Monoclinic
Space group	P2(1)/c
Unit cell dimensions	a = 7.7252(7)Å α = 90°.
	b = 26.715(3)Å β = 98.270(4)°.
	c = 11.0356(10)Å γ = 90°.
Volume	2253.9(4) $Å^3$
Z	4
Density (calculated)	1.702 Mg/m^3
Absorption coefficient	1.150 mm^{-1}
F(000)	1176
Crystal size	0.30 x 0.05 x 0.05 mm^3
Theta range for data collection	2.015 to 25.625°.
Index ranges	-9<=h<=9,-26<=k<=32,-13<=l<=10
Reflections collected	9268
Independent reflections	4078[R(int) = 0.0410]
Completeness to theta =25.625°	95.8%
Absorption correction	Empirical
Max. and min. transmission	0.945 and 0.788
Refinement method	Full-matrix least-squares on F^2
Data / restraints / parameters	4078/ 24/ 287
Goodness-of-fit on F^2	1.033
Final R indices [I>2sigma(I)]	R1 = 0.0424, wR2 = 0.0778
R indices (all data)	R1 = 0.0781, wR2 = 0.0882
Largest diff. peak and hole	0.802 and -0.844 e.$Å^{-3}$

Table S2. Crystal data and structure refinement for **3a**$^{2+}$.

Empirical formula	C26 H28 Cl2 N6 O13 Ru
Formula weight	804.51
Temperature	100(2) K
Wavelength	0.71073 Å
Crystal system	Monoclinic
Space group	P2(1)/n
Unit cell dimensions	a = 8.4167(6)Å α = 90°.
	b = 19.4697(12)Å β = 101.366(2)°.
	c = 19.9959(14)Å γ = 90°.
Volume	3212.5(4) Å^3
Z	4
Density (calculated)	1.663 Mg/m^3
Absorption coefficient	0.729 mm^{-1}
F(000)	1632
Crystal size	0.45 x 0.02 x 0.02 mm^3
Theta range for data collection	2.078 to 26.421°.
Index ranges	-10<=h<=10,-24<=k<=19,-25<=l<=22
Reflections collected	32844
Independent reflections	6595[R(int) = 0.0780]
Completeness to theta =26.421°	99.8%
Absorption correction	Empirica
Max. and min. transmission	0.986 and 0.565
Refinement method	Full-matrix least-squares on F^2
Data / restraints / parameters	6595/ 107/ 485
Goodness-of-fit on F^2	1.019
Final R indices [I>2sigma(I)]	R1 = 0.0469, wR2 = 0.1074
R indices (all data)	R1 = 0.0735, wR2 = 0.1208
Largest diff. peak and hole	1.667 and -1.096 e.Å^{-3}

Table S3. Crystal data and structure refinement for **3b**$^{2+}$.

Empirical formula	C26 H24 Cl2 N6 O11 Ru
Formula weight	768.48
Temperature	100(2) K
Wavelength	0.71073 Å
Crystal system	Monoclinic
Space group	P2(1)/n
Unit cell dimensions	a = 11.6059(3)Å α = 90°.
	b = 15.1634(4)Å β = 96.4100(10)°.
	c = 16.5717(4)Å γ = 90°.
Volume	2898.14(13) Å^3
Z	4
Density (calculated)	1.761 Mg/m^3
Absorption coefficient	0.798 mm^{-1}
F(000)	1552
Crystal size	0.04 x 0.04 x 0.04 mm^3
Theta range for data collection	1.826 to 38.097°.
Index ranges	-19<=h<=20,-26<=k<=25,-28<=l<=28
Reflections collected	74304
Independent reflections	15302[R(int) = 0.0236]
Completeness to theta =38.097°	96.3%
Absorption correction	Empirical
Max. and min. transmission	0.969 and 0.926
Refinement method	Full-matrix least-squares on F^2
Data / restraints / parameters	15302/ 0/ 425
Goodness-of-fit on F^2	1.036
Final R indices [I>2sigma(I)]	R1 = 0.0262, wR2 = 0.0659
R indices (all data)	R1 = 0.0323, wR2 = 0.0692
Largest diff. peak and hole	1.598 and -0.583 e.Å^{-3}

Figure S1. NMR spectra (400 MHz, 298 K, d_6-dmso) for complex *cis (out), cis*-$[Ru(Cl)_2(dmso)_2(HL)]$, **1**: (a) ^{1}H NMR, (b) COSY, (c) NOESY.

(a)

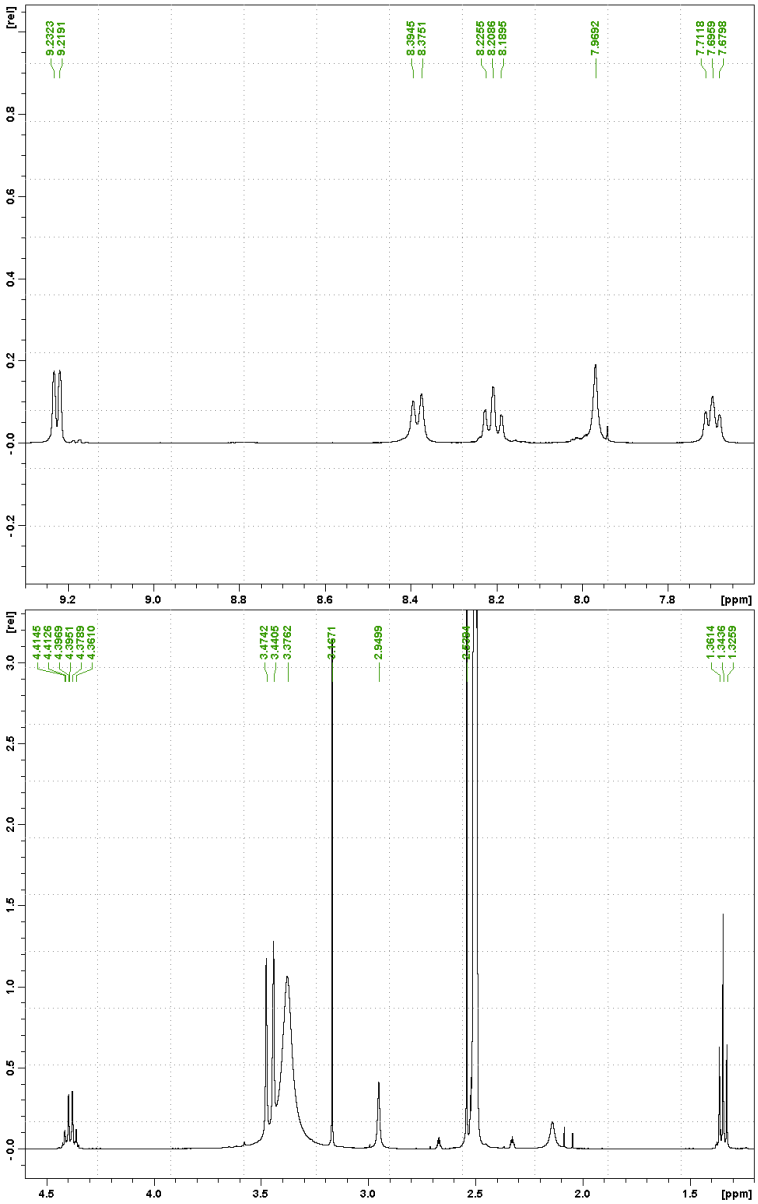

(b)

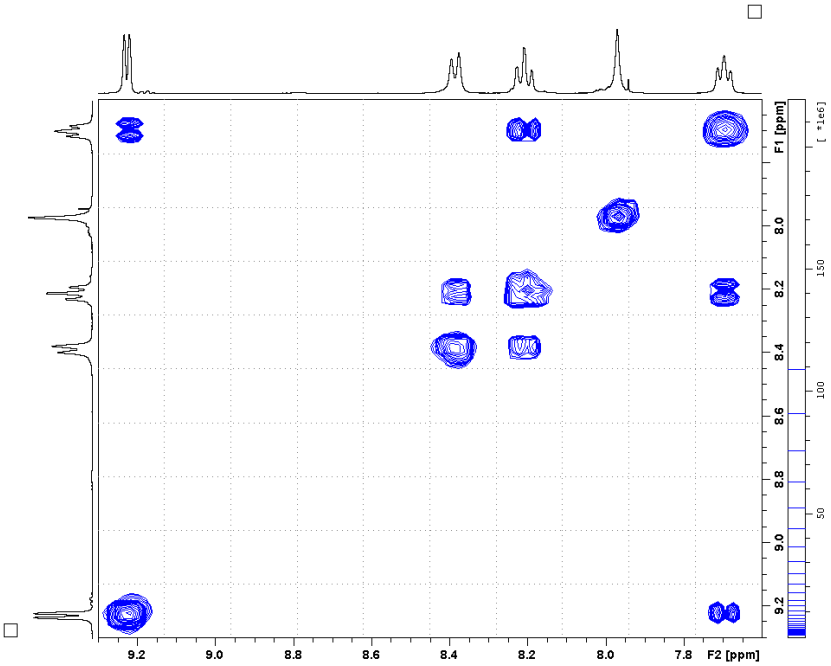

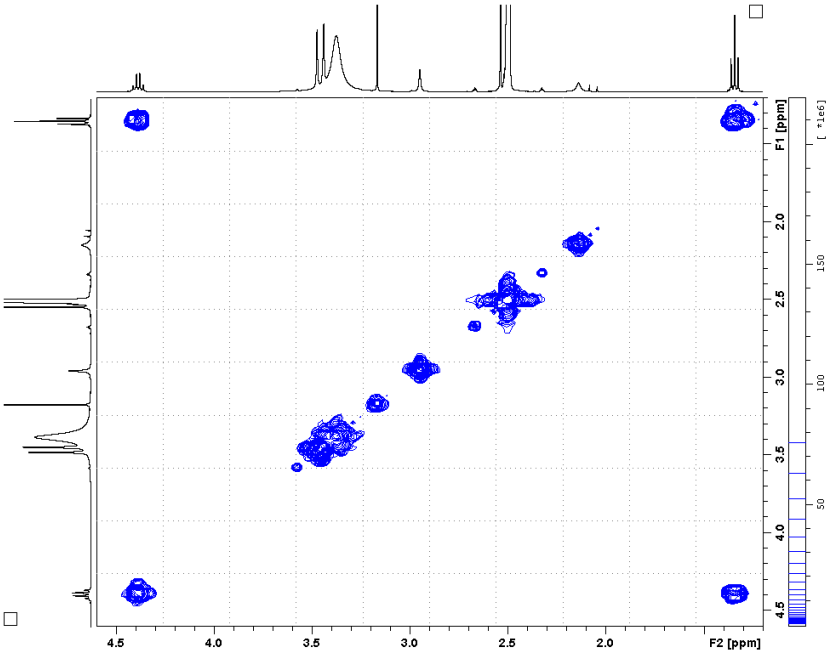

(c)

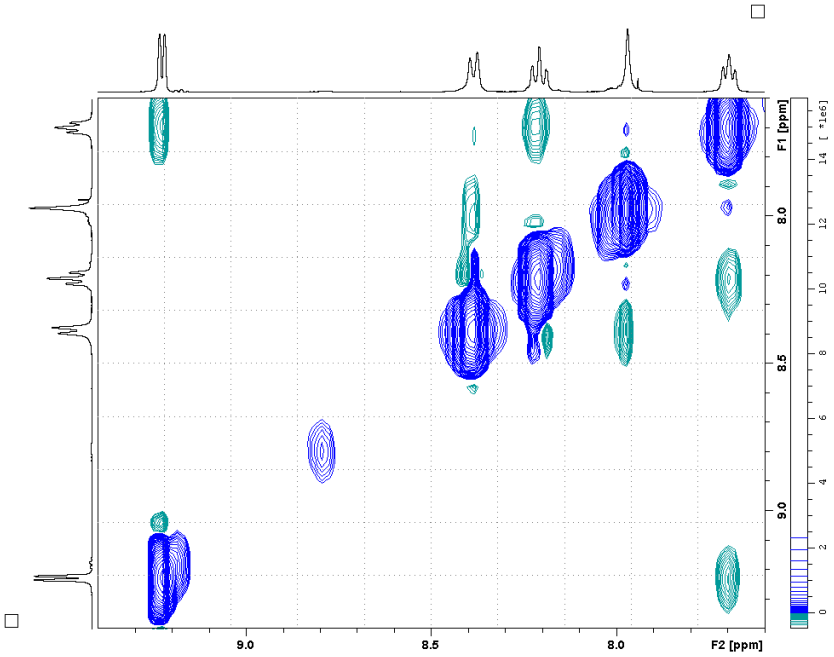

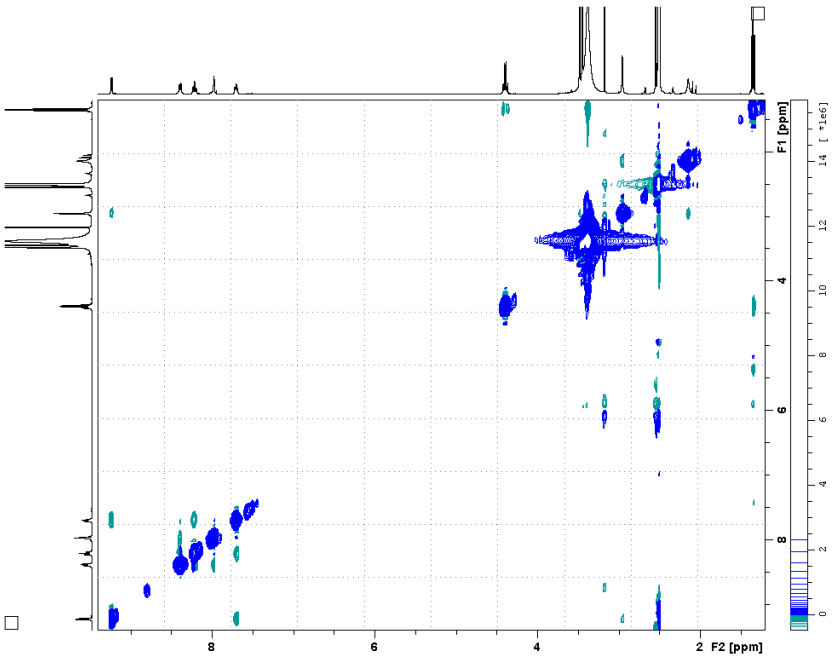

Figure S2. NMR spectra (500 MHz, 298 K, d_6-acetone) for complex *out*-[Ru(Cl)(HL)(trpy)](PF_6), **2a**$^+$: (a) ^{1}H NMR, (b) COSY, (c) NOESY.

(a)

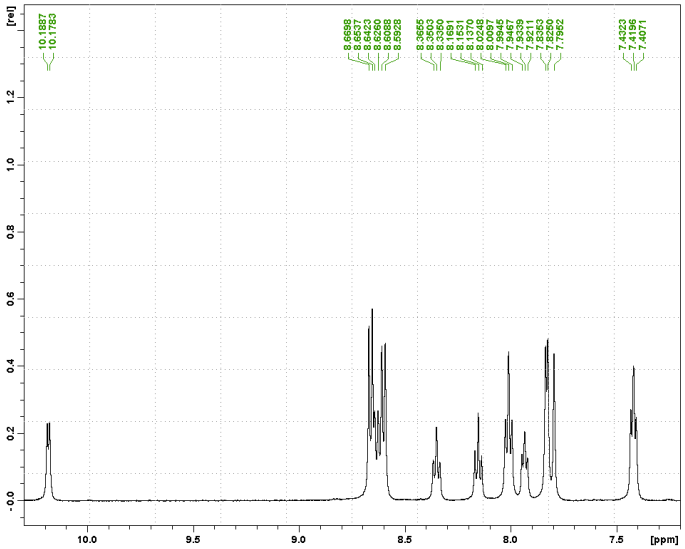

(b)

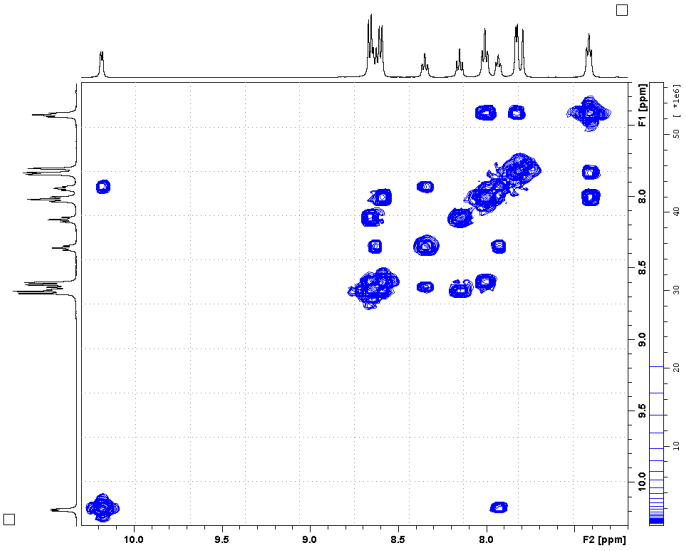

(c)

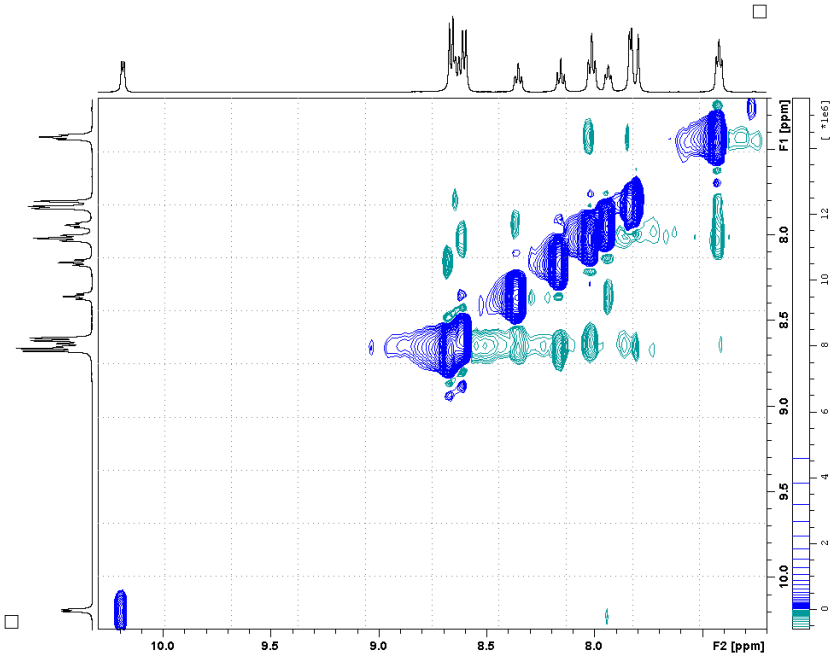

Figure S3. NMR spectra (500 MHz, 298 K, d_6-acetone) for complex *in*-[Ru(Cl)(HL)(trpy)](PF_6), **2b**$^+$: (a) ^{1}H NMR, (b) COSY.

(a)

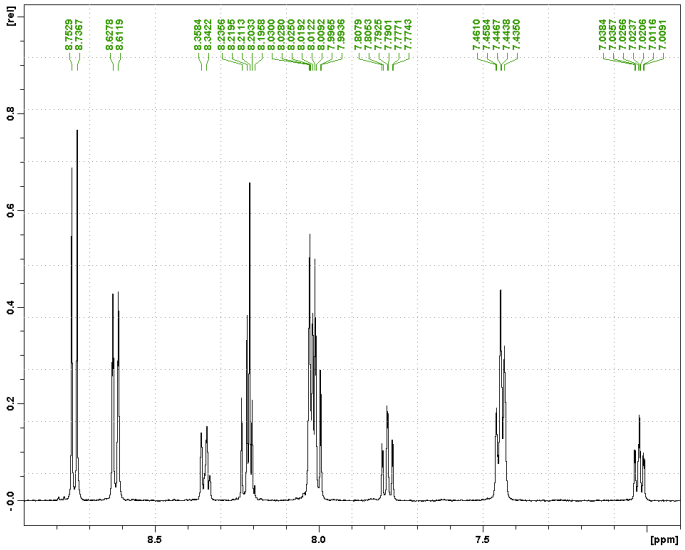

(b)

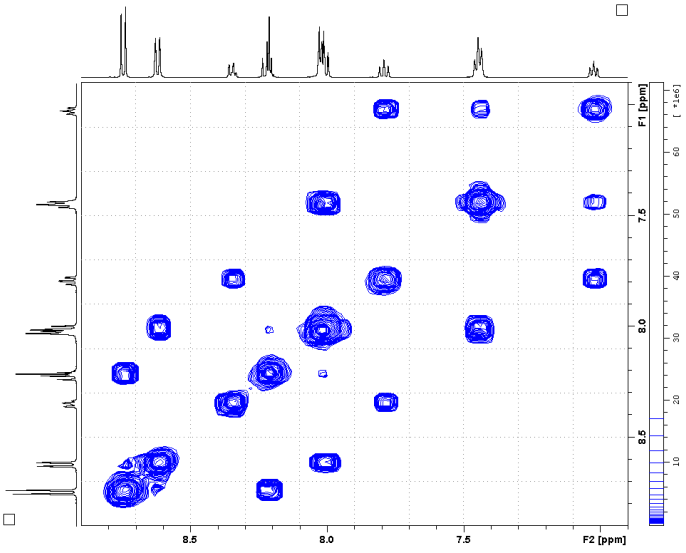

Figure S4. NMR spectra (500 MHz, 298 K, CF_3SO_3D 0.1 M in D_2O in presence of Sodium Ascorbate) for complex *out*-[Ru(HL)(trpy)(H_2O)](ClO_4)$_2$, **3a**$^{2+}$: (a) ^{1}H NMR, (b) COSY.

(a)

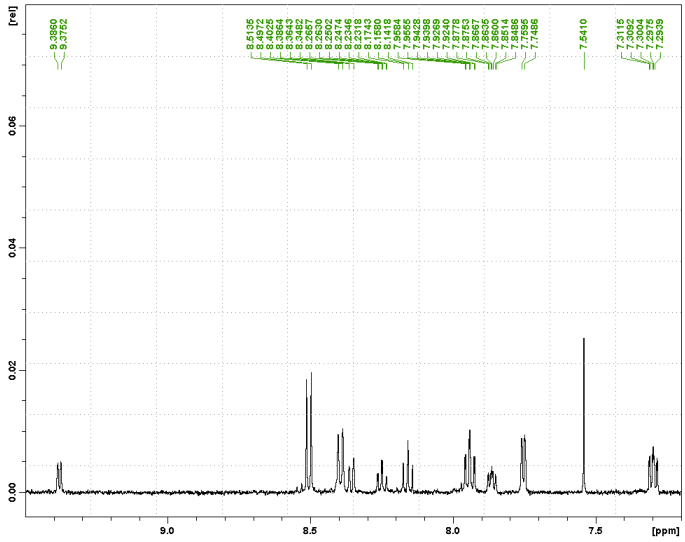

(b)

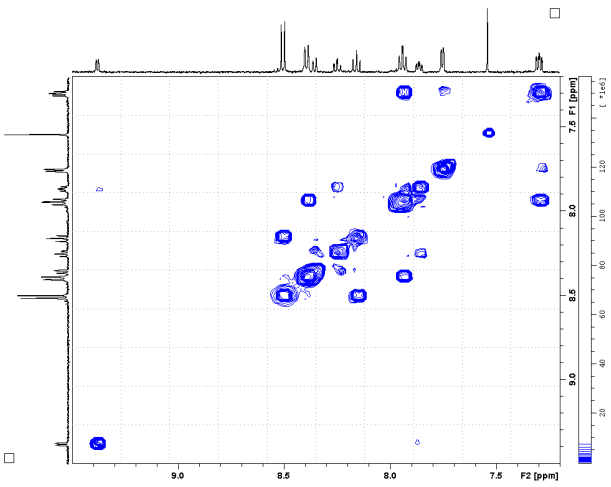

Figure S5. NMR spectra (500 MHz, 298 K, CF_3SO_3D 0.1 M in D_2O in presence of Sodium Ascorbate) for complex *in*-[Ru(HL)(trpy)(H_2O)](ClO_4)$_2$, **3b**$^{2+}$: (a) ^{1}H NMR, (b) COSY.

(a)

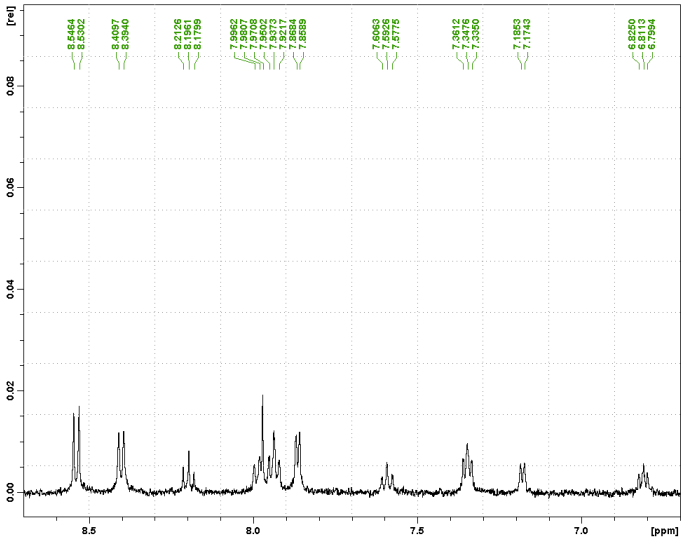

(b)

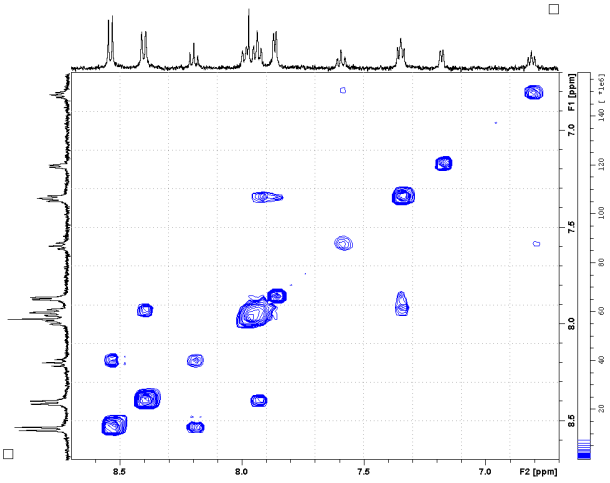

Figure S6. NMR spectra (400 MHz, 298 K, CF_3SO_3D 0.1 M in D_2O in presence of Sodium Ascorbate) for (from top to bottom): complex *out*-$[Ru(HL)(trpy)(H_2O)](ClO_4)_2$, **3a**$^{2+}$, before overnight irradiation; complex *out*-$[Ru(HL)(trpy)(H_2O)](ClO_4)_2$, **3a**$^{2+}$, after overnight irradiation; complex *in*-$[Ru(HL)(trpy)(H_2O)](ClO_4)_2$, **3b**$^{2+}$, before overnight irradiation; complex *in*-$[Ru(HL)(trpy)(H_2O)](ClO_4)_2$, **3b**$^{2+}$, after overnight irradiation.

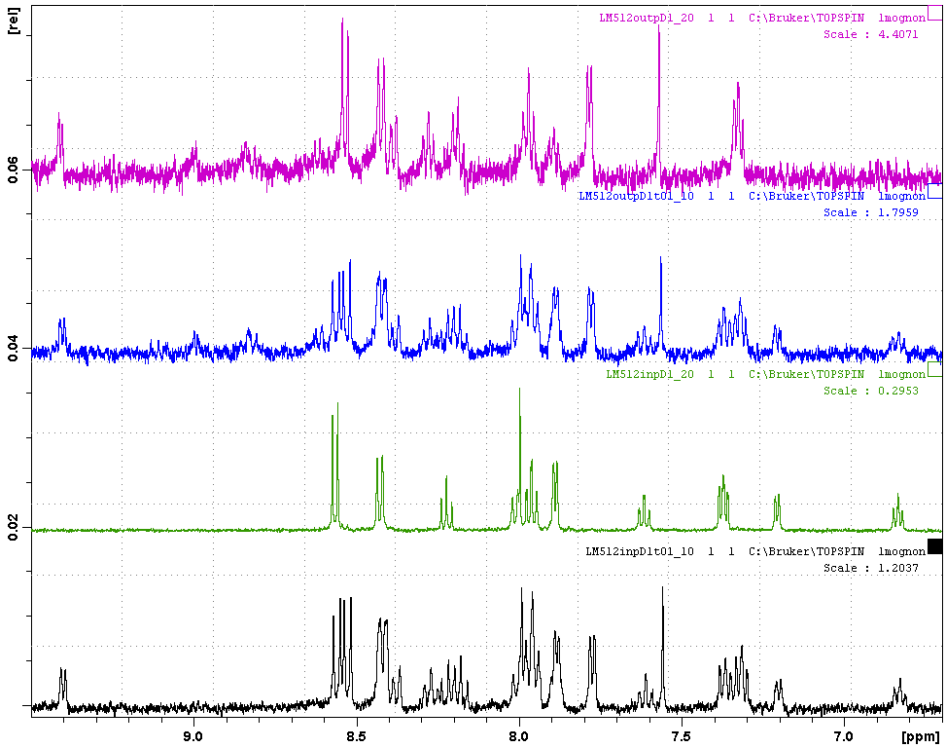

Figure S7. ESI-MS of complex *out*-[Ru(Cl)(HL)(trpy)](PF_6), **2a**$^+$, in MeOH and simulated isotopic distribution of the cation {Ru(Cl)(HL)(trpy)}$^+$.

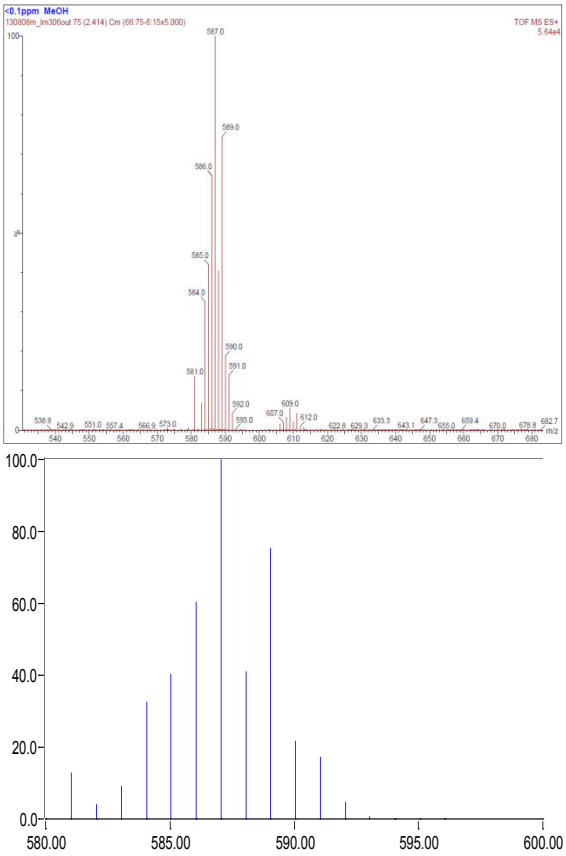

Figure S8. ESI-MS of complex *in*-[Ru(Cl)(HL)(trpy)](PF$_6$), **2b**$^+$, in MeOH and simulated isotopic distribution of the cation {Ru(Cl)(HL)(trpy)}$^+$.

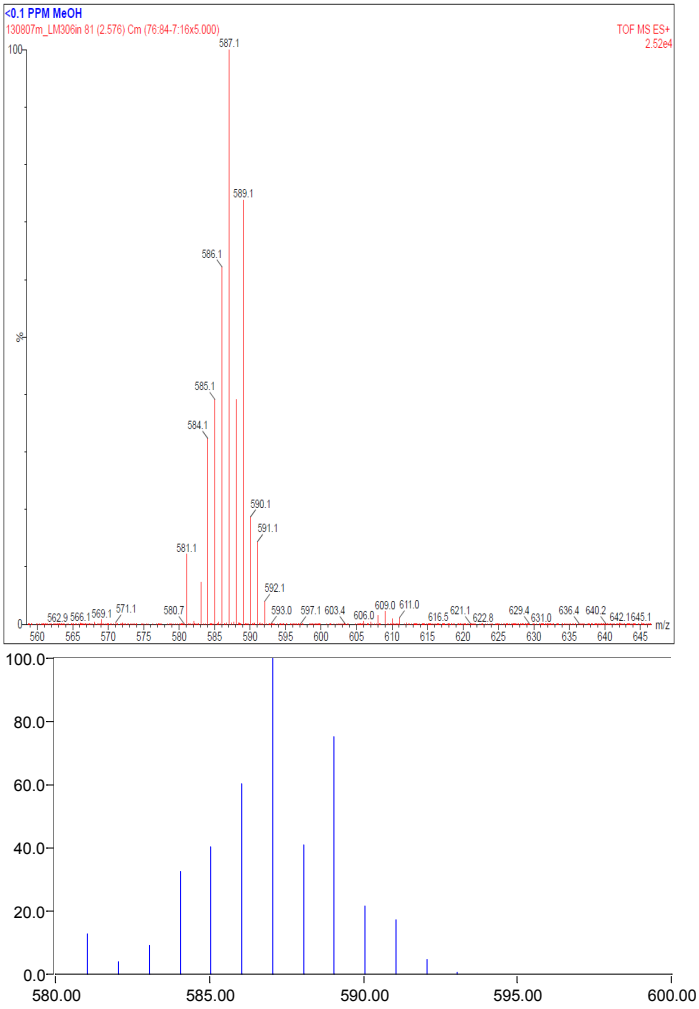

Figure S9. ESI-MS of complex *out*-[Ru(HL)(trpy)(H_2O)](ClO_4)$_2$, **3a**$^{2+}$, in MeOH and simulated isotopic distribution of the cation {Ru(OH)(HL)(trpy)}$^+$.

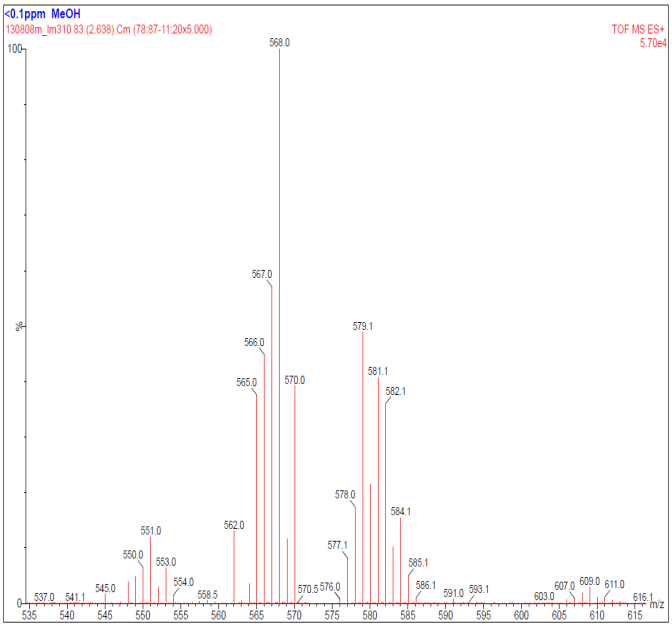

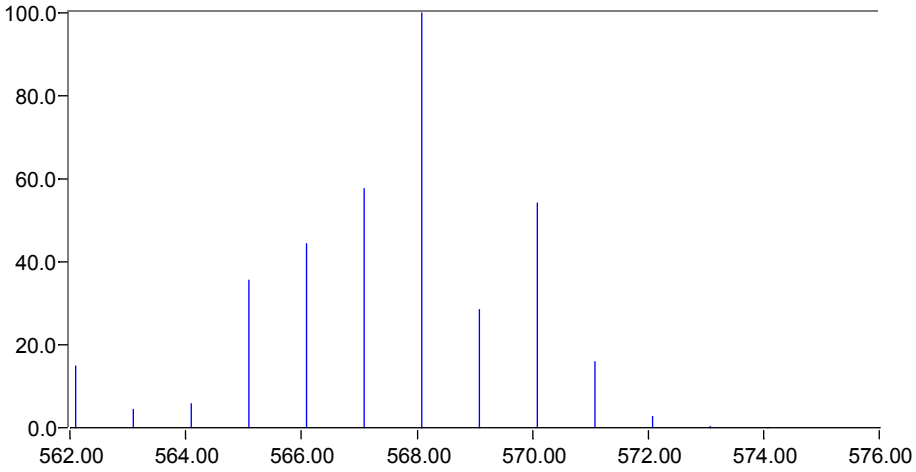

Figure S10. ESI-MS of complex *in*-[Ru(HL)(trpy)(H_2O)](ClO_4)$_2$, **3b**$^{2+}$, in MeOH and simulated isotopic distribution of the cation {Ru(OH)(HL)(trpy)}$^+$.

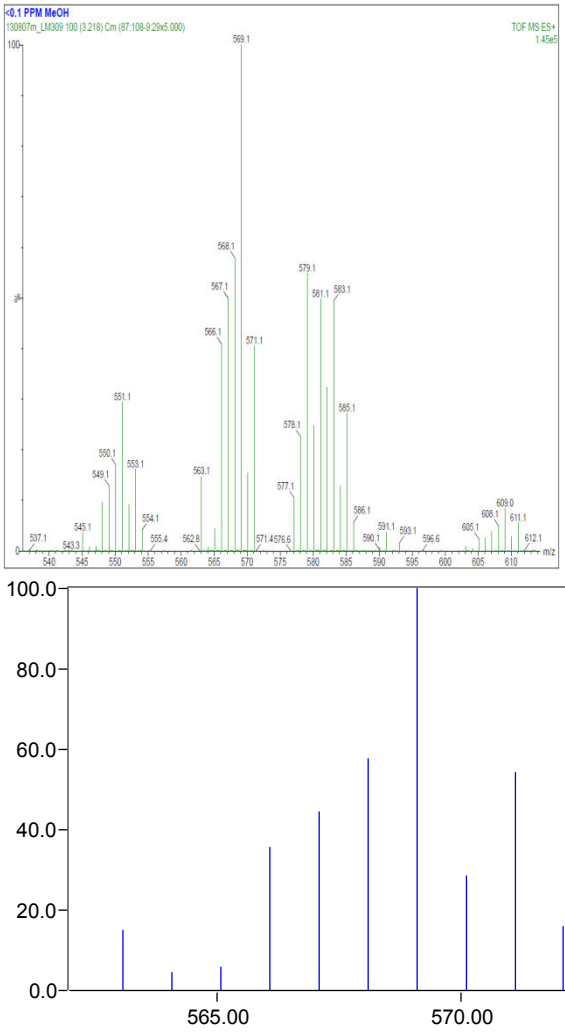

Figure S11. UV-Vis spectra in CH_2Cl_2 for complexes *cis(out)*, *cis*-$[Ru(Cl)_2(dmso)_2(HL)]$, **1**, *out*-$[Ru(Cl)(HL)(trpy)](PF_6)$, **2a**$^+$, and *in*-$[Ru(Cl)(HL)(trpy)](PF_6)$, **2b**$^+$.

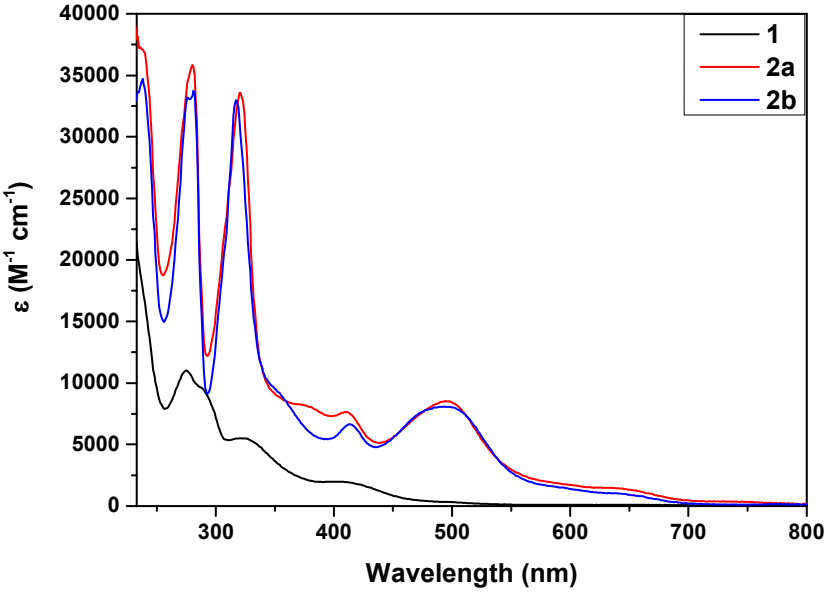

Figure S12. (a) UV-Vis spectra for complexes *out*-[Ru(HL)(trpy)(H_2O)](ClO_4)$_2$, **3a**$^{2+}$, and *in*-[Ru(HL)(trpy)(H_2O)](ClO_4)$_2$, **3b**$^{2+}$, in pH = 1 CF_3SO_3H, and redox titrations with [$(NH_4)_2Ce(NO_3)_6$] in pH = 1 CF_3SO_3H, of (left) **3a**$^{2+}$ (top) first equivalent, (middle) second equivalent and (bottom) absorbance versus equivalents added at selected wavelengths, and (right) **3b**$^{2+}$ (top) first equivalent, (middle) second equivalent and (bottom) absorbance versus equivalents added at selected wavelengths

(a)

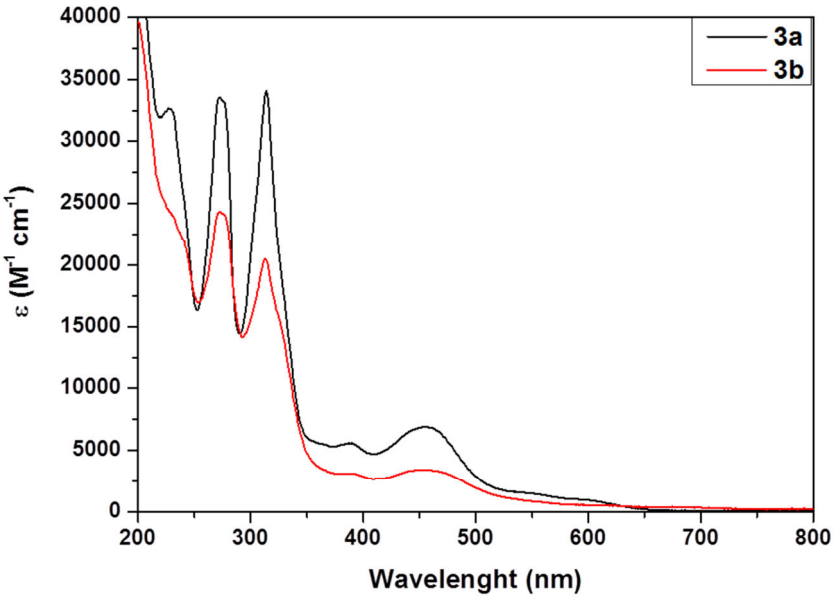

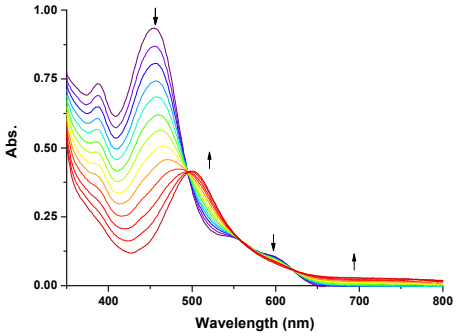

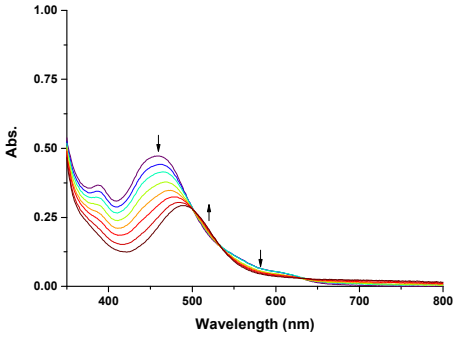

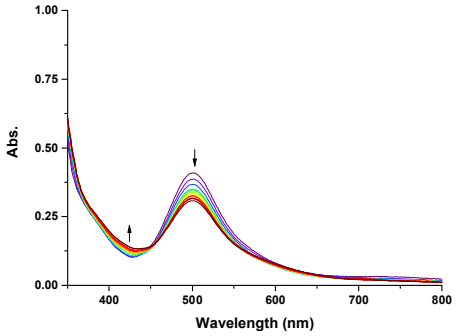

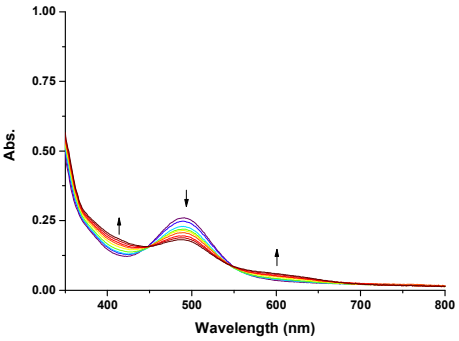

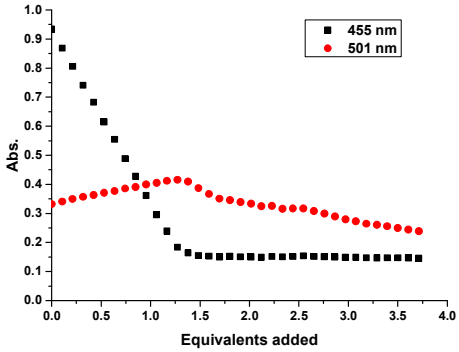

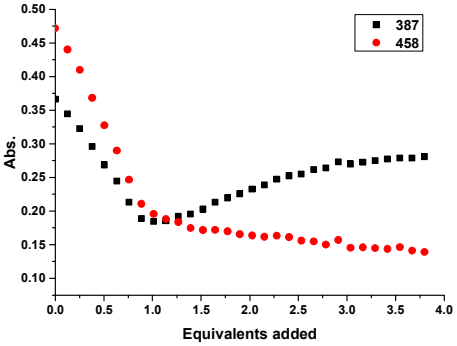

Figure S13. Cyclic voltammograms for complex *cis(out), cis*-$[Ru(Cl)_2(dmso)_2(HL)]$, **1**, in 0.1M TBAH, CH_2Cl_2, for the determination of the isomerization with a 2 minutes CPE (a) at 0.24 V, and (b) at 1.84 V, (c) plots for the determination of the reaction. Color code: black: 50 mV/s, red: 100 mV/s, green: 200 mV/s, blue: 300 mV/s, light blue: 400 mV/s, pink: 500 mV/s, yellow: 600 mV/s, dark yellow: 700 mV/s, dark blue: 800 mV/s, purple: 900 mV/s, brown: 1000 mV/s.

(a)

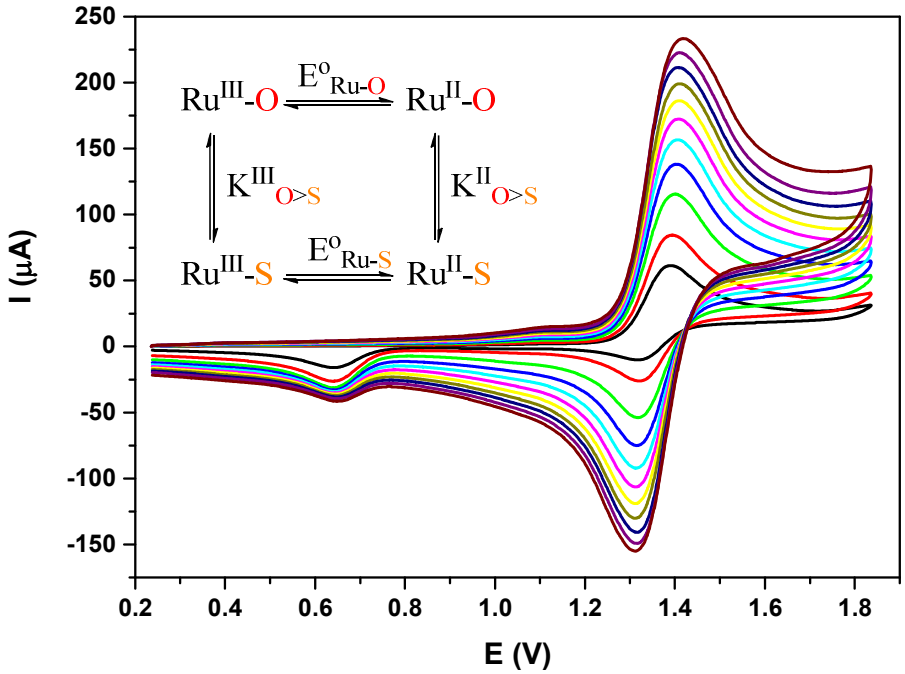

(b)

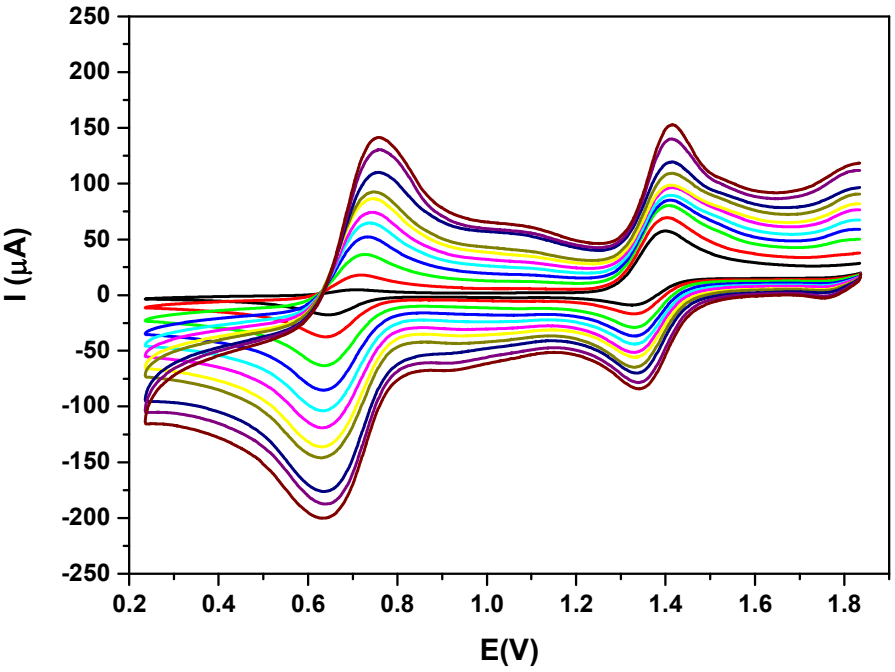

V

(c)

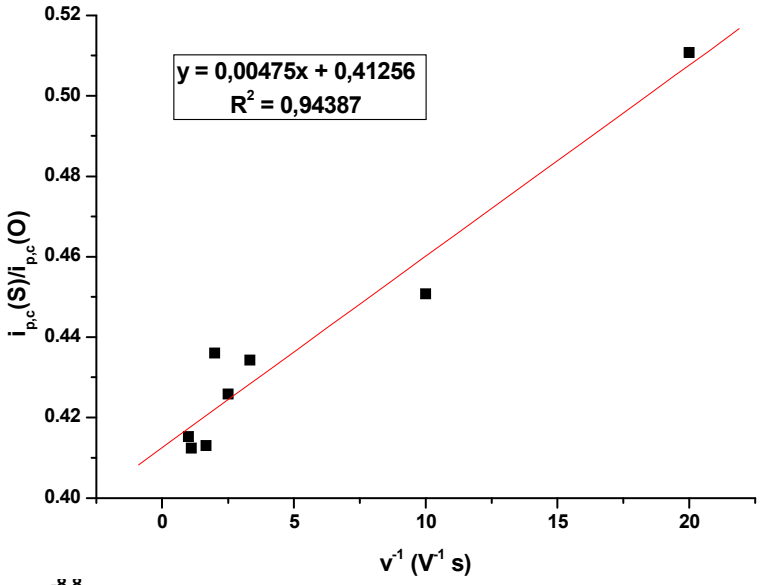
y = 0,00475x + 0,41256
R2 = 0,94387
ip,c(S)/ip,c(O)
v-1 (V-1 s)

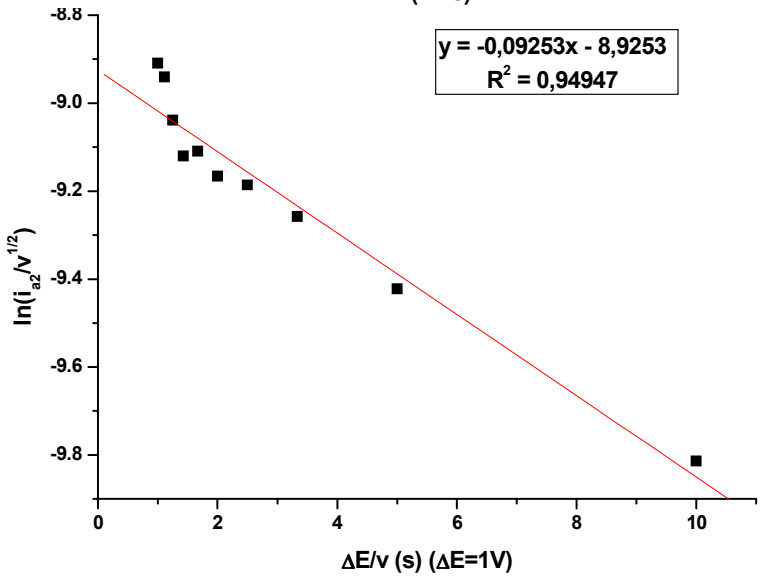
y = -0,09253x - 8,9253
R2 = 0,94947
ln(ia2/v1/2)
ΔE/v (s) (ΔE=1V)

Figure S14. Cyclic voltammogram for complexes (top) *out*-[Ru(Cl)(HL)(trpy)](PF_6), **2a**$^+$, and (bottom) *in*-[Ru(Cl)(HL)(trpy)](PF_6), **2b**$^+$, in 0.1M TBAH, CH_2Cl_2.

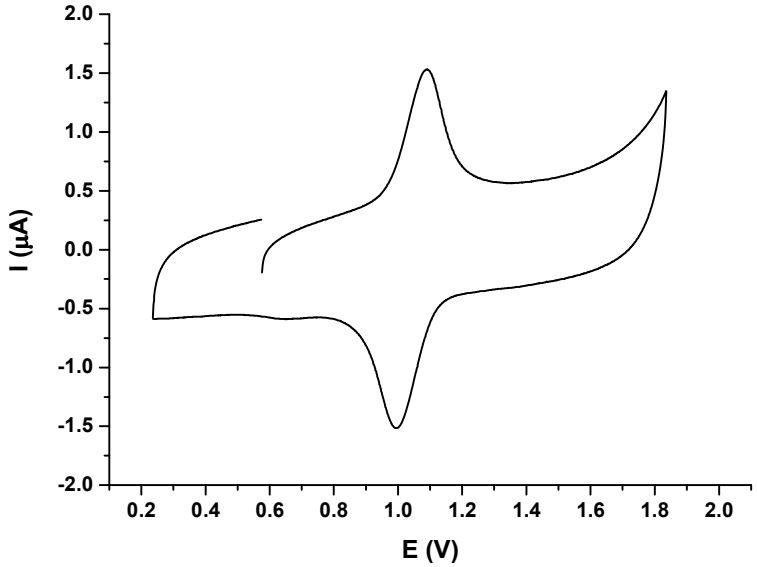

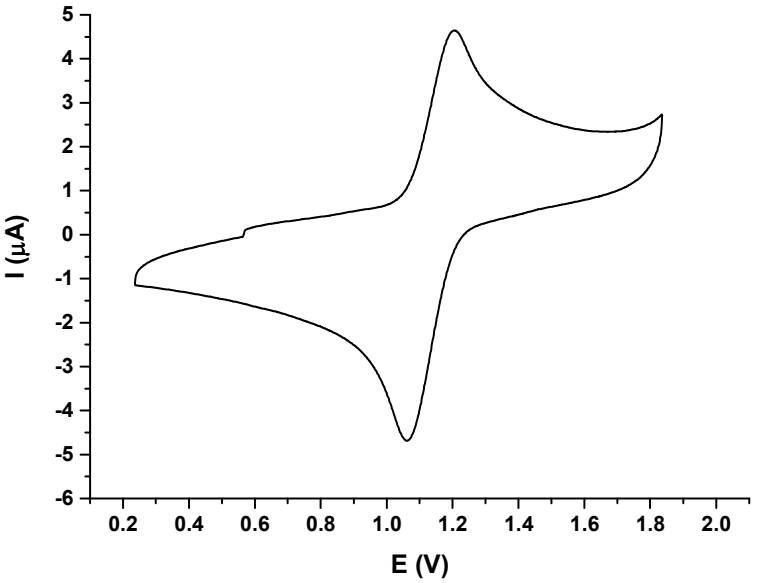

Figure S15. Cyclic voltammograms in (a) pH = 1 CF_3SO_3H and (b) pH = 7 phosphate buffer for complexes (top) *out*-[Ru(HL)(trpy)(H_2O)](ClO_4)$_2$, **3a**$^{2+}$, and (bottom) *in*-[Ru(HL)(trpy)(H_2O)](ClO_4)$_2$, **3b**$^{2+}$,

(a)

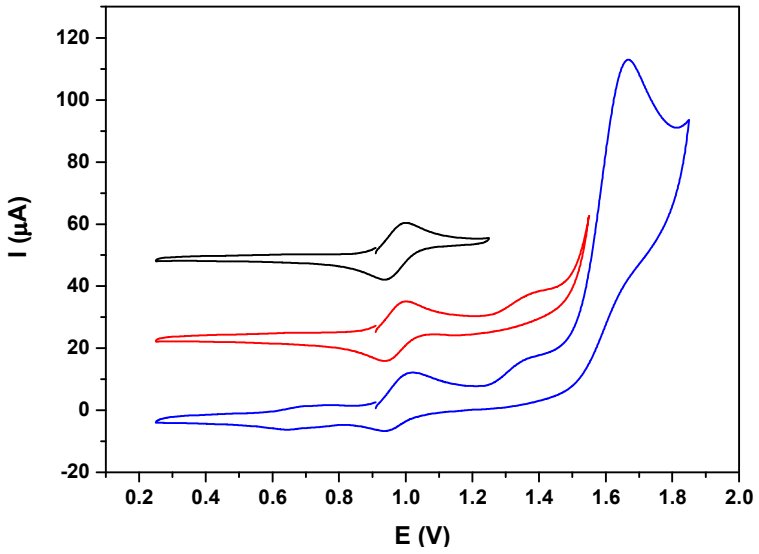

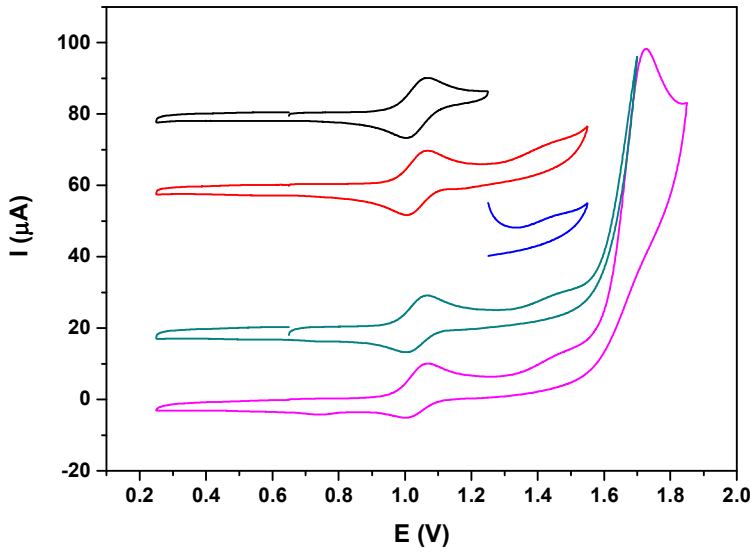

(b)

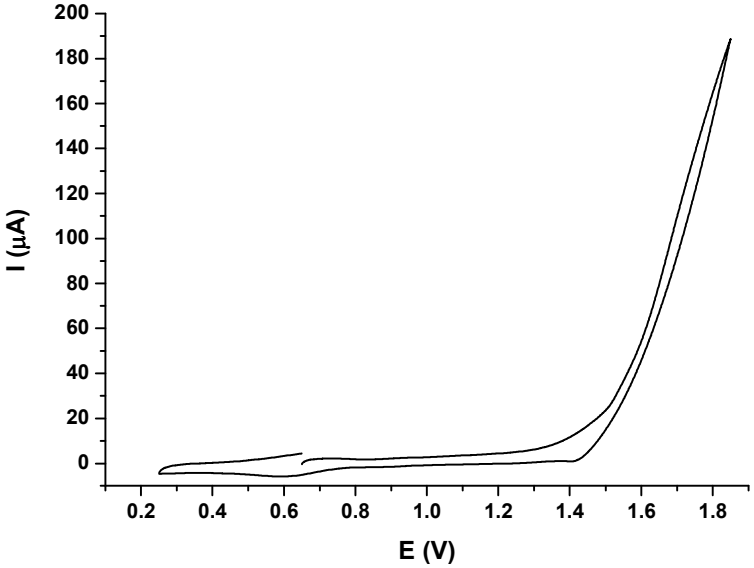

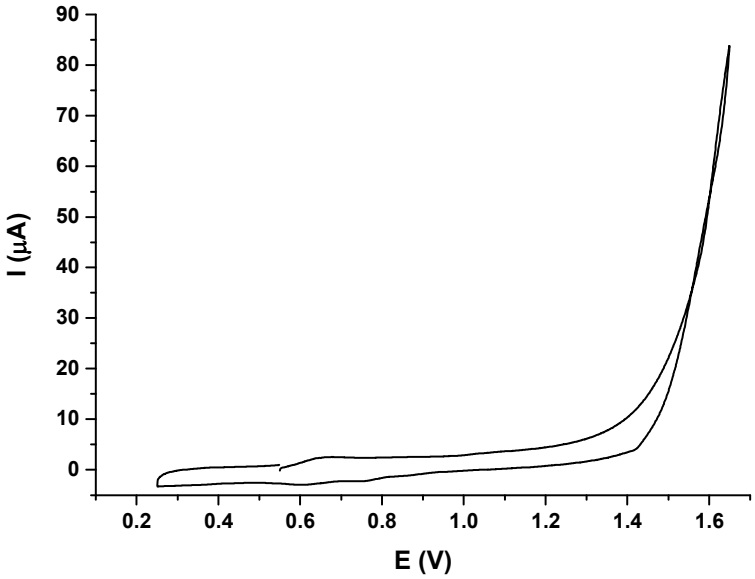

Figure S16. (a) CVs of 0.5 mM solutions of (top) **3a**$^{2+}$ and (bottom) **3b**$^{2+}$ at different scan rates. (b) Foot of the Wave analysis plots of i/i^0_p vs $1/\{1+\exp[(F/RT)(E^0_{PQ}-E)]\}$ at each scan rate. The insets show the plots of the $\log(k_{obs})$ vs $\log(v)$, the red line is the average value obtained from all the measurements. (c) DPV for the determination of E^0_{PQ}.

(a)

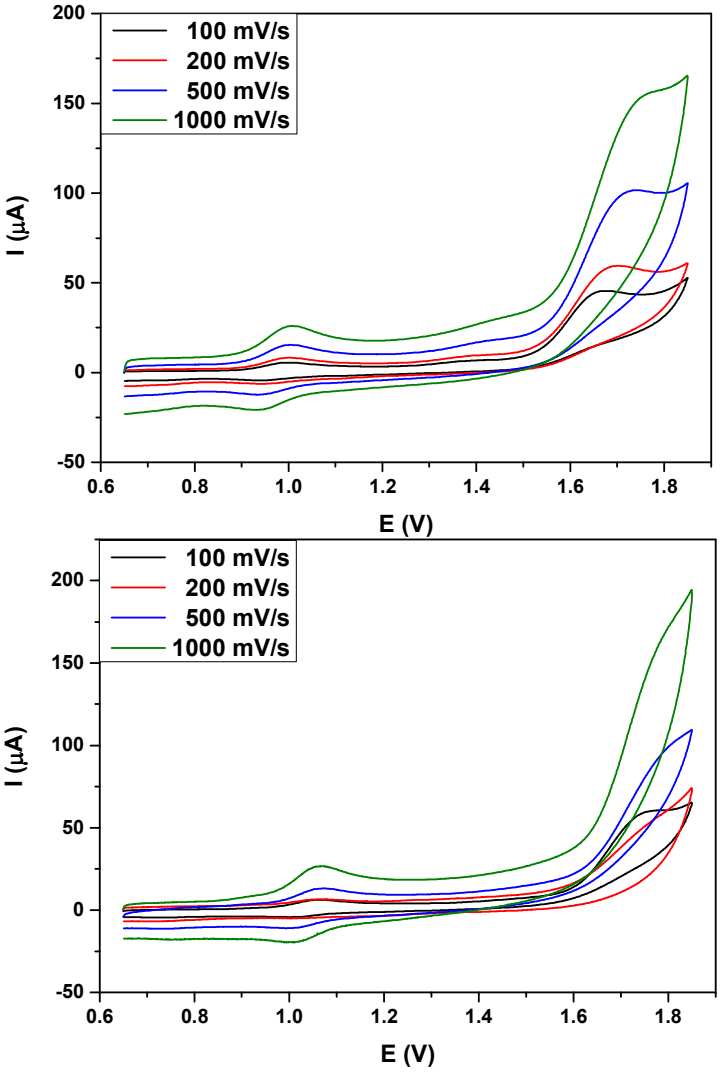

(b)

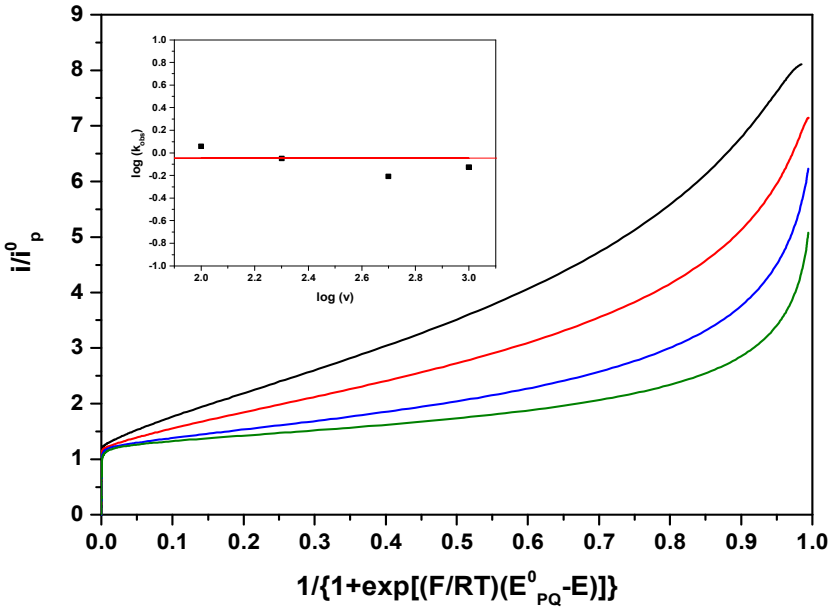

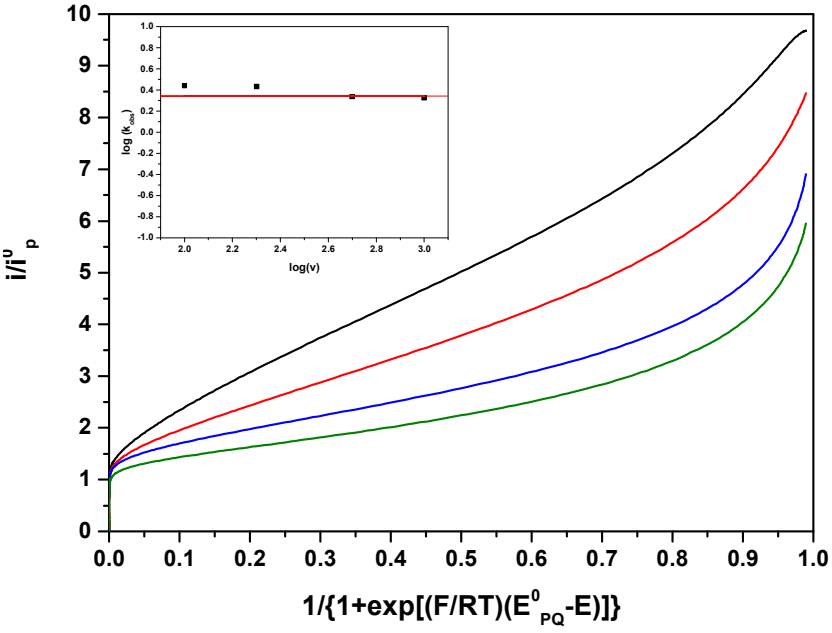

(c)

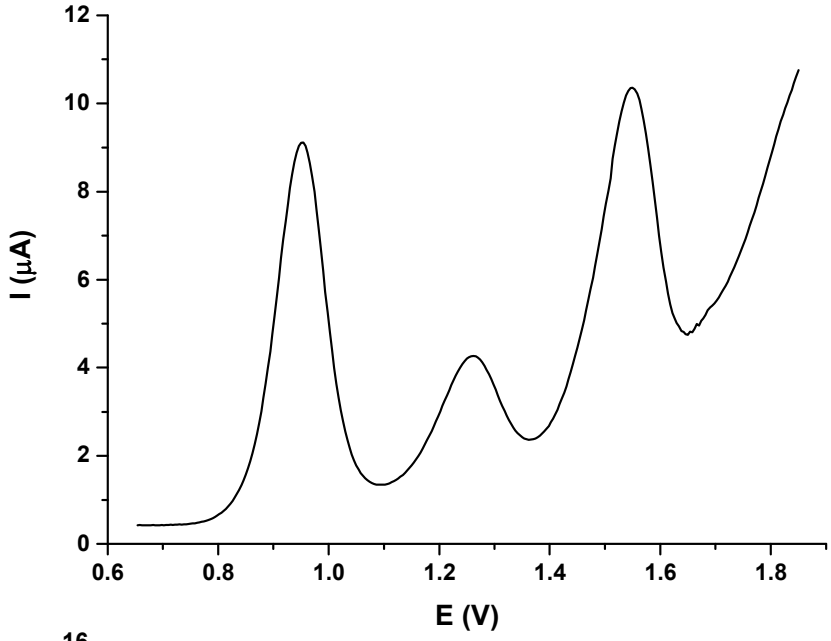
I (μA)
E (V)
0
2
4
6
8
10
12
0.6
0.8
1.0
1.2
1.4
1.6
1.8

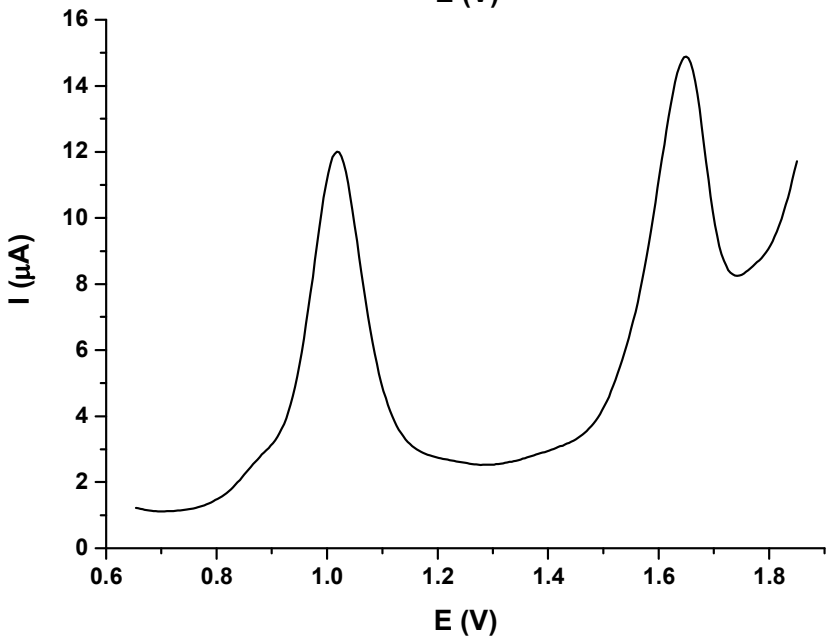
I (μA)
E (V)
0
2
4
6
8
10
12
14
16
0.6
0.8
1.0
1.2
1.4
1.6
1.8

Figure 17. (a) CVs of different solutions of (top) **3a**$^{2+}$ and (bottom) **3b**$^{2+}$ at 200mV/s. (b) Foot of the Wave analysis plots of i/i^0_p vs $1/\{1+\exp[(F/RT)(E^0_{PQ}-E)]\}$ at each concentration. The insets show the plot of the k_{obs} vs v, the red line is the average value obtained from all the measurements.

(a)

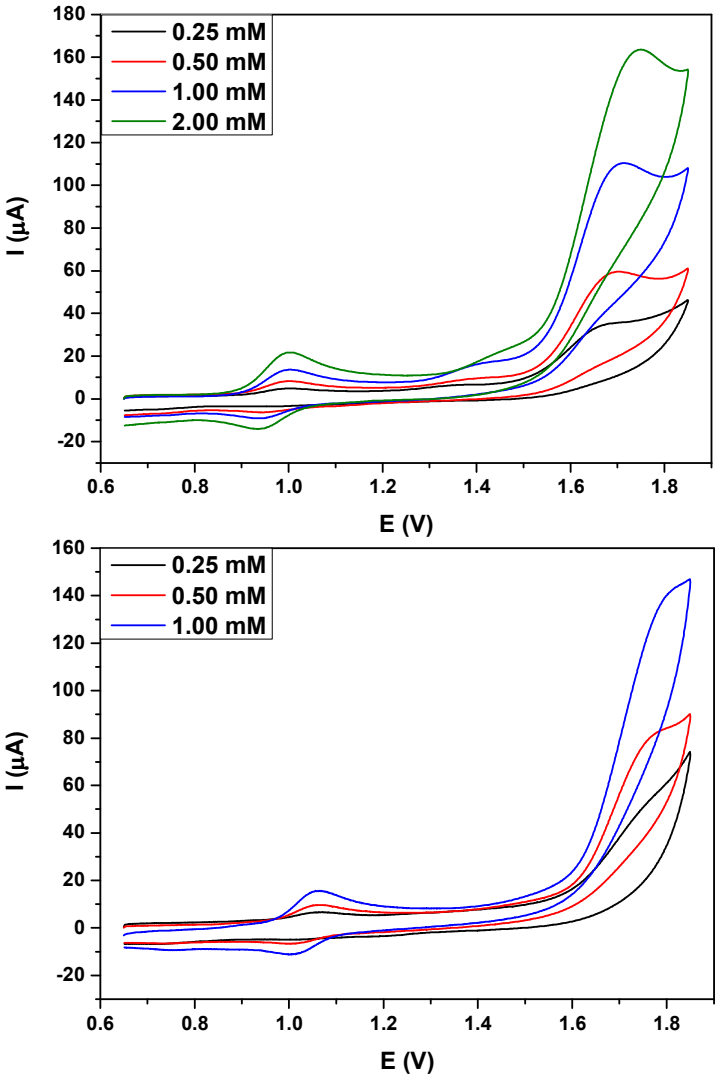

(b)

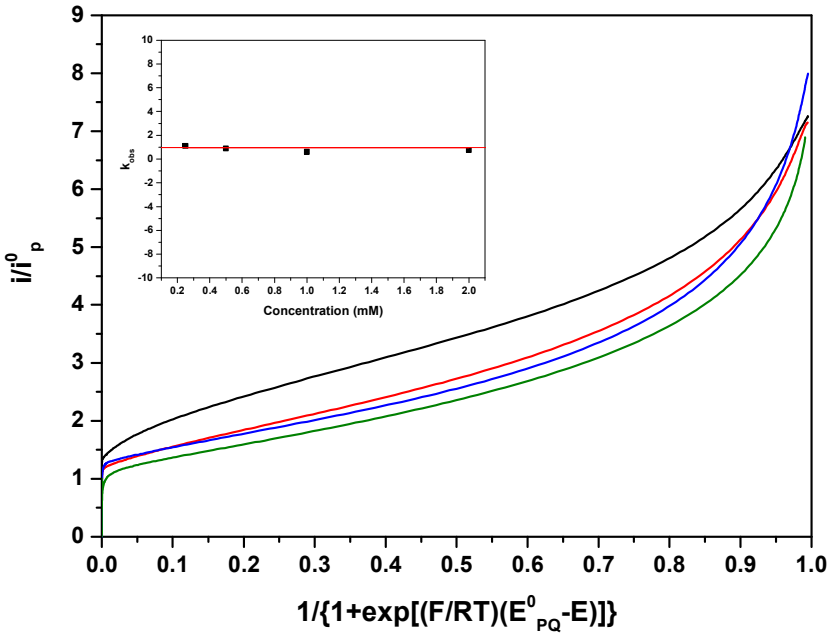
i/i^0_p
1/{1+exp[(F/RT)(E$^0_{PQ}$-E)]}
k_{obs}
Concentration (mM)

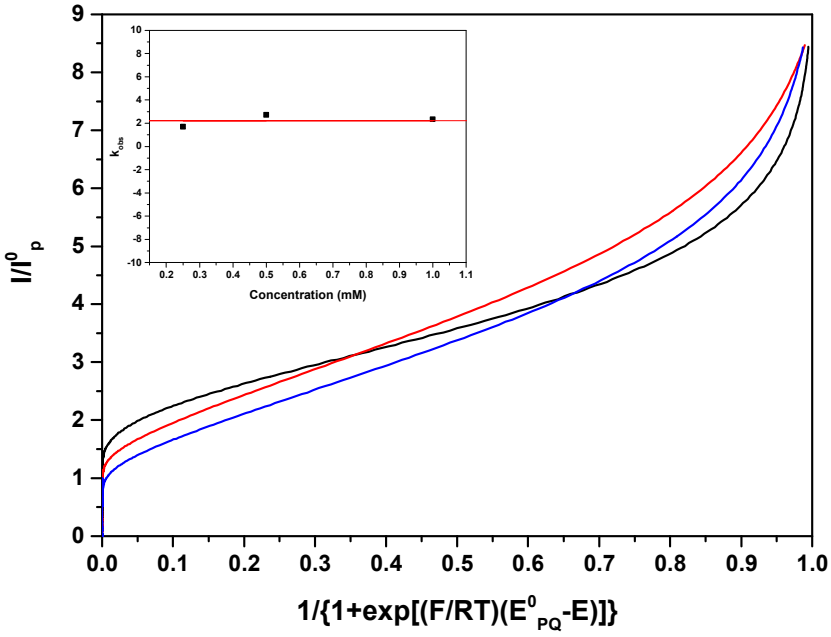
I/I^0_p
1/{1+exp[(F/RT)(E$^0_{PQ}$-E)]}
k_{obs}
Concentration (mM)

Figure S18. (a) DPV at selected pHs and (b) Pourbaix diagram for complexes (top) *out*-[Ru(HL)(trpy)(H_2O)](ClO_4)$_2$, **3a**$^{2+}$, and (bottom) *in*-[Ru(HL)(trpy)(H_2O)](ClO_4)$_2$, **3b**$^{2+}$. The orange line represents the potential for water oxidation. (c) Formulas for the simulation of the Pourbaix diagrams.

(a)

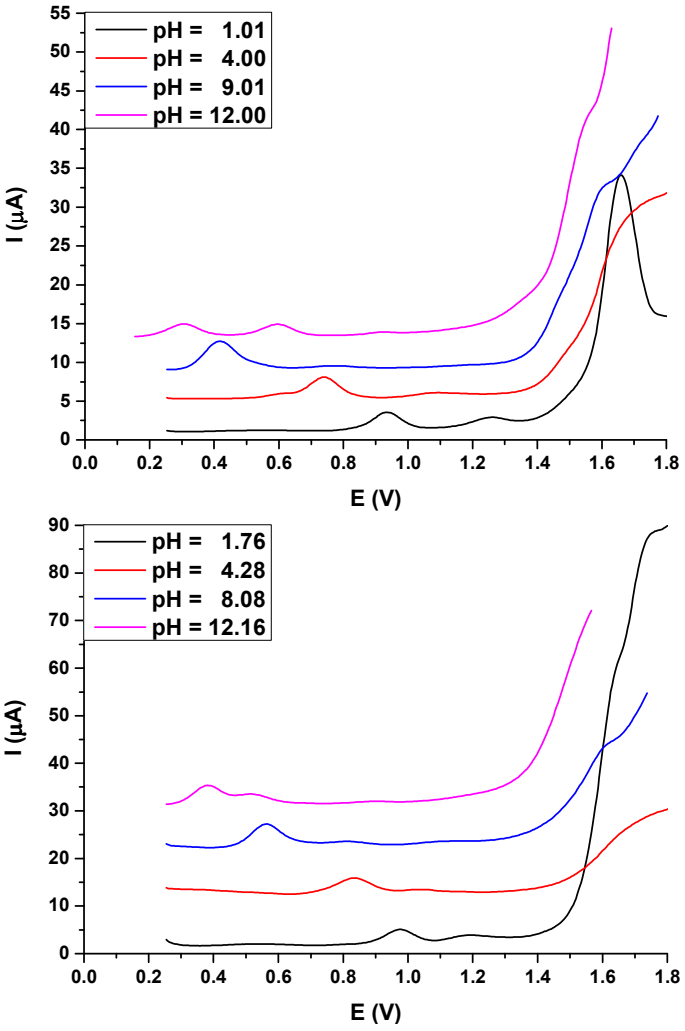

(b)

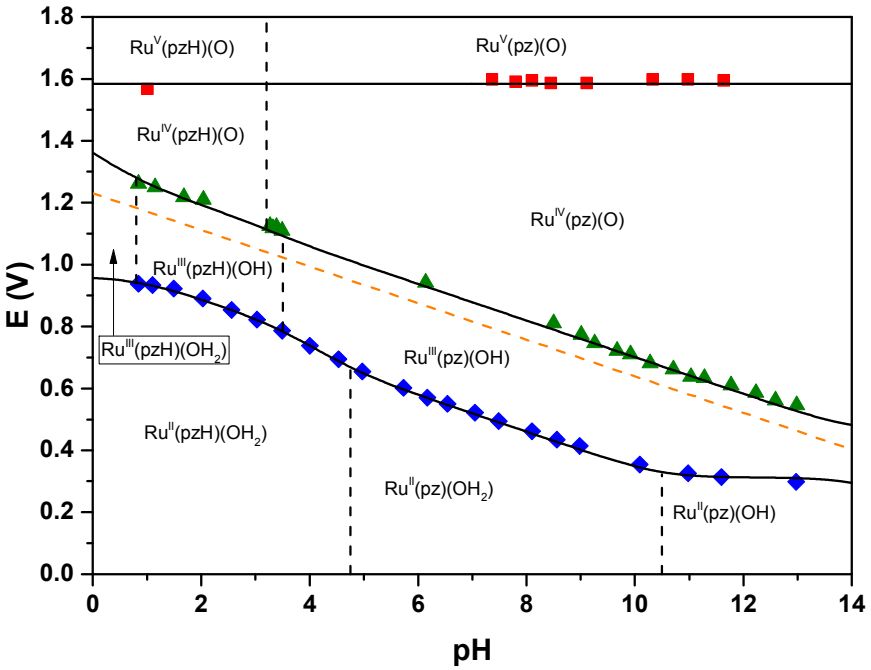
Ru^V(pzH)(O)
Ru^V(pz)(O)
Ru^IV(pzH)(O)
Ru^IV(pz)(O)
Ru^III(pzH)(OH)
Ru^III(pzH)(OH2)
Ru^III(pz)(OH)
Ru^II(pzH)(OH2)
Ru^II(pz)(OH2)
Ru^II(pz)(OH)
E (V)
pH

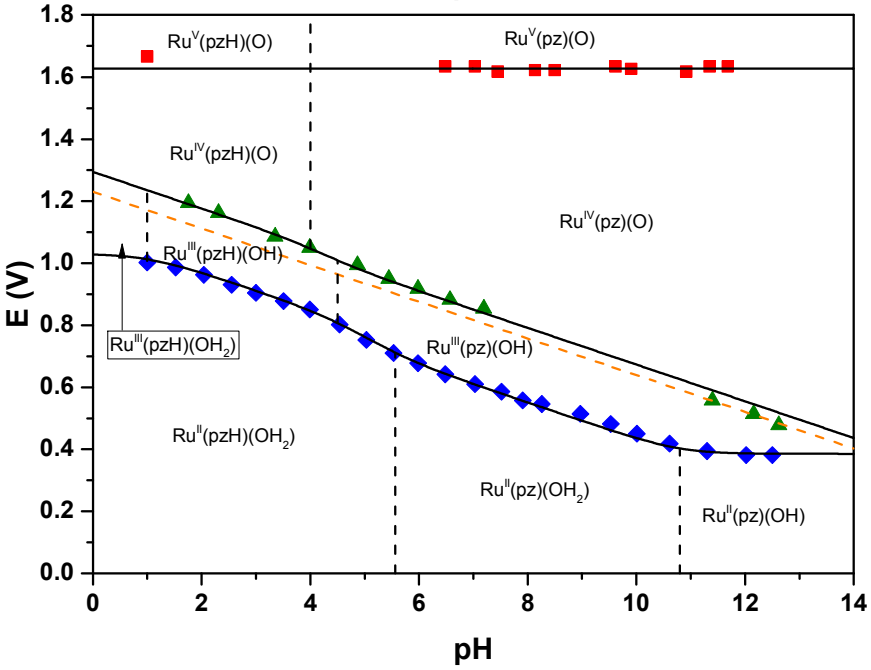
Ru^V(pzH)(O)
Ru^V(pz)(O)
Ru^IV(pzH)(O)
Ru^IV(pz)(O)
Ru^III(pzH)(OH)
Ru^III(pzH)(OH2)
Ru^III(pz)(OH)
Ru^II(pzH)(OH2)
Ru^II(pz)(OH2)
Ru^II(pz)(OH)
E (V)
pH

(c)

$$E(\mathrm{III/II}) = \left[E(\mathrm{III/II})_{\mathrm{pH=0}}\right] + \left(0.05916 * \log\left(\frac{[\mathrm{H^+}]^3 + [\mathrm{H^+}]^2\mathrm{K_{a1}^{II}} + [\mathrm{H^+}]\mathrm{K_{a1}^{II}K_{a2}^{II}} + \mathrm{K_{a1}^{II}K_{a2}^{II}K_{a3}^{II}}}{[\mathrm{H^+}]^3 + [\mathrm{H^+}]^2\mathrm{K_{a1}^{III}} + [\mathrm{H^+}]\mathrm{K_{a1}^{III}K_{a2}^{III}} + \mathrm{K_{a1}^{III}K_{a2}^{III}K_{a3}^{III}}}\right)\right)$$

$$E(\mathrm{IV/III}) = \left[E(\mathrm{IV/III})_{\mathrm{pH=0}}\right] + \left(0.05916 * \log\left(\frac{[\mathrm{H^+}]^3 + [\mathrm{H^+}]^2\mathrm{K_{a1}^{III}} + [\mathrm{H^+}]\mathrm{K_{a1}^{III}K_{a2}^{III}} + \mathrm{K_{a1}^{III}K_{a2}^{III}K_{a3}^{III}}}{[\mathrm{H^+}]^3 + [\mathrm{H^+}]^2\mathrm{K_{a1}^{IV}} + [\mathrm{H^+}]\mathrm{K_{a1}^{IV}K_{a2}^{IV}} + \mathrm{K_{a1}^{IV}K_{a2}^{IV}K_{a3}^{IV}}}\right)\right)$$

Figure S19. Manometric measurement for complexes (black) *out*-[Ru(HL)(trpy)(H_2O)](ClO_4)$_2$, **3a**$^{2+}$, and (red) *in*-[Ru(HL)(trpy)(H_2O)](ClO_4)$_2$, **3b**$^{2+}$, in terms of (a) pressure generated and (b) actual O_2 after on-line mass experiments. Conditions are: cat 1mM/CAN 100mM/pH = 1 triflic acid total volume 2 mL.

(a)

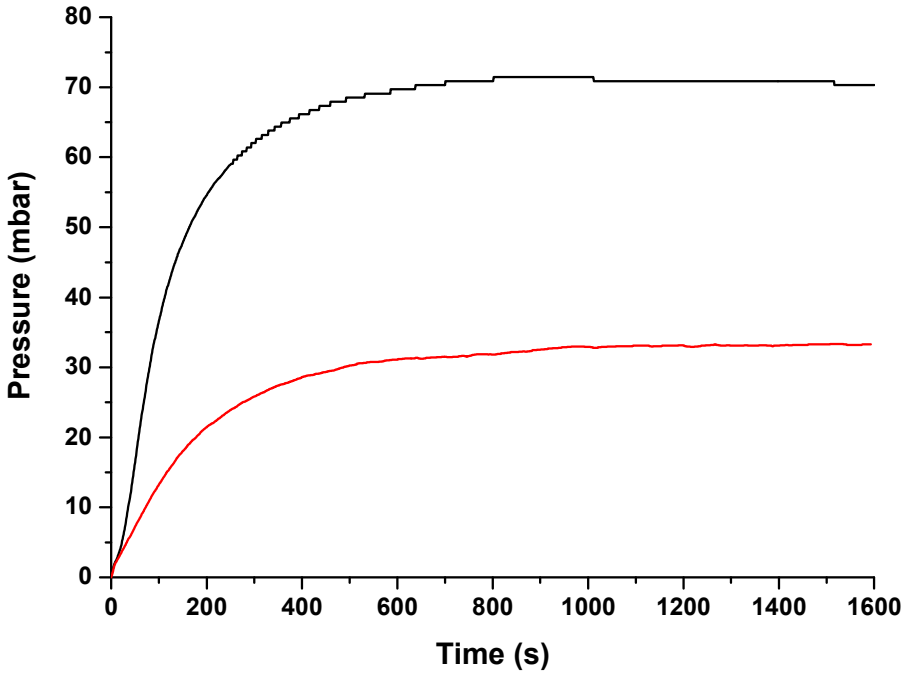

(b)

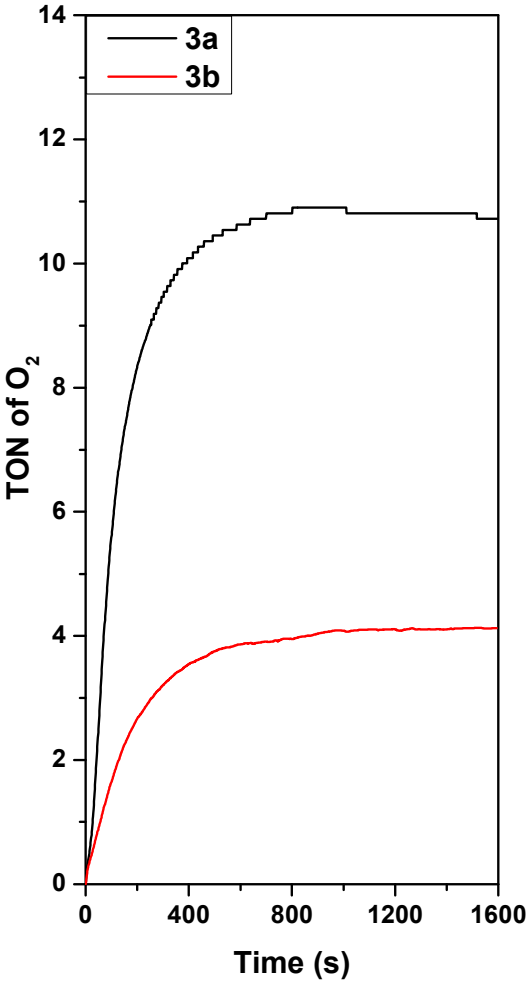

Figure S20. (a) On-line mass measurement for complexes (top) *out*-[Ru(HL)(trpy)(H_2O)](ClO_4)$_2$, **3a**$^{2+}$, and (bottom) *in*-[Ru(HL)(trpy)(H_2O)](ClO_4)$_2$, **3b**$^{2+}$, and (b) evolution of the ratios between O_2 and CO_2. Conditions are: cat 1mM/CAN 100mM/pH = 1 triflic acid total volume 2 mL.

(a)

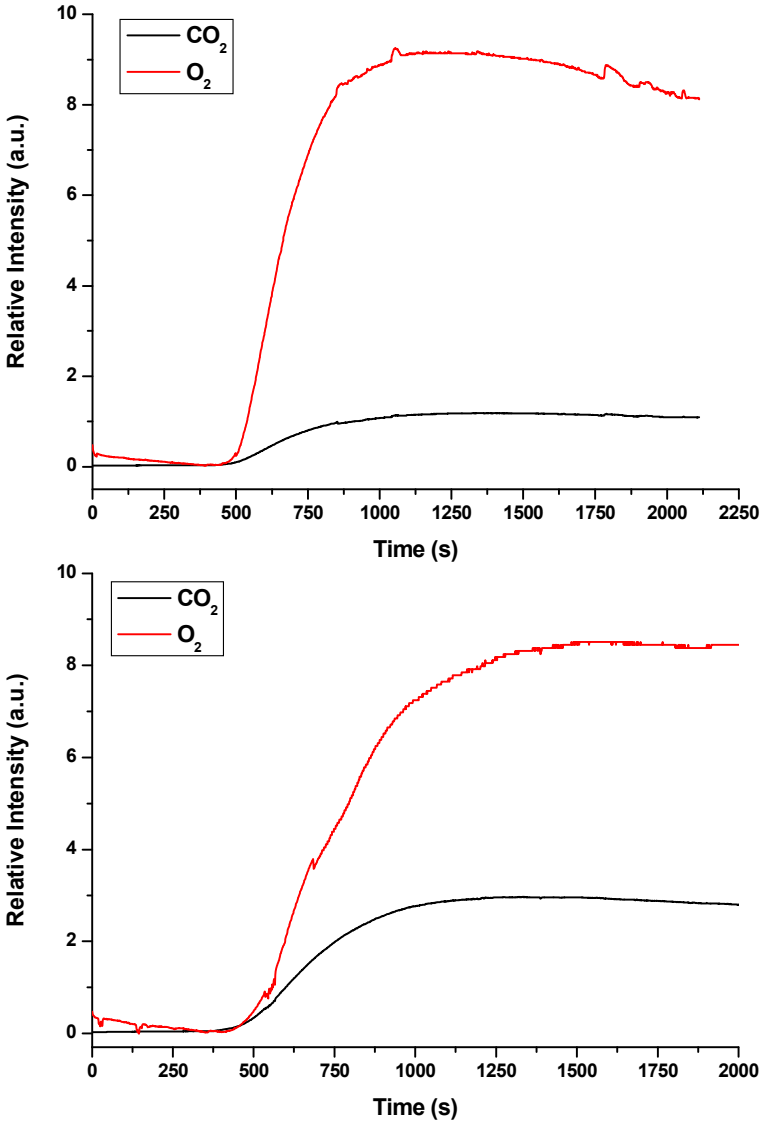

(b)

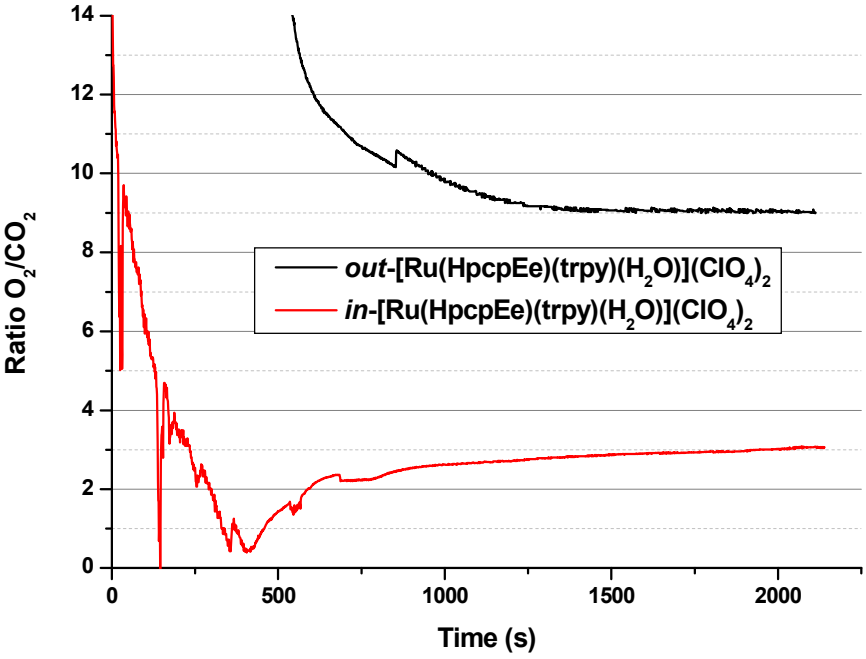

UNIVERSITAT ROVIRA I VIRGILI
MONONUCLEAR AND HETEROTRINUCLEAR RUTHENIUM COMPLEXES: SYNTHESIS AND WATER OXIDATION ACTIVITY.
Lorenzo Mognon
Dipòsit Legal: T 1359-2015

UNIVERSITAT ROVIRA I VIRGILI
MONONUCLEAR AND HETEROTRINUCLEAR RUTHENIUM COMPLEXES: SYNTHESIS AND WATER OXIDATION ACTIVITY.
Lorenzo Mognon
Dipòsit Legal: T 1359-2015

Chapter 6. Supported Single Site Isomeric Ru WOCs: Synthesis, Electrochemical Characterization, Reactivity and Anchoring

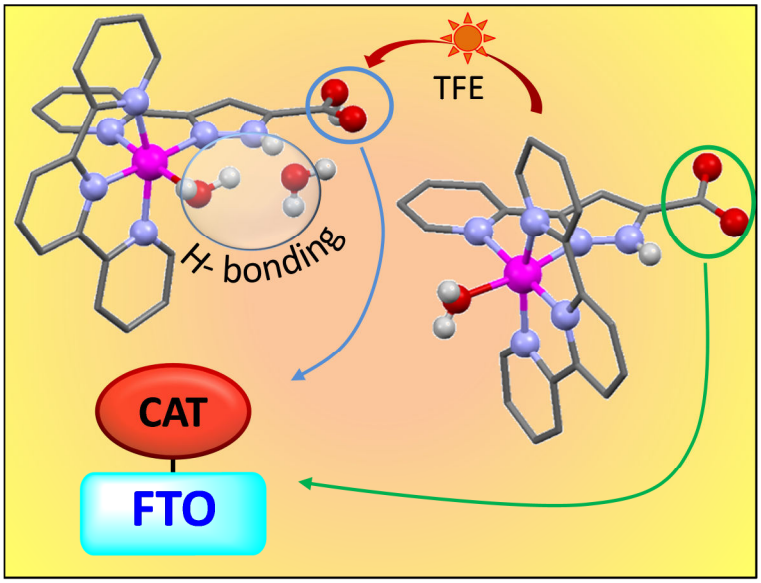

Modified mononuclear ruthenium complexes are synthesized and extensively characterized by spectroscopic and electrochemical methods. Homogeneous water oxidation is tested using Ce(IV) as sacrificial oxidant. The complexes are attached on solid support and characterized by electrochemical methods. Preliminary studies on heterogeneous water oxidation are carried out.

UNIVERSITAT ROVIRA I VIRGILI
MONONUCLEAR AND HETEROTRINUCLEAR RUTHENIUM COMPLEXES: SYNTHESIS AND WATER OXIDATION ACTIVITY.
Lorenzo Mognon
Dipòsit Legal: T 1359-2015

Chapter 6. Supported Single Site Isomeric Ru WOCs: Synthesis, Electrochemical Characterization, Reactivity and Anchoring.

UNIVERSITAT ROVIRA I VIRGILI
MONONUCLEAR AND HETEROTRINUCLEAR RUTHENIUM COMPLEXES: SYNTHESIS AND WATER OXIDATION ACTIVITY.
Lorenzo Mognon
Dipòsit Legal: T 1359-2015

Chapter 6. Supported Single Site Isomeric Ru WOCs: Synthesis, Electrochemical Characterization, Reactivity and Anchoring

Lorenzo Mognon,[a] Laia Francàs,[a] Jordi Benet-Buchholz,[a] and Antoni Llobet[a,b]

[a] Institute of Chemical Research of Catalonia (ICIQ), Avinguda Països Catalans 16, 43007 Tarragona, Spain

[b] Departament de Química, Universitat Autònoma de Barcelona, Cerdanyola del Vallès, 08193 Barcelona, Spain

6.1 Abstract

New mononuclear ruthenium complexes *out/in*-[Ru(H_2pcp)(trpy)(H_2O)]$^{2+}$ (**4a**$^{2+}$ and **4b**$^{2+}$, respectively, H_2pcp is 1*H*-Pyrazole-3-Carboxylic Acid, 5-(2-pyridinil)-,) are obtained by modification of previously described compounds. The new complexes are fully characterized by X-Ray diffraction, spectroscopic and electrochemical techniques. A hydrogen bond network is identified in the X-Ray structure of **4b**$^{2+}$, and its presence supports the rationalization of the electrochemical and acid/base properties. Both complexes are tested for homogeneous water oxidation, yielding values slightly higher than the starting compounds (TON of 17.7 for **4a**$^{2+}$ and 6.9 for **4b**$^{2+}$, and TOF_i of 88.9 × 10^{-3} s^{-1}

and 34.8 × 10^{-3} s^{-1}, respectively). A synthetic strategy to attach the complexes on conductive supports is developed. The films obtained are characterized by electrochemistry in organic solvent and preliminary tests on water oxidation catalysis are carried out.

6.2 Introduction

VI

Sunlight driven water splitting is a highly active research field, due to its importance in the much needed transition from fossil to solar fuels.[1] A photoelectrochemical cell is a device capable of capturing sunlight and use it to produce the water splitting reaction. For such a device to operate efficiently, a number of reactions need to occur simultaneously and in a synchronized manner.[2] In this perspective, water oxidation catalysis represents the main bottleneck. Ruthenium molecular catalysts in homogeneous phase have shown to be good candidates in virtue of relatively easy fine tuning of electrochemical properties, through careful tailored synthesis of the ligands.[3] Moreover, ligand modification can be employed to generate molecules suitable to anchor on oxide surfaces, avoiding deactivation pathways and favoring electronic communication with the electrode.[3a, 4]

Herein we report a modification to complexes **3a**$^{2+}$and **3b**$^{2+}$ presented in the previous chapter. The new complexes **4a**$^{2+}$ and **4b**$^{2+}$ are thoroughly characterized in solution and tested for water oxidation. A strategy for their anchor on Fluorine doped Tin Oxide (FTO) support is reported, together with preliminary tests on heterogeneous water oxidation.

6.3 Experimental Section

Preparations. Complexes *out/in*-[Ru(Cl)(HL)(trpy)](PF_6), **2a**(PF_6) and **2b**(PF_6) respectively, were prepared as previously reported in Chapter 5. FTO Pilkinton glass 2.5 mm of thickness, with a sheet resistance of 8 Ω and visible transmittance of 82-84.5 % was purchased from XOPGlass.

***out*-[Ru(H_2pcp)(trpy)(H_2O)](PF_6)$_2$, 4a(PF_6)$_2$.** In a 100 mL round-bottom flask, **2a**(PF_6) (100 mg, 0.136 mmol) is dissolved in 50 mL of ethanol and the mixture brought to reflux. A solution of 10 mL of $Ba(OH)_2$ 0.12 M is slowly added over 30 minutes and then the reaction refluxed for 4 hours. The organic fraction is then removed under vacuum and the resulting purple mixture is diluted with acetone and acidified with diluted H_2SO_4. Water is added to help the precipitation of $BaSO_4$, which is filtered over paper. Some drops of a saturated NH_4PF_6 aqueous solution are added and the solvent removed under vacuum until precipitation occurs. The reaction is left in fridge overnight and the solid filtered, washed with cold water and diethyl ether, and dried under vacuum. Yield: 25 mg (22.1%) Anal. Calcd for $C_{24}H_{20}F_{12}N_6O_3P_2Ru{\cdot}H_2O$: C, 33.96; H, 2.61; N, 9.89. Found: C, 33.96; H, 2.53; N, 9.84. ^{1}H NMR (500 MHz, pD = 1.0 deuterated trifluoromethansulfonic acid): δ = 9.40 (d, $^3J_{1\text{-}2}$ = 5.72 Hz, H1), 8.53 (d, $^3J_{16\text{-}17}$ = $^3J_{18\text{-}17}$ = 8.10 Hz, H16, H18), 8.42 (d, $^3J_{10\text{-}11}$ = $^3J_{24\text{-}23}$ = 7.98 Hz, H10, H24), 8.34 (d, $^3J_{4\text{-}3}$ = 7.95 Hz, H4), 8.27 (dd, $^3J_{3\text{-}4}$ = 7.95 Hz, $^3J_{3\text{-}2}$ = 7.67 Hz, H3), 8.18 (t, $^3J_{17\text{-}16}$ = $^3J_{17\text{-}18}$ = 8.10 Hz, H17), 7.96 (dd, $^3J_{11\text{-}10}$ = $^3J_{23\text{-}24}$ = 7.98 Hz, $^3J_{11\text{-}12}$ = $^3J_{23\text{-}22}$ = 7.73 Hz, H11, H23), 7.89 (dd, $^3J_{2\text{-}3}$ = 7.67 Hz, $^3J_{2\text{-}1}$ = 5.72 Hz, H2), 7.78 (d, $^3J_{13\text{-}12}$ = $^3J_{21\text{-}22}$ = 5.58 Hz, H13, H12), 7.55 (s, H7), 7.32 (dd, $^3J_{11\text{-}12}$ = $^3J_{11\text{-}10}$ = 7.73, $^3J_{12\text{-}13}$ = $^3J_{22\text{-}21}$ = 5.58 Hz, H12, H22). MALDI+ (Acetone): *m/z* = 523.1 ([Ru(L)(trpy)]$^+$). Cyclic Voltammetry (TFE, TBAH): $E_{1/2}$ = 0.75 V (ΔE_p = 78 mV); (pH = 1 CF_3SO_3H): $E_{1/2}$ = 0.97 V (ΔE_p = 50 mV).

in-[Ru(H_2pcp)(trpy)(H_2O)](PF_6)$_2$, 4b(PF_6)$_2$. In a 100 mL round-bottom flask, **2b**(PF_6) (100 mg, 0.136 mmol) is dissolved in 50 mL of ethanol and the mixture brought to reflux. A solution of 5 mL of NaOH 1 M is slowly added over 30 minutes and then the reaction refluxed for 4 hours. The organic fraction is then removed under vacuum and the resulting purple mixture is acidified with diluted HPF_6, adding acetone to help the dissolution. Once neutralized, a brown solid is precipitated by evaporating the organic solvent. The reaction is kept in fridge overnight and the solid filtered, washed with cold water and diethyl ether, and dried under vacuum. Yield: 44 mg (38.9%). Anal. Calcd for $C_{24}H_{20}F_{12}N_6O_3P_2Ru\cdot0.5(H_2O)\cdot0.5(EtOH)$: C, 34.77; H, 2.80; N, 9.73. Found: C, 34.59; H, 2.73; N,9.55.^{1}H NMR (500 MHz, pD = 1.0 deuterated trifluoromethansulfonic acid): δ = 8.57 (d, $^3J_{16\text{-}17}$ = $^3J_{18\text{-}17}$ = 8.19 Hz, H16, H18), 8.43 (d, $^3J_{13\text{-}12}$ = $^3J_{21\text{-}22}$ = 8.00 Hz, H13, H21), 8.23 (t, $^3J_{17\text{-}16}$ = $^3J_{17\text{-}18}$ = 8.19 Hz, H17), 8.02 (d, $^3J_{4\text{-}3}$ = 7.76 Hz, H4), 7.99 (s, H7), 7.97 (dd, $^3J_{12\text{-}13}$ = $^3J_{22\text{-}21}$ = 8.00 Hz, $^3J_{12\text{-}11}$ = $^3J_{22\text{-}23}$ = 7.66 Hz, H12, H23), 7.91 (d, $^3J_{10\text{-}11}$ = $^3J_{24\text{-}23}$ = 5.61 Hz, H10, H24), 7.62 (dd, $^3J_{3\text{-}4}$ = 7.76 Hz, $^3J_{3\text{-}2}$ = 7.61 Hz, H3), 7.38 (dd, $^3J_{11\text{-}12}$ = $^3J_{23\text{-}22}$ = 7.66 Hz, $^3J_{11\text{-}10}$ = $^3J_{23\text{-}24}$ = 5.61 Hz, H11, H22), 7.21 (d, $^3J_{1\text{-}2}$ = 5.83 Hz, H1), 6.84 (dd, $^3J_{2\text{-}3}$ = 7.61 Hz, $^3J_{2\text{-}1}$ = 5.83 Hz, H2). MALDI+ (Acetone): *m/z* = 523.2 ([Ru(L)(trpy)]$^+$). Cyclic Voltammetry (TFE, TBAH): $E_{1/2}$ = 0.94 V (ΔE_p = 163 mV); (pH = 1 CF_3SO_3H): $E_{1/2}$ = 1.02 V (ΔE_p = 85 mV).

Preparation of films 4a-FTO and 4b-FTO. The anchoring process on FTO films was carried out by soaking the film overnight in a 0.2 mM solution of the complex in trifluoroethanol (TFE). The films were cleaned in a neat TFE solution prior to measurement.

Instruments and measurements. Electrochemical experiments were performed in a one-compartment three electrode cell, using glassy carbon (ø = 3 mm) or an FTO film working electrode, a platinum disc as counter electrode (ø = 2 mm) and SSCE or $Hg/HgSO_4$ as reference electrodes in organic or aqueous solvents, respectively. All the potentials reported are referred to NHE. UV–vis spectroscopy was performed on a Cary 50 (Varian) UV–vis spectrometer using 1 cm quartz cells.

Online manometric measurements were carried out on a Testo 521 differential pressure manometer with an operating range of 0.1–10 kPa and accuracy within 0.5% of the measurements. The manometer was coupled to thermostatic reaction vessels for dynamic monitoring of the headspace pressure above each reaction solution. The manometer secondary port was connected to a thermostated reaction vessel containing the same solvent and headspace volume as the sample vial. Each measurement for a reaction solution (2.0 mL) was performed at 298 K.

X-ray Crystal Structure Determination. Crystals of **4a**$^{2+}$ and **4b**$^{2+}$ were obtained by slow cooling of saturated aqueous solutions of the complexes. The measured crystals were prepared under inert conditions immersed in perfluoropolyether as protecting oil for manipulation.

Data Collection: Crystal structure determination **4a**$^{2+}$ was carried out using a Bruker Smart 6000 diffractometer equipped with an CCD Smart 6000 area detector, a fix Chi stage, a Microfocus Source E025 IuS using CuK_α radiation, Quazar MX multilayer Optics as monochromator and an Oxford Cryosystems low temperature device Cryostream 700 plus (T = -173 °C).Crystal structure determinations for **4b**$^{2+}$ were carried out using a Apex DUO diffractometer equipped with a Kappa 4-axis goniometer, an APEX II 4K CCD area detector, a Microfocus Source E025 IuS using MoK_α radiation, Quazar MX multilayer Optics

as monochromator and an Oxford Cryosystems low temperature device Cryostream 700 plus (T = -173 °C).

Full-sphere data collection was used with ω and φ scans. *Programs used:* Data collection APEX-2,[5] data reduction Bruker Saint[6] V/.60A and absorption correction SADABS.[7,8]

Structure Solution and Refinement: Crystal structure solution was achieved using direct methods as implemented in SHELXTL[9] and visualized using the program XP. Missing atoms were subsequently located from difference Fourier synthesis and added to the atom list. Least-squares refinement on F^2 using all measured intensities was carried out using the program SHELXTL. All non hydrogen atoms were refined including anisotropic displacement parameters.

Comments to Structures: **4a**$^{2+}$: The asymmetric unit contains two independent molecules of the ruthenium metal complex coordinated to a water molecule, two PF_6 anions, four non-coordinated water molecules and one methanol molecule. One of the PF_6 anions is disordered in two orientations. The non-coordinated water molecules are disordered in six positions (ratio: 1:1:1:0.5:0.25:0.25). **4b**$^{2+}$: The asymmetric unit contains two independent molecules of the Ruthenium metal complex coordinated to a water molecule, 3.32 molecules of ClO_4 anions, 0.68 molecules of PF_6 anions and 7.5 non coordinated water molecules. The metal complex molecules are disordered in two shifted positions (molecule A: ratio 90:10; molecule B: ratio 95:05). Two of the ClO_4 anions are disordered sharing its positions with PF_6 anions (ratios: 69:31 and 63:37). In the case of the carboxylic acid groups present in the main molecule, it was confirmed by comparing the C-O distances, that they are protonated.

6.4 Results and Discussion

Synthesis and solid state structure. Two different synthetic strategies have been developed to synthetize the aqua-acid compounds **4a**$^{2+}$ and **4b**$^{2+}$ starting from the chlorido-ester compounds **2a**$^{+}$ and **2b**$^{+}$. They are shown in Scheme 1.

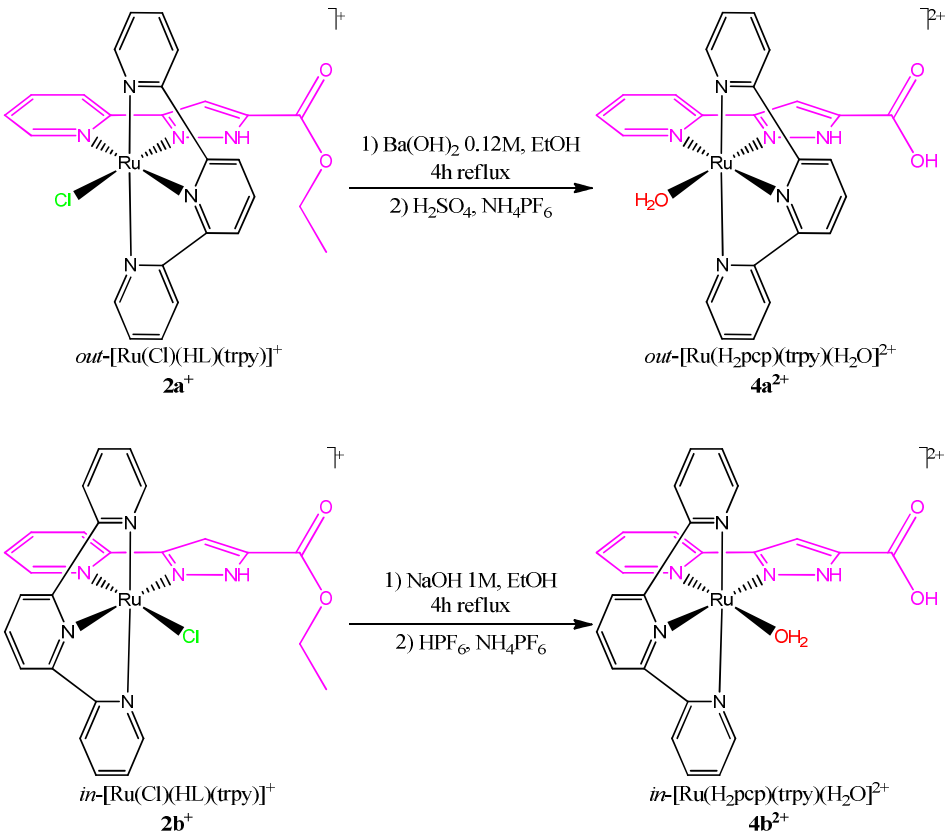

Scheme 1. Synthetic pathways for compounds **4a**$^{2+}$ and **4b**$^{2+}$.

Due to the high solubility of **4a**$^{2+}$ in water, a new synthetic route to remove undesired ions in solution previously to the precipitation of the complex has been developed. Successive 4 h reflux in presence of $Ba(OH)_2$ for ester

hydrolysis of **2a**$^{+}$ and addition of H_2SO_4 for acidification of the complex yields highly insoluble $BaSO_4$, which can be easily removed through filtration. Precipitation of the final product is then obtained with excess of PF_6^-, to isolate **4a**$^{2+}$ with a relatively low 22% yield, once again due to the high solubility of the complex.

Compound **4b**$^{2+}$ is synthesized following a standard procedure for ester hydrolysis,[4b] consisting in a 4h reflux of **2b**$^{+}$ in presence of NaOH and subsequent acidification of the solution with HPF_6 to give **4b**$^{2+}$ in 39% yield.

It is interesting to note how, while the main objective of the reactions in base is the hydrolysis of the ester moiety, the highly alkaline conditions favor the substitution of the chlorido ligands for the more catalytically useful aqua moiety. This kind of substitution reactions are generally carried out by Ag(I), which presents two major drawbacks: (a) in presence of a free site in a multinucleating ligand, Ag^+ can coordinate, thus lowering the yield of the synthesis,[10] and (b) Ag(I) is an oxidant, and can generate traces of Ru(III) in the final mixture, lowering the yield and the purity of the isolated compound, and hampering its NMR characterization.

Monocrystals of the two complexes were obtained from saturated aqueous solutions and their crystal structures solved by means of X-Ray diffraction analysis. Their ORTEP view is presented in Figure 1 and all crystallographic data can be found in the Supporting Information (Tables S1 and S2). Both present a symmetry plane containing the H_2pcp ligand and bisecting the terpyridine. The coordination environment of the ruthenium atom is that of a distorted octahedron, very similar to previously reported d^6 Ru(II).[11]

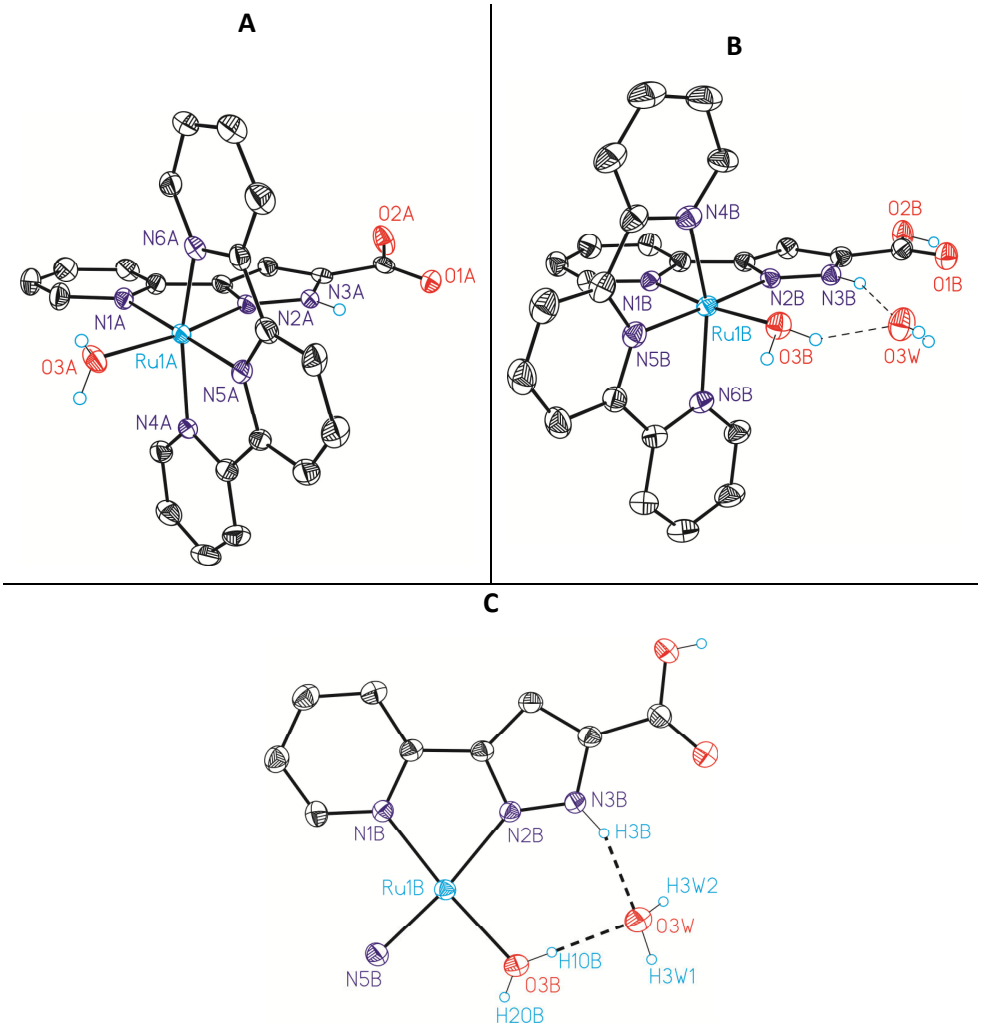

Figure 1. ORTEP drawing (thermal ellipsoids 50 %) of complexes (a) **4a**$^{2+}$, (b) **4b**$^{2+}$, and (c) focus on the hydrogen bond network in **4b**$^{2+}$. Non relevant hydrogen atoms have been omitted in the sake of clarity.

An interesting feature of the crystal structure of **4b**$^{2+}$ is the presence of a hydrogen bond (Figure 1C) between the non coordinated pyrazole nitrogen and a free water (H(3B)-O(3W) = 1.902(6) Å, N(3B)-O(3W) = 2.730(7) Å, N(3B)-H(3B)-O(3W) = 161.5(4)°) and another one between the aqua ligand and the

same free water molecule (H(1OB)-O(3W) = 1.813(6) Å, O(3B)-O(3W) = 2.725(7) Å, O(3B)-H(1OB)-O(3W) = 153.1(3)°). This fact provokes the elongation of the interested bonds: the one between the pyrazolic nitrogen and its proton (N(3B)-H(3B) = 0.860(5) Å, against 0.81(2) Å for **3b**$^{2+}$, see previous chapter), and the one between the proton and the oxygen of the water molecule coordinated to the Ru metal center (O(3B)-H(1OB) = 0.982(5) Å for the involved hydrogen against O(3B)-H(2OB) = 0.863(6) Å for the not involved one).

Spectroscopic Properies. ^{1}H NMR spectra of the complexes were recorded in pD =1 CF_3SO_3D in D_2O and are presented in Figure 2 and in the Supporting Information (Figures S1 and S2). The signals could be assigned based on integrals, symmetry considerations previously reported and bidimensional COSY experiments. As for **4a**$^{2+}$, an additional feature for the determination of the pyridilic system of the H_2pcp ligand is the deshielding effect of the aqua ligand on H1, which places the proton at 9.40 ppm.[11c, 12]

The optical properties of the complexes were investigated by UV-vis in 0.1 M triflic acid aqueous solutions and are shown in the Supporting Information (Figure S5). As the cromophores of the two species are the same, the spectra are basically identical. The typical π-π* transitions due to the aromatic ligands can be seen below 350 nm, and lower intensity MLCT dπ-π* between 400 and 650 nm.[12-13] Spectrophotometric redox titrations using Ce(IV) as oxidant confirmed the molecular weight and the purity of the compounds, and are displayed in Figure 3 for **4a**$^{2+}$ and in the Supporting Info for **4b**$^{2+}$.

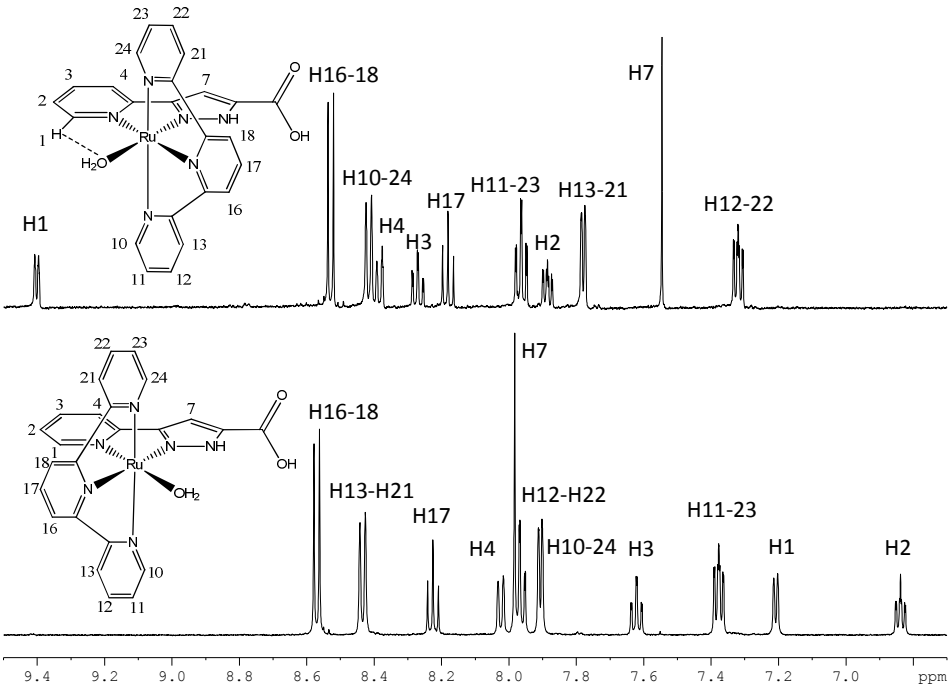

Figure 2. ^{1}H-NMR spectra in CF_3SO_3D 0.1 M in D_2O (500 MHz, 298 K) and assignment for complexes (top) **4a** $^{2+}$ and (bottom) **4b**$^{2+}$.

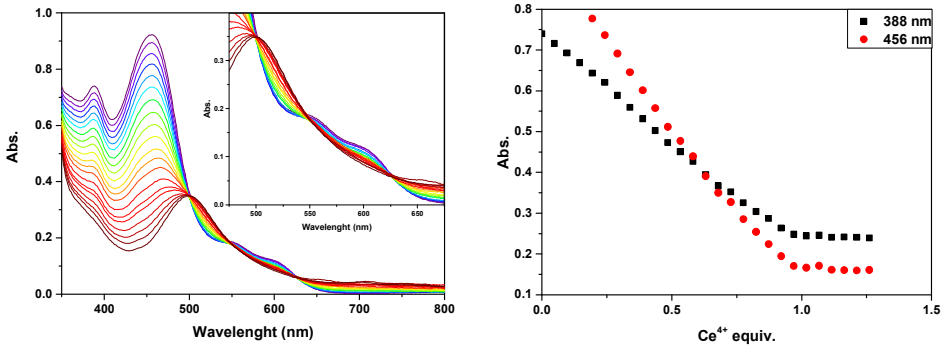

Figure 3. (Left) UV-Vis redox titration for Ru(II)->Ru(III) with $[(NH_4)_2Ce(NO_3)_6]$ in pH=1 CF_3SO_3H for **4a**$^{2+}$, and (right) absorbances at selected wavelengths.

Redox properties in homogeneous phase. The redox properties of complexes **4a**$^{2+}$ and **4b**$^{2+}$ were investigated by means of cyclic voltammetry (CV) and differential pulse voltammetry (DPV) in aqueous solutions, using 0.1 M CF_3SO_3H for measurements at pH = 1.0 and the appropriate phosphate buffer for measurement at other pH, and in solutions 0.1 M of TBAH [(nBu$_4$N)(PF$_6$)] in trifluoroethanol (TFE). All the CVs were run with a scan rate of 50 mV/s, and are shown in Figure 4 and in the SI (Figure S6). The redox potentials reported are referred to the NHE electrode.

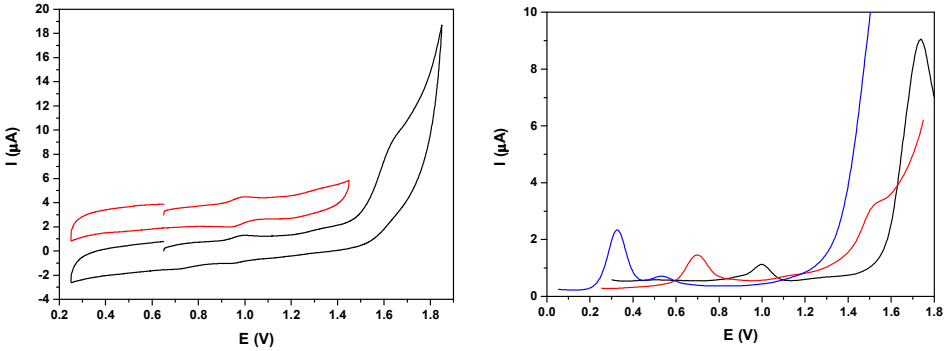

Figure 4. Electrochemical characterization for complex **4a**$^{2+}$. (Left) Cycling voltammetry in pH = 1 CF_3SO_3H , and (right) differential pulse voltammetry at selected pHs (black 2.1, red 7.0, blue 12.0).

At pH = 1 the complex **4a**$^{2+}$presents a chemically and electrochemically reversible wave at 0.97 V (ΔE_p = 50 mV), assigned to the Ru(III)/Ru(II) couple. A second wave can be hinted around 1.35 V in the anodic wave, with a very broad cathodic wave, assigned to the Ru(IV)/Ru(III) redox couple. A large electrocatalytic wave is observed at higher potentials, starting approximatively around 1.5 V. In the returning scan the Ru(III)/Ru(II) wave is less intense (i_a/i_c = 2.41) and a new wave can be seen around 0.7 V. When the scan is reversed at

1.45 V, avoiding higher potentials, the intensity of the Ru(III)/Ru(II) couple is fully recovered (i_a/i_c = 0.99), indicating that a decomposition reaction is taking place simultaneously as the water oxidation reaction.

All the redox waves observed are pH dependent, as reported in the Pourbaix diagram in Figure 5, where the zones of stability of the different species, relative to pH and potential, are reported. Due to the presence of four possible acid-base equilibriums, the evolution of the redox couples over the pH range has been simulated using the following equation, adapted from previous reported cases with fewer equilibriums :[14]

$$E(\mathrm{n'/n}) = \left[E(\mathrm{n'/n})_{\mathrm{pH=0}}\right] + \left(0.05916 * \log\left(\frac{[\mathrm{H^+}]^3 + [\mathrm{H^+}]^2\mathrm{K^n_{a1}} + [\mathrm{H^+}]\mathrm{K^n_{a1}K^n_{a2}} + \mathrm{K^n_{a1}K^n_{a2}K^n_{a3}}}{[\mathrm{H^+}]^3 + [\mathrm{H^+}]^2\mathrm{K^{n'}_{a1}} + [\mathrm{H^+}]\mathrm{K^{n'}_{a1}K^{n'}_{a2}} + \mathrm{K^{n'}_{a1}K^{n'}_{a2}K^{n'}_{a3}}}\right)\right) \quad \textbf{Eq.1}$$

where $E(\mathrm{n'/n})_{\mathrm{pH=0}}$ is the potential for the n'/n redox couple, with n' = n+1, at pH = 0 and K^X_{an} is the n^{th} acid–base constant for the specie in oxidation state X. Equation 1 allowed to estimate the values of the pK_a reported in Table 1, together with relevant thermodynamic and kinetic values of related complexes.

It is interesting to note how the potentials at pH = 1 for **4a**$^{2+}$ are not much different from the potentials observed for the ester homologue **3a**$^{2+}$ in the same conditions, indicating that the electronic effects of the –COOH moiety are quite similar to those of -COOEt. Sweeping to basic pHs the potentials for the Ru(III)/Ru(II) couple drops with a steeper slope than the ester case, ending reaching a plateau 50 mV lower at around pH = 12.

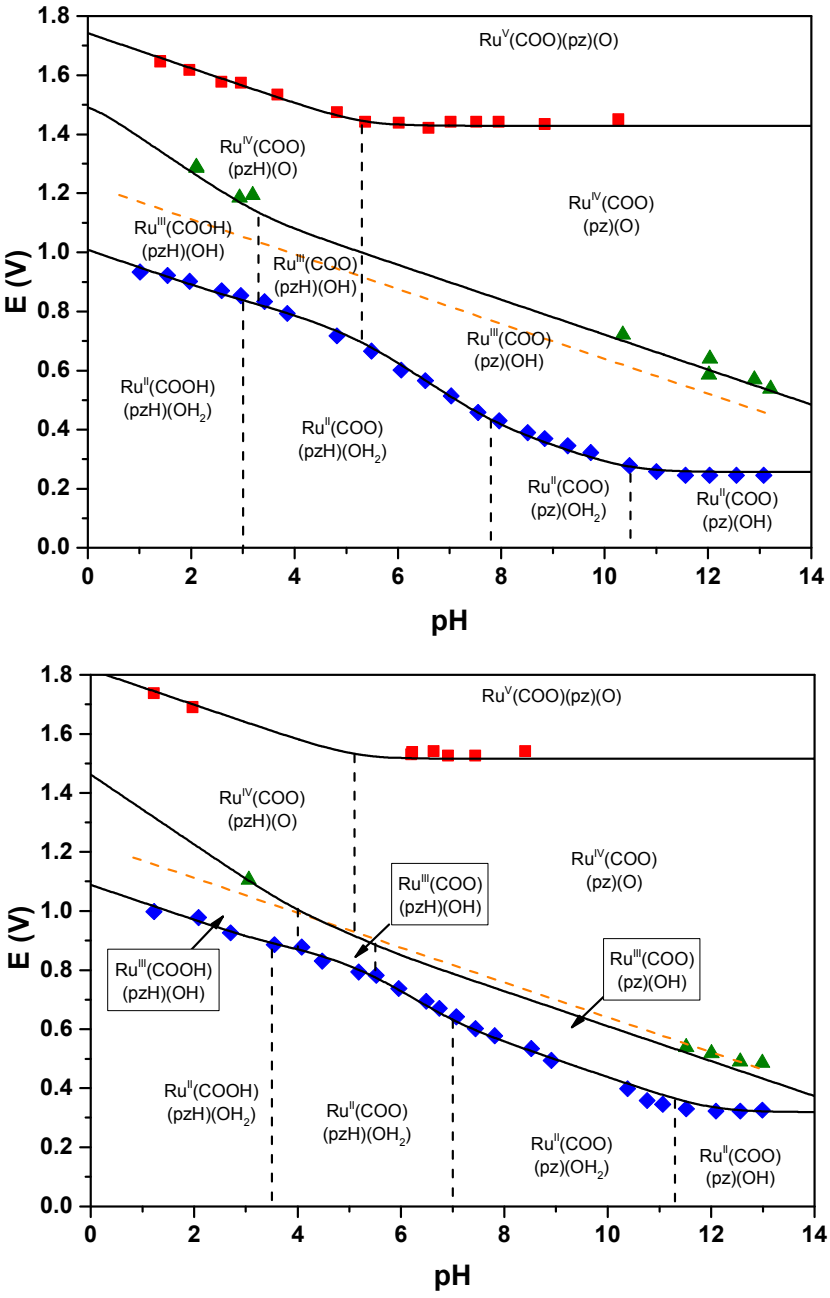

Figure 5. Pourbaix diagrams for complexes (top) **4a**$^{2+}$, and (bottom) **4b**$^{2+}$. The orange line represents the potential for water oxidation.

Table 1. Thermodynamic and catalytic data for **4a**$^{2+}$ and **4b**$^{2+}$ and for related Ru-aqua complexes described in the literature at pH = 7.0.

Entry	Complex[a]	$E_{1/2}$(V) *vs.* NHE				ΔE[c]	$pK_{a,II}$[d]	$pK_{a,III}$[d]	$pK_{a,III}$[e] pyrazole	$TOF_i \cdot 10^3$ (TON)[f]
		IV/III	III/II	IV/II[b]	V/IV					
1[14]	*out*-[Ru(Hbpp)(trpy)(H_2O)]$^{2+}$, ***out*-1**	0.85	0.48	0.67		370	11.1	2.8	6.88/5.43	
2[g]	*out*-**3a**$^{2+}$	0.88	0.52	0.70	1.59	360	10.5	0.8	4.75/3.5/3.2	58.2 (10.8)
3[g]	*in*-**3b**$^{2+}$	0.85	0.61	0.73	1.54	240	10.8	1.0	5.6/4.5/4.0	15.4 (4.2)
4	*out*-**4a**$^{2+}$	0.90	0.51	0.71	1.43	390	10.5	--	7.8/5.3/5.3	88.9 (17.7)
5	*in*-**4b**$^{2+}$	0.79	0.63	0.71	1.52	160	11.3	--	7.0/5.5/5.1	34.8 (6.9)
6[11a]	[Ru(bpy)(trpy)(H_2O)]$^{2+}$	0.83	0.72	0.78	1.86	110	9.8	1.7		15.1 (18.3)
7[15]	[R (4,4'-$(MeO)_2$-bpy)(trpy)(H_2O)]$^{2+}$	0.82	0.64	0.76		240	11.2	3.2		
8[15]	[Ru(4,4'-$(HOOC)_2$-bpy)(trpy)(H_2O)]$^{2+}$	0.89	0.75	0.82		140	10.4	1.2		
9[11a]	[Ru(6,6'-F_2-bpy)(trpy)(H_2O)]$^{2+}$	--	--	0.80[h]	1.93	--	10.4	--		1.7 (7.8)

[a]Ligand abbreviations: 4,4'-$(MeO)_2$-bpy is 4,4'-dimethoxy-2,2'-bipyridine; 4,4'-$(HOOC)_2$-bpy is 4,4'-dicarboxy-2,2'-bipyridine. [b]Calculated as [$E_{1/2}$ (IV/III)+$E_{1/2}$ (III,II)]/2. [c]$\Delta E = E_{1/2}$ (IV/III)-$E_{1/2}$ (III,II) in mV. [d]$pK_{a,II}$ and $pK_{a,III}$ represent the pK_a of the corresponding Ru^{II}-OH_2 and Ru^{III}-OH_2 species, respectively. [e]pKa for the pyrazole proton, at the different oxidation states II/III/IV. [f]TOF_i stands for initial Turn Over Frequencies in cycles per second and TON for Turn Over Numbers. This values are extracted for the catalytic reactions involving 1.0 mM Cat/100 mM Ce(IV) in a 0.1 M triflic acid solution with a total volume of 2 mL. [g]See previous Chapter. [h]Two electron process.

On the other hand, the bigger difference is presented by the Ru(V)/Ru(IV) couple, which already at neutral pH is 150 mV lower. The reason for the drop in potential resides in the double negative charge present on the ligand due to the double proton loss, which increases the electron density on the metal center, stabilizing the Ru(V) oxidation state. The electrochemical properties of **4b**$^{2+}$ are quite similar to those of the *out* isomer, and are presented in Figure 5 and in the Supporting Information. As for the ester case, the different *trans* effects generated from the change in the relative coordination of the ligand, influence the differences between the IV/III and III/II couples ΔE, which are 390 mV for **4a**$^{2+}$ and 160 mV for **4b**$^{2+}$ at pH = 7. Another interesting fact raised from the comparison of the Pourbaix diagram for **4a**$^{2+}$ and **4b**$^{2+}$ and the data in Table 1 is the shifting of the pK_a values of the Ru(II) oxidation state. The pK_a of the acid moiety and the aqua group are both higher in the *in* **4b**$^{2+}$ than in the *out* **4a**$^{2+}$, in similar manner as previously reported (See Chapter 5).[14] However for the pK_a corresponding to the deprotonation of the pyrazole moiety the tendency is reversed, being almost one unit higher for **4a**$^{2+}$ than for **4b**$^{2+}$. This observation is in agreement with the presence of the same hydrogen bonding found in the solid state in solution. The pK_a of the aqua ligand, which also participates in the hydrogen bond network, is not affected by it because the network breaks once the most acid proton, the pyrazolic one, is lost.

To check the stability of the complexes in anchoring conditions, their electrochemical properties were analyzed also in trifluoroetanol (TFE), and the results are showed in Figure 6 and in the Supporting Information. In the scanned potential range they both present a single wave corresponding to the Ru(III)/Ru(II) couple, **4a**$^{2+}$ at 0.75 V (ΔE_p = 78 mV), and **4b**$^{2+}$ at 0.90 V (ΔE_p = 113 mV). The absence of further waves at higher potentials could indicate a

substitution of the aqua ligand, necessary to reach Ru(IV)=O, with a CF_3CH_2OH from the solution (Eq.2). Furthermore, when exposed to ambient light for 15 hours, **4a**$^{2+}$ shows the appearance of a second wave at higher potentials, around 0.9 V, which grows bigger with time. Treating in the same way **4b**$^{2+}$ leaves the signal mostly unaffected. We interpret this behavior as an isomerization from **4a**$^{2+}$ to **4b**$^{2+}$, favored by a hydrogen bond system similar to that seen in the crystal structure of **4b**$^{2+}$ and corroborated by the shift of the pK_a value of the pyrazolic proton.

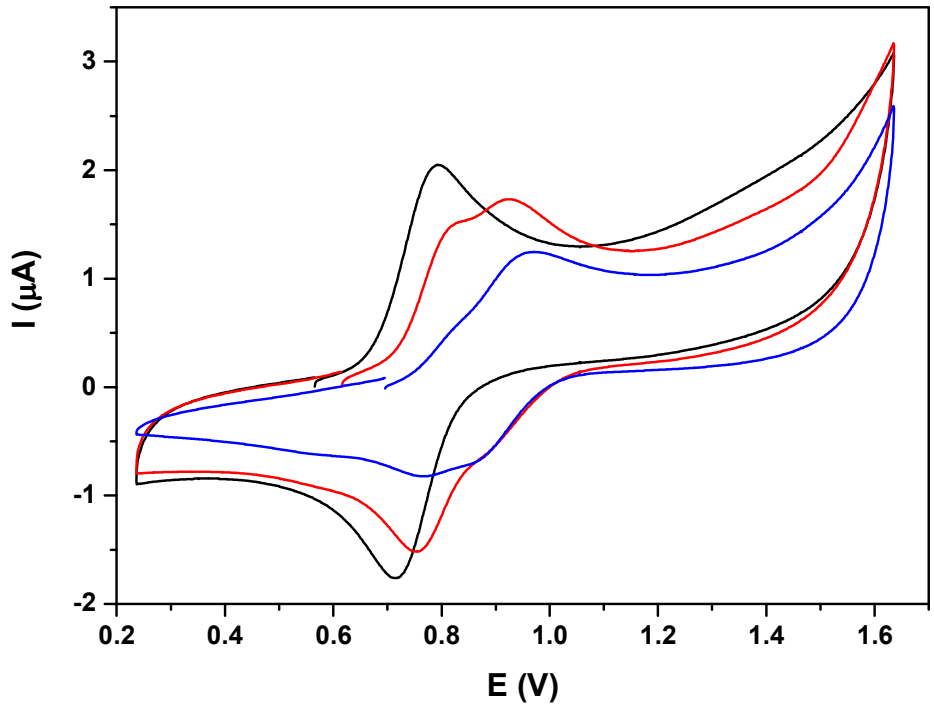

Figure 6. Cyclic voltammograms for complex **4a**$^{2+}$, in trifluoroethanol before irradiation (black), after 15h irradiation (red) and after 63 h irradiation (blue).

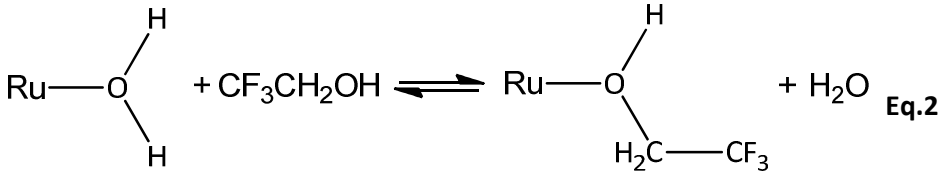

Eq.2

Reactivity. The complexes were tested for chemical water oxidation at pH = 1 with $[(NH_4)_2Ce(NO_3)_6]$ (CAN). Manometric measurements showed activity for both complexes and the reactions finish in less than 20 minutes (Figure 7). On-line mass experiments were performed in the same conditions to investigate the nature of the gas evolved. As reported in Figure S8, both complexes generate CO_2, probably due to ligand oxidation, because of the high potential needed for the catalysis as was observed in the electrochemical characterization. The manometric values corrected for the on-line mass data are TON = 17.7 and $TOF_i = 88.9 \times 10^{-3}$ s^{-1} for **4a**$^{2+}$ and TON = 6.9 and $TOF_i = 34.8 \times 10^{-3}$ s^{-1} for **4b**$^{2+}$.Comparing to the case of the esters, the ratio O_2/CO_2 is even more favorable to the oxygen, 11.1 for **4a**$^{2+}$ and 6.2 for **4b**$^{2+}$. This could be due to the acid moiety being less electro withdrawing than the ester. This yields a less electronegative and less activated (and thus less prone to be oxidized) carbon atom, slowing down the deactivation pathway, which is known to start as a bimolecular pathway in the most activated position,[16] and favoring the oxygen formation.

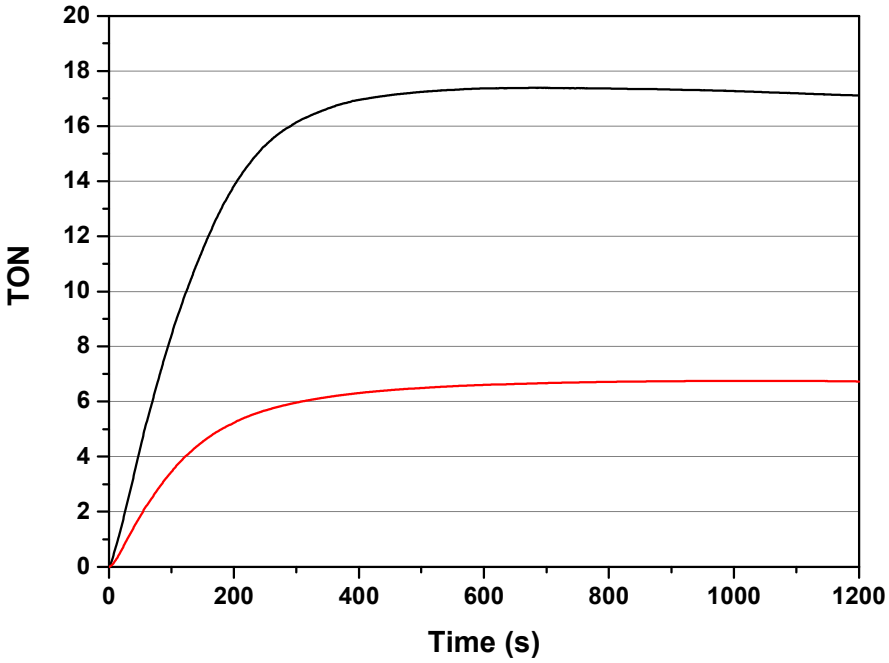

Figure 7. Manometric measurement for complexes (black) **4a**$^{2+}$, and (red) **4b**$^{2+}$, corrected for the values obtained from the on-line mass experiments. Conditions are: cat 1mM/CAN 100mM/pH = 1 triflic acid total volume 2 mL.

Attachment of the catalysts and reactivity tests. The presence of a free carboxylic acid allows the attachment of the catalyst to a metal oxide surface via the presence of the superficial residual hydroxyls. The latter react with the acid moiety forming a covalent bond (Eq.3). Following this strategy the complexes were attached onto Fluorine doped Tin Oxide (FTO) films by soaking the latter in 0.2 mM solutions of the catalysts in TFE for 15 hours, away from light to avoid isomerization. The films thus obtained were then cleaned in neat TFE and electrochemically characterized in solutions 0.1 M of TBAH [(nBu$_4$N)(PF$_6$)] in TFE.

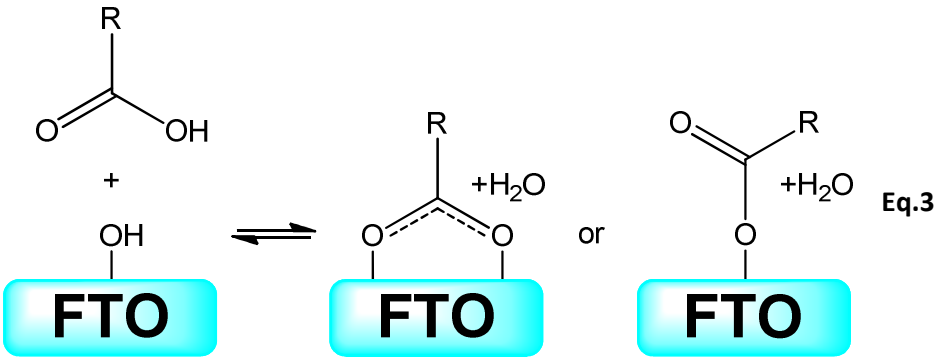

Eq.3

VI

A graphical representation of the possible disposition of the complexes on the FTO films is presented in Scheme 2, and the CVs of the supported catalysts are shown in Figure 8 and in the supporting info. **4a-FTO** shows a wave at 0.88 V, 130 mV higher than in homogeneous conditions, while **4b-FTO** shows a wave at 0.99 V, at the same potential as the homogeneous. As in the case of the homogeneous characterization, the absence of waves at higher potentials is interpreted as a substitution of the labile H_2O ligand with CF_3CH_2OH.

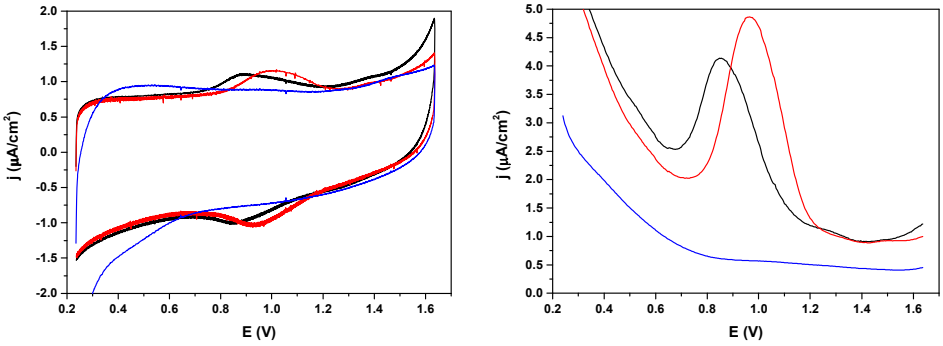

Figure 8. (Left) Cyclic voltammetry and (right) DPV of **4a-FTO** (black), **4b-FTO** (red) and bare FTO (blue).

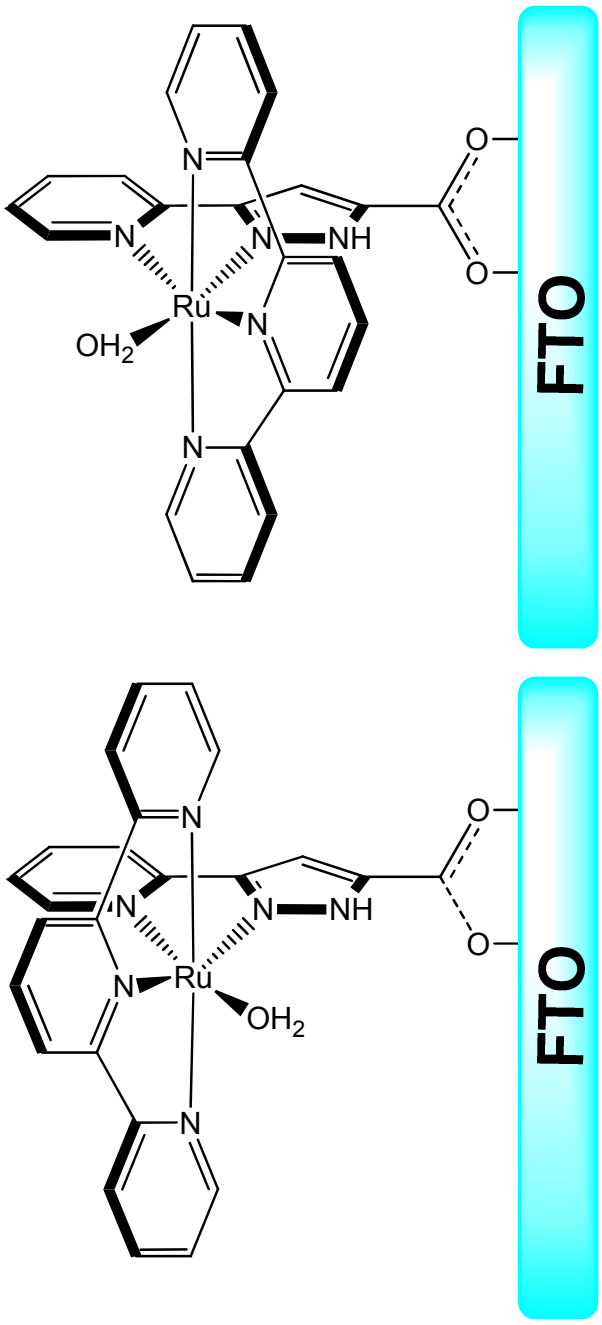

Scheme 2. Possible structures of films (top) **4a-FTO** and (bottom) **4a-FTO**.

Assuming that the observed waves correspond to the monoelectronic redox couples Ru(III)/Ru(II), their integrals, which correlates to the charge passed, can be used to calculate the surface coverage Γ, according to:

$$\Gamma = \frac{Q}{FA} \qquad \textbf{Eq.4}$$

where Q is the charge passed in Coulomb, F is the Faraday constant(F = $9.6485 \cdot 10^4$ C mol^{-1}) and A is the area of the surface analyzed (in our case 1.5 cm^2). The values obtained, 2.77 pmol cm^{-2} for **4a-FTO** and 4.52 pmol cm^{-2} for **4b-FTO**, are orders of magnitude lower than literature for similar systems.[17] A possible reason for this behavior could be the intrinsic reactivity of the carboxylic acid attached to a pyrazol moiety. This group is electron rich and, in the equilibrium illustrated in Eq.3, it disfavors the formation to the bond, being the carboxylate form more favored. This behavior can be observed also in the Pourbaix diagram, where the pK_a for the carboxylic acid is below pH = 4, while common values for a carboxylic acid are 4.76 for the acetic acid and 4.2 for the benzoic acid. This is also in agreement with the fact that the lowest pK_a value corresponds to compound **4a**$^{2+}$, which is also the one giving the lowest surface coverage.

The reactivity of the films toward water oxidation was tested by adding increasing aliquots of water to the electrolytic solutions, and measuring the intensity of the electrocatalytic current. The results are shown in Figure 9 and in the Supporting Information (Figure S10). Both films show activity towards water oxidation, and as expected, **4a-FTO** is more active. This difference in activity is in agreement with the difference seen in homogeneous catalysis and with the electrochemistry in homogeneous aqueous media.

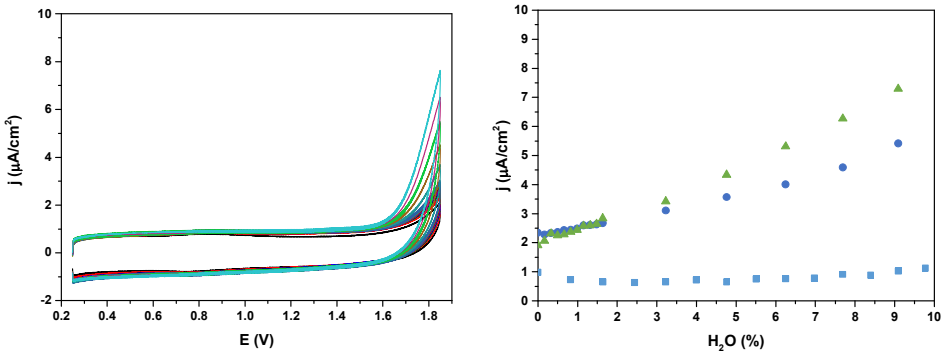

Figure 9. Successive additions of H_2O to the TFE electrolytic solution: (left) **4a-FTO**, and (right) current densities at 1.85 V. Green triangles: **4a-FTO**, blue circles: **4b-FTO**, light blue squares: bare FTO.

The analysis of the DPV before and after the addition of water (Figure S11) shows how in presence of water the CF_3CH_2OH ligand is substituted by an aqua moiety: the waves shift to slightly lower potentials, and a new weak wave appears at higher potentials, possibly attributable to the Ru(IV)/Ru(III) couple.

On the other hand, for both isomers the CVs show decreasing intensity of the Ru(III)/Ru(II) wave, indicating detachment of the complexes from the surface, as consequence of the equilibrium in Eq. 3.

It's remarkable how, despite the low surface coverage and the detachment equilibrium, both supported complexes still present activity toward oxidation, encouraging a deeper study of the system.

6.5 Conclusions

In this chapter two complexes, **4a**$^{2+}$ and **4b**$^{2+}$, have been synthesized, characterized and tested for water oxidation in homogenous phase, a protocol

for their support on FTO has been appointed, and the films thus obtained have been characterized and tested for water oxidation. It has been showed how the presence of multiple acid base equilibria in the ligand can dramatically change the redox properties of the complex, with differences in potential of up to 160 mV at pH = 7. A hydrogen bond network has been identified in the crystal structure of **4b**$^{2+}$, and its effects on the pK_a of the species have been rationalized. Both complexes showed water oxidation activity, with TON of 17.7 for **4a**$^{2+}$ and 6.9 for **4b**$^{2+}$, and TOF_i of 88.9 × 10^{-3} s^{-1} and 34.8 × 10^{-3} s^{-1}, respectively. Mass analyses of the evolved gas indicated that the system is slightly more rugged than the esterified counterpart. Both complexes have been successfully anchored on FTO, and their electrocatalytic performances tested, showing an as expected higher activity for complex **4a**$^{2+}$, although notable leaching has been observed.

VI

Finally, highlighting the versatility of carefully tailored ruthenium complexes, complex **4b**$^{2+}$ shows the right characteristics not only to perform homogenous and heterogeneous water oxidation, as hereby presented, but can also function as a scaffold for an asymmetric homonuclear WOC, or for an heterodinuclear WOC.

I performed the synthesis, the characterization, and the electrochemical experiments and reactivity experiments of all the complexes presented. The experiments on the heterogeneous part and rationalization of the whole system were carried out in collaboration with Dr. Laia Francàs. X-Ray structure analyses were carried out by Dr. J. Benet-Bucholz.

6.6 References

(1) Berardi, S.; Drouet, S.; Francas, L.; Gimbert-Surinach, C.; Guttentag, M.; Richmond, C.; Stoll, T.; Llobet, A. *Chem. Soc. Rev.* **2014,** *43*, 7501-7519.

(2) a) Youngblood, W. J.; Lee, S.-H. A.; Kobayashi, Y.; Hernandez-Pagan, E. A.; Hoertz, P. G.; Moore, T. A.; Moore, A. L.; Gust, D.; Mallouk, T. E. *J. Am. Chem. Soc.* **2009,** *131*, 926-927; b) Luo, J.; Im, J.-H.; Mayer, M. T.; Schreier, M.; Nazeeruddin, M. K.; Park, N.-G.; Tilley, S. D.; Fan, H. J.; Grätzel, M. *Science* **2014,** *345*, 1593-1596.

(3) a) Neudeck, S.; Maji, S.; López, I.; Meyer, S.; Meyer, F.; Llobet, A. *J. Am. Chem. Soc.* **2013,** *136*, 24-27; b) Richmond, C. J.; Matheu, R.; Poater, A.; Falivene, L.; Benet-Buchholz, J.; Sala, X.; Cavallo, L.; Llobet, A. *Chem. Eur. J.* **2014,** *20*, 17282-17286.

(4) a) Liu, F.; Cardolaccia, T.; Hornstein, B. J.; Schoonover, J. R.; Meyer, T. J. *J. Am. Chem. Soc.* **2007,** *129*, 2446-2447; b) Francàs, L.; Sala, X.; Benet-Buchholz, J.; Escriche, L.; Llobet, A. *ChemSusChem* **2009,** *2*, 321-329.

(5) Data collection: APEX II, versions v2009.1-02 and v2013.4-1; Bruker AXS Inc.: Madison, WI, 2007.

(6) Data collection: APEX II, versions v2009.1-02 and v2013.4-1; Bruker AXS Inc.: Madison, WI, 2007.

(7) Data collection: APEX II, versions v2009.1-02 and v2013.4-1; Bruker AXS Inc.: Madison, WI, 2007.

(8) Blessing, R. *Acta Crystallogr. Sect. A* **1995,** *51*, 33-38.

(9) Sheldrick, G. *Acta Crystallogr. Sect. A* **2008,** *64*, 112-122.

(10) Mognon, L.; Benet-Buchholz, J.; Rahaman, S. M. W.; Bo, C.; Llobet, A. *Inorg. Chem.* **2014,** *53*, 12407-12415.

(11) a) Maji, S.; López, I.; Bozoglian, F.; Benet-Buchholz, J.; Llobet, A. *Inorg. Chem.* **2013,** *52*, 3591-3593; b) Planas, N.; Christian, G.; Roeser, S.; Mas-Marzá,

E.; Kollipara, M.-R.; Benet-Buchholz, J.; Maseras, F.; Llobet, A. *Inorg. Chem.* **2012,** *51*, 1889-1901; c) Roeser, S.; Farràs, P.; Bozoglian, F.; Martínez-Belmonte, M.; Benet-Buchholz, J.; Llobet, A. *ChemSusChem* **2011,** *4*, 197-207; d) Farràs, P.; Maji, S.; Benet-Buchholz, J.; Llobet, A. *Chem. Eur. J.* **2013,** *19*, 7162-7172; e) Romero, I.; Rodriguez, M.; Llobet, A.; Collomb-Dunand-Sauthier, M.-N.; Deronzier, A.; Parella, T.; Stoeckli-Evans, H. *J. Chem. Soc., Dalton Trans.* **2000**, 1689-1694.

(12) Mognon, L.; Benet-Buchholz, J.; Rahaman, S. M. W.; Bo, C.; Llobet, A. *Inorg. Chem.* **2014**.

(13) a) Haga, M.; Dodsworth, E. S.; Lever, A. B. P. *Inorg. Chem.* **1986,** *25*, 447-453; b) Wong, C.-Y.; Che, C.-M.; Chan, M. C. W.; Leung, K.-H.; Phillips, D. L.; Zhu, N. *J. Am. Chem. Soc.* **2004,** *126*, 2501-2514; c) Kannan, S.; Ramesh, R.; Liu, Y. *J. Organomet. Chem.* **2007,** *692*, 3380-3391.

(14) Sens, C.; Rodríguez, M.; Romero, I.; Llobet, A.; Parella, T.; Benet-Buchholz, J. *Inorg. Chem.* **2003,** *42*, 8385-8394.

(15) Wasylenko, D. J.; Ganesamoorthy, C.; Henderson, M. A.; Koivisto, B. D.; Osthoff, H. D.; Berlinguette, C. P. *J. Am. Chem. Soc.* **2010,** *132*, 16094-16106.

(16) Francàs, L.; Sala, X.; Escudero-Adán, E.; Benet-Buchholz, J.; Escriche, L.; Llobet, A. *Inorg. Chem.* **2011,** *50*, 2771-2781.

(17) Chen, Z.; Concepcion, J. J.; Jurss, J. W.; Meyer, T. J. *J. Am. Chem. Soc.* **2009,** *131*, 15580-15581.

Supporting Information for

Supported Single Site Isomeric Ru WOCs: Synthesis, Electrochemical Characterization, Reactivity and Anchoring

Lorenzo Mognon,[a] Laia Francàs,[a] Jordi Benet-Buchholz,[a] and Antoni Llobet[a,b]

[a] Institute of Chemical Research of Catalonia (ICIQ), Avinguda Països Catalans 16, 43007 Tarragona, Spain

[b] Departament de Química, Universitat Autònoma de Barcelona, Cerdanyola del Vallès, 08193 Barcelona, Spain

Table 1. Crystal data and structure refinement for **4a**$^{2+}$.

Empirical formula	C24.50 H25 F6 N6 O5.50 P Ru
Formula weight	737.54
Temperature	100(2) K
Wavelength	1.54178 Å
Crystal system	Monoclinic
Space group	P2(1)/c
Unit cell dimensions	a = 16.1528(7)Å α= 90°.
	b = 16.7817(7)Å β = 90.6893(17)°.
	c = 21.4156(10)Å γ = 90°.
Volume	5804.7(4) Å^3
Z	8
Density (calculated)	1.688 Mg/m^3
Absorption coefficient	5.691 mm^{-1}
F(000)	2968
Crystal size	0.40 x 0.20 x 0.05 mm3
Theta range for data collection	2.736 to 66.616°.
Index ranges	-16<=h<=18,-19<=k<=19,-24<=l<=24
Reflections collected	22011
Independent reflections	8643[R(int) = 0.0418]
Completeness to theta =66.616°	84.2%
Absorption correction	Empirical
Max. and min. transmission	0.764 and 0.484
Refinement method	Full-matrix least-squares on F^2
Data / restraints / parameters	8643/ 266/ 879
Goodness-of-fit on F^2	1.067
Final R indices [I>2sigma(I)]	R1 = 0.0688, wR2 = 0.1918
R indices (all data)	R1 = 0.0739, wR2 = 0.2012
Largest diff. peak and hole	2.815 and -1.046 e.Å^{-3}

Table 2. Crystal data and structure refinement for **4b**$^{2+}$.

Empirical formula	C24H27.50Cl1.66F2.07N6O13.37P0.34Ru
Formula weight	823.68
Temperature	100(2) K
Wavelength	0.71073 Å
Crystal system	Triclinic
Space group	P-1
Unit cell dimensions	a = 10.2023(4)Å α = 71.7848(18)°.
	b = 17.3572(7)Å β = 81.901(2)°.
	c = 19.5242(8)Å γ = 87.855(2)°.
Volume	3251.3(2) Å^3
Z	4
Density (calculated)	1.683 Mg/m^3
Absorption coefficient	0.720 mm^{-1}
F(000)	1666
Crystal size	0.04 x 0.02 x 0.01 mm^3
Theta range for data collection	1.235 to 32.115°.
Index ranges	-14<=h<=15,-25<=k<=25,-28<=l<=28
Reflections collected	32844
Independent reflections	20563[R(int) = 0.0303]
Completeness to theta =32.115°	90.200005%
Absorption correction	Empirical
Max. and min. transmission	0.993 and 0.849
Refinement method	Full-matrix least-squares on F^2
Data / restraints / parameters	20563/ 2488/ 1574
Goodness-of-fit on F^2	1.100
Final R indices [I>2sigma(I)]	R1 = 0.0776, wR2 = 0.2148
R indices (all data)	R1 = 0.1154, wR2 = 0.2606
Largest diff. peak and hole	3.797 and -1.239 e.Å^{-3}

Figure S1. NMR spectra (500 MHz, 298 K, CF_3SO_3D 0.1 M in D_2O) for complex *out*-$[Ru(H_2pcp)(trpy)(H_2O)]^{2+}$, **4a**$^{2+}$: (a) ^1H NMR, (b) COSY.

(a)

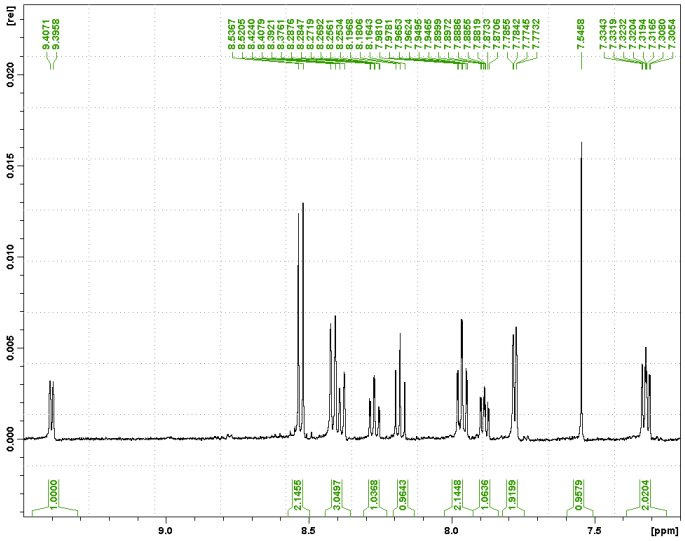

(b)

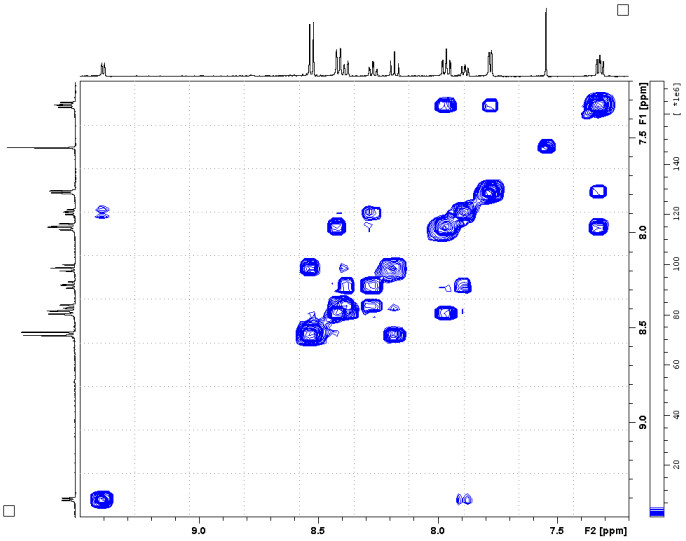

Figure S2. NMR spectra (500 MHz, 298 K, CF_3SO_3D 0.1 M in D_2O) for complex *in*-[Ru(H_2pcp)(trpy)(H_2O)]$^{2+}$, **4b**$^{2+}$: (a) ^{1}H NMR, (b) COSY.

(a)

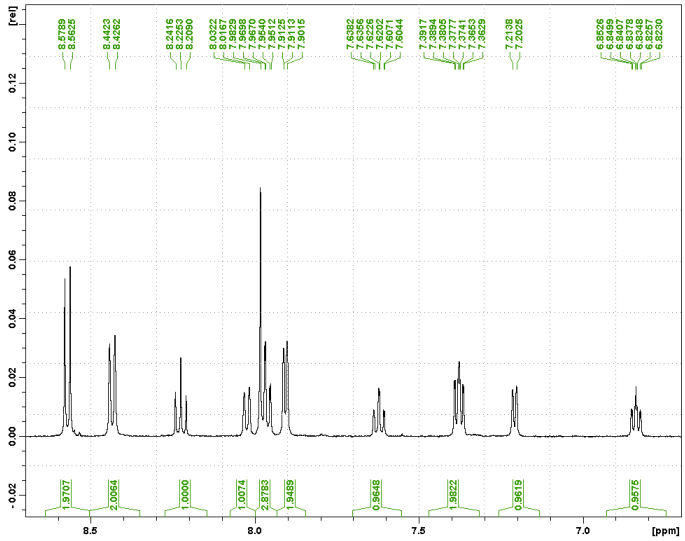

(b)

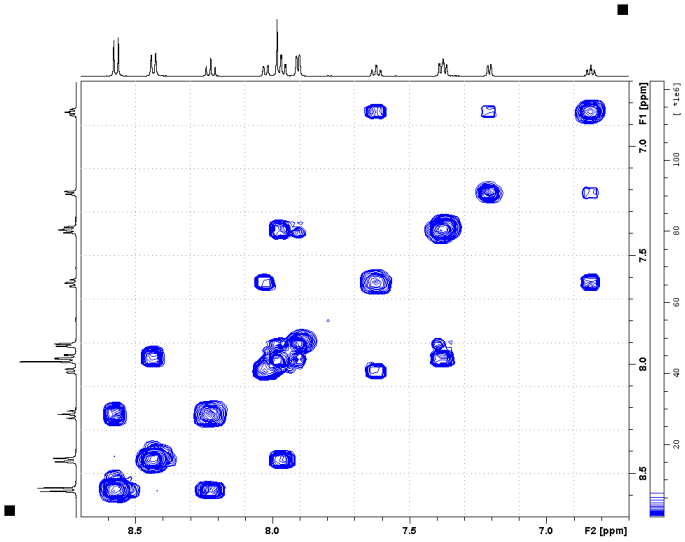

Figure S3. MALDI+ of complex *out*-[Ru(H_2pcp)(trpy)(H_2O)] $^{2+}$, **4a^{2+}**, in acetone (black) and simulated isotopic distribution of the cation {Ru(OH)(H_2pcp)(trpy)}$^{+}$ (blue).

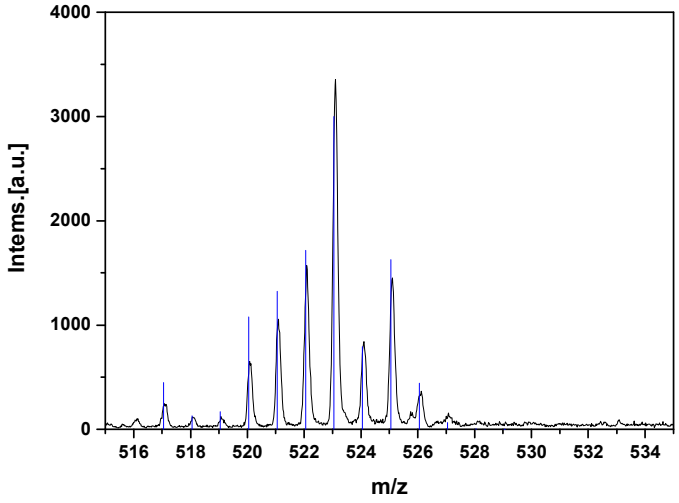

Figure S4. MALDI+ of complex *in*-[Ru(H_2pcp)(trpy)(H_2O)] $^{2+}$, **4b^{2+}**, in acetone (black) and simulated isotopic distribution of the cation {Ru(OH)(H_2pcp)(trpy)}$^{+}$ (blue).

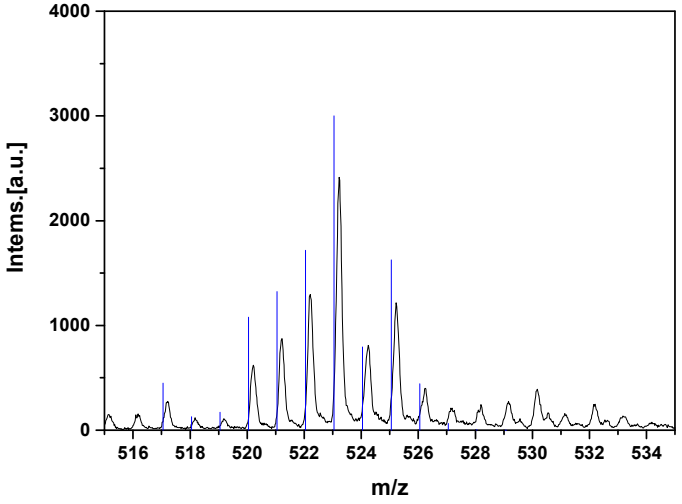

Figure S5. (a) UV-Vis spectra for complex *out*-$[Ru(H_2pcp)(trpy)(H_2O)]^{2+}$, **4a**$^{2+}$ (black), and *in*-$[Ru(H_2pcp)(trpy)(H_2O)]^{2+}$, **4b**$^{2+}$ (red)**,** in pH = 1 CF_3SO_3H, (b) redox titration for Ru(II)->Ru(III) with $[(NH_4)_2Ce(NO_3)_6]$ in pH = 1 CF_3SO_3H, (c) absorbances at selected wavelengths, (d) spectra for the Ru(II) (black) and Ru(III) (red) species of (left) **4a**$^{2+}$ and (right) **4b**$^{2+}$.

(a)

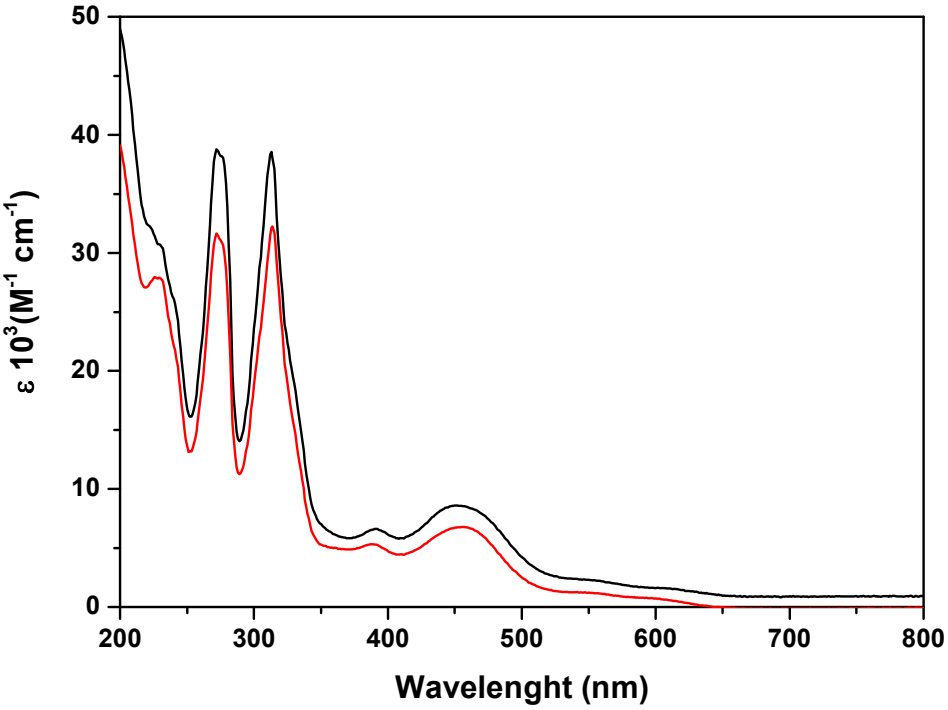

VI

(b)

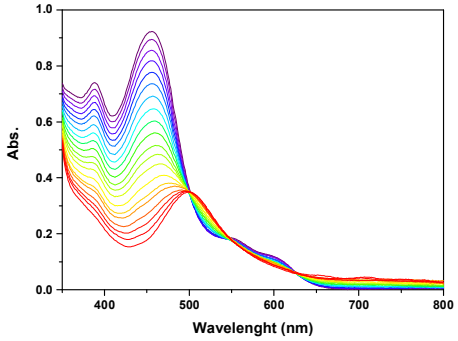
Abs.
Wavelenght (nm)

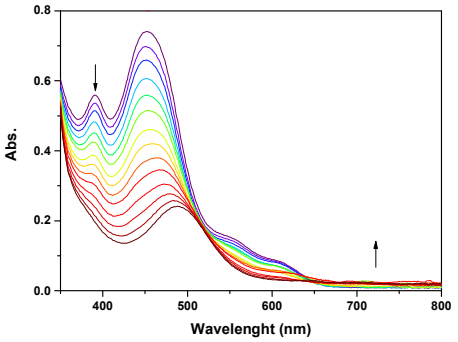
Abs.
Wavelenght (nm)

(c)

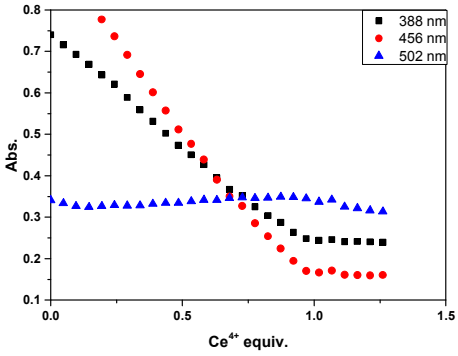
388 nm
456 nm
502 nm
Abs.
Ce4+ equiv.

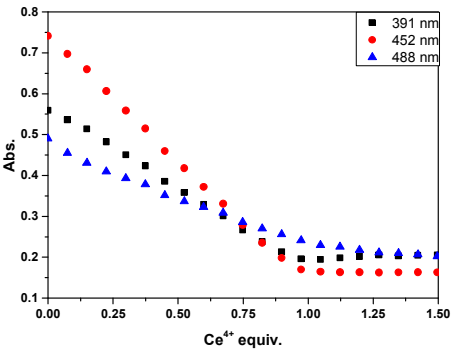
391 nm
452 nm
488 nm
Abs.
Ce4+ equiv.

(d)

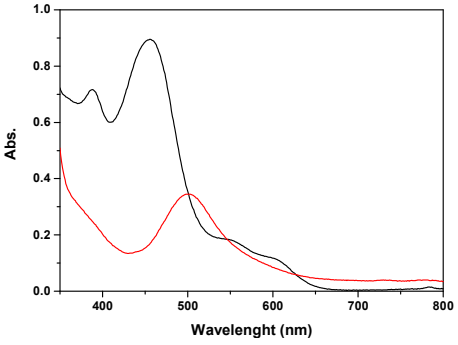
Abs.
Wavelenght (nm)

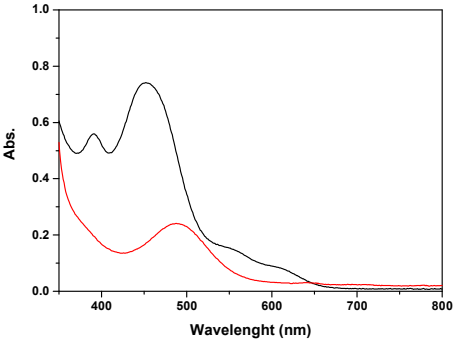
Abs.
Wavelenght (nm)

Figure S6. Cyclic voltammograms for complex *in*-[Ru(H_2pcp)(trpy)(H_2O)]$^{2+}$, **4b^{2+}**, in (a) pH = 1 CF_3SO_3H , and in (b) trifluoroethanol before irradiation (black), and after 15h irradiation (red).

(a)

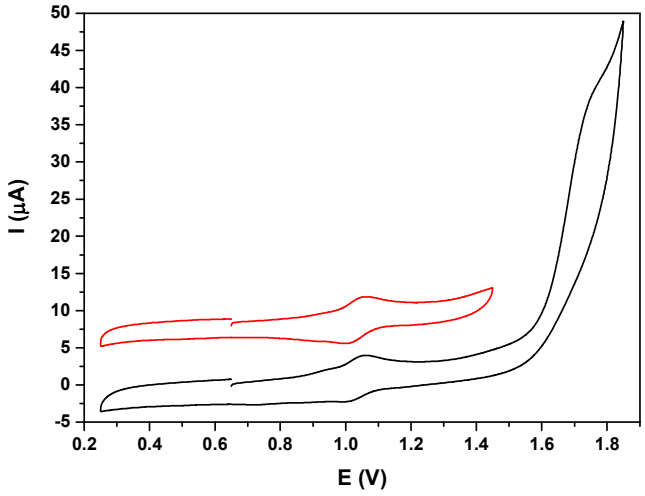

(b)

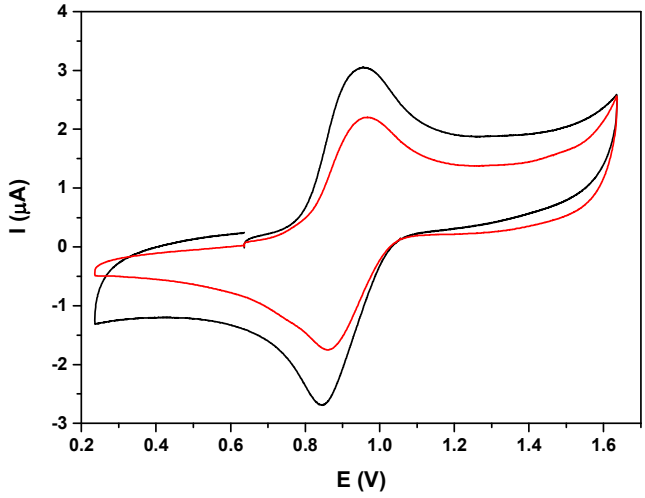

Figure S7. DPV at selected pHs (black 1.2, red 6.6, blue 12.0) for complex *in*-$[Ru(H_2pcp)(trpy)(H_2O)]^{2+}$, $\mathbf{4b}^{2+}$.

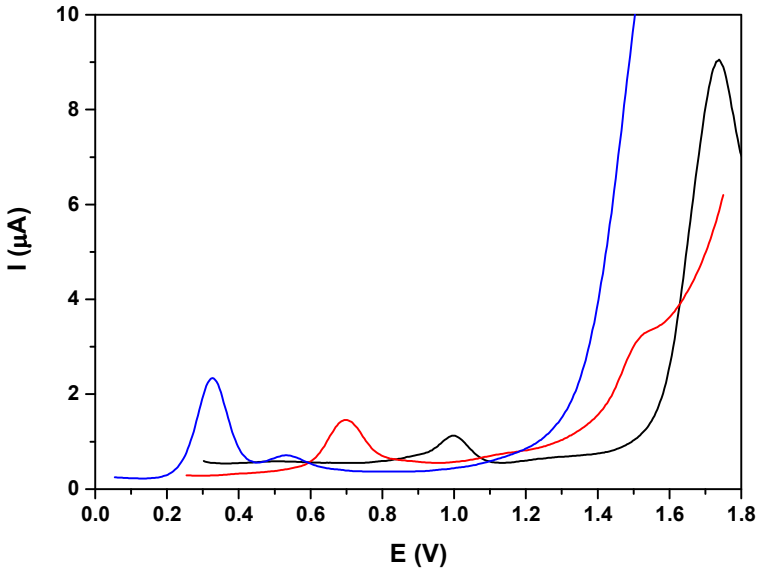

Figure S8. On-line mass measurement for complexes (a) *out*-[Ru(H_2pcp)(trpy)(H_2O)]$^{2+}$, **4a**$^{2+}$, and (b) *in*-[Ru(H_2pcp)(trpy)(H_2O)]$^{2+}$, **4b**$^{2+}$**,** (black: oxygen, red carbon dioxide). (c) Evolution of the ratios between O_2 and CO_2 (black **4a**$^{2+}$, red **4b**$^{2+}$). Conditions are: cat 1mM/CAN 100mM/pH = 1 triflic acid total volume 2mL.

(a)

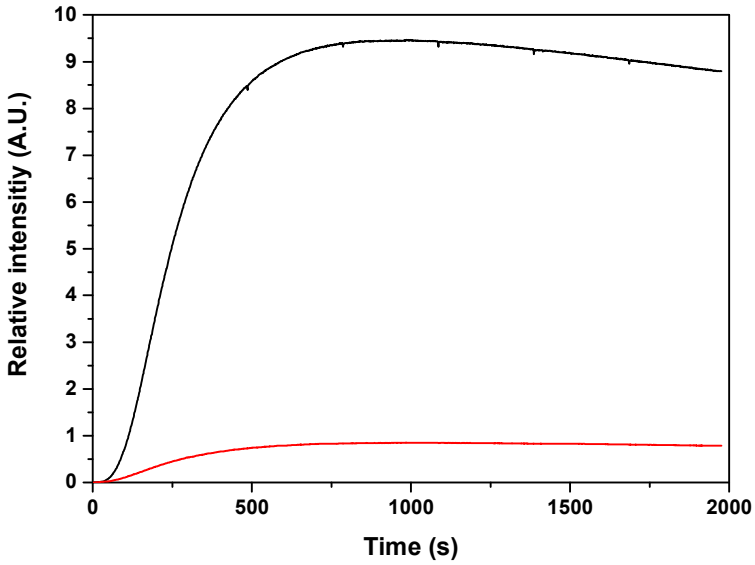

(b)

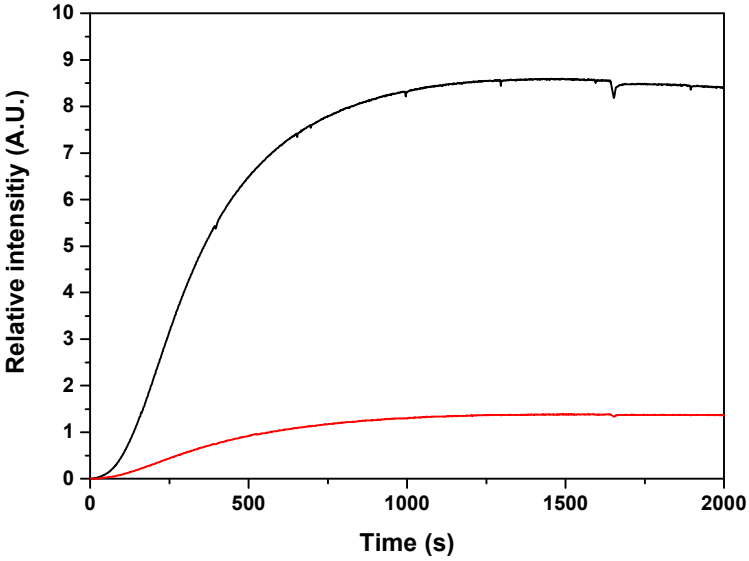

(c)

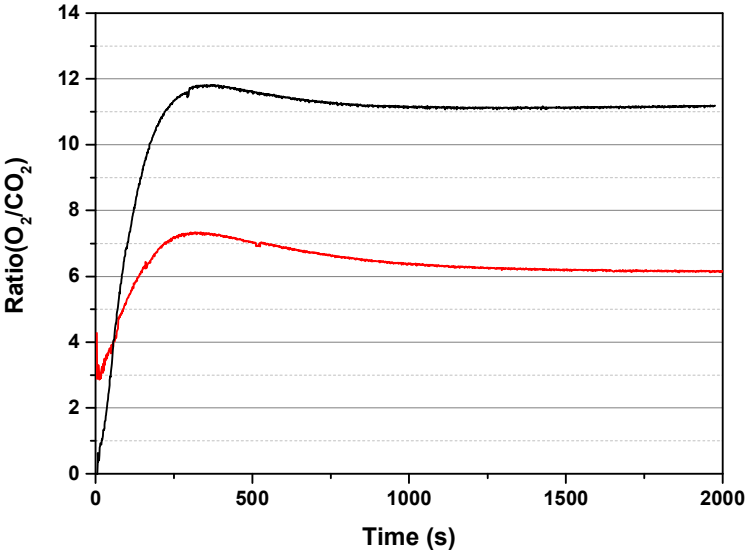

Figure S9. Comparison of homogenous (red) and heterogenous (black) CV for (a) **4a**$^{2+}$ and (b) **4b**$^{2+}$.

(a)

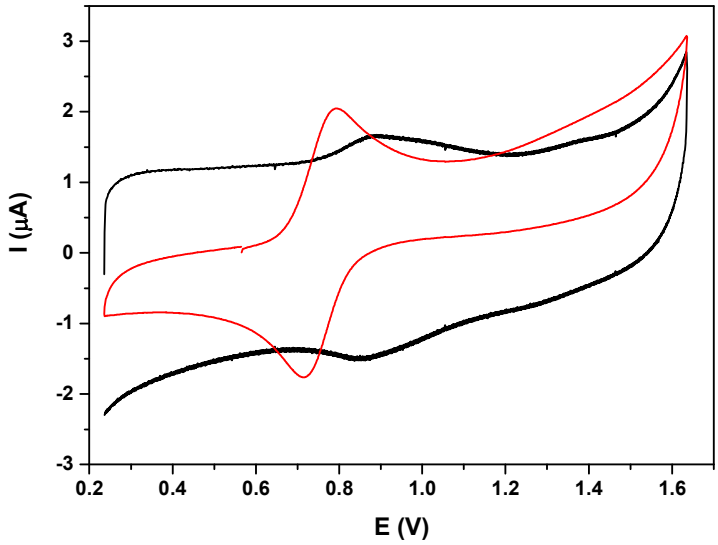

(b)

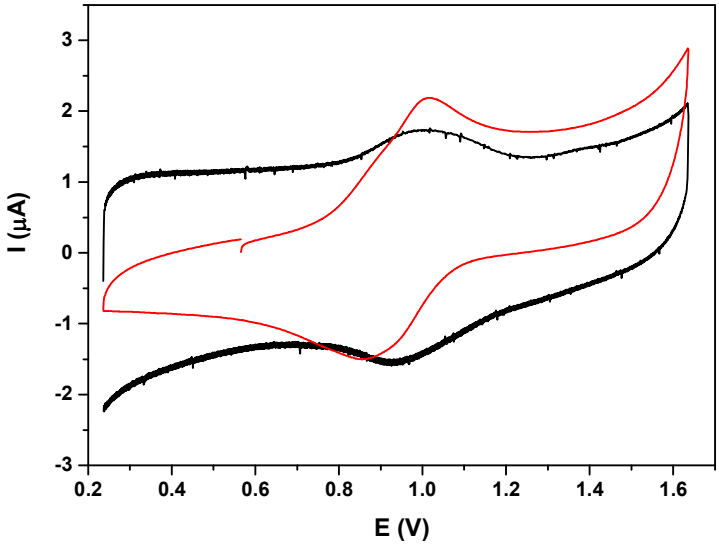

Figure S10. Successive additions of H_2O to the TFE electrolythic solution: (top left) **4a-FTO**, (top right) **4b-FTO**, (bottom left) bare FTO, (bottom right) current densities at 1.85 V. Green triangles: **4a-FTO**, blue circles: **4b-FTO**, light blue squares: bare FTO.

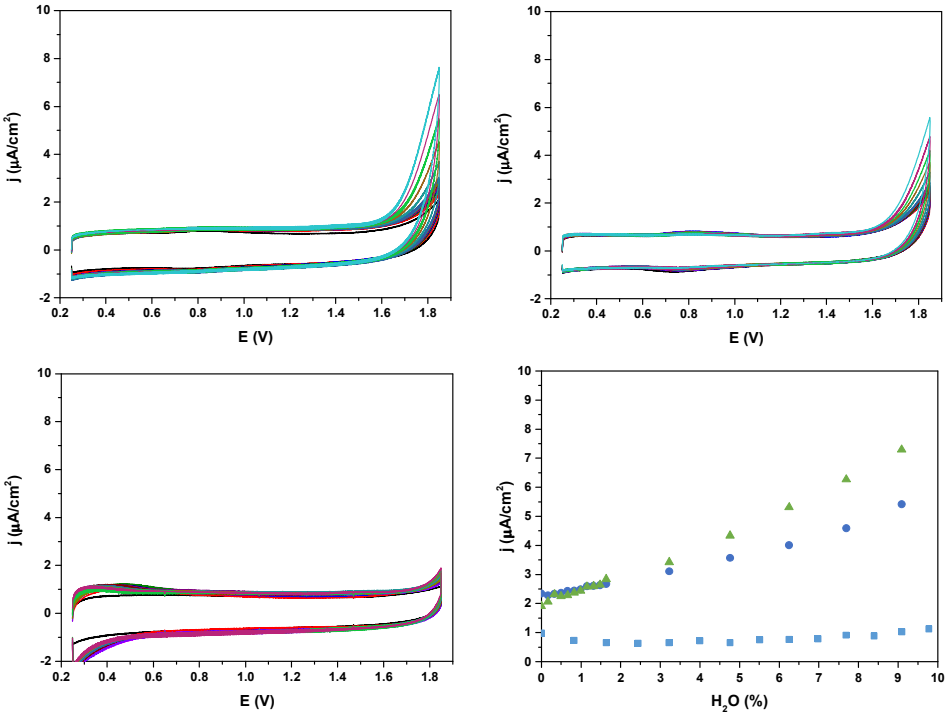

Figure S11. Normalized DPV of (a) **4a@FTO** and (b) **4b@FTO**, in TFE (black) and 2% H_2O in TFE (red).

(a)

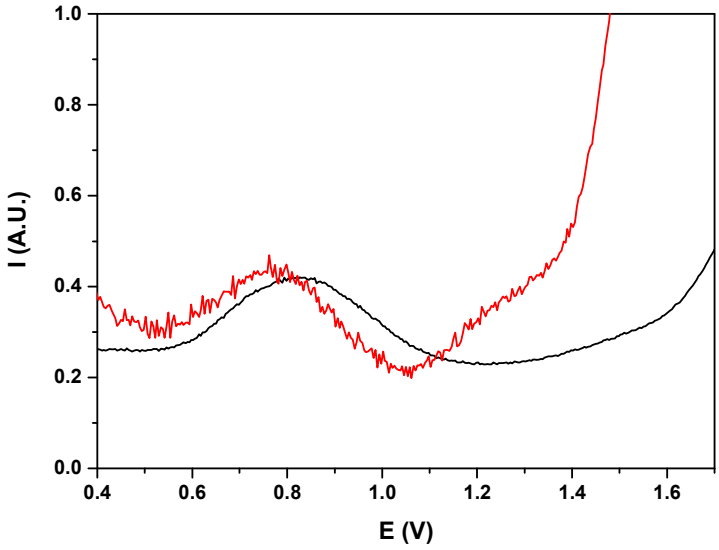

(b)

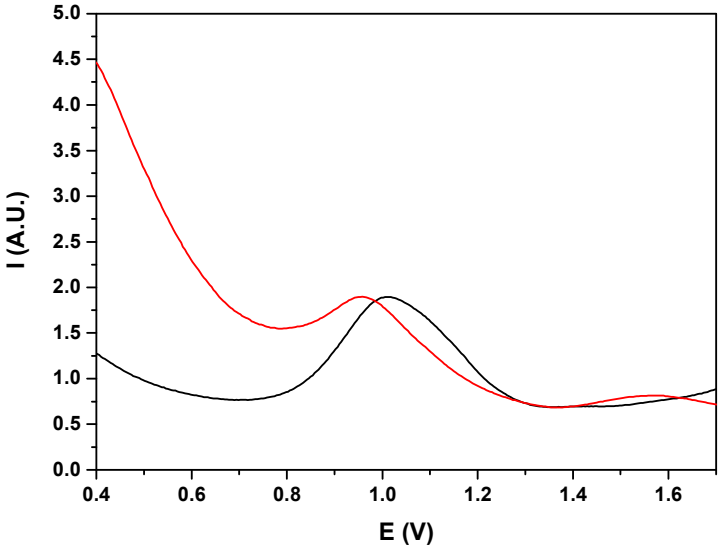

UNIVERSITAT ROVIRA I VIRGILI
MONONUCLEAR AND HETEROTRINUCLEAR RUTHENIUM COMPLEXES: SYNTHESIS AND WATER OXIDATION ACTIVITY.
Lorenzo Mognon
Dipòsit Legal: T 1359-2015

Chapter 7. Summary and Conclusions

UNIVERSITAT ROVIRA I VIRGILI
MONONUCLEAR AND HETEROTRINUCLEAR RUTHENIUM COMPLEXES: SYNTHESIS AND WATER OXIDATION ACTIVITY.
Lorenzo Mognon
Dipòsit Legal: T 1359-2015

Chapter 7. Summary and Conclusions

Chapter 3

- ✓ Five new complexes: *out*-{[RuCl(trpy)][$ZnCl_2$](μ-bpp)}, ***out*-2**; *out, out*-{[RuCl(trpy)]$_2$(μ-[Zn(bpp)$_2$])}$^{2+}$, ***out*-3**; *out, out*-{[Ru(trpy)(H_2O)]$_2$(μ-[Zn(bpp)$_2$])}$^{4+}$, ***out*-4**; *in, in*-{[RuCl(trpy)]$_2$(μ-[Zn(bpp)$_2$])}$^{2+}$, ***in*-3**; and *in, in*-{[Ru^{III}(trpy)]$_2$(μ-[Zn(bpp)$_2$(H_2O)] μ-(O)}$^{4+}$, ***in*-5**; bearing both ruthenium and zinc atoms, have been successfully synthesized and characterized.
- ✓ The electronic communication between the ruthenium centers in ***out*-3** and ***in*-3** has been electrochemically evaluated and the slightly stronger coupling found in ***in*-3** has been explained in terms of the Zn-Cl contacts seen in the X-Ray structure.
- ✓ The irreversible isomerization process from ***out*-3** to ***in*-3** has been followed by NMR spectroscopy and rationalized with the help of DFT calculation.
- ✓ The higher stability in aqueous media of ***in*-5** respect to ***out*-4** is determined by the oxo-bridge connecting the two ruthenium centers. The same oxo-bridge is unstable when the complex is reduced to (II/II) redox state, breaking apart the molecule.

Chapter 4

- ✓ Six new complexes: $\{[Ru(trpy)]_2(\mu\text{-}[Co(bpp)_2][(\mu\text{-}Cl)_2])\}^{2+}$, **$Ru_2Co\text{-}Cl_2$**; $\{[Ru(trpy)]_2(\mu\text{-}[Co(bpp)_2][(\mu\text{-}AcO)_2])\}^{2+}$, **$Ru_2Co\text{-}OAc_2$**; $\{[Ru(H_2O)(trpy)]_2(\mu\text{-}[Co(H_2O)_2(bpp)_2])\}^{4+}$, **$Ru_2Co\text{-}(H_2O)_4$**; $\{[Ru(trpy)]_2(\mu\text{-}[Mn(bpp)_2][(\mu\text{-}Cl)_2])\}^{2+}$, **$Ru_2Mn\text{-}Cl_2$**; $\{[Ru(trpy)]_2(\mu\text{-}[Mn(bpp)_2][(\mu\text{-}AcO)_2])\}^{2+}$, **$Ru_2Mn\text{-}OAc_2$**; $\{[Ru(H_2O)(trpy)]_2(\mu\text{-}[Mn(H_2O)_2(bpp)_2])\}^{4+}$, **$Ru_2Mn\text{-}(H_2O)_4$**; were synthesized and characterized.
- ✓ Electrochemical experiments on **$Ru_2Co\text{-}OAc_2$** and **$Ru_2Mn\text{-}OAc_2$** showed for both complex three metal based redox processes, fully assigned, and highlighted the electronic communication between the two ruthenium centers in both complexes ($\Delta E(Ru_2(III,III)/(Ru_2(III,II)$ - $Ru_2(III,II)/(Ru_2(II,II))$ = 170 mV for **$Ru_2Co\text{-}OAc_2$** and 100 mV for **$Ru_2Mn\text{-}OAc_2$**).
- ✓ Electrochemical characterization at pH = 7 showed large electrocatalytic waves at 1.3 V vs NHE for **$Ru_2Co\text{-}(H_2O)_4$** and 1.3 for **$Ru_2Mn\text{-}(H_2O)_4$**. This difference in potential translated to the activity in photoinduced water oxidation, where the Co containing complex generated 50 TON with a TOF_i of 0.21 s^{-1}, while the Mn containing one generated a much lower 8 TON.

VII

- ✓ Complex **Ru_2Co-$(H_2O)_4$** was tested for chemically activated water oxidation, using Oxone as chemical oxidant, yielding 13 TON. Labelled water experiments on the same system allowed the definition of a mechanism where the only active site is the cobalt center, and a redox tautomerism is present.

Chapter 5

- ✓ Five new complexes: *cis(out), cis*-$[Ru(Cl)_2(HL)(dmso)_2]$, **1**; *out*-$[Ru(Cl)(HL)(trpy)]^+$, **2a**$^+$; *in*-$[Ru(Cl)(HL)(trpy)]^+$, **2b**$^+$; *out*-$[Ru(HL)(trpy)(H_2O)]^{2+}$, **3a**$^{2+}$; *in*-$[Ru(HL)(trpy)(H_2O)]^{2+}$, **3b**$^{2+}$; were synthesized and characterized. HL is 1H-Pyrazole-3-Carboxylic Acid, 5-(2-pyridinil)-, ethyl ester, used for the first time as ligand in this work. Two different synthetic routes were appointed for isomeric **2a**$^+$ and **2b**$^+$, allowing to obtain more of one or the other compound.
- ✓ The linkage isomerism presented by a dmso moiety in **1** was investigated by electrochemical methods, and thermodynamic and kinetic data were extracted.
- ✓ Electrochemical characterization of **3a**$^{2+}$ and **3b**$^{2+}$ at different pHs allowed the construction of Pourbaix diagrams, which in turn

helped to contextualize the effect of the electronwithdrawing ester on the redox and acid –base properties of the complexes.

- ✓ Foot-of-the-wave analysis was applied to electrochemical experiments on **3a**$^{2+}$ and **3b**$^{2+}$, yielding values of k_{obs} of 1.00 s^{-1} and 2.23 s^{-1} respectively.
- ✓ Complexes **3a**$^{2+}$ and **3b**$^{2+}$ were tested for CAN driven water oxidation, giving values of TON of 10.8 and 4.2; and TOF_i of 58.2 x 10^{-3} s^{-1} and 15.4 x 10^{-3} s^{-1}, respectively.

VII

Chapter 6

- ✓ Two new complexes: *out*-[Ru(H_2pcp)(trpy)(H_2O)]$^{2+}$, **4a**$^{2+}$; *in*-[Ru(H_2pcp)(trpy)(H_2O)]$^{2+}$, **4b**$^{2+}$; were synthesized and characterized.
- ✓ The crystal structure of **4b**$^{2+}$ showed the presence of a hydrogen bond network between a pyrazolic nitrogen, the aqua ligand and a free water molecule.
- ✓ The construction of Pourbaix diagrams for both species highlighted a shift of the pK_a of the pyrazolic proton of **4b**$^{2+}$ towards acidic pH. This unusual behavior has been explained in terms of the stability induced by the hydrogen bond network. The Pourbaix diagrams also showed a dramatic drop in potential for the Ru(V)/Ru(IV) couple at neutral and basic pH for both

complexes, due to the accumulation of negative charges on the ligand.

✓ Electrochemical characterization in CF_3CH_2OH indicated both a very fast substitution of the aqua ligand for a solvent molecule, and a slow isomerization under light irradiation from the *out* to the *in* isomer, probably due to a hydrogen bond system similar to the one observed in solid state.

✓ Both complexes have been tested for homogeneous water oxidation with CAN as sacrificial oxidant, with values of TON of 17.7 and 6.9; and TOF_i of 88.9 x 10^{-3} s^{-1} and 34.8 x 10^{-3} s^{-1}, for **4a**$^{2+}$ and **4b**$^{2+}$ respectively.

✓ A strategy to attach the complexes on FTO has been developed, and the films **4a-FTO** and **4b-FTO** thus obtained have been characterized by electrochemistry, and preliminary studies on heterogeneous water oxidation show a higher activity for **4a-FTO** than **4b-FTO**.

UNIVERSITAT ROVIRA I VIRGILI
MONONUCLEAR AND HETEROTRINUCLEAR RUTHENIUM COMPLEXES: SYNTHESIS AND WATER OXIDATION ACTIVITY.
Lorenzo Mognon
Dipòsit Legal: T 1359-2015

UNIVERSITAT ROVIRA I VIRGILI
MONONUCLEAR AND HETEROTRINUCLEAR RUTHENIUM COMPLEXES: SYNTHESIS AND WATER OXIDATION ACTIVITY.
Lorenzo Mognon
Dipòsit Legal: T 1359-2015

UNIVERSITAT ROVIRA I VIRGILI
MONONUCLEAR AND HETEROTRINUCLEAR RUTHENIUM COMPLEXES: SYNTHESIS AND WATER OXIDATION ACTIVITY.
Lorenzo Mognon
Dipòsit Legal: T 1359-2015